RETURN TO ANL LIBRARY LIBRARY

ANALYTICAL MODELING OF THERMAL DISCHARGES

A Review of the State of the Art

by

Barry A. Benedict, Jerry L. Anderson,
and Edgar L. Yandell, Jr.

U of C-AUA-USAEC

ARGONNE NATIONAL LABORATORY, ARGONNE, ILLINOIS

Prepared for the U.S. ATOMIC ENERGY COMMISSION
under Contract W-31-109-Eng-38

The facilities of Argonne National Laboratory are owned by the United States Government. Under the terms of a contract (W-31-109-Eng-38) between the U. S. Atomic Energy Commission, Argonne Universities Association and The University of Chicago, the University employs the staff and operates the Laboratory in accordance with policies and programs formulated, approved and reviewed by the Association.

MEMBERS OF ARGONNE UNIVERSITIES ASSOCIATION

The University of Arizona
Carnegie-Mellon University
Case Western Reserve University
The University of Chicago
University of Cincinnati
Illinois Institute of Technology
University of Illinois
Indiana University
Iowa State University
The University of Iowa
Kansas State University
The University of Kansas
Loyola University
Marquette University
Michigan State University
The University of Michigan
University of Minnesota
University of Missouri
Northwestern University
University of Notre Dame
The Ohio State University
Ohio University
The Pennsylvania State University
Purdue University
Saint Louis University
Southern Illinois University
The University of Texas at Austin
Washington University
Wayne State University
The University of Wisconsin

NOTICE

This report was prepared as an account of work sponsored by the United States Government. Neither the United States nor the United States Atomic Energy Commission, nor any of their employees, nor any of their contractors, subcontractors, or their employees, makes any warranty, express or implied, or assumes any legal liability or responsibility for the accuracy, completeness or usefulness of any information, apparatus, product or process disclosed, or represents that its use would not infringe privately-owned rights.

Printed in the United States of America
Available from
National Technical Information Service
U.S. Department of Commerce
5285 Port Royal Road
Springfield, Virginia 22151
Price: Printed Copy $7.60; Microfiche $1.45

ANL/ES-18
Heat Rejection
and Utilization

ARGONNE NATIONAL LABORATORY
9700 South Cass Avenue
Argonne, Illinois 60439

ANALYTICAL MODELING OF THERMAL DISCHARGES

A Review of the State of the Art

by

Barry A. Benedict, Jerry L. Anderson,*
and Edgar L. Yandell, Jr.**
(Vanderbilt University)

Environmental Statement Project

April 1974

* Now at Civil Engineering Department, Memphis State University
**Now at U. S. Army Corps of Engineers, Mobile, Alabama

TABLE OF CONTENTS

Page

LIST OF SYMBOLS 19

ABSTRACT 35

I. OBJECTIVES AND PURPOSE 35

II. INTRODUCTION TO HEATED DISCHARGES 37

A. Possible Broad-classification Schemes 37

1. Use of the Word "Model" 37
2. Near Field, Far Field, Broad Thermal Trends 37
3. River, Lake, Estuary 38
4. Type of Discharge Model 38

B. Basic Parameters in Heated-Discharge Problem 39

1. Effect of Location: x/D_o, y/D_o, z/D_o 41
2. Turbulence Levels: Re_a and Re_j 42
3. Buoyancy Considerations: $\Delta\rho/\rho_o$, F_a, F_j 42
   a. Upstream and Downstream Motion: F_a 42
   b. Degree of Vertical Mixing: F_j 43
4. Receiving-water Density Structure: C_{ds} 45
5. Initial Discharge Conditions: C_s, θ_o' β_o', k 48
6. Geometry Effects: z_1/H, z_2/H, x/D_o, D_o/H, S_b, W/D_o . . 49
7. Wind Effects: C_w, θ_1 51
8. Surface Heat Exchange: K 52
9. Degree of Unsteadiness: C_u 53
10. Physical Modeling 53

C. Comments 54

III. HEAT-BUDGET EQUATION 55

A. Introduction 55

B. Components of Heat-Budget Equation 55

1. Net Short-wave Solar Radiation, $Q_s - Q_{sr}$ 55
2. Net Atmospheric Radiation, $Q_a - Q_{ar}$ 56
3. Back Radiation, Q_{br} 57
4. Energy Used by Evaporation, Q_e 58
5. Energy Conducted from a Body of Water, Q_h 61
6. Inflow and Outflow Heat, Q_v 61
7. Conclusion 62

C. Equilibrium Temperature 63

1. Edinger-Geyer Method 63
   a. General Development 63
   b. Numerical Example 68

CONTENTS (Continued)

Page

2. Hogan *et al.* Method 70
   a. General Development 70
   b. Numerical Example 71
3. Thackston and Parker Method 72
4. Brady *et al.* Method 73
   a. General Formulation 73
   b. Numerical Example 75

D. Conclusion 76

IV. STRATIFICATION OF HEATED-WATER DISCHARGES 77

A. Basic Equations 77

B. Specific Examples of Wedges 81

1. Condenser-water Discharge Channel, Zone B 83
   a. General Formulation 83
   b. Numerical Example 84
2. Middle Region between Intake and Outlet, Zone C 85
   a. General Formulation 85
   b. Numerical Example 86

C. Summary and Conclusions 88

V. SURFACE DISCHARGES OF HEATED WATER 89

A. Introduction 89

1. Entrainment versus Diffusion Concept 89
2. Jet Models and Diffusion Models 94
3. Zone of Flow Establishment 96
   a. General 96
   b. Similarity of Profiles 97
   c. Length of Zone of Flow Establishment 98
   d. Angle at End of ZOFE 99
   e. Notation at Orifice and End of ZOFE 99
4. Pressure Difference across Jet 100
5. Inclusion of Buoyancy Effects on Models 101
6. General Comments on Formulation of Momentum Equations . 101
7. Comments on Choice of Similar Profiles 102
8. Time of Exposure of Organisms 102
9. Consideration of Surface Cooling Effects 105
10. Accounting for Limited Dilution Water 106
11. Accounting for Horizontal Variation of Ambient Temperature 108

B. Selection of Models for Discussion 108

C. Stolzenbach-Harleman Model 109

CONTENTS (Continued)

Page

1. Assumptions 110
2. Verification 112
3. Limitations and Ranges of Applicability 114
4. Data Needed 115
5. Numerical Example 115
   a. Basic Output 115
   b. Time of Exposure and Surface Area 117
6. Notation 118

D. Motz-Benedict Model 118

1. Assumptions 118
2. Verification 120
3. Data Needed 122
4. Limitations and Ranges of Applicability 124
5. Numerical Example 124

E. Pritchard's Model 128

1. Model Assumptions 128
2. Model Equations 129
   a. Initial Two-dimensional Distances and Contours . . . 130
   b. Areas within Isotherms 131
3. Inclusion of Vertical Mixing 132
4. Inclusion of Surface Cooling in Models 134
5. Time-of-exposure Calculations 136
6. Model Verification 137
7. Limitations and Ranges of Applicability 139
8. Data Needed 139
9. Numerical Example 140
   a. Data 140
   b. Lengths, Widths, Areas (No Cooling) 140
   c. Adjustment for Surface Cooling 141
   d. Time of Exposure 146
   e. Inclusion of Vertical Mixing 148
10. Summary on Pritchard's Model 149
11. Notation 149

F. Model by Sundaram, Easterbook, Piech, and Rudinger 150

1. Model Assumptions 150
2. Model Equations 152
   Jet Mixing Region 152
3. Equations for Diffusion Region 155
4. Relating Near- and Far-field Solutions 156
   Time of Exposure and Surface Areas 156
5. Verification 158
6. Limitations and Ranges of Applicability 158
7. Data Needed for Model 158
8. Numerical Example 158

CONTENTS (Continued)

Page

G. Conclusions 163

1. Discussion 163
2. Notation 163

H. Other Near-field Models 164

1. Hoopes-Zeller-Rohlich Model 164
2. Carter's Model 165

I. Other Far-field Models 166

J. Surface Discharges--Transient Conditions 168

1. Near-field Models 169
2. Far-field Estimates 170
   Segmented Model for Partially Mixed Estuary 170
3. Time-varying Model for Homogeneous Estuary 174
4. Other Finite-difference Models 176

K. Surface Discharges--Conclusions 176

1. Three-dimensional Models and Vertical Mixing 177
2. Effect of Velocity Ratio 177
3. Situations not Covered by Current Near-field Models . . 178
4. Far-field Estuary Models 178
5. Model Verification 179
6. Model Implementation and Interpretation of Results . . . 179

VI. SINGLE-PORT SUBMERGED DISCHARGES 182

A. Theory and Application of Submerged Jets 183

1. Introduction 183
2. Jets in General 183
3. Axis of Reference 184
4. General Assumptions for Submerged Jet Models 185
5. Entrainment in Submerged Jets 185
6. Typical Similar Profile--Velocity, Buoyancy, and Tracer 188
7. Pressure Drag 190

B. Development of the General Equations for a Round, Buoyant Jet 190

1. Equation of Continuity 190
2. Equation of Momentum 191
3. Density Deficiency 194
4. Continuity of Tracer 194
5. Geometric Relationships 195
6. Conclusions 195

CONTENTS (Continued)

Page

C. Round, Buoyant Jets in a Stagnant Environment 195

D. Round, Buoyant Jets in a Stagnant Uniform Environment . . . 196

1. Basic Equations 196
2. Normalization of Governing Parameters 196
3. Time of Exposure 199

E. Discharge of a Round, Buoyant Jet into a Stagnant, Linearly Stratified Environment 201

1. Basic Equations 201
2. Fan and Brooks' Solution 201
3. Ditmars' Solution 201
4. SYMJET and PLUME Models 202
5. Time of Exposure 203

F. Round, Buoyant Jets in a Stagnant Environment--Application to a Practical Problem 204

1. Round, Buoyant Jet into a Stagnant, Uniform Environment 204
2. Round, Buoyant Jets into a Stagnant, Stratified Environment 210

G. Round Jets into Stagnant Environments--Summary and Conclusions 215

H. Discharge of a Round, Buoyant Jet into a Flowing Stream . . 216

I. Discharge of a Round, Buoyant Jet in a Flowing, Uniform Environment 217

1. General Equations--Fan's Model 217
2. Abraham's Model 219
3. Time of Exposure 219

J. Discharge of a Round, Buoyant Jet in a Flowing, Stratified Environment 220

1. Introduction 220
2. General Equations 220

K. Round, Buoyant Jets in a Flowing Environment--Application to a Practical Problem 221

1. Introduction 221
2. Round, Buoyant Jet in a Flowing, Uniform Environment . . 221

L. Round Jets into a Flowing Environment--Summary and Conclusions 225

CONTENTS (Continued)

Page

M. Buoyant, Slot Jets 226

N. Buoyant, Slot Jets into a Stagnant Environment--General Equations 227

O. A Buoyant, Slot Jet in a Stagnant Uniform Environment . . . 228

1. Fan and Brooks 228
2. Cederwall and Brooks 230
3. Time of Exposure 230

P. A Buoyant, Slot Jet in a Stagnant, Stratified Environment . 231

1. Basic Equations 231
2. Fan and Brooks 231
3. Time of Exposure 234

Q. Practical Application of Buoyant-slot-jet Models 235

1. General Considerations 235
2. Buoyant, Slot Jets in a Stagnant, Uniform Environment . 235
3. Numerical Example--Stagnant, Uniform Environment 236
4. Buoyant, Slot Jets in a Stagnant, Stratified Environment 238

R. Slot Jets--Conclusions 240

S. Surface Layers from Submerged Jets 241

T. Estuarine Conditions 242

U. Single-Port Submerged Jets--Summary and Recommendations . . 243

VII. Submerged, Multiport Diffusers 245

A. Jet Interference 245

B. Diffusers in Stagnant, Arbitrarily Stratified Waters 246

1. Model Formulation 246
2. Data and Output from Computer Program 247
3. Model Applicability and Usefulness 248

C. Deeply Submerged Diffusers in a Stagnant Environment 249

1. Experimental Findings 249
2. Numerical Example 251

D. Multiport Diffusers in a Shallow, Flowing Environment . . . 252

1. Experimental and Analytical Findings 252
2. Numerical Example 254

CONTENTS (Continued)

Page

E. Multiport Diffusers into Stagnant, Intermediate Depths . . . 255

1. Experimental Findings 255
2. Numerical Example 257

F. Conclusions--Multiport Diffusers 258

VIII. COOLING PONDS 260

A. Introduction 260

B. Hydraulic Classification of Cooling Ponds 260

1. Completely Mixed Ponds 260
2. Plug-flow Ponds 261
3. Actual Ponds 263
4. Pond Optimization 264

C. Equilibrium-temperature Model for Cooling Ponds 265

1. Once-through Cooling Ponds 265
2. Recirculating Cooling Pond 268

D. First Trial Model for Cooling Ponds 269

E. Cooling-pond Model--Steady State and Transient 272

1. Case I: Mixed, Steady State, No Vertical Temperature Gradient 273
2. Case II: Mixed Pond, Steady State with Vertical Temperature Gradient 275
3. Case III: Mixed Pond, Transient Operation, No Vertical Temperature Gradient 276
4. Case IV: Mixed Pond, Transient Operation, with a Specified Linear Vertical Temperature Gradient . . . 279
5. Case V: Plug-flow Pond, Steady State, No Vertical Temperature Gradient 279
6. Case VI: Plug-flow Pond, Steady State, with a Specified Linear Vertical Temperature Gradient 284
7. Case VII: Plug Flow, Transient, No Vertical Gradient . 284
8. Case VIII: Plug Flow, Transient Operation, with a Specified Linear Vertical Temperature Gradient . . . 288

F. Expected Accuracy from Idealized Models 288

G. Entrance Entrainment Model 289

H. Active-region Model 291

I. Evaporation Losses from Ponds 295

CONTENTS (Continued)

Page

1. Completely Mixed Ponds 295
2. Plug-flow Pond 298

J. Deep-pond Modeling 299

1. General Model Assumptions and Development 300
2. Available Models 302
3. Application of Deep-reservoir Models to Cooling Ponds . 302
4. Summary on Deep-reservoir Models 302
5. Models for Other Deep-pond Cases 302
6. Summary on Deep-pond Modeling 304

K. Conclusion 304

APPENDIX A: Shirazi *et al.* Model, Including the Effect of Ambulent Turbulence on Buoyant Jets 307

APPENDIX B: Koh-Fan Jet Model, Modified for Changes in Zone of Flow Establishment 309

ACKNOWLEDGMENTS 310

REFERENCES 311

LIST OF FIGURES

No.		Page
2.1	General Heated Discharge	40
2.2	Density Profiles in Two-layer Flow	44
2.3	Typical Stratified Reservoir Profile	47
2.4	Effect of Ambient Stratification	48
2.5	Effect of Ambient Current	49
2.6	Lateral Boundary Effects	50
3.1	Clear-sky Solar Radiation	58
3.2	Brunt C Coefficient from Air Temperature, T_a, Ratio Measured Solar Radiation to Clear-sky Radiation	58
3.3	Saturated Air Temperature or Water Temperature vs Saturated Vapor Pressure	65
3.4	Exchange Coefficient, K, Based on Lake Hefner Evaporation Formula	66
3.5	E_3 from Air Vapor Pressure, P_a, and E_2 from Air Temperature, T_a	68
3.6	M - T_{EQ} Correction for Use in Eq. 3.27	68
3.7	Normal Temperature Psychrometric Chart	69
3.8	Heat-exchange Coefficient on July 1; Monthly Average for Average Weather Conditions	73
3.9	Equilibrium Temperature on July 1; Monthly Average for Average Weather Conditions	74
3.10	Cooling Coefficient, K, from Wind Speed, W, and Average Temperature, T_a	75
4.1	Flow Stratification in Vicinity of Power Plant	78
4.2	Two-layered Stratified Flow	79
4.3	Critical Flow Sections in Two-layer Flow	82
4.4	Vertical Temperature and Velocity Profile of Warrior River Mile 228.2 near Green County Steam Plant, 8/12/70	82
4.5	Cross Section along Centerline of Outlet Channel	84
4.6	Relative Shape of Warm-water Wedge for No Recirculation	86

FIGURES (Continued)

No.		Page
4.7	Variation in Relative Wedge Length with Densimetric Froude Number	88
5.1	Entrainment of Fluid	91
5.2	Reduction of Entrainment as a Function of Richardson Number	92
5.3	Schematic View of Thermal Plume	92
5.4	Definition Sketch for Zone of Flow Establishment	97
5.5	Zone of Flow Establishment	99
5.6	Schematic for Graphically Calculating Exposure Time	105
5.7	Longitudinal Distribution in the Chesapeake Bay of the Sectional Mean Relative Concentration and Temperature Rise	107
5.8	Schematic of Heated Surface Discharge	110
5.9	Geometrical Characteristics of the Jet	111
5.10	Dilution in the Stable Region of Buoyant Discharges	113
5.11	Maximum Jet Depth vs. F_j as Calculated by Theory	114
5.12	Theoretical Calculation of Jet Structure for Example	116
5.13	Calculated Isotherms for Example	117
5.14	Definition Sketch for Motz-Benedict Model	120
5.15	Entrainment Coefficient as a Function of Velocity Ratio	121
5.16	Observed Values and Fitted Curve for Initial Angle vs. Velocity Ratio	122
5.17	Observed Values and Fitted Curve for Length of Establishment Zone vs. Velocity Ratio	123
5.18	Temperature Decrease for Motz-Benedict Example	125
5.19	Isotherms for Motz-Benedict Example	126
5.20	Definition Sketch for Pritchard Model	130
5.21	Pritchard Idealized Isotherm	132
5.22	Predicted Isotherms for Pritchard Example	147
5.23	Variation of Plume Depth for Numerical Example	148

FIGURES (Continued)

No.		Page
5.24	Two-step Method of Plume Analysis	151
5.25	Velocity Distribution for Turbulent Two-dimensional Jet	154
5.26	Decay of Temperature along Plume Centerline for Lake Surface Temperature = 70°F and Discharge Temperature = 85°F	154
5.27	Isotherms in Diffusion Zone by Sundaram *et al.* Model	162
5.28	Segmented Model for Partially Mixed Estuary	170
6.1	Schematic Diagram of Reference Axis	184
6.2	Schematic of a Simplified Section of a Jet with Counter-rotating Vortices	188
6.3	Typical Jet Cross Section for a Discharge into a Flowing, Ambient Environment	189
6.4	Schematic Diagram of Ambient-velocity and Drag-force Components	192
6.5	Schematic Diagrams of Round, Buoyant Jet Problems Studied	196
6.6	Trajectories and Half-width b/b_o of Horizontal Round, Buoyant Jets in a Stagnant, Uniform Ambient Fluid Based on $\alpha = 0.082$	197
6.7	Dilution of Horizontal, Round, Buoyant Jets in Stagnant, Uniform Environments	198
6.8	Theoretical Solutions of Dilution, D_i, for Horizontal, Buoyant Jet in Stagnant Receiving Water of Uniform Density	200
6.9	Terminal Height of Rise ξ_t for Horizontal, Round, Buoyant Jets in a Linearly Density-stratified Environment	202
6.10	Terminal Horizontal Coordinate η_t for Horizontal, Round, Buoyant Jets in a Linearly Density-stratified Environment	202
6.11	Terminal Volume-flux Parameter μ_t for Horizontal, Round, Buoyant Jets	203
6.12	Density Profile for Ditmars' Example Problem	203
6.13	ZOFE for an Inclined, Round, Buoyant Jet	206
6.14	Predicted Temperature Decrease for Example Problem Using Hirst's Model	214
6.15	Comparison of the Predicted Jet Trajectories for Stagnant-environment Numerical Example	214

FIGURES (Continued)

No.		Page
6.16	Comparison of Observed and Theoretical Trajectory, Half-widths, $r_{0.5}/D_o$, and Centerline Dilution Ratios, D, of a Buoyant Jet in a Uniform Cross Stream: $F_j = 20$ and $k = 4$	218
6.17	Comparison of Observed and Theoretical Trajectory, Half-widths, $r_{0.5}/D_o$, and Centerline Dilution Ratios, D, of a Buoyant Jet in a Uniform Cross Stream: $F_j = 20$ and $k = 8$	218
6.18	Variations of the Entrainment Coefficient, α, and the Reduced Drag Coefficient, C_d' for Buoyant Jets in Uniform Cross Stream for a 90° Discharge	219
6.19	Integration Scheme for Evaluating Time of Exposure	220
6.20	Comparison of the Predicted Temperature Decrease for Numerical Example for a Flowing Environment	223
6.21	Comparison of the Predicted Jet Trajectories for Numerical Example for a Flowing Environment	224
6.22	Graphical Integration for the Time of Exposure Using Fan's Model	224
6.23	Schematic Diagrams of Slot-buoyant-jet Problems Studied	228
6.24	Trajectories and Half-widths, b/b_o, for Slot, Buoyant Jets in a Stagnant, Uniform Environment: $\Theta_o' = 0°$	229
6.25	Dilution of Slot, Buoyant Jets in Stagnant, Uniform Environment: $\Theta_o' = 0°$	229
6.26	Experimental Jet Trajectory for a Horizontal, Buoyant Slot Jet in Stagnant Environment, Compared With Fan and Brooks Theory Based on $\alpha = 0.16$ and $\lambda = 0.89$	231
6.27	Experimental Centerline Dilution for a Horizontal, Buoyant Slot Jet in Stagnant Environment, Compared with Theory of Fan and Brooks Based on $\alpha = 0.16$ and $\lambda = 0.89$	231
6.28	Terminal Height of Rise ξ_t for Slot Buoyant Jets, $\Theta_o' = 0°$, in Linearly Stratified Environment	232
6.29	Terminal Horizontal Coordinate η_t for Slot Buoyant Jets, $\Theta_o' = 0°$, in a Linearly Stratified Environment	232
6.30	Terminal Volume Flux Parameter μ_t for Slot Buoyant Jets, $\Theta_o' = 0°$, in Linearly Stratified Environment	233
6.31	Zone of Flow Establishment for an Inclined Slot Buoyant Jet	236
7.1	Two Ways in Which Jets from a Multiport Diffuser Can Interact	245

FIGURES (Continued)

No.		Page
7.2	Predicted Trajectories of Multiple Buoyant Jets in a Uniform Environment	247
7.3	Predicted Jet Centerline Excess Temperature of Multiple Buoyant Jets in Uniform Environment	248
7.4	Predicted Trajectories of Multiple Buoyant Jets in a Stratified Environment	249
7.5	Minimum Dilution along the Center of Merging Buoyant Jets from a Manifold in Stagnant Receiving Water of Uniform Density	250
7.6	Jet Interference vs. Nozzle Spacing and Submergence at Froude Number $F_j = 20$	256
7.7	Jet Interference vs. Froude Number at Spacing $W/D_o = 10$	256
8.1	Flow-through Curves for Completely Mixed and Plug-flow Ponds	262
8.2	Results for Nashville, Tennessee	271
8.3	Effect of Pond Surface Area on Amount of Cooling for Various Seasons: Nashville, Tennessee	272
8.4	f_1 vs. Equilibrium Temperature or Steady-state Mixed Pond Temperature	274
8.5	Linear Temperature Profile	276
8.6	f_2 vs. $\Delta\Theta$ for Equilibrium Temperature of 80°F	278
8.7	Transient Pond Temperature for 800-acre, Completely Mixed Pond	280
8.8	Transient Effluent Temperature for 800-acre, Plug-flow Pond	288
8.9	Results from Examples for Steady-state, Completely Mixed and Plug-flow Ponds	288
8.10	Schematic Drawing of Entrance Entrainment Model	290
8.11	Temperature Excess of Shallow Pond with Entrance Mixing	291
8.12	Definition of Main Flow and Tributary Sidearm for Shape-factor Computations	293
8.13	Partitioning of Cooling Lake for Alternative Scheme and for Inflow-Outflow Formulations	294
8.14	Evaporation Loss Parameter for Mixed Pond in Steady State as a Function of Temperature	297

FIGURES (Continued)

No. Page

8.15 Evaporation Loss Parameter vs. Temperature for a Plug-flow Pond Operating in Steady State 299

8.16 Schematic Diagram of Reservoir Problem 300

LIST OF TABLES

No.		Page
3.1	Coefficients for Various Evaporation Formulas, Expressed in lb/ft^2-day	59
3.2	Comparison of Amounts of Heat Loss By Various Components of Heat Budget Equation	62
3.3	Summary of Equations of Three Different T_{EQ} Calculating Methods	64
5.1	Values of Entrainment Coefficient	121
5.2	Data for Motz-Benedict Example	125
5.3	Example Predictions, Motz-Benedict Model	126
5.4	Length, Width, and Area for Example Case, With No Cooling	141
5.5	Surface Cooling Coefficient, as a Function of Wind Speed, Natural Surface Water Temperature, and Excess Temperature	142
5.6	Areas Within Isotherms, For Example, With Surface Cooling Included	144
5.7	Near-field Model Applicability	178
5.8	Characteristics of Models	181
6.1	Comparison of Predicted Values for Example Problem Using Fan, Cederwall, and Hirst	215
6.2	Comparison of Predicted Results Using Fan and Hirst Models	225
6.3	Modeling Capabilities in Flowing Environments	227
6.4	Applicability of Single Port Models	244
7.1	Applicability of Submerged Multiport Diffuser Information	258
7.2	Ranges of Parameters for Studies Reported	259
8.1	Comparison of Completely Mixed and Plug-flow Ponds	266
8.2	Results from Example Problem for Once-through Cooling	268
8.3	Results from Example Problem for Recirculating	270
8.4	Calculations for Transient Example	279
8.5	Computation of Lake Shape Factor	293
8.6	Lake Shape Factor for Alternative Scheme	294

LIST OF SYMBOLS

This list of symbols is not all-inclusive. Those symbols that are introduced only once, defined at that point, and used only at that place in the text for discussion or clarification are generally not included in this list.

Efforts have been made to retain some consistency of symbols from chapter to chapter. Occasional variances from this enable the text to remain closer to the symbols used in the basic references. For this reason, some of the symbols in Chapters III and VIII duplicate those in other chapters. Because these chapters are rather distinct from those on discharge mechanisms, no problem is seen from such duplication. The reader should review all the definitions for any symbol to assure himself that he is using the correct definition.

A	Surface area of the pond or other body of water
A_C	Characteristic area subjected to ambient flow for purposes of determining pressure drag
A_c	Area within desired isotherm
A_i	Surface area along the main flow path from the discharge to the center of the mouth of each sidearm
A_n	Area inside isotherm number n
$(A_n)_{m,c}$	Area within nth isotherm, corrected for cooling (see Eq. 5.54)
A_p	Area of discharge port
A_R	Cross-sectional area of river or estuary
A_x	Cross-sectional area of estuary (for Eq. 5.92)
$A_{\Delta T}$	Surface area within the ΔT isotherm
A'	Channel-aspect ratio for Stolzenbach-Harleman model = $2z_o/B_o$
a,b	Coefficients used in evaporation formulas (see Table 3.1)
a_1	8.9×10^{-2}
a_2	3.5×10^{-3}
a_3	5.68×10^{-6}
a_4	1.13×10^{-6}

SYMBOLS (continued)

a_6	1.9176×10
a_7	5.85×10^{-2}
a_8	7.923×10^{-2}
a_{12}	3.73×10^{3}
a_{13}	3.73×10^{2}
a_{14}	4.73×10^{-3}
B	Bowen ratio
B_o	Initial width of slot or rectangular jet
B_{ov}	Width of virtual orifice
b	Half-width of jet = $\sqrt{2}\ \sigma$ (Chapter V), or characteristic length (frequently called jet half-width) described by Eq. 6.4 (Chapter VI)
b_m	Maximum width of an isotherm
b_o	Half-width at end of zone of flow establishment (ZOFE)
b_R	Width of river
C	Cloud cover, tenths
C_B	Brunt coefficient
C_D	Drag coefficient
C_d	Drag coefficient
C'_d	$C_d\ \sqrt{2}/\alpha\pi$
C_{ds}	Coefficient indicating density structure of the receiving waters
C_M	Meyer-evaporation-equation constant
C_p	Specific heat capacity of water
C_s	Dimensionless shape factor, indicating influence of orifice shape on discharge action
C_u	Coefficient indicating unsteadiness of the flow
C_w	Wind-stress coefficient

SYMBOLS (continued)

C_{x_i}	Coefficient in river-diffusion equation (Eq. 5.7)
C_1, C_2	Constants for Q_{cs} calculation (a function of latitude)
C_3, C_4	Curve-fitting constants that are a function of cloud cover and P_a
$C(\beta)$	The x-axis intercepts of the straight lines that approximate the T_s-versus-P_s curve for each 10°F segment
c	Concentration of the material under discussion
c_0	Initial concentration of substance of discharge point
D	Dilution, or dilution with respect to discharged point
D_i	Unadjusted dilution, or dilution with respect to the end of the zone of flow establishment
D_L	Longitudinal dispersion (mixing) coefficient; or local jet dimension (Chapter VII only)
D_o	Initial diameter of round jet
D_{x_i}	The diffusion coefficient in the x_i direction
d	Day of the year (1-365)
d_s	Incremental length along jet axis
E	Coefficient of entrainment; or evaporation rate (Chapter VIII only)
E'	Diffusion coefficient
E_n	Vertical exchange coefficient in partially mixed estuary
E_r	Rate at which ambient fluid is entrained
F_a	Densimetric Froude number of the ambient flow = $U_a/\sqrt{g(\Delta\rho/\rho_o)H}$
F_D	Drag force
F_d	Drag force due to pressure differences
F_{DL}	Densimetric Froude number of discharge load = $Q_L/[z_1\sqrt{(\Delta\rho/\rho)g\ z_1}]$

SYMBOLS (continued)

F_j	Densimetric Froude number of discharge = $U_o/\sqrt{g(\Delta\rho/\rho_o)D_0}$ (D_o replaced by z_o for rectangular orifice)
F_L	Local densimetric Froude number = $U_j/\sqrt{g(\Delta\rho/\rho_o)b}$ for submerged plumes; or local densimetric Froude number = $\bar{U}/\sqrt{g(\Delta\rho/\rho)z_L}$ for surface plumes
F_s	Total shape factor
F_1	Densimetric Froude number in upper layer
F_2	Densimetric Froude number in lower layer
f_b	Dimensionless Darcy-Weisbach friction factors for bottom
f_i	Dimensionless Darcy-Weisbach friction factors for interface; or shape factor for each sidearm (Chapter VIII only)
f_1	Summation term defined by Eq. 3.30
$f(\zeta)$	Lateral similarity function for velocity in Stolzenbach-Harleman[131] model (Eq. 5.22)
g	Acceleration due to gravity
H	Total depth of receiving-water body at point of discharge
H_{plant}	Rated capacity of plant
H_R	Absorbed radiation, Btu/ft^2-day
$H_{rejected}$	Heat rejected by plant
h_i	Enthalpy of term i, Btu/lb$_m$; or mean depth at the mouth of each sidearm (Chap. VIII only)
h_{max}	Maximum depth of bottom of jet
h_{mu}	Enthalpy of the makeup water
h_o	Initial horizontal momentum flux
h_{POND}	Enthalpy of the pond water
h_p	Enthalpy of the precipitated water
h_s	Enthalpy of the seepage water

SYMBOLS (continued)

K	Surface cooling coefficient (see Chapter III)
K_H	Eddy-diffusion coefficient
$K_{M_{jet}}$	Eddy diffusivity of the jet region
k	Velocity ratio = U_o/U_a
k'	$k + \cos \Theta_o$
k_H	Constant in 4/3 law
L	Length of the warm-water wedge (Chapter IV only); or distance from intake to outlet of a pond (Chapter VIII only)
L_c	Length of conduit leading to outfall
L_s	Characteristic length scale of diffusion phenomenon
M_E	Mass rate of water loss by evaporation
M_i	Mass transfer rate due to flow i, lb_m/ft^2-day
m	Momentum-flux parameter
n	Manning's roughness coefficient; or inverse spreading ratio in Pritchard's model (taken as 6)
P_a	Water-vapor pressure in the air, mm Hg
P'_a	Water-vapor pressure in the air, psia
P_{EQ}	Saturation vapor pressure at equilibrium temperature, T_{EQ}
P_s	Saturation vapor pressure at water surface temperature, T_s
P_1	$U_a/(k_H B_{ov}^{1/3})$
P_2	$KB_{ov}/(\rho C_p U_a z_0)$
Q	Volume flow rate past given section of jet (used in all chapters except III and VIII); or increase in energy stored in the body of water, Btu/ft^2-day (used in Chapters III and VIII)
Q_a	Incoming long-wave radiation from the atmosphere, Btu/ft^2-day
Q_{ar}	Reflected long-wave radiation, Btu/ft^2-day

SYMBOLS (continued)

Q_{br}	Back radiation emitted by the body of water, Btu/ft^2-day
Q_{cs}	$Q_s - Q_{sr}$ = net clear sky solar (short-wave radiation) Btu/ft^2-day
Q_e	Energy used by evaporation, Btu/ft^2-day
Q_h	Heat added to the cooling water by the power plant (all chapters except III), or energy conducted from the body of water as sensible heat, Btu/ft^2-day
Q_i	Inflow to a layer in deep reservoir model
Q_L	Discharge per unit length of manifold = $\pi U_o D_o^2/4W$
Q_l	Lower-layer flow in partially mixed estuary
Q_o	Condenser-water discharge
Q'_o	Outflow from a layer in deep-reservoir model
Q_p	Heated-water discharge
Q_{pp}	Waste thermal energy imposed on the pond
Q_R	River discharge
Q_s	Short-wave radiation incident to the water surface, Btu/ft^2-day
Q_{sr}	Reflected short-wave radiation, Btu/ft^2-day
Q_u	Upper-layer flow in partially mixed estuary
Q_v	Net energy brought into the body of water in inflow, including precipitation, and accounting for outflow, Btu/ft^2-day (Chapters III and VIII); or vertical flow between layers in partially mixed estuary (Chapter V)
Q'_v	Vertical advective flow rate past elevation z
q_p	Intake flow of the pond
$q_{p,n}$	Pollutant discharge into nth segment of estuary
q_r	Inflow rate
R	Hydraulic radius (Eq. 4.9)
R'	Fresh-water inflow to estuary
R_{ar}	Q_{ar}/Q_a = atmospheric reflectivity

SYMBOLS (continued)

Re_a	Reynolds number of ambient flow = $U_a H/\nu$ (or some other representative length may be used instead of H)
Re_j	Reynolds number of initial discharge or jet = $U_o D_o/\nu$ or $U_o B_o/\nu$
R_h	Relative humidity
R_i	Bulk Richardson number = $1/F_L^2$
R_{sr}	Q_{sr}/Q_s = solar reflectivity
r	Radial distance from centerline
$r_{0.5}$	Radial distance from jet centerline to the point at which $\Delta T/\Delta T_c = 0.5$
r_i	$KA/(\rho C_p q_p)$
S	Dimensionless jet axis distance for Motz-Benedict[93] model (see Eq. 5.32)
S_b	Bottom slope
S_e	Slope of energy grade line (Eq. 4.8)
S_i	Surface area of each sidearm
S_l	Salinity of lower layer of partially mixed estuary
S_u	Salinity in upper layer of partially mixed estuary
S_v	Salinity on boundary between upper and lower layers in partially mixed estuary
s_c	Distance at which isotherm crosses jet axis
s_e	Length of zone of flow establishment (ZOFE)
s_t	Distance along axis to point where desired temperature contour crosses plume axis
T	Temperature at point of interest; or stratification parameter = $(\rho_o - \rho_1)/[-D_o(d\rho_a/dz)]$ (D_o replaced by B_o for slot jets)
T_A	Average temperature between T_{SAT} and T_{EQ}
T_a	Air temperature, °F (Chapters III and VIII); or water temperature at the condenser intake when water is taken from the river--is equal to the ambient water temperature of river if recirculation is prohibited (Chapter IV)

SYMBOLS (continued)

T_c	Time of travel in conduit leading to outfall; or temperature of water entering the condensers (Chapter VIII only)
T_{EFF}	Effluent temperature
T_{EQ}	Equilibrium temperature
T_{IN}	Intake temperature of a pond
T_o	Initial discharge temperature
T_p	Pond temperature
T_{RO}	Outlet temperature of a cooling lake
T_s	Surface-water temperature, °F
T_{SAT}	The saturated or wet-bulb air temperature corresponding to T_a at R_h, °F
T_t	Total time of travel from condensers to a given temperature rise contour
$T(z)$	Variation of ambient temperature with depth
T_{ZOEF}	Time spent in zone of established flow (ZOEF)
T_{ZOFE}	Time spent in zone of flow establishment (ZOFE)
T_w	Ambient water temperature
T_1	Initial jet temperature
t_r	Flow-through time
$t_{\Delta T}$	Time to reach ΔT isotherm along jet axis
$t(\zeta)$	Lateral similarity function for temperature in Stolzenbach-Harleman[131] model (Eq. 5.23)
t'	Detention time of a pond
U	Jet centerline velocity (except in Chapter VI)
$\overline{U}$	Average plume velocity at the given location
U_a	Ambient velocity at point of interest (may vary over receiving body)
U_{am}	Maximum ambient velocity for nonuniform ambient velocities

SYMBOLS (continued)

$U_a(y)$	Variation of ambient velocity, U_a, with distance y from shoreline
U_C	Characteristic velocity component for defining pressure drag
U'_c	Velocity in conduit to outfall (usually = U_o for open-channel discharges)
U_f	Fresh-water flow velocity
U_i	Instantaneous velocity in river or estuary for Eq. 5.2
U_j	Velocity of jet at centerline (Chapter VI)
U_{max}	Maximum tidal velocity (Eq. 5.91)
U_o	Initial jet velocity, or $u_o + U_a \cos \Theta_o$ (Chapter VI only)
U(s)	Velocity as a function of distance along axis, s
U_w	Wind speed
U_1	Average velocity in the upper layer for two-layer flow
U_2	Average velocity in the lower layer for two-layer flow
U_η	Velocity at distance η from centerline
u = u(s)	Jet centerline velocity at s (Chapter VI only)
$u^*(s,r,\phi)$	Local jet velocity
u_o	Initial discharge velocity of jet (Chapter VI only)
u^*	Friction velocity = $\sqrt{gRS_e}$
V	Volume of the pond
v_i	Entrainment velocity
W	Spacing between discharge ports, $W \to \infty$ implies a single port (all chapters except III and VIII); or wind speed, mph (Chapters III and VIII)
W_i	Width at the mouth of each sidearm
W_p	Wetted parameter
W_r	Width of ambient receiving stream/width of discharge channel or port

SYMBOLS (continued)

w	Nominal jet half-width
w_t	Jet half-width at terminal location
$\tilde{w}$	Dimensionless jet half-width
x,y,z	Standard Cartesian coordinates, usually oriented such that the ambient velocity, U_a, is located along the x axis
x,y	Distances measured from virtual origin for Sundaram model only
x	Distance from pond intake to some point of interest (Chapter VIII)
x_t	Horizontal terminal location of jet into a stratified environment
x_1	Representative distance of discharge point of interest from nearest shoreline
$\tilde{x}$	x/B_{ov} (see Eq. 5.74)
y_{max}	Maximum penetration of jet away from shoreline into cross-current
$y_{\Delta T}$	Distance along jet axis to point where ΔT isotherm crosses the axis (Pritchard's model)
$\tilde{y}$	y/B_{ov} (see Eq. 5.74)
ZOEF	Zone of established flow
ZOFE	Zone of flow establishment
z_c	Critical depth of mixing for Pritchard's model (Chapter V); or critical depth for two-layer flow (Chapter IV)
z_L	Depth of heated layer at the section of interest
z_m	Height at which alternate-side jets merge
z_o	Depth of rectangular (slot or open channel) orifice
Z_R	Total depth of river
z_t	Vertical terminal location of jet into a stratified environment
z_y	Plume thickness at distance y from orifice
z_1	Submergence of orifice (distance below water surface); or thickness of the upper layer in two-layer flow (Chapter IV only)

SYMBOLS (continued)

z_2	Distance orifice is located above bottom boundary of receiving body; or thickness of the bottom layer in two-layer flow (Chapter IV only)
α	Coefficient of entrainment
(α,β,γ)	Empirical coefficients for jet trajectory equation in model of Sundaram et al.[133] (see Eq. 5.64)
α_r	Entrainment coefficient for round jet, usually taken as 0.082
α_s	Entrainment coefficient for slot jet, usually taken as 0.16
α_{sz}	Vertical-entrainment coefficient, buoyant case
α_z	Vertical-entrainment coefficient, nonbuoyant case
β	Angle that the projection of the s axis on the xy plane makes with the x axis along a local point along jet axis (all chapters except III and VIII); or the slope of the straight lines that approximate the T_s-versus-P_s curve for each 10°F segment (Chapters III and VIII)
β_*	$90°-\beta$
β'	Slope of temperature gradient
β_a	Coefficient of the form, $\beta_a = C_3 + C_4P_a$
β_o	Jet angle with respect to x axis in xy plane at end of ZOFE
β_o'	Initial jet angle with respect to x axis in xy plane
$(\Delta A_n)_m$	Incremental area of nth isotherm, no cooling allowed, i.e., area between nth and (n - 1)st isotherms, or $A_n - A_{n-1}$; subscript m implies mixing only
$(\Delta A_n)_{m,c}$	Incremental area of nth isotherm, mixing (m) and cooling (c) both included
Δh	Heat of vaporization of water
ΔT	Temperature rise at a specific point; generally taken to mean temperature rise on jet centerline, but occasionally used as temperature rise at a point on the lateral profile of temperature
$\Delta\overline{T}$	New average temperature rise over cross section after adjustment for vertical mixing in Pritchard's model
$\Delta T'$	Temperature rise adjusted to include background temperature buildup

SYMBOLS (continued)

ΔT_c	Centerline temperature rise, or temperature rise across the condensers (Chapter VIII only)
ΔT_n	Temperature rise of nth isotherm
$\Delta \overline{T}_n$	Average temperature rise between ΔT_n and ΔT_{n-1}
ΔT_o	Initial discharge temperature rise
ΔT_{ov}	Temperature rise at virtual origin
ΔT_s	Temperature rise at water surface
$\Delta T_{surface}$	Temperature rise, above ambient, at the water surface
ΔT_η	Temperature rise at distance η from centerline
$(\Delta \Gamma_n)_m$	Rate of excess heat loss between isotherms based on area calculated without cooling
$(\Delta \Gamma_n)_{m,c}$	Rate of excess heat loss between isotherms based on area calculated, including mixing and cooling
$\Delta \Theta$	$\Theta_{ss} - \Theta_t$
$\Delta \rho$	Density difference between receiving fluid and discharge fluid
δ	A scale factor that relates the coordinates distances on the jet trajectory to T, the stratification parameter, and F_j
ε	Operational efficiency of plant
ε_w	Emissivity of water surface = 0.97
ζ	Dimensionless lateral distance for Stolzenbach-Harleman[131] lateral-similarity profiles (see below Eq. 5.23)
ζ_c	Dimensionless jet distance along axis for submerged jets (See particular section of Chapter VI for the precise definition for a given model.)
η	Lateral distance from jet centerline
η_1	Distance required to reach the critical depth of mixing
η_t	Dimensionless terminal horizontal coordinate
Θ	Angle that a tangent to the s axis makes with the xy plane (all chapters except III and VIII); or pond-water temperature referenced to 32°F (Chapters III and VIII)

SYMBOLS (continued)

$\overline{\Theta}$	Bulk average temperature of the pond
Θ_a	$T_a - 32°F$
Θ_{EQ}	$T_{EQ} - 32°F$
Θ_0'	Initial angle of discharge with respect to xy plane
Θ_s	Pond-surface temperature referenced to 32°F
Θ_{ss}	Steady-state pond temperature
Θ_1	Angle of wind direction to ambient current
κ	Constant in 4/3 law
λ^2	Turbulent Schmidt number
λ_r	Spreading ratio for round jet, usually taken as 1.16
λ_s	Spreading ratio for slot jet, usually taken as 1.0
μ	Volume-flux parameter
μ_t	Terminal volume-flux parameter
ν	Kinematic viscosity of the fluid
ξ_c	Critical depth divided by the depth of the river
ξ_t	Dimensionless terminal jet height
ρ	Fluid mass density; or jet-centerline density
ρ_A	Mass density of air
ρ_a	Ambient density
ρ_o	Reference density; or ambient density at point of interest
$\rho(z)$	Variation of ambient density with depth
ρ_1	Initial jet density; or density of water in upper layer (Chapter IV only)
ρ_2	Density of water in lower layer
σ	Standard deviation of Gaussian lateral distribution (all chapters except III and VIII); or Stefan-Boltzmann Constant = 4.12×10^{-8} Btu/ft^2-day-°R^4 (Chapters III and VIII)

SYMBOLS (continued)

τ_b	Shear stress at the bottom
τ_i	Shear stress at the interface in two-layer flow
τ_w	Stress on water surface due to wind
ϕ	Angular rotation of radial coordinate r
ϕ'	Background excess temperature occurring due to limited-dilution water
ϕ_z	Solar-radiation flux past elevation z
$\int_A$	Integration or summation over entire cross section of jet

Subscripts and Superscripts

Chapter IV

'	Zone C
B	Zone B
C	Critical control section
a	Section in which ambient conditions prevail
0	Section at which condenser discharges into river

Chapter V

Sub m	Mixing only
Sub m,c	Mixing and cooling both included

Chapter VI

'	With respect to the discharge location
Sub 0	Initial value
Sub t	Terminal point
(s,r,ϕ)	Following a variable, references the physical location of that variable
(s)	Following a variable, references the location along the s axis of that variable

SYMBOLS (continued)

*	Value at a point located by s, r, and ϕ
"e"	Distances in the zone of flow establishment (ZOFE)

Chapter VIII

0	Value at x = 0 or t = 0
CM	Completely mixed pond
PLUG	A plug-flow pond
i	An initial or intake value
f	A value at some specific point
t	A value at some time, t

ANALYTICAL MODELING OF THERMAL DISCHARGES

A Review of the State of the Art

by

Barry A. Benedict, Jerry L. Anderson,
and Edgar L. Yandell, Jr.

ABSTRACT

This work describes available techniques for mathematical modeling for discharges of heated waters into rivers and lakes and for the operation of cooling ponds. General factors affecting heated-water discharges are discussed, including entrainment and diffusion, receiving-water stratification and flow rate, among others. The general elements of the heat budget are also reviewed. For all models presented, assumptions and model limitations are included, along with the basic theory, necessary equations, available verification, and numerical examples. Solutions are included for important cases of the warm-water wedge. Four models for surface discharges of heated water are reviewed in depth. Several others are referenced.

Submerged discharges, both single and multiple port, are covered. Both round and slot jets are included, and the availability of models for stratified and nonstratified receiving waters, and for stagnant or flowing receiving waters, is considered. For the single-port discharges, as well as the surface-discharge models, means of estimating times of exposure are presented.

Cooling-pond analysis emphasizes idealized pond behavior, with discussion on the behavior and analysis of real ponds. The effect of choice of evaporation formula on pond design is assessed.

I. OBJECTIVES AND PURPOSE

Concern over the problems due to thermal pollution is apparent. Several fine references detail a number of the major concerns.[75,99,100] Many of these works are being continually supplanted piece by piece as researchers, design engineers, and government agencies continue to produce new findings, improved designs or theories, and additional evidence of impact.

Numerous agencies are charged with evaluating the environmental impact of proposed projects. Although it is not yet an accomplished fact, the National Environmental Policy Act (NEPA) of 1970 is expected to eventually cause the

consideration of environmental impact to be a standard part of the total decision-making process. NEPA currently requires preparation of draft environmental-impact statements by the appropriate agency. These draft statements are reviewed and commented upon by interested agencies, and these comments are then incorporated into a final environmental-impact statement on the proposed project. This statement becomes part of the total package of information available as a basis for necessary decisions. The statement is made available to the public through the National Technical Information Service (NTIS).

Because of the rather diverse audience, the environmental-impact statement must satisfy two very distinct, often difficult to reconcile, goals. First, it must provide sufficient technical background and strong enough use of available theories and techniques to satisfy rigorous review by knowledgeable government personnel. Secondly, it must couch the report in such language that the public can understand the findings and make its own assessments. Numerous models have been suggested for the means of reaching the public. Some have suggested making the statement understandable to the high-school science teacher; others have suggested more or less sophisticated receivers than this.

Even if one resolves the problem of communication, there are many problems in the technical area. With the growth in experimental findings, design alternatives, and theoretical models, those charged with evaluating projects face a real task in reducing the available information to a usable set of operational techniques.

The specific concern of this report is the analysis of the discharge of heated waters, presumably from power-generating stations, but possibly from other sources. Evaluation of the impact must, of course, bear on the biological consequences of any given discharge. This report, however, limits itself directly to the problem of the physical description of the temperature distributions resulting from heated-water discharges. To this end, selected currently available models will be presented in brief form, with discussion designed to enable evaluation of appropriate models for given uses. In addition, means will be provided to extend the present uses of models to include estimates for time of exposure of organisms to a given temperature, information of real concern to biologists evaluating thermal effects. Much emphasis will be placed on imparting physical insight to problems and providing needed background for this purpose. It is hoped that such information will not only serve the technical worker trying to use present techniques, but will also help communicate effectively with the public.

This report then is designed to aid in both the implementation of the technical assessments and the writing for public consumption demanded by environmental-impact statements as required by NEPA. One should recognize, however, that many people in and out of the government are charged with, or interested in, assessment of potential environmental problems. It is therefore expected that this report could be quite helpful to an entire array of other such people.

II. INTRODUCTION TO HEATED DISCHARGES

The discussion of heated discharges can begin in many ways. Numerous characterization or classification schemes exist. There are, however, some definitions and physical parameters so basic they must be introduced before any detailed studies begin. It seems well at this point to place the heated-discharge problem in a framework that would set the tone for the rest of this report.

A. Possible Broad-classification Schemes

1. Use of the Word "Model"

One word that is frequently confusing, even among trained people in the field, is the word "model." As used in this report, it denotes a theoretical formulation designed to describe a physical process. This may mean one equation or several equations, all based on conceptions of what happens in the given physical phenomenon.

Some authors use the word "model" to denote a small-scale version of the problem built and operated according to certain laws designed to make the physical model behave like the prototype. In this report, the term "physical model" will be applied to these small-scale physical structures. Hence, one might speak of a physical model of a given heated discharge on, e.g., the Chesapeake Bay.

2. Near Field, Far Field, Broad Thermal Trends

One common means of classifying *regions* affected by heated discharges or the *models* to describe them, is by the distinction between near and far fields. The near field can be defined as the region in which the effects of the conditions at the point of discharge--for example, orifice size and shape, effluent velocity, and temperature rise--still influence the temperature distribution in the receiving water. Most, if not all, temperature standards are presently stringent enough that they must be met within the near field. Eventually, the water in a heated discharge reaches a point at which it is no longer influenced by the conditions at the point of discharge. At this point, it becomes completely subject to the motion of the ambient fluid and any dispersion or diffusion resulting from this ambient motion. The region totally subject to ambient conditions is then known as the far field. There is a transition zone between the near and far fields, and there is no universally accepted criterion for defining the exact limits of either field.

The terms near and far field are frequently applied to theoretical models for describing temperature distributions in the receiving waters. Any model for the near field must encompass the full characteristics of the jet discharge, as well as the dynamics of the interaction between the heated effluent and the ambient fluid. A far-field model, however, needs only describe the motion of the ambient currents, while also satisfying the basic requirements of conservation of mass and heat.

The present state of knowledge is such that no one model approach handles both near- and far-field cases, though some are used that link different

approaches for the two regions. To determine whether required temperature standards are met, usually only a near-field model is needed. However, those charged with going beyond standards to assess impact may well wish to evaluate far-field effects also. In summary, the terms near and far field arise not only as physically descriptive terms, but also because of the limits of current modeling knowledge.

Anyone interested in studying the impact of a heated discharge may have to define the effect of a local discharge (or series of such discharges) on the overall thermal (and density stratification) trends in the receiving-water body. This concern is basic to the design of cooling ponds, for example. However, in lakes and impounded rivers, the effect on broad thermal trends also bears investigation. For example, if a more intense stratification existed in a reservoir due to a power-plant discharge, dissolved-oxygen levels might be reduced below a desirable level. The mathematical modeling of these broad thermal trends is discussed in Sec. VIII J. Further details of such efforts appear in Refs. 75, 99, and 100. The important thing to see here is the progression away from the local point of heated discharge through near and far fields and on to a broad thermal effect.

3. River, Lake, Estuary

One means of classifying heated discharges is by the type of receiving body into which they are discharged. The classes "river", "lake", and "estuary" frequently occur. Numerous differences can be cited, but the following features are those most usually distinctive of each. Rivers are bodies of water in which the far bank plays a real role in the action of the heated discharge. That is, the far bank inhibits the motion of the discharge and reduces its mixing. A lake has no far-boundary influence. An estuary is usually subjected to distinctly unsteady (periodic) flows. There are other differences and many points of similarity.

If appropriate assumptions are made, many techniques currently available are applicable in all three cases. Emphasis in this report will then be placed on the available methods, with discussion as to the usefulness of these methods in the various circumstances.

4. Type of Discharge or Model

Another classification scheme is based on the type of discharge or model thereof. Major categories would usually include:

- Submerged discharges
- Surface discharges
  - Downstream
  - Upstream wedges
- Cooling ponds
- Deep reservoirs (broad thermal structure).

The current report is following this scheme with added subcategories. This breakdown has numerous advantages to the user. For example, the present models available for handling submerged discharges do not differ among river, lake, and estuary. It is much easier to present (and read), in one place, the

material on submerged jets with discussion on slight differences of interpretation or application at different sites. This report catalogs the available techniques by groups that are as physically recognizable as any other. It, in addition, seems to enable a more coherent presentation of the present state of knowledge. Therefore, while this scheme is adopted, the earlier classifications will be used as subsets to try to provide adequate coverage.

B. Basic Parameters in Heated-discharge Problem

Consider now a very general heated-discharge situation, as shown in Fig. 2.1. Although this is shown as a multiport diffuser, increase of the port spacing, W, to infinity (or a decrease to zero) would yield the case of a single port. In addition, reduction of the vertical submergence, Z_1, to zero would yield a surface discharge. By appropriate choice of angle, β_1', and reducing x_1 to zero, the discharge becomes one located on the shoreline. Therefore, with some imagination, Fig. 2.1 can be extended to cover almost all cases of concern in power-plant discharges.

A general dimensionless, functional relationship could be developed for the temperature at any point in the receiving-water body for this case:

$$\frac{T - T_w}{T_o - T_w} = fn\left(\frac{x}{D_o}, \frac{y}{D_o}, \frac{z}{D_o}, \frac{\Delta\rho}{\rho_0}, C_s, \Theta_0', \beta_0', k, \frac{z_1}{H}, \frac{z_2}{H}, \frac{x_1}{D_o}, \frac{D_o}{H}, \frac{W}{D_o}, Re_a, Re_j, F_a, F_j, K, C_w, \Theta_1, C_u, C_{ds}, S_b\right), \tag{2.1}$$

where T = temperature at point of interest,

T_o = initial discharge temperature,

T_w = ambient water temperature,

x,y,z = standard Cartesian coordinates, oriented so that the ambient velocity, U_a', is located along the x-axis,

D_o = diameter of discharge port,

B_o = width of rectangular, or slot, discharge port (note that D_o in Eq. 2.1 can be replaced by B_o for a rectangular orifice),

$\Delta\rho$ = density difference between receiving fluid and discharge fluid,

ρ_0 = ambient density at point of interest,

C_s = dimensionless shape factor, indicating influence of orifice shape on discharge action,

Θ_0' = initial angle of discharge with respect to xy plane,

β_0' = initial angle of discharge with respect to xz plane,

k = velocity ratio = U_o/U_a,

U_o = initial jet velocity,

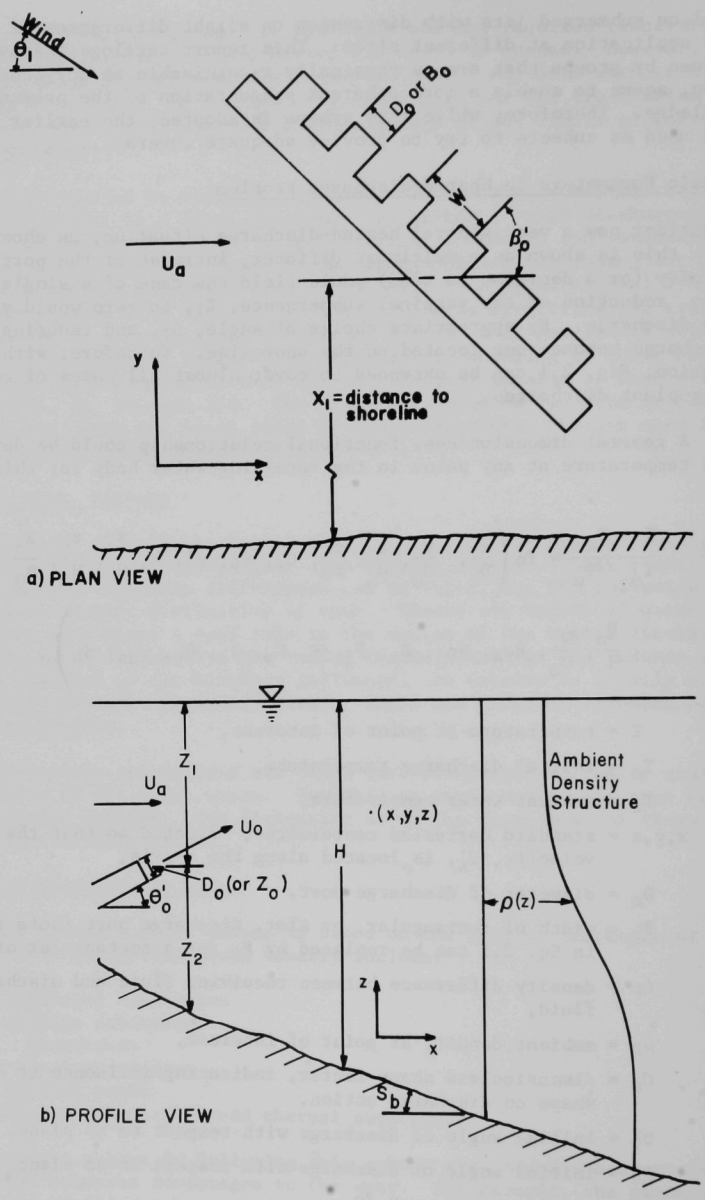

Fig. 2.1. General Heated Discharge.

U_a = ambient velocity at point of interest (may vary over receiving body),

z_1 = submergence of orifice (distance below water surface),

z_2 = distance orifice is located above bottom boundary of receiving body,

x_1 = representative distance of discharge point of interest from nearest shoreline,

H = total depth of receiving-water body at point of discharge,

W = spacing between discharge ports ($W \to \infty$ implies a single port),

Re_a = Reynolds number of ambient flow = $U_a H/\nu$ (or some other representative length may be used instead of H),

Re_j = Reynolds number of initial discharge or jet = $U_o D_o/\nu$ or $U_o B_o/\nu$,

ν = kinematic viscosity of the fluid,

F_a = densimetric Froude number of the ambient flow = $U_a/\sqrt{g \frac{\Delta\rho}{\rho_0} H}$,

g = acceleration due to gravity,

F_j = densimetric Froude number of discharge = $U_o/\sqrt{g \frac{\Delta\rho}{\rho_0} D_o}$ (D_o replaced by z_o for rectangular orifice),

z_o = depth of rectangular (slot or open channel) orifice,

K = surface-cooling coefficient (see Chapter III on the heat balance),

C_w = wind-stress coefficient,

Θ_1 = angle of wind direction to ambient current,

C_u = coefficient indicating unsteadiness of the flow,

C_{ds} = coefficient indicating density structure of the receiving waters, and

S_b = slope of bottom boundary of receiving waters.

Other elements could probably have been included. However, those presently considered in any available models are encompassed by the parameters in Eq. 2.1. Note that several "coefficients" have been introduced--C_s, C_u, and C_{ds}--which may not be quantifiable. The intent is to indicate important influences in the problem. A better insight into the heated-discharge problem can be gained by reviewing the parameters shown in Eq. 2.1.

1. Effect of Location: x/D_o, y/D_o, z/D_o

Clearly, the location of a point with respect to the discharge location is important, and no elaboration is needed here. The location of a point in either the far or near field may determine the techniques used to predict temperatures at that point.

2. Turbulence Levels: Re_a and Re_j

The two Reynolds numbers have been introduced to emphasize the importance of ambient turbulence (Re_j). In natural systems, the flow is expected to be fully turbulent, and hence the effect of differences in Reynolds numbers is negligible. However, it is particularly important to observe the Reynolds number when laboratory results are being used to verify theoretical models. If the laboratory model is not functioning in the fully turbulent range, results may not be useful for application to field situations. It is commonly assumed that values of the Reynolds number above 3000 for both jet[4,101] and ambient flows are necessary. Although this is the accepted figure (often due to laboratory and facility constraints), it is still preferable to attain higher Reynolds numbers in the laboratory to ensure good similarity to field conditions.

3. Buoyancy Considerations: $\Delta\rho/\rho_0$, F_a, F_j

A major factor in the motion of a heated discharge is the buoyancy force created by density differences between the ambient water and the heated effluent. The term $\Delta\rho/\rho_0$ appears in both densimetric Froude numbers, F_a and F_j. However, it is important to include the density-difference term separately so it can be noted that $\Delta\rho$ can be either positive or negative. The typical heated discharge is warmer, and hence lighter, than the receiving water. In this case, $\Delta\rho/\rho_0$ is positive. However, a power plant can draw cold water from the bottom of a lake, heat it, and return it to the lake surface still colder and heavier than the surrounding ambient surface waters. In this case, $\Delta\rho/\rho_0$ is negative, and the discharge is called a negatively buoyant jet or a sinking jet. If this situation exists, the problem of meeting temperature-rise standards does not exist. There may still be other impacts to be investigated, such as introduction of materials into the hypolimnion and possible impact on the benthos.

At present, no method exists to predict the behavior of a negatively buoyant, surface discharge. For this reason and because temperature standards (in present forms) are not threatened by this type of discharge, no further discussion will be offered on negatively buoyant jets.

a. Upstream and Downstream Motion: F_a. The ambient densimetric Froude number, F_a, can be interpreted in much the same way as the standard Froude number, F ($= U_a/\sqrt{gH}$), for open channels. The latter number indicates the ability of a surface disturbance to move upstream. If F is greater than one, the flow is supercritical, and no wave will move upstream against the flow. If F is less than one, a wave will move upstream as well as downstream. In a similar fashion, a value of F_a greater than one (theoretically) will ensure that no buoyancy-induced movement of the heat upstream will occur; if F_a is less than one (theoretically), heat can and will move upstream. In practice,[24,47,61] the critical number for F_a is more like 0.75, instead of 1.0.

The essence of the present topic can be seen by considering a surface discharge moving very slowly (essentially no initial momentum) onto the surface of a completely stagnant receiving body. The heated plume would be expected to spread by buoyancy-induced motion equally in the positive and negative x directions as it attempted to "ride" over the surface of the heavier receiving water. As an ambient current is added, however, the upstream buoyant velocities are counteracted by mainstream ambient velocities, resulting in a shorter upstream protrusion of the heated water. This upstream portion of the heated

plume is called a wedge. Specifics of the wedge are detailed in Chapter IV. As the ambient velocity, U_a, is increased, the wedge length is eventually reduced to zero.

A numerical example with typical river values will help in visualizing the importance of F_a. Consider a power plant discharging water from a surface canal at 90°F into a body of water whose temperature is 65°F. Assume that

z_o = discharge-canal depth = 5 ft,

B_o = discharge-canal width = 40 ft,

Q_p = heated-water discharge = 730 cfs,

H = receiving stream depth = 30 ft, and

U_a = ambient velocity = 1.0 ft/sec.

Then

ρ_a = ambient water density = 0.99856 g/cm^3,

ρ_1 = initial discharge water density = 0.99498 g/cm^3, and

$\Delta\rho$ = initial density difference = 0.00358 g/cm^3.

The equation for F_a includes a term $\Delta\rho/\rho$. Here the choice of ρ is not too critical (ρ_1, ρ_a, or an average), as the percentage difference is slight. It is convenient to use ρ_a here. Then

$$\Delta\rho/\rho = 0.00358/0.99856 = 0.00359 .$$

Finally,

$$F_a = 1.0/\sqrt{32.3(0.00359)(30)} = 0.54 .$$

This implies that some upstream movement is expected. If the ambient velocity were increased to 2.0 ft/sec, F_a would equal 1.08, and no upstream movement of heat would be indicated. It is pointed out in Chapter IV that plants for whom the predicted wedge is too long probably have exceeded any conceivable temperature standards.

b. Degree of Vertical Mixing: F_j. The other commonly used densimetric Froude number is F_j, which is a measure of the relative importance of inertial forces (numerator) and buoyancy forces (denominator). For this reason, it is an important indicator of the effect of the density gradient between the ambient water and the heated effluent. A very high value of F_j indicates that buoyant forces are small compared with inertial forces. Hence, it may be possible to treat the discharge by simpler models for nonbuoyant discharges. If, however, buoyant forces are large enough to inhibit vertical mixing, then F_j will have a much lower value. Work by several people[37,64] has shown that vertical mixing is negligible for F_j less than 1.0. Figure 2.2 shows density profiles in so-called two-layer flow. If there is a sharp density gradient, any lighter

particle trying to move from the upper to the lower "layer" will be forced back up by buoyancy. Similarly, any particle trying to go from the lower to the upper "layer" will be forced back down, since it is heavier. As the velocities increase (and F_j increases), the energies imparted to particles become greater, enabling them more and more frequently to overcome the buoyant forces and to mix from one layer to the other.

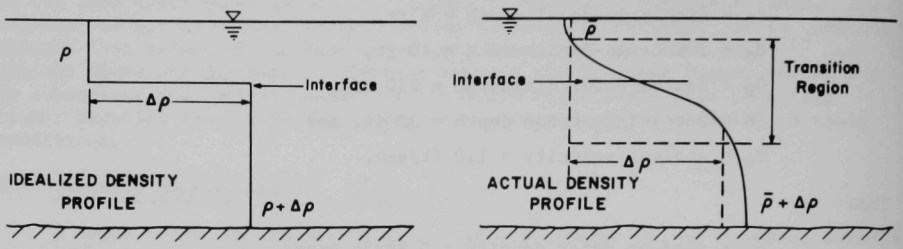

Fig. 2.2. Density Profiles in Two-layer Flow.

An example calculation for F_j using typical values might help give more physical perspective to this discussion. Consider the same basic case used in Sec. a above. A power plant discharges water from a surface canal at 90°F into a body of water whose temperature is 65°F. Assume that (as before)

z_o = discharge-canal depth = 5 ft,

B_o = discharge-canal width = 40 ft, and

Q_p = heated-water discharge = 730 cfs.

Also,

U_o = initial jet velocity = 730/[40(5)] = 3.65 ft/sec, and

$\Delta\rho/\rho$ = 0.00358/0.99856 = 0.00359.

Finally,

$$F_j = 3.65/\sqrt{32.2(0.00359)(5)} = 4.8.$$

Therefore, for this case, initial mixing would be slightly three-dimensional (some vertical mixing). If the discharge canal had been 200 ft wide (B_o), for the same discharge, U_o would equal 0.73 ft/sec and F_j would be 0.96, implying very little vertical mixing initially. Actually, in the latter case, F_j would become 1.0. (See Chapter IV for details.) Hence, one can design his discharge structure to achieve much or little initial vertical mixing.

It can be seen then that F_j is a measure of whether the jet experiences mixing in the vertical direction. The terms "two-dimensional" and "three-dimensional" are frequently applied to those cases without and with vertical mixing. Thus, a two-dimensional model is one for which F_j is assumed sufficiently close to 1.0 to ignore vertical mixing. Typically, such a model would be expected to be conservative, inasmuch as it omits one mode of mixing, if in fact vertical mixing is important.

particle trying to move from the upper to the lower "layer" will be forced back up by buoyancy. Similarly, any particle trying to go from the lower to the upper "layer" will be forced back down, since it is heavier. As the velocities increase (and F_j increases), the energies imparted to particles become greater, enabling them more and more frequently to overcome the buoyant forces and to mix from one layer to the other.

An example calculation for F_j using typical values might help give more physical perspective to this discussion. Consider the same basic case used in Sec. a above. A power plant discharges water from a surface canal at 90°F into a body of water whose temperature is 65°F. Assume that (as before)

z_o = discharge-canal depth = 5 ft,

B_o = discharge-canal width = 40 ft, and

Q_p = heated-water discharge = 730 cfs.

Also,

U_o = initial jet velocity = 730/[40(5)] = 3.65 ft/sec, and

$\Delta\rho/\rho$ = 0.00358/0.99856 = 0.00359.

Finally,

$$F_j = 3.65/\sqrt{32.2(0.00359)(5)} = 4.8.$$

Therefore, for this case, initial mixing would be slightly three-dimensional (some vertical mixing). If the discharge canal had been 200 ft wide (B_o), for the same discharge, U_o would equal 0.73 ft/sec and F_j would be 0.96, implying very little vertical mixing initially. Actually, in the latter case, F_j would become 1.0. (See Chapter IV for details.) Hence, one can design his discharge structure to achieve much or little initial vertical mixing.

It can be seen then that F_j is a measure of whether the jet experiences mixing in the vertical direction. The terms "two-dimensional" and "three-dimensional" are frequently applied to those cases without and with vertical mixing. Thus, a two-dimensional model is one for which F_j is assumed sufficiently close to 1.0 to ignore vertical mixing. Typically, such a model would be expected to be conservative, inasmuch as it omits one mode of mixing, if in fact vertical mixing is important.

4. Receiving-water Density Structure: C_{ds}

The density structure of the receiving-water body can be very significant. The receiving body may range from a completely homogeneous density to a highly stratified receiving body. The homogeneous body of water would be characterized either by a very shallow depth, usually less than 30 ft, and/or a very high flow-through. Flow-through implies volume rate of flow into and out of the water

body of concern. If the body of water is shallow, wind mixing alone would suffice to continually mix the water and retain a uniform density throughout. For a high flow-through, mixing would also be sufficient to retain a uniform density. The latter is exhibited, for example, in many rivers.

If the water body is not shallow and/or the flow-through is not high compared to the volume of the water body, then a stratified condition may be obtained in the ambient water body. This situation frequently occurs in lakes, impounded rivers, and reservoirs. Perhaps one way to see what occurs in the density structure of a lake, for example, would be to briefly discuss the changes occurring in that lake throughout a normal year. For more discussion on this topic, see Ref. 100, from which the following is abstracted.

At the end of a winter season, the lake is usually isothermal, that is, of constant temperature from top to bottom, and at a relatively low temperature. As atmospheric temperatures begin to rise when the spring season begins, the addition of heat energy across the air-water interface becomes greater than the loss of energy across that interface. As a result, the surface layers of the lake begin to heat up and become lighter than the underlying colder waters.

Figure 2.3 is an example of the temperature structure and strata in a typical lake. The upper layers, of more nearly uniform temperatures due to continued wind mixing, are referred to as the epilimnion. The lower, denser regions of the lake, again of more nearly uniform temperature, are referred to as the hypolimnion. The transition between these two layers, or the region of more intense thermal gradients, is called the metalimnion, or the clinolimnion. The position of most intense thermal gradient is frequently called the thermocline. As indicated in Fig. 2.3, some authors refer to the entire region of sharp temperature change as the thermocline. As the lake moves into the summer months, the temperature differential between the surface and bottom layers increases and the intensity of stratification increases also. As the summer progresses, the thermocline moves deeper into the reservoir. In the southeastern United States, the thermocline exists from about April to November. In a deep reservoir, the thermocline may be 30-50 ft below the water surface.

As the fall season approaches and atmospheric temperatures begin to drop, more heat energy is lost across the air-water interface than is gained. The surface layers then begin to cool, eventually becoming heavier than those layers beneath them. This precipitates "overturn", the process by which the lake is mixed to again approach isothermal conditions. From this point on, the lake continues to lose heat uniformly throughout the winter. Where the climate is such that the water temperature goes below 4°C, the point of maximum density of water, two overturns may occur each year. In this case, the lake is known as a dimictic lake. When one overturn occurs, limnologists classify the lake as monomictic.

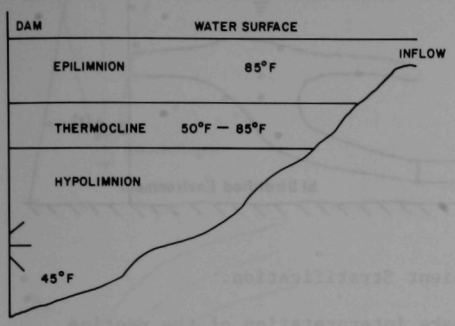

Fig. 2.3.

Typical Stratified Reservoir Profile.[100]

Not only is this density structure in the lake of importance to the motion of a heated discharge, it is also important in terms of water-quality problems within the lake. Just as a heated discharge on the surface might be expected not to mix down into the lower layers of the lake, oxygen transferred from the atmosphere would not be expected to reach the lower regions of the lake. Hence, dissolved oxygen levels in the bottoms of many deep impoundments or lakes frequently approach zero in the summer months.

Three different forms of motion of an effluent may occur, depending upon the relation of the effluent density to the receiving-water density. The problem of frequent concern in thermal pollution is the case of an overflow. This would be typified by a hotter water discharge, which remained on the surface of the lake. It could also be represented by a submerged discharge, which, by virtue of being lighter than the receiving water, rose to the surface and remained there. A second extreme case occurs if the effluent is heavier than the receiving water. It may then plunge to the bottom and flow along the bottom of the lake. Such flows are called "underflows." This is frequently true for discharges containing sediments or salts such as might occur from desalting plants, dredging operations, or the inflow of a stream heavily laden with sediment. As noted earlier, a discharge from a power plant could, in fact, still be a negatively buoyant discharge. This discharge could fall into the intermediate category, that is, an interflow. Water discharged into a receiving body tends to seek its own density level. It may overshoot that level because of momentum. Figure 2.4 illustrates this case for a submerged jet. When the jet is discharged into a uniform ambient environment and is warmer than the receiving body, it tends to rise completely to the surface. If it is discharged, however, into a body of water with a vertical density gradient, it may take the form shown in Fig. 2.4b. The plume spreads out into a horizontal layer below the surface. Also, there is frequently a slight hump above the point where the plume begins to spread out into the horizontal direction. The "hump" is the result of the plume tending to overshoot its point of neutral density due to momentum. Since lighter fluid exists above this horizontal layer that is formed, a heavier fluid exists below it. A relatively stable layer may be formed in which little vertical mixing occurs.

In a discussion of ambient density structure, one must not neglect horizontal variations in ambient temperature. Pritchard[110] presents an example of data taken on Lake Michigan by Beer and Pipes,[14] where the temperature varied in the ambient receiving water from 48°F at the shoreline to 43°F

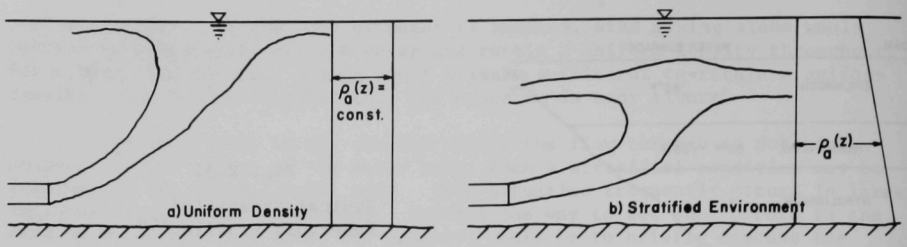

Fig. 2.4. Effect of Ambient Stratification.

6000 ft offshore. This variation would make interpretation of the meeting of existing or proposed temperature standards very difficult. As noted in Sec. V.A.11, it also makes more difficult the application of existing models for prediction of the action of heated discharges.

The density structure of the receiving water body is an important parameter. Many useful results can be obtained from considering the ambient fluid as having uniform density. However, it will frequently be necessary to consider at least vertical stratification, and in some instances, horizontal temperature variations within the receiving body. These topics will be defined in depth in the appropriate ensuing chapters, particularly Chapters VI and VII.

5. Initial Discharge Conditions: C_s, Θ_0', β_0', k

The initial angle of the discharge with respect to the ambient velocity as expressed by the angles Θ_0' and β_0' clearly influences the direction and final location of the heated discharge plume. The velocity ratio, k (defined as the initial jet velocity, U_o, divided by the ambient velocity, U_a), is an important parameter in determining the trajectory of the heated discharge. Consider a discharge directed along the y axis. For k approaching infinity (no ambient current), the discharge would essentially continue to have its axis on the y axis. As the ambient current was increased and therefore k decreased, the plume would be deflected more and more downstream. Eventually, as k approached 1 or less, the plume would essentially be swept immediately along the x axis, after a very short initial transition region. This process is familiar to anyone who has watched the smoke exiting from a smokestack. For no wind, the plume goes straight up; as the wind speed increases, the smoke plume bends over more and more. Figure 2.5 illustrates this effect. Therefore, it can be seen that for values of k greater than 1, any predictive model should consider the value of k and hence its effect on the location of the heated plume. Such predictive models, as will be detailed again in Sec. V.A.2 are usually called jet models. For lower values of k such that the plume is immediately swept downstream, the value of k itself might be less important and a model neglecting the influence of the velocity ratio on trajectory of the discharge might be satisfactory. These models are frequently called diffusion models. Both types of models are discussed in Chapter V. The effect of the initial velocity ratio, k, will be evident both in that chapter and in Chapter VI.

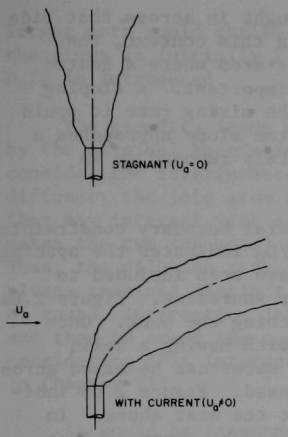

Fig. 2.5.

Effect of Ambient Current.

A further characteristic of the initial discharge, which is of importance, is the shape of the discharge or orifice. This may range from a rectangular or trapezoidal open channel, which discharges at the surface, to a round or slot port or some other shape discharge port beneath the surface. The techniques for dealing with, for example, the slot and the round jet are not too different. Yevjevich[146] has indicated that the velocity profiles of both a round and a slot jet approach a circular or elliptical shape at some distance downstream, this distance being slightly greater the larger the discrepancy in the two dimensions of the slot. In addition, there would not be much difference in the action of a single slot jet and a number of round jets placed immediately next to each other with no spacing in between, if the size were chosen to correspond with that of the slot jet. Shape is an important factor in the very early regions of a discharge. For this reason, Chapters V and VI provide information to handle at least the most basic cases, which are circular and rectangular ports for the submerged case and the rectangular discharge for the surface condition.

6. Geometry Effects: z_1/H, z_2/H, x_1/D_0, D_0/H, S_b, W/D_o

The confining geometry of the receiving-water body can play a significant role if it interacts with the jet. In addition, if there is more than one discharge port, the discharges may interact with one another. This could be extended to the case of the discharge plumes from two or more power plants interacting with one another under certain conditions. Two parameters, z_1/H and z_2/H, give some measure of the location of the discharge with respect to the free surface and the bottom boundary of the receiving body. This can be seen in Fig. 2.1b. The location of a submerged discharge with respect to the surface may be controlling in how much dilution or mixing is obtained before the discharge reaches the surface. Very near the surface, for example, it has little time and little water with which to mix before it reaches the surface and spreads out as a horizontal layer, where the mixing rate may be considerably decreased. If the discharge is very near the bottom and is swept along near the bottom, for example, by a high ambient velocity or by having an initial angle that directs the jet near the bottom, mixing of fluid into the heated discharge may again be inhibited simply because there is a solid boundary on

one side of the discharge. Hence, no water can be brought in across that side and the rate of dilution is considerably decreased. In this context, the bottom slope, S_b, of the receiving body of water in the area where a heated discharge plume might make contact with the bottom is important. A sloping surface may enable the plume to more nearly approach the mixing rate it would obtain if there were no bottom boundaries. If the bottom slope approaches a high enough value, eventually the bottom may be completely removed as an influence.

Figure 2.6 illustrates the possible impact of lateral boundary constraints on the motion of a heated discharge. The parameter x_1/D_o indicates the spacing to the near shoreline. A corrollary parameter could have been included to indicate the spacing from the discharge port to the far shoreline. Figure 2.6a illustrates a plume extending across the river and reaching the bank. Once the plume has reached the far bank, it again is faced with having a solid boundary in contact with one portion of the plume. No water can be mixed across this solid boundary, hence, the dilution rate is decreased. Figure 2.6b indicates a heated plume being swept immediately up against the near shore. In like fashion, the dilution rate is reduced. The plume may be swept against the shore by the high value of ambient velocity relative to the jet discharge velocity (implying a low k). It could also be pushed against the shore by a shoreward ambient current generated by the wind. Due to reduced mixing caused by such conditions, plumes have been known to persist for several miles downstream from a power-plant site.

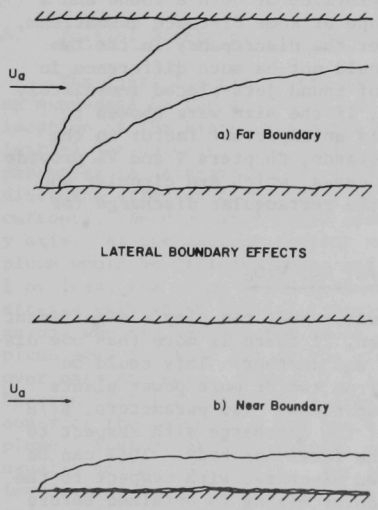

Fig. 2.6.

Lateral Boundary Effects.

The size of the orifice relative to the total receiving depth and distances to the free surface and/or bottom is also important. For example, the discharge from a 5-ft-dia port 10 ft from the bottom would be affected more immediately by this boundary than would the discharge from a 2-in. port also located 10 ft from the bottom, all other conditions being equal. Assuming, for simplicity, the same linear rate of spreading for each plume, the edge of the plume from the

larger port would strike the bottom first. This is because the lower edge of the plume is initially 2 ft 5 in. closer to the bottom. Hence, the parameter D_o/H is introduced.

The geometry items discussed to this point have concerned interference by the physical boundaries of the ambient water body. It is important to consider the interference between two heated discharges. In a multiport diffuser, the jets grow as they mix with ambient water. As they spread, they may interact with one another if initial spacing was small enough. This makes the two (or more) discharge plumes compete for the same dilution water. Thus, the dilution rate is decreased over that which would be obtained if all plumes remained distinct and did not interact. One common approach for a set of round, interacting jets is to treat them as single jets until they interfere, and then to treat the combined system as a single slot jet.[73] Details of considering this interaction are thus important and are discussed in depth in Chapter VII.

It would be inappropriate to dismiss the subject of geometry effects without noting that many of the parameters cited are not well handled (if at all) by current theoretical models. This becomes evident in later chapters, but free-surface (Z_1/H) and lateral (X_1/D_o) constraints especially are not well established. There is, in addition, not yet good field evidence to verify most of the attempts at including bottom slope or jet interference. Hence, inclusion of geometry effects in predictions of thermal-plume action still remains as much an art as a science in some areas.

7. Wind Effects: C_w, Θ_1

The effects of wind on the temperature distribution resulting from a heated discharge may be many and varied. Wind, for example, is an important factor in the heat exchange occurring across the air-water interface. Here, however, the concern is the effect of wind on plume location. References 99, 100, 104, and 147 discuss this. The coefficient C_w is used in

$$\tau_w = \rho_A \, C_w \, U_w^2, \tag{2.2}$$

where τ_w = stress on water surface due to wind,

ρ_A = mass density of air,

C_w = wind-stress coefficient, and

U_w = wind speed.

The angle Θ_1, with respect to the direction of the ambient velocity, is included to indicate the component that might be included in the x- or y-direction momentum equations, as suggested by Zeller.[147]

There is some disagreement over whether the wind-stress term should be included in the standard equations used for surface discharges. Policastro and Tokar[104] provide the essential background quite well. If the ambient velocity U_a (both magnitude and direction) is adequately defined, then it seems inappropriate to include the wind shear as an added term in the basic momentum equation. This is true because the momentum input due to the wind

shear has already been accounted for by defining the U_a resulting from that force. Including the wind shear again would really mean that the wind effect had been included twice. For this reason, current models are discussed in the light of adequately assessing the ambient velocity and neglecting any additional considerations of the wind.

Data have been obtained from numerous sources for the effect of the wind in inducing a current.[68,102] For making a rough assessment of the velocities generated solely due to wind (which may then have to be superimposed on some gravity-generated currents), we can assume that the surface-water velocity is approximately 1/30 of the average wind speed near the surface of the water. Wind effects probably are not directly felt more than about 30 ft below the water surface. Hence, one should first assume some expected critical wind condition (often toward shore) lasting several hours (long enough to cause the plume to shift its location and currents to fully develop). Then, velocity and direction can be estimated for U_a and this ambient current included in the appropriate predictive model.

Although not mentioned separately, the effect of waves generated by wind stresses (as well as by other sources) is a factor that may well be important. This is especially so for predictions in the ocean environment. Mixing may be enhanced by these waves, although no present model adequately accounts for these wave effects.

With these suggestions, and the realization that present knowledge does not allow a more adequate handling of wind, further discussion on wind in Chapter V will be minimal.

8. Surface Heat Exchange: K

As the heated discharge is mixing with ambient fluid, it is also exchanging heat with the atmosphere across the air-water interface.

The cooling coefficient K may take several forms. The most common can be expressed by

$$\text{Heat lost to atmosphere} = K(\text{Surface area})\ (T - T_{EQ})\ , \qquad (2.3)$$

where K = heat-exchange coefficient,

T = water temperature, and

T_{EQ} = equilibrium temperature.

The equilibrium temperature is the temperature the water surface would approach if atmospheric conditions remained constant indefinitely. Ways to calculate this temperature appear in Chapter III. It can be demonstrated (and is, in Chapter V) that this surface cooling plays an insignificant role in the near-field region. In this zone, dilution and physical-mixing processes play the major role in decreasing the temperature. Even though temperature differentials are large near the discharge, the surface areas available for exchange are too small to allow any significant heat loss. However, by the time plume-temperature rises (temperature rise = plume

temperature minus ambient temperature) are down to 1 or 2°F, areas have been large enough to enable important amounts of cooling. For this reason, calculations of temperatures in the far-field region must include surface cooling or they will yield a vastly inflated estimate of the area influenced by the plume.

9. Degree of Unsteadiness: C_u

C_u, again, is a fictitious coefficient introduced to illustrate the possible existence of unsteady flows and their impact on heated-discharge distributions. This is of special concern in estuaries and on the open coast, although it may also be of interest in rivers or impoundments where unsteady flows exist. A general review of the status of estuarine modeling is given by Ward and Espey.[140] There is a true lack of knowledge on the effects of unsteadiness on mixing, and hence on temperatures in the near-field region. Most assessments simply take the slack-tide condition and treat it as a steady-flow input to one of the models. This is likely a too conservative approach, although it can give reasonable first results.

Models do exist for attempting to handle the far-field problem. Lee and Harleman[79] and others have developed finite-difference solutions to the one-dimensional dispersion equation in estuaries. This equation, with surface cooling included, can estimate how long it takes a parcel of heated water to be flushed out of the estuary system, or at least how long it takes for dissipation of the excess heat to the atmosphere. In addition, some two-dimensional (shallow) estuaries have been treated by finite-difference procedures.[140] These techniques are referred to in Chapter V.

One should mention the tool that has been heavily relied upon for predictions where unsteady flows exist, especially when coupled with unusual geometry. The use of physical models has been extensive in thermal work. A review by Silberman and Stefan,[125] done for Argonne National Laboratory, assesses the state of the art in this area. Parker and Krenkel[99,100] and Acker[4] also present useful information on this topic. Recently, helpful information has begun to appear on model repeatibility and model-prototype correlations. The accuracy of physical models can only be fully evaluated by comparison with good field data.

In short, unsteadiness is a problem that has not yet been well handled, especially in the near field. Predictive ability in highly unsteady systems is frankly an unknown quantity with low reliability attached to many of the assumptions made. First-cut approaches do exist, however, and these are presented in the appropriate chapters.

10. Physical Modeling

Due to limitations of time and space, physical modeling is not discussed in depth in this report. It is, however, an important tool, and those reviewing power plants are often confronted with results obtained from such physical scale models. A rather thorough review has been prepared by Silberman and Stefan.[124] Since it is completely directed to the study of heat motion by physical models, it is the most extensive such work available. The work by Parker and Krenkel[100] also reviews much of the basic literature. Ackers[4] presents a concise summary of requirements for such models and shares some of the rather broad experience gained in Great Britain.

As with any tool, there are pitfalls. Harleman[49] discusses the use of physical models for estuaries, with interesting comments on present inadequacies in use of models for general water-quality problems. One should not retreat to physical models too hastily; they are expensive, and verification is difficult. This is especially true where no prototype discharge yet exists. In fact, a major need in physical modeling of thermal discharges is the collection of adequate prototpye data to check the results obtained from physical models. Data of this sort are available, such as that presented by Hindley *et al.*[53] Much more is needed.

The reader who must review results from physical models is encouraged to go to the suggested sources for information. In this report, comments will be made where the state of analytical modeling seems to dictate a need for at least considering physical models.

C. Comments

This chapter sets a framework and makes a general introudction to the problem of heated discharges. It has purposely been kept low-key. The remaining chapters attack the problems of available predictive techniques, with discussion, analysis, and appropriate examples. For added general background, see the references mentioned.

III. HEAT-BUDGET EQUATION

A. Introduction

The heat-budget equation is best defined as a complete summation of the rate of heat into, rate of heat out of, and rate of change of heat storage of an isolated body. Such an equation will allow one not only to predict the present heat content of a body but also to describe the response of this body if certain components in the equation change. Of concern to the reader in the following chapters is the form the heat-budget equation takes for such bodies as cooling ponds, rivers, lakes, etc.

The following equation is a complete heat-budget equation (often called the energy-budget equation) for such bodies of water. The components of the heat budget per unit surface area per unit time are written as[145]

$$Q_s - Q_{sr} + Q_a - Q_{ar} - Q_{br} - Q_e - Q_h + Q_v = Q \ , \tag{3.1}$$

where Q_s = short-wave radiation incident to the water surface,

Q_{sr} = reflected short-wave radiation,

Q_a = incoming long-wave radiation from the atmosphere,

Q_{ar} = reflected long-wave radiation,

Q_{br} = back radiation emitted by the body of water,

Q_e = energy used by evaporation,

Q_h = energy conducted from the body of water,

Q_v = net energy brought into the body of water in inflow, including precipitation and accounting for outflow, and

Q = increase in energy stored in the body of water.

Most of these components, however, cannot be measured, or the measured information needed is not available. Methods to estimate the components are discussed in the following sections.

The main objective in this chapter is to show how the heat-budget equation is applied to bodies of water. This application serves as the basis for surface-cooling calculations in the following chapters. The general format of this chapter is first to discuss the various methods used to calculate the value of the individual components in the heat-budget equation. Then, the heat budget is reduced to the form used in surface-cooling calculations.

B. Components of Heat-Budget Equation

1. Net Short-wave Solar Radiation, $Q_s - Q_{sr}$

Short-wave radiation is that portion of the sun's radiation with wavelengths shorter than 4 μm. According to Wein's Law, the radiation at these wavelengths accounts for about 99% of the sun's radiation energy. The amount

of short-wave radiation striking the earth's surface is reduced as it passes through the atmosphere by absorption by ozone; scattering, and diffuse reflection by particulate matter; and absorption and scattering by water vapor. The short-wave radiation reaching the earth is a function of latitude, time of day, and season of the year.

Thackston and Parker,[136] based on work by Raphael,[112] derived the following equation for absorbed clear-sky solar solar radiation, in Btu/ft^2-day, via a polynomial fitting using a nonlinear, least-squares method (absorbed solar radiation is the incident minus the reflected solar radiation):

$$Q_{cs} = 24[C_1 - C_2 \sin (2\pi d/366 + 1.710)] , \tag{3.2}$$

where C_1 and C_2 are constant and are functions of latitude and d is the day of the year (1-365). The absorbed solar radiation for other than clear skies is

$$Q_s - Q_{sr} = 24[(1 - 0.0071C^2)Q_{cs}] , \tag{3.3}$$

where C is the cloud cover, in tenths of sky.

Edinger and Geyer[32] and Hogan *et al.*[56] discuss using a pyrheliometer to measure Q_s directly. This method seems to be the best approach because the average daily values for Q_s are published by most large Weather Bureau stations, based on recorded instantaneous values of solar radiation. Edinger and Geyer used solar reflectivity, $R_{sr} = Q_{sr}/Q_s$, to determine the reflected short-wave radiation. They assumed R_{sr} constant at an average value of 0.05. Hogan *et al.* use a series of plots by Anderson,[6] based on the Lake Hefner studies, that allows one to find R_{sr}. In these plots, R_{sr} is a function of sun altitude, cloud cover, and altitude of clouds. They point out, however, that R_{sr} is in the range of 0.04-0.12 for the United States. The reader is referred to Ref. 6 for additional discussion on R_{sr}. Use of $R_{sr} = 0.05$ results in the following equation for absorbed short-wave radiation:

$$Q_s - Q_{sr} \text{ (Btu/ft}^2\text{-day)} = Q_s(1 - 0.05) = 0.95Q_s , \tag{3.4}$$

where Q_s on the right side of the equation is from Weather Bureau data.

2. <u>Net Atmospheric Radiation, $Q_a - Q_{ar}$</u>

Atmospheric radiation is from electromagnetic radiation given off by the gases that constitute the earth's atmosphere and has wavelengths up to 120 μm. Due to the long wavelengths, another name for atmospheric radiation is long-wave radiation. Unlike solar radiation, atmospheric radiation is present at night as well as during the day. Atmospheric radiation is a function of ozone, water vapor, and carbon dioxide content and distribution in the atmosphere, and the atmospheric temperature.

Koberg[71] presented the following empirical equation for atmospheric radiation:

$$Q_a = \sigma\varepsilon(T_a + 460)^4(C_B + 0.031\sqrt{P_a}\ ) \ , \tag{3.5}$$

where Q_a = atmospheric radiation, Btu/ft^2-day,

σ = Stefan-Boltzman constant = 4.12×10^{-8} Btu/ft^2-day-°R^4,

T_a = air temperature, °F, measured 6 ft above water surface,

C_B = Brunt coefficient, and

P_a = water-vapor pressure in air, mm Hg, measured 6 ft above water surface.

The only unknown value on the right side of Eq. 3.5 is C_B. To calculate the value of C_B, one reads the value of clear-sky solar radiation from Fig. 3.1 as a function of month of year and latitude. One can then calculate the ratio of the measured solar radiation to clear-sky radiation. Using this ratio and the air temperature, one can get C_B from Fig. 3.2.

Edinger and Geyer[32] and Hogan *et al.*[56] used a value of atmospheric reflectivity ($R_{ar} = Q_{ar}/Q_a$) of 0.03. Therefore the absorbed atmospheric radiation would be

$$Q_a - Q_{ar} = 0.97\sigma\varepsilon(T_a + 460)^4(C_B + 0.03\sqrt{P_a}\ ) \ . \tag{3.6}$$

Thackston and Parker[136] used the same type of procedure as above and arrived at the following general form by using a nonlinear, least-squares curve-fitting technique:

$$Q_a - Q_{ar} = 24[1.66 \times 10^{-9}\beta_a(T_a - 460)^4] \ , \tag{3.7}$$

where β_a is a coefficient of the form $\beta_a = C_3 + C_4P_a$; C_3 and C_4 are curve-fitting constants that are a function of cloud cover. See Ref. 7 for additional information on Q_a and Ref. 63 for information on Q_{ar}.

3. Back Radiation, Q_{br}

Water radiates almost like a perfect black body. The amount of back radiation can be computed from the Stefan-Boltzman fourth-power radiation law,

$$Q_{br} = \varepsilon_w\sigma(T_s + 460)^4 \ , \tag{3.8}$$

where Q_{br} = the back radiation from the water surface in Btu/ft^2-day,

ε_w = the emissivity of the water surface, assumed constant at 0.97, and

T_s = the surface water temperature in °F.

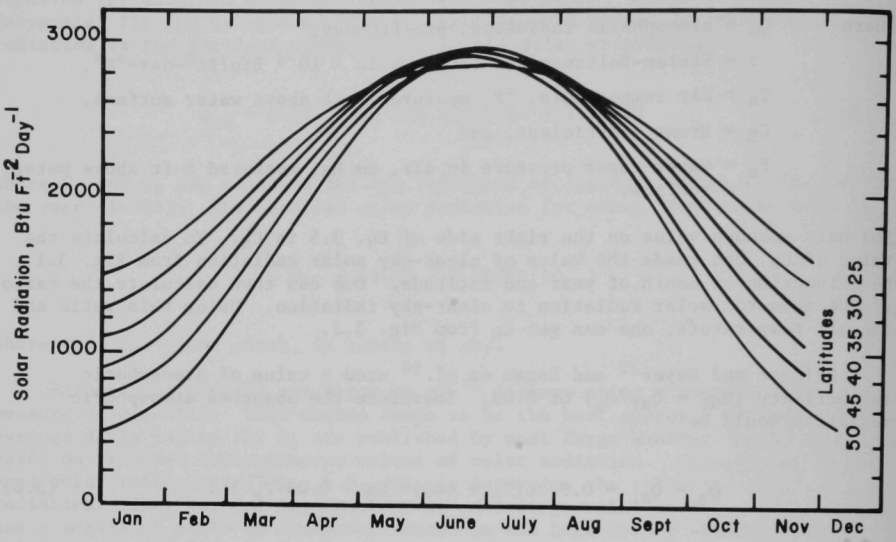

Fig. 3.1. Clear-sky Solar Radiation.[71]

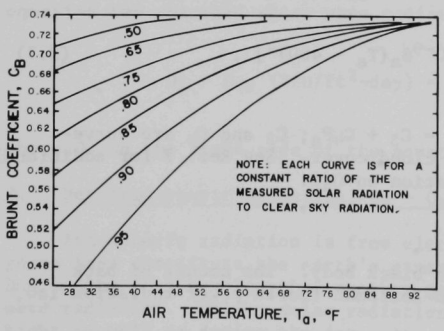

Fig. 3.2.

Brunt C Coefficient from Air Temperature, T_a, Ratio Measured Solar Radiation to Clear-sky Radiation.[71]

4. Energy Used by Evaporation, Q_e

The energy used by evaporation is a major term in the heat-budget equation. Evaporation can account for 40-70% of the heat transfer from a body of water.[56]

It is therefore important to make evaporation calculations as accurate as possible. A general form of the evaporation term is

$$Q_e = (a + bW)(P_s - P_a) \ , \tag{3.9}$$

where Q_e = the energy loss by evaporation in Btu/ft^2-day,

a and b = coefficients depending on the evaporation formula used (see Table 3.1),

W = the wind speed in mph, and

P_s = the saturated vapor pressure of water determined from the water surface temperature, T_s.

Table 3.1. Coefficients for Various Evaporation Formulas, Expressed in lb_m/ft^2-day

Formula	*a*	*b*
Lake Hefner	0	12.4
Lake Colorado City	0	18.1
Meyer	70.5	7.05

Note that the elevation at which W and P_a are determined must be specified, as well as the time period over which these values are averaged. Both these factors will affect the numerical value of the coefficients a and b in Eq. 3.9.

Inspection of Eq. 3.9 reveals two main meteorological variables that affect evaporation. First, the driving force is $P_s - P_a$, which measures the relative difference between the amount of water vapor the air can hold and the amount it presently holds. The greater the water-vapor content of the air, the greater the value of P_a, and the smaller the rate of evaporation for a given P_s. The other major term in Eq. 3.9 is the wind speed. Its relation to evaporation is one of determining how long a single volume of air will remain in contact with the water. The greater the wind speed, the less time a single volume of air, with its increasing P_a value due to water contact, will remain in contact with the water. Therefore, higher wind speeds retain a higher driving force. The proper values of a and b in Eq. 3.9 for a specific location are ideally chosen based on evaporation studies performed in that area. However, care should be used any time one is dealing with evaporation coefficients. As discussed earlier, wind speed has an effect on evaporation; therefore, when determining these coefficients, one is concerned not only with the general location but also with factors influencing wind speed, such as local topography, shape of the body of water, and total surface area of the body of water.

Of the formulas available in the literature, the following three evaporation formulas are in major use:

the Lake Hefner equation,[89]

$$M_E = 0.614W(P_s - P_a) \; ; \tag{3.10}$$

the Lake Colorado City equation,[72]

$$M_E = 0.897W(P_s - P_a) \; ; \tag{3.11}$$

and the Meyer Equation,[85]

$$M_E = C_M(0.349)\ 1 + \frac{W}{10}\ (P_s - P_a) \; , \tag{3.12}$$

where M_E = the mass transfer in lb/day-ft^2;

W = the wind speed in miles per hour:

measured at an elevation of 26 ft above the water surface and taken as the average over 3 hr for Eq. 3.10;

measured at an elevation of 26 ft above the water surface and taken as the average over 24 hr for Eq. 3.11;

measured at an elevation of 25 ft above the water surface and taken as the average over one month for Eq. 3.12;

P_s = the saturated water-vapor pressure of water determined from the water surface temperature, T_s, in mm Hg;

P_a = water vapor pressure in air, mm Hg:

measured at the same elevation above the water surface and averaged over the same time period as the values of W indicated above; and

C_M = a constant ranging from 10 to 15 and is a function of certain features of the body of water and frequency of available meteorological measurement; assume C_M = 10 for this report.

To convert these equations from mass transfer to heat transfer, one multiplies by the heat of vaporization. The heat of vaporization is a function of water temperature; however, assuming a constant heat of vaporization will result in an error of only about 1-2% for the ranges of temperatures expected in application. Based on a heat of vaporization of 1041 Btu/lb$_m$ (corresponding to a water temperature of about 100°F), Table 3.1 shows the values of a and b for Eq. 3.9 based on Eqs. 3.10-3.12 and based on the same units used in those equations for W, P_s, and P_a.

In comparing these three equations, note that the Meyer equation is the only one that has evaporation at W = 0 (corresponding to a ≠ 0). Edinger and Geyer[32] have a similar table in their report, but they used 970 Btu/ft^3

(corresponding to a water temperature of 212°F) for the heat of vaporization. This results in an error of about 7% in their values of a and b. However, later sections of this report will use their values of a and b when their equations are used for example calculations.

Again it shoud be pointed out that Q_e is a major term in the heat-budget equation and yet one of the most difficult to determine. As shown later, major differences in the final values of certain calculations using the heat-budget equation can be reached just by using two different evaporation equations of the type presented by Eqs. 3.9-3.11.

5. Energy Conducted from a Body of Water, Q_h

The loss of heat due to conduction can be either positive (corresponding to $T_a < T_s$) or negative (corresponding to $T_a > T_s$). The rate at which heat is conducted between the air-water interface is a function of the product of a heat-transfer coefficient and a driving force, $T_s - T_a$. It is commonly assumed that the heat of conduction can also be related to the same variables as the heat of mass transfer (evaporation). Making use of this relationship, Q_h was related to evaporative energy by Bowen,[17] by use of the Bowen ratio, B, where

$$B = \frac{Q_h}{Q_e} , \tag{3.13}$$

in which $B = 0.26(T_s - T_a)/(P_s - P_a)$, in which T_s and T_a are in °F, and P_s and P_a in mm Hg; P_a is evaluated at the same elevation and over the same averaging period as indicated for the evaporation equation being used (Eq. 3.10, 3.11, or 3.12); T_a is the air temperature, evaluated at the same elevation and averaged over the same time as P_a.

6. Inflow and Outflow Heat, Q_v

Water flowing into the main water body brings heat energy with it; water flowing out of the main body takes heat energy away. A major factor in many heat budgets is the net gain or loss of energy due to such inflows and outflows. The net heat brought into a body of water as inflow includes such terms as precipitation, all tributary waters, groundwater, and any other water that enters the main body. The net heat extracted from the body of water in outflow includes all terms, such as seepage, that describe water leaving the main body. Therefore, when stated in heat-loss terms, the individual components of Q_v are both negative and positive. Using the notations of this chapter, where M_i is the mass-transfer rate, we can write

$$Q_v = \frac{\sum_{i=1}^{m} h_i M_i}{A} , \tag{3.14}$$

where M_i = the mass-transfer rate in lb_m/day for term i (positive for inflows and negative for outflows),

h_i = the enthalpy in Btu/lb_m for term i, and

A = the surface area of the body of water in ft^2.

The value of enthalpy, h_i, can be expressed as

$$h_i = \Delta T_i C_p \ , \tag{3.15}$$

where ΔT_i = the difference in the temperature of the body of water and the temperature of the waters leaving and entering, in °F, and

C_p = the specific heat of water = 1.0 Btu/lb_m - °F.

Care should be taken in determining the signs of the components because, although inflow and outflow have positive and negative heat-transfer signs, respectively, the sign of h_i can be negative, thereby reversing these signs.

7. Conclusions

Table 3.2 gives a relative comparison of the amount of heat transfer by each component of the heat-budget equation. The values of heat transfer in this table are expressed in ranges. Because the individual components are functions of different meteorological conditions, corresponding values within given ranges will not occur simultaneously. For example, peak values of all components will not occur at the same time.

Table 3.2. Comparison of Amounts of Heat Transfer by Various Components of Heat-budget Equation

Component	*Range of Heat Loss, Btu/ft²-day*
Q_s	400-2800
Q_a	2400-3200
Q_{br}	2400-3600
Q_e	500-2000
Q_h	-320-+420
Q_{sr}	40-200
Q_{ar}	70-120

C. Equilibrium Temperature

Consider a body of water with no net energy change due to inflows and outflows; i.e., $Q_v = 0$. This means that all energy transfer is across the air-water interface. Subject that water body to constant meteorological conditions. Eventually, the water-body surface will approach a constant temperature such that the system is in equilibrium. At this condition, the heat entering the water surface would exactly balance the heat leaving. The temperature at this equilibrium point is called the equilibrium temperature, T_{EQ}. Thus T_{EQ} is a steady-state surface temperature satisfying Eq. 3.1 with Q = net energy change = 0. In natural systems, meteorological conditions will not remain constant, even for short times, much less long enough to attain T_{EQ} for that set of parameters. However, the difference between T_{EQ} and the actual water-surface temperature, T_s, is a good measure of the rate at which the water surface will gain or lose heat. The rate of heat exchange will decrease as T_s approaches T_{EQ}. Use of T_{EQ} in surface heat-exchange calculations will considerably simplify the use of the energy budget. The following equation uses T_{EQ} to express the energy-budget equation for $Q_v = 0$:

$$Q = -K(T_s - T_{EQ}) \ . \tag{3.16}$$

This form is desirable because of it simplicity. It states that the amount of heat transferred across the air-water interface, Q, is equal to a cooling coefficient, K, times the driving force, $T_s - T_{EQ}$.

Equation 3.1 is reduced to the following form when calculating T_{EQ}:

$$Q_s - Q_{sr} + Q_a - Q_{ar} - Q_{br} - Q_e - Q_h = 0 \ . \tag{3.17}$$

There are a number of methods to determine T_{EQ} using Eq. 3.17. Each method will be discussed separately.

1. Edinger-Geyer[32] Method

a. General Development. Edinger and Geyer use the term "absorbed radiation," H_R, and define it as

$$H_R = Q_s + Q_a - Q_{sr} - Q_{ar} \ . \tag{3.18}$$

The approach they use to calculate the terms on the right side of Eq. 3.18 are discussed previously and summarized in Table 3.3. Substituting Eq. 3.18 into Eq. 3.17 gives

$$H_R - Q_{br} - Q_e - Q_h = 0 \ . \tag{3.19}$$

Table 3.3. Summary of Equations of Three Different T_{EQ} Calculating Methods

Term/Method	*Edinger-Geyer*[32]	*Hogan et al.*[56]	*Thackston-Parker*[136]
Q_s	Measured	Measured	$Q_o = 24\{C_1 - C_2 \sin[(2\pi d/366 + 1.71]\}$ C_1 and C_2 = fn(latitude) $Q_s = (1 - 0.0071\ C^2)Q_o$
Q_{sr}	$R_{sr} = 0.05$	R_{sr} = fn(height of clouds, cloud cover, sun altitude)[a]	Included in Q_s above
Q_a	$Q_a = \varepsilon_w \sigma (T_a + 460)^4 (C_B + 0.031 P_a)$[a] C_B = fn(month, T_a, Q_s)		$Q_a = 24[1.66 \times 10^{-9} \beta_a (T_a + 460)^4]$[b] β_a = fn(cloud cover, P_a)
Q_{ar}	$R_{ar} = 0.03$		
Q_{br}	$Q_{br} = 0.97\sigma(T_s + 460)^4$		
Q_e	General form: $Q_e = (a + bW)(P_s - P_a)$	Meyer's coefficients	Lake Hefner coefficients
Q_h	$Q_c = 0.26(a + bW)(T_s - T_a)$		$Q_c = 24[0.0543 x W x P x (T_a - T_s)]$ $P = (29.92)/\exp \frac{32.15 \times E}{1545(T_a + 460)}$ E = elevation in ft

[a]*Requires reading values from a figure.*

[b]$\beta_a = C_1 + C_2 P_a$, *where the value of C determines which of a set of 11* C_1 *and* C_2 *to use.*

Equation 3.19 is physically relating the fact that if a body of water is at T_{EQ}, then the total energy input across the air-water interface (H_R) must equal the total energy output across this interface. Substituting the equations from Table 3.3 for the Q's into Eq. 3.19 gives

$$H_R = 0.97\sigma(T_s + 460)^4 + (a + bW)(P_s - P_a) + 0.26(a + bW)(T_s - T_a) \ , \quad (3.20)$$

where P_s is the water-vapor pressure at T_s and W, P_a, and T_a are evaluated at an elevation corresponding to the evaporation formula used (see definitions following Eq. 3.12).

At this point in the development of this method, the term "cooling coefficient" must be defined.

The following assumptions are made so that Eq. 3.17 can be expressed as a function of the first power of T_s, as in Eq. 3.16:

1. $\varepsilon_w\sigma(T_s + 460)^4 = \varepsilon_w\sigma(460)^4\left[6\left(\frac{T_s}{460}\right)^2 + 4\left(\frac{T_s}{460}\right) + 1\right]$.

2. $0.051(T_s^2 - T_{EQ}^2) = 0$; this must be done to eliminate this term from Eq. 3.18.

3. $P_s = C(\beta) + \beta T_s$,

   $P_{EQ} = C(\beta) + \beta T_{EQ}$, and

   $P_s - P_{EQ} = \beta(T_s - T_{EQ})$,

where β is the slope of the straight-line approximation illustrated in Fig. 3.3 for each 10°F increment and $C(\beta)$ is the x-axis intercept for the same lines.

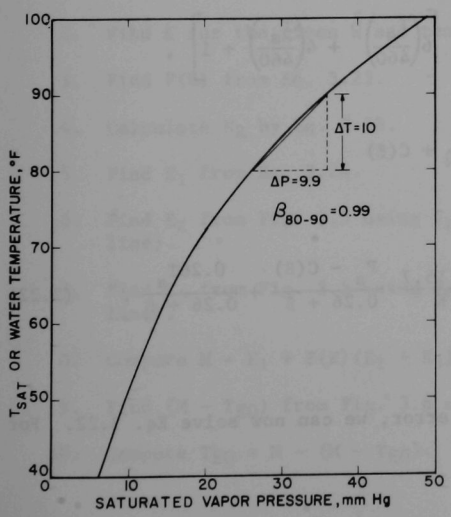

Fig. 3.3

Saturated Air Temperature or Water Temperature vs. Saturated Vapor Pressure.[32]

Application of these assumptions to Eq. 3.16 yields this equation for K (in Btu/ft^2-day-°F):

$$K = 15.7 + (0.26 + \beta)(a + bW) \ . \tag{3.21}$$

Figure 3.4 is a plot of K versus wind speed for various β's or T_{EQ} ranges for the Lake Hefner evaporation formula. Now that K has been evaluated, one can proceed to determine T_{EQ}.

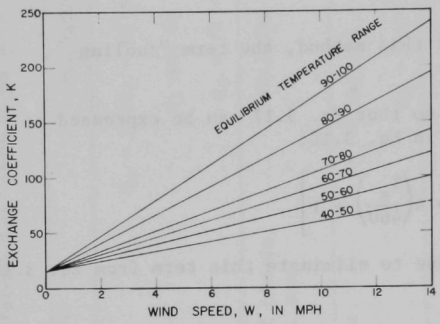

Fig. 3.4.

Exchange Coefficient, K, Based on Lake Hefner Evaporation Formula.[32]

Returning to Eq. 3.20 and substituting

$$a + bW = \frac{K - 15.7}{0.26 + \beta} \ ,$$

$$\varepsilon_w \sigma (T_s + 460)^4 = \varepsilon_w \sigma (460)^4 \left[6\left(\frac{T_s}{460}\right)^2 + 4\left(\frac{T_s}{460}\right) + 1 \right] \ ,$$

and

$$P_{EQ} = \beta T_{EQ} + C(\beta)$$

into Eq. 3.20 results in

$$T_{EQ} + \frac{0.051 T_{EQ}^2}{K} = \frac{H_R - 1801}{K} + \frac{K - 15.7}{K} \ \frac{P_a - C(\beta)}{0.26 + \beta} + \frac{0.26 T_a}{0.26 + \beta} \ , \tag{3.22}$$

where $T_s = T_{EQ}$.

Knowing H_R, P_a, T_a, and K, by trial and error, we can now solve Eq. 3.22. For convenience, define the following terms:

$$F(K) = \frac{K - 15.7}{K} , \tag{3.23}$$

$$E_1 = \frac{H_R - 1801}{K} , \tag{3.24}$$

$$E_2 = \frac{0.26T_a}{0.26 + \beta} , \tag{3.25}$$

$$E_3 = \frac{P_a - C(\beta)}{0.26 + \beta} , \tag{3.26}$$

and

$$M = T_{EQ} + \frac{0.051T_{EQ}^2}{K} . \tag{3.27}$$

Substituting Eqs. 3.23-3.27 into Eq. 3.22 gives

$$M = E_1 + F(K)(E_2 + E_3) . \tag{3.28}$$

Figures 3.5 and 3.6 are nomograms that solve Eq. 3.28. The steps in calculating T_{EQ} using the nomograms are:

1. Assume a temperature range.
2. Find K for the given W and temperature range from Fig. 3.4.
3. Find F(K) from Eq. 3.23.
4. Calculate H_R by Eq. 3.18.
5. Find E_1 from Eq. 3.24.
6. Find E_2 from Fig. 3.5 using T_a and the temperature range (along solid line).
7. Find E_3 from Fig. 3.5 using P_a and the temperature range (along dotted line).
8. Compute $M = E_1 + F(K)(E_2 + E_3)$.
9. Find $(M - T_{EQ})$ from Fig. 3.6 using values of M and K.
10. Compute $T_{EQ} = M - (M - T_{EQ})$.

11. Check to see that this computed value falls within the selected temperature range. If it does not, choose a new range based on the value of T_{EQ} given in step 10 and repeat the computations.

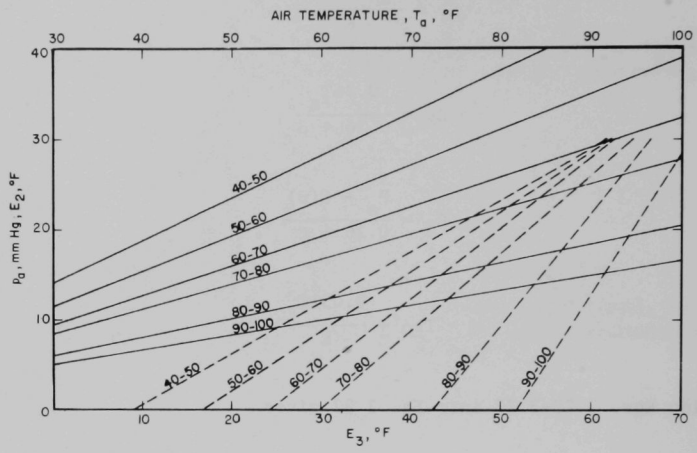

Fig. 3.5. E_3 from Air Vapor Pressure, P_a, and E_2 from Air Temperature, T_a.[32]

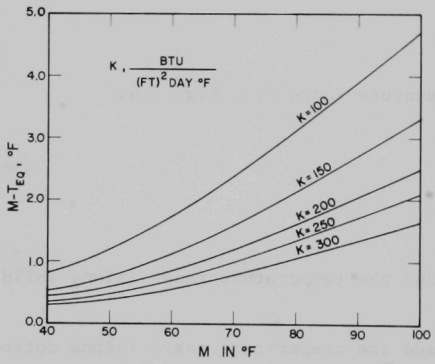

Fig. 3.6.

M - T_{EQ} Correction for Use in Eq. 3.27.[32]

b. Numerical Example. To help understand the Edinger-Geyer method, we present the following data as an example problem:

latitude = 36° (Nashville, Tennessee),

Month = June,

T_a = air temperature = 75°F,

R_h = relative humidity = 73%,

W = wind speed = 6.6 mph,

C = cloud cover = 6.3/10, and

Q_s = solar radiation = 539 langleys/day = 1990 Btu/ft^2-day.

The solution is:

Step 1: Assume a temperature range of 80-90°F.

Step 2: From Fig. 3.4 (Lake Hefner evaporation equation) at W = 6.6 mph and temperature range 80-90°F, find K = 98 Btu/ft^2-day-°F.

Step 3: F(K) = (K - 15.7)/K = (98 - 15.7)/98 = 82.3/98 = 0.84.

Step 4: It is now required to calculate the atmospheric- and solar-radiation terms to evaluate H_R. To compute the atmospheric radiation, it is necessary to calculate the water-vapor pressure in the air, P_a. The value of P_a is the saturated water-vapor pressure at the wet-bulb temperature, T_{SAT}. However, since the value of T_{SAT} is not recorded by the Weather Bureau, one must calculate it using T_a and the relative humidity. Figure 3.7 allows this calculation to be done graphically.

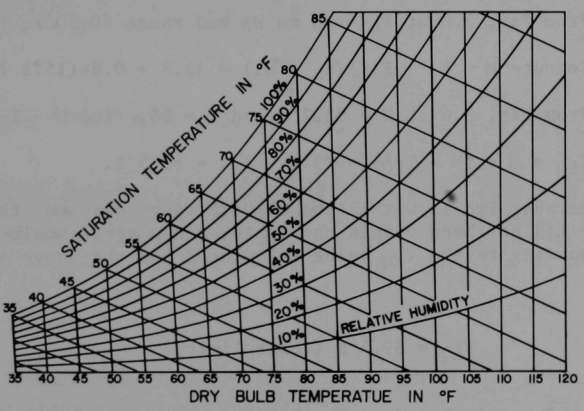

Fig. 3.7. Normal Temperature Psychrometric Chart.

a. From Fig. 3.7 at T_a = 75.0°F and relative humidity = 73%, find saturated air temperature at 68.6°F = T_{SAT}. From Fig. 3.3 at T_{SAT} = 68.6°F, find P_a = 18 mm Hg.

b. From Fig. 3.1 at month = June and latitude = 36°, find clear-sky solar radiation = 2950 Btu/ft^2-day.

c. Ratio of measured solar radiation to clear sky is 1990/2950 = 0.674. From Fig. 3.2 at T_a = 75°F and ratio = 0.674, find C_B = 0.74.

d. $Q_a = 4.5 \times 10^{-8}(T_a + 460)\ (C_B) + 0.031\sqrt{e_a}\ )$

$= 4.5 \times 10^{-8}(75 + 460)^4(0.74 + 0.031\sqrt{18}$

$= 4.5 \times 10^{-8}(5.35 \times 10^2)^4(0.74 + 0.132)$

$= 3220$ Btu/ft^2-day.

e. $Q_{sr} = 0.05\ Q_r = (0.05)(1990) = 99.50$ Btu/ft^2-day.

$Q_{ar} = 0.03\ Q_a = (0.03)(3220) = 96.60$ Btu/ft^2-day.

$H_R = Q_s + Q_a - Q_{sr} - Q_{ar} = 1990 + 3220 - 99.5 - 99.6$

$= 5014$ Btu/ft^2-day.

Step 5: $$E_1 = \frac{H_R - 1801}{K} = \frac{5014 - 1801}{98} = 32.8°F\ .$$

Step 6: From Fig. 3.5 at T_a = 75°F and range 80-90°F, find E_2 = 15.5°F.

Step 7: From Fig. 3.5 at P_a = 18 mm Hg and range 80-90°F, find E_3 = 57°F.

Step 8: Compute $M = E_1 + F(K)(E_2 + E_3) = 32.8 + 0.84(15.5 + 57) = 93.7$°F.

Step 9: From Fig. 3.6 at M = 93.7°F and K = 98, find $M - T_{EQ} = 4.2$.

Step 10: $T_{EQ} = M - (M - T_{EQ}) = 93.7 - 4.2 = 89.5$°F.

Step 11: Because T_{EQ} is within the 80-90°F range assumed, the answer is correct. If it had not been within the range, a new range would have been assumed corresponding to the T_{EQ} value calculated and the above steps repeated.

$$T_{EQ} = 89.5°F \text{ (lower limit)}\ .$$

This value of T_{EQ} is based on the Lake Hefner evaporation equation, which gives the minimum K of any of the evaporation equations presented by Edinger and Geyer. Using the same procedure but applying the Meyer evaporation equation result in values of K = 167 Btu/ft^2-day-°F and T_{EQ} = 82.1°F (upper limit).

2. Hogan *et al.*[56] Method

a. General Development. This method basically takes Eq. 3.17 and substitutes into it the component equations listed under Hogan *et al.* in Table 3.3. Using various expansion techniques, they arrive at

$$0 = [H_R - a_5 - (a_{12} + a_{13}W)(a_1 - \theta_a a_{14} - P_a')]$$
$$- [a_6 + (a_{12} + a_{13}W)(a_2 + a_{14})]\theta_{EQ} \tag{3.29}$$
$$- [a_7 + (a_{12} + a_{13}W)a_3]\theta_{EQ}^2 - [a_3 + (a_{12} + a_{13}W)a_4]\theta_{EQ}^3 ,$$

where H_R = same as previous H_R, except for different R_{sr},

P_a' = the water-vapor pressure in the air in psia,

$\theta_{EQ} = T_{EQ} - 32°F$,

$\theta_a = T_a - 32°F$, $a_6 = 19.176$,

$a_1 = 0.089$, $a_7 = 5.85 \times 10^{-2}$,

$a_2 = 3.50 \times 10^{-3}$, $a_8 = 7.923 \times 10^{-2}$,

$a_3 = 5.68 \times 10^{-6}$, $a_{12} = 3730$,

$a_4 = 1.13 \times 10^{-6}$, $a_{13} = 373$, and

$a_5 = 2358.74$ $a_{14} = 0.00473$.

T_a, P_a', and W are all taken as one-month averages of values measured at an elevation of 25 ft above the water surface.

To avoid having to solve this third-order equation each time, the equation is plotted in Fig. 8.4 for various values of $a_{12} + a_{13}W$ and f_1, in which

$$f_1 = H_R - a_5 - (a_{12} + a_{13}W)(a_1 - \theta_a a_{14} - P_a') . \tag{3.30}$$

b. Numerical Example. To help the reader understand this method, the following example is worked using the data given in the Edinger-Geyer example. The only additional data needed is R_{sr}; assume $R_{sr} = 0.007$ for this example.

$$f_1 = [H_R - a_5 - (a_{12} + a_{13}W)(a_1 - \theta_a a_{14} - P_a')] .$$

$H_R = (Q_s - Q_{sr}) + (Q_a - Q_{ar})$,

$Q_s = 1990$ Btu/ft^2-day,

$Q_{sr} = 0.07(Q_s) = (0.07)(1990) = 139.30$ Btu/ft^2-day,

$Q_a = Q_a$ (previous example) $= 3220$ Btu/ft^2-day,

$Q_{ar} = 0.03\ Q_a = (0.03)(3220) = 96.60$ Btu/ft^2-day,

$H_R = (1990 - 139) + (3220 - 97) = 4974$ Btu/ft^2-day,

$\theta_a = T_a - 32°F = 75 - 32 = 43°F$,

$P_a' = 18$ mm Hg $= (18)(0.01934)$ psia $= 0.348$ psia,

$a_{12} + a_{13}W = 3730 + (373)(6.6) = 6190$,

$$f_1 = \{4974 - 2359 - (6190)[0.089 - (43)(0.00473) - 0.348]\}$$

Using Fig. 8.4 at $f_1 = 5475$ and $a_{12} + a_{13}W = 6190$, find $T_{EQ} = 82.3°F$.

Note that the Edinger-Geyer method gave a $T_{EQ} = 82.1°F$ for the Meyer evaporation equation as compared to $T_{EQ} = 82.3°F$ for the Hogan *et al.* method, which assumes the same coefficients. However, use of the Lake Hefner evaporation equation results in $T_{EQ} = 89.5$, or better than 7°F higher than the Meyer T_{EQ}. This range of T_{EQ} is pointed out in an effort to show just how important the choice of evaporation formula can be.

3. Thackston-Parker[136] Method

Table 3.3 shows that the Thackston-Parker method requires no plots. Therefore, given (1) month of the year, (2) latitude of the location, (3) elevation of the location, (4) dry-air temperature, (5) relative humidity, (6) wind speed, and (7) cloud cover, this method can be computerized using a trial-and-error method to determine T_{EQ}.

The trial-and-error approach is based on Eq. 3.16 and states that if the correct value of T_{EQ} is assumed, then the value of $T_s - T_{EQ} \approx 0$. This can be expressed in equation form as

$$Q = -K(T_s - T_{EQ}) = 0 \ . \tag{3.31}$$

To use this approach, one calculates the value of Q from Eq. 3.16 based on an initial assumed value of T_{EQ_1} (1 corresponding to the first assumed temperature). If the value of Q is zero as required in Eq. 3.31, then T_{EQ_1} is the correct answer. However, if $Q \neq 0$, then one can rearrange Eq. 3.16 in the following form:

$$T_s - T_{EQ} = -Q/K \ , \tag{3.32}$$

in which

$$K = 24[15.7 + (0.01025 + \eta)333W] \tag{3.33}$$

and

$$\eta = \frac{9501}{(T_{EQ_1} + 460)^2} \exp\left[17.62 - \frac{9501}{T_{EQ_1} + 460}\right] . \tag{3.34}$$

Since the Lake Hefner equation (Eq. 3.10) is used for evaporation, W must be evaluated as a 3-hr average at 26 ft above the water surface. The value of

$T_s - T_{EQ}$ Iis then added to T_{EQ_1} to get T_{EQ_2}, and the procedure is repeated with T_{EQ_2} replacing all T_{EQ_1}. Thackston and Parker use a computer program based on this procedure, with the computer program terminating at the point where $T_s - T_{EQ}$ from Eq. 3.32 becomes less than 0.1°F.

Using the technique described above and the average and extreme (upper 10%) values for the required meteorological variables for 88 locations throughout the United States, Thackston and Parker arrive at average and extreme contour plots for T_{EQ} and K for the United States. Figure 3.8 shows an example of the contours for K, and Fig. 3.9 shows an example of the contours for T_{EQ}. They also use this technique to calculate monthly average and extreme values for T_{EQ} and K for the individual locations (see Fig. 8.2).

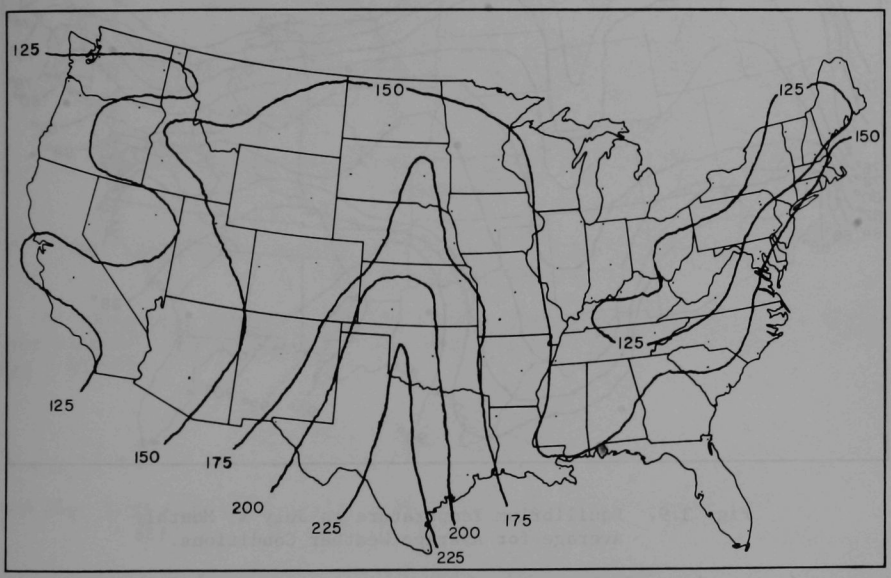

Fig. 3.8. Heat-exchange Coefficient on July 1; Monthly Average for Average Weather Conditions.[136]

4. Brady *et al.*[18] Method

a. General Formulation. Brady *et al.* use field data to arrive at the following equation for T_{EQ}:

$$T_{EQ} = T_{SAT} + Q_s/K \ , \tag{3.35}$$

where T_{SAT} is the dew-point temperature calculated from measured values of T_a and relative humidity, Q_s is the measured solar radiation, and K is calculated from

$$K = 15.7 + (\beta + 0.26)(70 + 0.7W^2) \ . \tag{3.36}$$

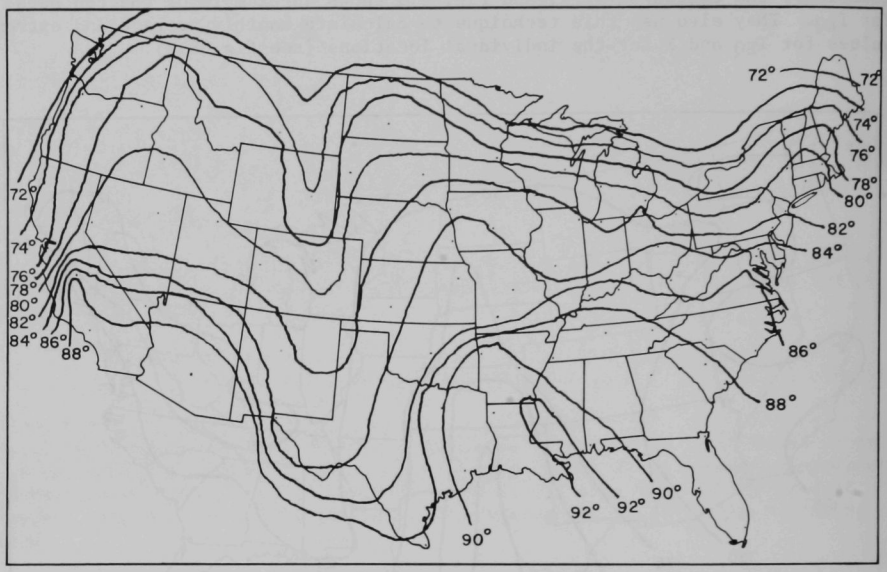

Fig. 3.9. Equilibrium Temperature on July 1; Monthly Average for Average Weather Conditions.[136]

Here, β is the slope of the vapor-pressure curve and is calculated by

$$\beta = 0.255 - 0.0085T_A + 0.000204T_A^2 \ , \tag{3.37}$$

where T_A is the average temperature between T_{SAT} and T_{EQ}.

To use this procedure, one assumes a value of T_{EQ} to calculate T_A and then works Eqs. 3.37, 3.36, and 3.35, in that order. This results in a new value of T_{EQ} from Eq. 3.35. If this new T_{EQ} is not equal to the old assumed T_{EQ}, then use the new T_{EQ} to calculate T_A and repeat the process. To eliminate calculating Eqs. 3.36 and 3.37 each trial, Fig. 3.10 is provided to allow one to get K directly, using T_A and W.

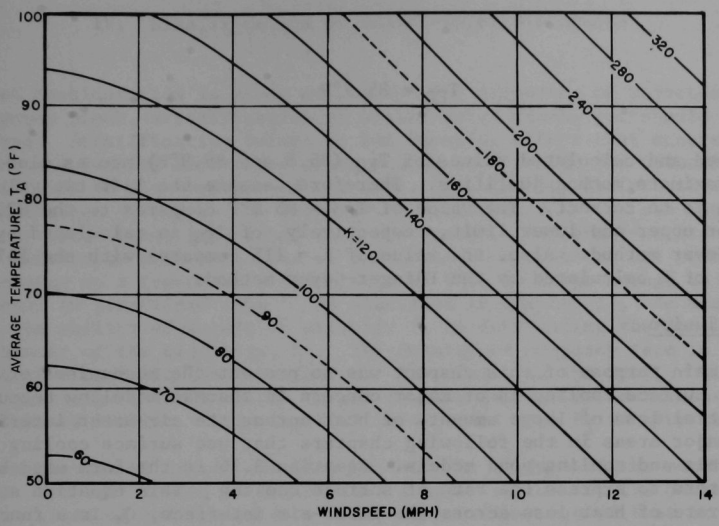

Fig. 3.10. Cooling Coefficient, K, from Wind Speed, W, and Average Temperature, T_a.[18]

b. Numerical Example. Use the same meteorological data as in the Edinger-Geyer example. Assume T_{EQ} = 80.0°F. From Fig. 3.7 at R_h = 73% and T_a = 75°F, T_{SAT} = 68.6°F.

$$T_A = (T_{EQ} + T_{SAT})/2 = 74.3°F \ .$$

From Fig. 3.10 at W = 6.6 and T_A = 74.3, K = 117 Btu/ft^2-day-°F.

$$T_{EQ} = T_{SAT} + Q_s/K = 68.6°F + \frac{1990 \text{ Btu/ft}^2\text{-day-°F}}{117 \text{ Btu/ft}^2\text{-day-°F}} = 85.6°F \ .$$

Since T_{EQ} = 85.6°F is not the original assumption, the process must be repeated.

$$T_A = (68.6 + 85.6)/2 = 72.1°F \ .$$

This value of T_A results in

$$K = 115 \text{ Btu/ft}^2\text{-day-°F}$$

and

$$T_{EQ} = 85.9°F \ .$$

The assumed and calculated values of T_{EQ} (85.6 and 85.9°F) are as close as this approximate method justifies. Therefore, assume the last two values of K and T_{EQ} to be correct. The value of T_{EQ} = 85.9°F compares to the 82.1 and 89.5°F for upper and lower limit, respectively, of T_{EQ} as calculated by the Edinger-Geyer method. Also, the value of K = 115 compares with the 167 and 98 values of K calculated by the Edinger-Geyer method.

D. Conclusion

The main purpose of this chapter was to present the mechanisms of surface cooling. Surface cooling is of major concern in thermal modeling because of the potential loss of large amounts of heat across the air-water interface. The two major areas in the following chapters that use surface cooling are far-field models and cooling-pond models. Equation 3.16 is the form used by most investigators to express the rate of surface cooling. This equation states that the rate of heat loss across the water-air interface, Q, is a function of a cooling coefficient, K, and a driving force, $T_{EQ} - T_s$. If one knows the value of T_s, then only the values of K and T_{EQ} need be determined. The value of K is merely a function of wind speed and air temperature. Depending on the method used to calculate T_{EQ}, K can be easily calculated. With K and T_s known, only the value of T_{EQ} needs to be determined to find the value of Q.

This chapter discussed four methods of calculating the equilibrium temperature, T_{EQ}. Of the methods discussed, the most general one was the Edinger-Geyer[32] method. The Hogan *et al.*[56] and the Thackston-Parker[136] methods lacked this generality because these methods chose specific evaporation coefficients. Therefore, when the meteorological data are available to apply the Edinger-Geyer method, we feel it to be the best of the three.

When meteorological data are not available or when a rough estimate of the equilibrium temperature is desired, then the Brady *et al.*[18] method is suggested. Use of the plots of equilibrium temperature presented by Thackston and Parker also offers an initial estimate.

IV. STRATIFICATION OF HEATED-WATER DISCHARGES

When consideration is given to a means for disposing of rejected heat from a power plant, stratification of heated-water discharges should be considered. Stratification refers to the layering effect that occurs when waters have a density difference great enough to override the natural tendencies of all liquids to mix when placed together. The density difference in power-plant discharges is due to the temperature differences of the two waters, the hotter water being less dense than the cooler. Harleman[47] states, "A density difference between layers of the order of a tenth of one percent, corresponding to a temperature difference of 6°F, is large enough to be significant in stratified flow." As discussed in Chapter II, one means of stating the ability of waters to stratify is by determining the densimetric Froude number of the discharge, F_j. The density or buoyancy term in F_j is $\Delta\rho/\rho$, which appears in the denominator. Therefore, as the density difference, $\Delta\rho$, becomes larger, the buoyancy forces causing stratification become stronger and F_j becomes smaller. Some layering is expected when F_j is very close to 1.0.

When the heated waters are floated onto the surface of the receiving body of water, vertical mixing is inhibited. A major reason for the decrease in the temperature of the heated waters may then be the rate of heat exchange or dissipation to the atmosphere. Recirculation of the heated water through the intake is always a possibility. Such problems related to the stratification of heated waters have drawn much attention in the past. However, due to recent stringent temperature discharge regulations, the use of the technique of layering the warm water may be limited in its scope of application. Still, the alternative is avilable and is being considered in environmental-impact statements.[129]

Analytical tools are available for evaluating the thermal impact of an existing power station where layering does occur. Bata[13] solved the hydrodynamic equations proposed for two-layer flow by Schijf and Schönfeld.[121] Harleman and Stolzenbach[52] and Harleman[47] present laboratory results of a physical model that verify the applicability of the equations in two-layer flow systems. Polk *et al.*[105] present data from field investigations of heated discharges at four power plants located in the Southeast. The field investigations verified the ability of the solution presented by Bata to predict the arrested warm-water wedge length.

A. Basic Equations

Harleman[47] presents an excellent discussion of two-layer flow theory as applied to mechanics of condenser water discharge from thermal power plants. Terminology and symbols in this chapter will follow those used by Harleman, which will differ slightly from other chapters in this report. A schematic is presented in Fig. 4.1, dividing the locale of the power plant into five specific regions and defining symbols. The general description of the zones is: A, river section downstream from the discharge channel; B, discharge channel; C, river section between the discharge channel and intake structure; D, intake structure; and E, river section upstream of the intake structure. The water at the condenser intake from the river has a temperature of T_a, and the temperature of the discharge water, T_o, is $T_a + \Delta T_o$,

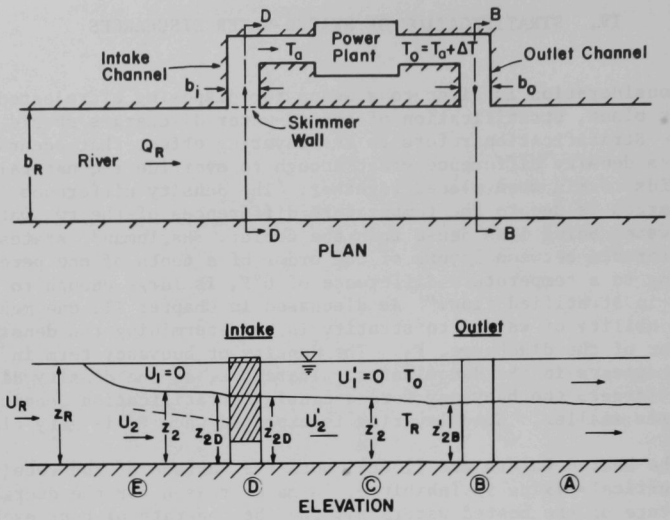

Fig. 4.1. Flow Stratification in Vicinity of Power Plant.[47]

where ΔT_o is the temperature rise across the condensers. If recirculation is prohibited, T_a will equal the ambient temperature of the river.

To simplify the mathematics, the flows in these several regions will be treated as two-layer flows. Figure 2.2 illustrates the relationship between this assumed profile and actual profiles. Each layer is considered homogeneous, with a density difference, $\Delta\rho$, between the two layers. This assumes that no mixing occurs across the interface, and that the heated water is in essence "riding up" over the colder water. Polk *et al.*[105] indicated that the density of the upper layer was difficult to determine without measurements. Figure 4.2 details a two-layer flow system. Other assumptions are made to make tractable the mathematics of one-dimensional equations of motion and continuity for both layers:

a. Flows are assumed steady.

b. For the range of temperature under consideration, density varies linearly with temperature.

c. The total depth is constant. The free-surface Froude number, F, based on the average velocity of the entire flow, is assumed to be small compared to unity. Hence, changes in the total depth, z_R, are neglected, and it is assumed that

$$z_R = z_1 + z_2 = \text{constant} \ , \tag{4.1}$$

where z_R is the total depth, z_1 is the thickness of the upper layer, z_2 is the thickness of the bottom layer, U_1 and U_2 are the average velocities in the upper layer and lower layer, respectively, and τ_i and τ_b are the shear stresses at the interface and bottom.

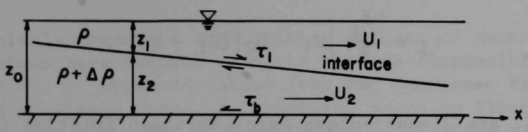

Fig. 4.2. Two-layered Stratified Flow.[47]

These assumptions can be combined with the momentum and mass-conservation relations to describe the system. Essentially, a balance must be obtained between changes in momentum of the flowing fluid and forces acting on the system. Here, those forces include (1) friction between the two layers and at the channel bottom; (2) buoyancy forces caused by the density difference, $\Delta\rho$; and (3) forces due to the weight of water (hydrostatic pressure).

Harleman[45] develops the following equation, using the equations of motion and continuity, to describe the slope of the interface, dz_2/dx:

$$\frac{dz_2}{dx} = \frac{\dfrac{\tau_b - \tau_i}{\rho g z_2} - \dfrac{\tau_i}{\rho g z_1}}{\dfrac{\Delta\rho}{\rho}\left(F_2^2 + F_1^2 - 1\right)}, \tag{4.2}$$

in which F_1 and F_2 are the densimetric Froude numbers of the upper and lower layers,

$$F_1 = \frac{U_1}{\sqrt{g\,\dfrac{\Delta\rho}{\rho}\,z_1}} \tag{4.3}$$

and

$$F_2 = \frac{U_2}{\sqrt{g\,\dfrac{\Delta\rho}{\rho}\,z_2}} \tag{4.4}$$

with $\Delta\rho = \rho_2 - \rho_1$.

The bottom and interfacial shear stresses are given by

$$\tau_b = \frac{\rho f_b}{8} |U_2| U_2 \tag{4.5}$$

and

$$\tau_i = \frac{\rho f_i}{8} |U_1 - U_2| (U_1 - U_2) , \tag{4.6}$$

in which f_b and f_i are dimensionless Darcy-Weisbach friction factors for the bottom and interface. Note that the values of τ_b and τ_i may be positive or negative, depending on the direction of U_1 and U_2. The values of f_i, the interfacial friction factor, are determined using a Moody diagram for turbulent flow in smooth pipes. The value of f_i is thus a function of the Reynolds number calculated using

$$R_e = \frac{4\bar{u}z_2}{\nu_2} \tag{4.7}$$

where $\bar{u}$ is the average stream velocity, z_2 is the average lower layer depth, and ν_2 is the kinematic viscosity of the lower layer fluid.

The bottom friction factor, f_b, is determined from

$$S_e = \frac{f_b}{4R} \frac{\bar{u}^2}{2g} , \tag{4.8}$$

where R is the hydraulic radius, and S_e is the slope of energy grade line.

The hydraulic radius, R, is defined by

$$R = \frac{A_R}{W_p} , \tag{4.9}$$

in which A_R is the cross-sectional area of flow and W_p is the wetted perimeter. For example, if a river had a wide rectangular channel of width b_R and depth z_R, then $A_R = b_R z_R$ and W_p is $b_R + 2z_R$. If b_R is much greater than z_R (e.g., by a factor of 20), then R will be approximately equal to z_R.

The value of S_e can be obtained using the Manning formula defined in

$$\bar{u} = \frac{1.489}{n} (R)^{2/3} (S_e)^{1/2} , \tag{4.10}$$

in which n = Manning's roughness coefficient. Values of Manning's "n" can be obtained from various governmental agencies who are responsible for river control. Polk *et al.*[105] obtained values from the Tennessee Valley Authority (TVA) and the United States Corps of Engineers, based on flood slope studies. In addition, Chow[25] and Barnes[12] give examples of "n" along with pictures of the site. Equations 4.5 and 4.6 are substituted into Equation 4.2 to obtain the rate of change of the interface shown in

$$\frac{dz_2}{dx} = \frac{\frac{f_b}{8gz_2} |U_2| U_2 - \frac{f_i}{8gz_2} \frac{z_R}{z_R - z_2} |U_1 - U_2| (U_1 - U_2)}{\frac{\Delta\rho}{\rho} \left(F_2^2 + F_1^2 - 1 \right)} . \tag{4.11}$$

Equation 4.11 is the general equation for the interfacial slope in a two-layer stratified flow. The solution of this first-order differential equation requires one boundary condition. Physically, the depth and slope of the interface must be known at some location, called a control section. Frequently, a control section is taken at a point where the interface is assumed to change rapidly. The depth at such a point is called critical depth, z_c. Figure 4.3 shows four cases of critical depth control, where

$$\xi_c = z_c / z_R . \tag{4.12}$$

At the control sections shown, $dz_2/dx \to \infty$. Hence, the denominator in Eq. 4.11 must equal zero, as shown in (dividing through by $\Delta\rho/\rho$)

$$F_2^2 + F_1^2 - 1 = 0 . \tag{4.13}$$

Equation 4.11 can be integrated in a closed analytical form for certain cases or numerically integrated for all general cases. For the example in Fig. 4.3b, the arrested warm-water wedge, $U_1 = 0$. This allows for a closed analytical solution. Equation 4.13 is important, as it is the necessary equation for the determination of the critical depth, z_c.

B. Specific Examples of Wedges

Harleman[47] discusses five zones when analyzing the development of a warm-water wedge as shown in Fig. 4.1. Application to some of the zones will be made to indicate simplification of Eq. 4.13. In several of the cases, it will

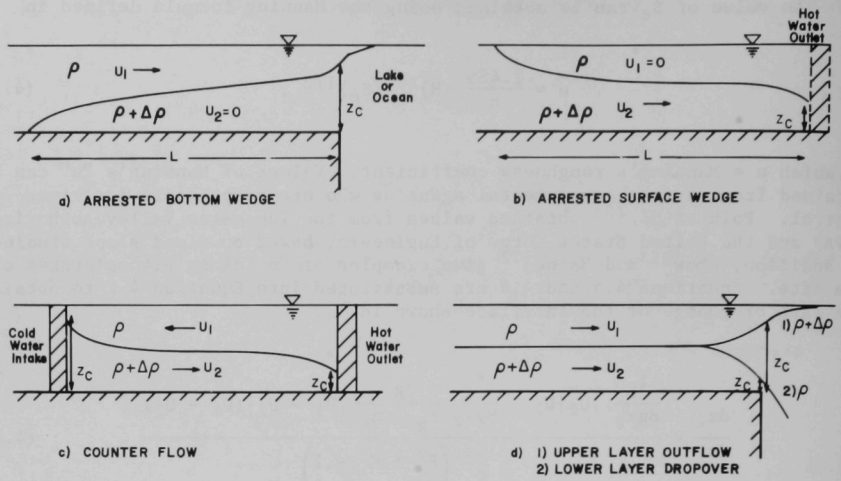

Fig. 4.3. Critical Flow Sections in Two-layer Flow.[52]

be assumed that the velocity in one layer is zero. This is not the real situation. However, for a steady-state condition to exist, the average velocity in that layer must be zero. A cell of circulating fluid caused by the moving layer is developed in the assumed stagnant layer. The interface acts as a moving boundary which prevents the formation of a steep vertical velocity gradient and entrainment of the ambient waters. Figure 4.4 clearly indicates this circulatory pattern in an arrested warm water edge, as shown in Fig. 4.3b.

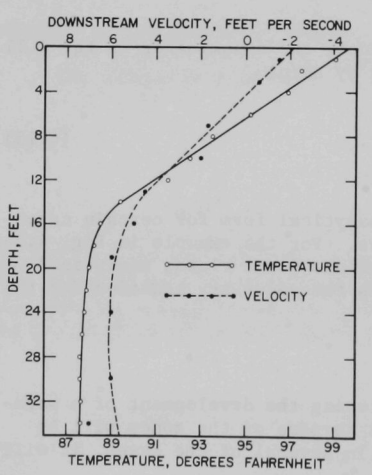

Fig. 4.4.

Vertical Temperature and Velocity Profile of Warrior River Mile 228.2 near Green County Steam Plant, 8/12/70.[105]

1. Condenser-water Discharge Channel, Zone B

One of the most important cases of wedges in present-day thermal-discharge analysis is that which occurs when a cold-water wedge intrudes into the discharge canal. In this case an analysis must be made of the actual depth and velocity at the point where the channel discharges into the receiving-water body. This depth and velocity are needed for the various surface-discharge models used in Chapter V.

a. General Formulation. The condenser-water discharge channel is shown in Fig. 4.5 with a cold-water intrusion. This is the same as an arrested bottom wedge, shown in Fig. 4.3a. The simplifying assumption is that $U_2 = 0$. Therefore, the equation for the slope of the interface is expressed by

$$\frac{dz_{2B}}{dx} = \frac{\dfrac{-f_i}{8gz_{2B}} \dfrac{z_o}{z_o - z_{2B}} U_{1B}^2}{\dfrac{\Delta\rho}{\rho}\left(F_{1B}^2 - 1\right)}$$

where z_o is the initial depth in the channel. With reference to Fig. 4.5, at the junction of the discharge channel and river, the condenser water undergoes a rapid expansion as it is spread laterally and longitudinally in the river. Hence, the critical section occurs at the junction. Referring to Eq. 4.13, then $(F_{1B})_c = 1$, which follows from the concept of rapid changing of the interface at the junction. The continuity equation is

$$U_o z_o = U_{1B} z_{1B} \ . \tag{4.15}$$

in which U_o and z_o are the velocity and depth in the discharge cannel upstream from the intruded river water. Hence, the upstream Froude number, F_o, can be related to F_1 by

$$F_{1B} = F_o \left(\frac{z_o}{z_o - z_{2B}}\right)^{3/2} , \tag{4.16}$$

in which

$$F_o = \frac{U_o}{\sqrt{g \dfrac{\Delta\rho}{\rho} z_o}} \ . \tag{4.17}$$

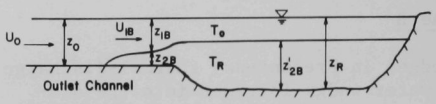

Fig. 4.5.

Cross Section along Centerline of Outlet Channel.[48]

Then, if $(F_{1B})_c$ is 1 at the junction, the depth of the upper layer is given by

$$\frac{z_o - (z_{2B})_c}{z_o} = F_o^{2/3} , \tag{4.18}$$

in which the depth $(z_{2B})_c = z_o - (z_{1B})_c$.

b. Numerical Example. Consider a thermal discharge of Q_o = 600 cfs into a discharge channel 100 ft wide by 15 ft deep. The temperature of the discharge water is 72.5°F with ρ_1 = 0.99768. The temperature of the receiving stream is 59°F with ρ_2 = 0.99913. Will there be a cold-water intrusion, and to what depth will the channel be reduced?

Use continuity to calculate the discharge velocity U_o:

$$U_o - Q_o/z_o b_o = 600/(15)(100) = 0.4 \text{ ft/sec} .$$

Calculate the channel densimetric Froude number using Eq. 4.17.

$$F_o = \frac{U_o}{\frac{\Delta\rho}{\rho} g z_o} = \frac{0.4}{\sqrt{(0.00145)(32.2)(15)}} = 0.48 .$$

The theoretical criterion for the development of a cold-water wedge is $F_o < 1$, as discussed in Chapter II. If $F_o > 1$, the wedge will be expelled from the channel and the jet will entrain ambient fluid and mixing will occur. However, if F_o is very small, the length of the cold-water wedge may be longer than the length of the discharge channel. Therefore, based on the above discussion, a cold-water wedge will intrude into the channel. Hence, using Eq. 4.18 to solve for the depth of $(z_{1B})_c$, we obtain

$$(z_{1B})_c = z_o F_o^{2/3} = 15(0.48)^{2/3} = 9.15 \text{ ft} .$$

The thickness of the cold-water wedge at the junction will be 15 - 9.15 = 5.85 ft. The velocity at the outlet would then become

$$(U_o)_c = \frac{Q_o}{(z_{1B})_c\ b_o} = \frac{600}{(9.15)(100)} = 0.656 \text{ ft/sec} .$$

The new depth, $(z_{1B})_c$, and velocity, $(U_o)_c$, can then be used as input to some appropriate surface-discharge model. If mixing is minimized at the outlet channel, then the same depth of the heated layer will occur in the river adjacent to the outlet channel. Equation 4.14 can be integrated numerically or in closed analytical form to give the interfacial profile.

2. Middle Region between Intake and Outlet, Zone C

a. General Formulation. The middle region is shown in Fig. 4.1 as Zone C. The specific assumption for the evaluation of Eq. 4.11 is that the mean velocity in the upper layer is equal to zero, or $U_1' = 0$. Therefore, $F_1 = 0$. Harleman[47] presents the following equation to evaluate the warm-water wedge in the middle zone:

$$\frac{dz_2'}{dx} = \frac{\dfrac{(U_2')^2}{8gz_2'} f_b' + f_i' \dfrac{z_R}{z_R - z_2'}}{\dfrac{\Delta\rho}{\rho}\left[(F_2)^2 - 1\right]} , \tag{4.19}$$

in which the primes denote Zone C.

With reference to Eq. 4.13, the critical control section will occur at $(F_2')_c = 1$. If $F_2 < 1$, the slope of the interface will be negative. Wigh[143] concluded that there will be no intrusion of a warm-water wedge in the region upstream of the outlet if the Froude number, F_a, of region upstream of the wedge is > 1. The Froude number is calculated using

$$F_a = \frac{Q_R - Q_o}{b_R\sqrt{g\,\dfrac{\Delta\rho}{\rho}\,z_R^3}}$$

where Q_R is the river discharge, Q_o is the condenser-water discharge, and b_R is the average width of the river.

Keulegan[69] showed that for salt wedges under flowing fresh water, the critical value of the densimetric Froude number is approximately 0.75. Harleman[47] states that in practice the value need only be greater than 0.7 to be effective in preventing upstream intrusion of the warm water-wedge in the middle region. Polk *et al.*[105] illustrated that for values of $F_a < 0.4$, the choice of critical calues of F_a is irrelevant. Bata[13] presents a normalized curve of x/L vs. $z_1/(z_1)_c$ for the control section occurring at the outlet. This plot is shown in Fig. 4.6, where L is the length of the

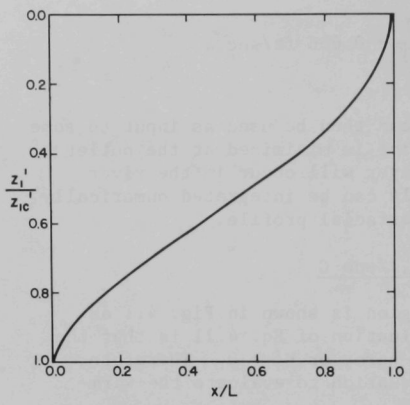

Fig. 4.6.

Relative Shape of Warm-water Wedge for No Recirculation.[13]

warm-water wedge and x is the distance upstream to some section where z_1' is the depth of the upper layer. The value of $(z_1')_c$ is found using

$$(z_1')_c = z_R F_a^{2/3}. \tag{4.21}$$

b. Numerical Example. Consider the previous example to be discharging into a river with an average width of 300 ft and an average depth of 25 ft. The flow is 6000 cfs. Will there be an upstream wedge? Using Eq. 4.20, calculate F_a:

$$F_a = \frac{Q_R - Q_o}{b_R \frac{\Delta\rho}{\rho} g z_R^3} = \frac{6000 - 600}{300\sqrt{0.00145(32.2)(25)^3}} = 0.667 < 0.75 .$$

Therefore, there will be a wedge upstream. Calculate the river flow for no wedge formation:

$$Q_R - Q_o = 0.7(300)\sqrt{(0.00145)(32.2)(25)^3} = 5660 \text{ cfs} .$$

Hence, $Q_R = 5660 + 600 = 6260$ cfs. Since $F_o < 0.75$, the theory predicts an upstream wedge, but it will be very short. The depth of warm water at the outlet will be 9.15 ft, as shown previously. Therefore, the ratio $z_1'/z_R = 9.15/25 = 0.366$. Using Eq. 4.21, calculate the critical depth ratio:

$$(z_1')_c/z_R = F_a^{2/3} = (0.667)^{2/3} - 0.764 ;$$

$$(z_1')_c = 0.764(25) = 19.1 \text{ ft} .$$

The value of L/z_R may be found by using the integrated form of Eq. 4.19, as shown by Polk *et al.*[105] in Fig. 4.7, using the critical F_a as 0.75, and for illustration using $f_b = 0.034$ and $f_i = 0.0068$. From Fig. 4.7, a relative value of L/z_R for $F_a = 0.667$ is 5. For other values of f_b and f_i, the relative lengths may be found by integrating Eq. 4.19 from some control section as a function of F_a. Therefore, the length, L, from some control section will be 125 ft. However, the depth ratio, $z_1'/(z_1')_c$, at the outlet channel is 9.15/19.1 = 0.479. So, by entering Fig. 4.6, we see that the outlet channel is already effectively located at x = 0.61 from some fictitious control section. Hence, the wedge upstream will only be 0.4L upstream from the outlet channel, or 0.4(125) = 50 ft.

As a further example, consider the discharge from the same power plant to be $Q_o = 1300$ cfs, and Q_R has decreased to 5000 cfs. Using the continuity relationship to evaluate U_o, one can then use Eq. 4.17 to calculate the discharge-channel Froude number, F_o, as follows:

$$U_o = 1300/(15)(100) = 0.867 \text{ ft/sec} ;$$

$$F_o = \frac{0.867}{\sqrt{0.00145(32.2)(15)}} = 1.03 > 1 .$$

Therefore, there will be no cold-wedge intrusion. Also, assume no mixing takes place at the outlet.

The Froude number for the river will be

$$F_a = \frac{5000 - 1300}{300\sqrt{0.00145(32.2)(25)^3}} = 0.46 < 0.75 .$$

There will be a warm-water-wedge intrusion upstream. From Eq. 4.21, the critical depth ratio is

$$(z_1')_c/z_R = F_o^{2/3} = (0.46)^{2/3} = 0.596 .$$

Also,

$$(z_1')/z_R = 15.0/25.0 = 0.600 > 0.596 .$$

Hence, the critical section will be at the outlet. Therefore, enter Fig. 4.7 for these given sets of conditions when $F_a = 0.46$ and $L/z_R = 40$. Therefore, the length of the wedge will be 1000 ft. Figure 4.6 can be used to plot the profile from the discharge channel to the end of the warm-water wedge. If the depth ratio of discharge depth to river depth, z_1'/z_R, is greater than the ratio $(z_1')_c/z_R$, it may be assumed that the discharge will go through critical depth at the junction.

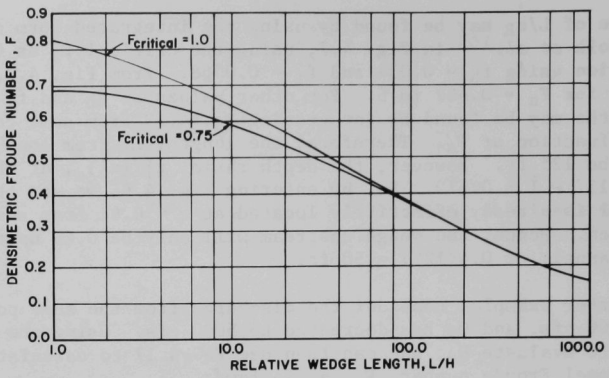

Fig. 4.7. Variation in Relative Wedge Length with Densimetric Froude Number.[105]

Another important consideration is the recirculation of heated waters. If the wedge should extend upstream past the intake structure, there exists the possibility of recirculating, or taking into the plant, heated water from the warm-water wedge. Harleman[47] presents design considerations for a skimmer wall to avoid recirculation and develops the continuation of the wedge upstream of the intake canal.

C. Summary and Conclusions

Due to recent temperature regulations, the technique of layering the warm water on the surface of a receiving body is limited in its scope of application. However, it is still being considered in evaluating the thermal impact of heated discharges on the environment as an alternative to other methods of discharge. It is also important in determining the actual velocity and depth of a surface discharge for low densimetric Froude numbers.

The analytical tools are available and have been experimentally verified. Polk *et al.*[105] presented field data from four southeastern plants to verify the models of Bata[13] and Harleman.[46] However, Polk *et al.* noted that some mixing did occur that precluded using the condenser discharge temperature. The average temperatures of the wedge were calculated using that portion of the vertical temperature profile above the depth that indicated an average velocity of zero in the upper layer. However, no attempt was made to formulate a general model to describe the amount of temperature decrease observed at the different sites. Edinger and Yanogida[36] proposed heat-balance equations at the discharge to be used in conjunction with the stratified flow equation to account for downstream advection of the heat plus a loss due to surface cooling from the warm-water wedge.

V. SURFACE DISCHARGES OF HEATED WATER

A. Introduction

One of the most common means of disposing of heated waters is to discharge them to the receiving-water body by a surface channel or canal or some closed conduit discharging at the water surface. Most older plants use this disposal method. Many new ones still use this method primarily because it is the least expensive alternative for disposal of the waste heat generated in the power process. This chapter reviews the principles on which most commonly used models for predicting the effects of heated discharges are based, the assumptions that have been made and their development, the information needed to use the models, limitations or questions concerning the models, and some examples of application. In addition, comments will be made concerning the verification evidence that exists for the models.

No attempt will be made in this chapter to present the complete details of any model. Several references exist, including those by Parker and Krenkel[99,100] and Policastro and Tokar,[104] which give details on several available models. In addition, reference will be made to the more specific reports available for the models discussed. The work by Policastro and Tokar is especially significant since it takes 12 current models and discusses them all in a common format. This study is currently being extended at Argonne National Laboratory, and reports will be issued comparing the results obtained by use of the several models. The reader should be especially alert to the issuance of these reports as they should begin to provide real information as to the validity of the results obtained from the given models. Therefore, the emphasis in this chapter will be placed upon a review of the general principles and physical reasoning for the models. Sufficient description will be provided to enable the reader to decide whether to obtain the detailed version of the model development.

Before any discussion of specific models ensues, several phenomena common to surface discharges (and in some instances to submerged discharges) should be discussed. The following paragraphs review these points and clarify the distinctions.

1. Entrainment versus Diffusion Concept

Two words frequently seen in a discussion of surface discharges are "entrainment" and "diffusion." Both relate to the mixing of ambient water into the discharge as it moves into the ambient body. When heated water is discharged into a receiving stream or lake, it gathers into itself fluid from the surrounding water body as it moves. The entrainment and diffusion concepts are two commonly used means of trying to express the rate at which this mixing occurs. Although they will frequently be presented as entirely separate modes of mixing, it should be clear that both are closely related.

Entrainment can be considered to be caused by the eddies generated due to shear caused by one fluid stream being introduced into another fluid stream with a vector-velocity difference. This means that the two fluid streams have different velocities and/or are at an angle to one another. The magnitude

of the shearing stresses, i.e., the eddying and the mixing, will increase with increasing vector-velocity differences.

As an example, consider a discharge such that the initial discharge velocity, U_o, equals the ambient velocity, U_a. If this discharge is parallel to the ambient stream, it should move smoothly into the main stream. Here, the vector-velocity difference is zero. If, on the other hand, the discharge is at 90° to the main flow, one can visualize considerable interaction between the two streams. In this case, the vector-velocity difference is U_o. One can also visualize enhanced mixing by discharging parallel to the ambient current, but at a speed quite different from that of the ambient current.

The entrainment expression for mixing is based upon the premise by Morton *et al.*[92] that such mixing into the plume should be proportional to some characteristic local velocity. Early studies were for jets discharged into a stagnant environment, and, typically, the centerline velocity of the plume at any given location was chosen as the representative velocity. In this scheme, one could consider a fictitious entrainment velocity, v_i. An expression for this is

$$v_i = EU, \tag{5.1}$$

in which E = coefficient of proportionality, called entrainment coefficient, and U = jet centerline velocity. Hence, the rate of change of mass flow past a given section of the plume can be expressed as this inflow velocity, v_i, times the circumferential area available for this entrainment. Initial jet studies considered circular jets; the circumferential area was $2\pi bds$, where b is the representative radius and ds is the incremental length along the jet axis. The expression for the change of mass flux along the centerline axis (the s axis) of the plume can then be expressed as

$$\frac{dQ}{ds} = 2\pi bEU, \tag{5.2}$$

in which Q = volume flow rate past given section of jet.

The entrainment concept has been extended by Fan[38] and others to the case of a jet discharged into a flowing ambient environment. In this case, rather than using the centerline velocity, U, it is chosen to represent the key velocity as some form of difference between the centerline velocity and a corresponding ambient velocity component. Again, for a round submerged jet, Fan has modified the continuity equation by replacing U by $|U_j - U_a|$, in which the velocity-difference expression is a vector difference. Other authors, as noted later, have chosen different expressions.

Figure 5.1 illustrates a typical portion of a plume and the entrainment of fluid into that plume. Equation 5.2 needs to be modified for a surface discharge, especially one of a non-circular section, to reflect the geometry of that discharge form. For example, for a rectangular discharge, the entrainment laterally into the plume would occur over a rectangular area along the

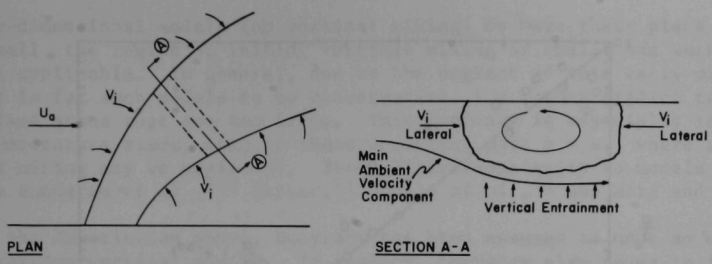

Fig. 5.1. Entrainment of Fluid.

sides of the plume. There would, in addition, under appropriate circumstances, be entrainment across the bottom of the discharge plume. This would ordinarily proceed at a reduced rate due to the density gradient inhibiting mixing. As mentioned in Chapter II, a densimetric Froude number for the plume can be evaluated at a local point as shown in

$$F_L = \frac{\overline{U}}{\sqrt{g \frac{\Delta\rho}{\rho} z_L}} , \tag{5.3}$$

in which z_L is the depth of heated layer at the section of interest and $\overline{U}$ is the average plume velocity at the given location.

This local densimetric Froude number, F_L, is often replaced in the literature by the bulk Richardson number, R_i, which equals $1/F_L{}^2$, or

$$R_i = \frac{g \frac{\Delta\rho}{\rho} z_L}{\overline{U}^{\,2}} . \tag{5.4}$$

Ellison and Turner[37] performed experimental work to define the relationship between vertical entrainment and R_i. Their results showed that vertical entrainment was essentially zero for R_i greater than about 0.8 (F_L less than about 1.1). Figure 5.2 shows the results obtained by Ellison and Turner expressing this degree of entrainment, with a mathematical expression fitted to the data by Stolzenbach and Harleman.[131] In this figure, α = E, the entrainment coefficient, and α_0 = the entrainment coefficient with no buoyancy effect.

Figure 5.1 illustrates another important phase of the mixing process, which is in addition to the *simple gathering in of fluid by shearing action.* If an ambient current exists, it will attempt to separate around the jet, much as around a solid body. As shown in Fig. 5.1, this crosscurrent will generate a vortex acting laterally in the jet, a feature that enhances mixing. The strength of the vortex depends on the value of U_a, the ambient velocity.

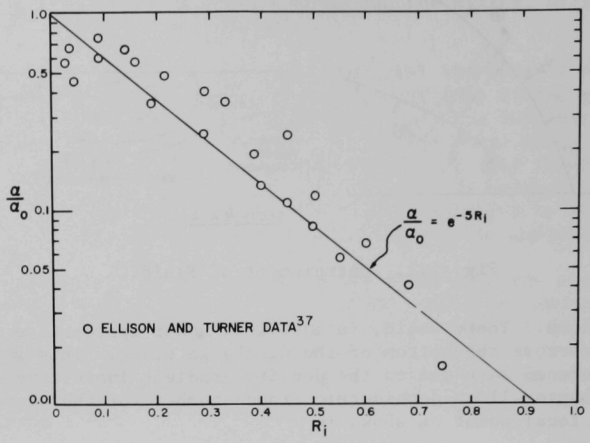

Fig. 5.2. Reduction of Entrainment as a Function of Richardson Number.[131]

Consider the development of a typical plume, reviewing the variation in F_L and vertical entrainment along the plume. Figure 5.3 is adapted from the report by Sundaram *et al.*[133], although others have used a similar plume description. If the initial densimetric Froude number, F_j, is greater than 1.1, some vertical mixing will occur since inertial forces are greater than bouyant forces. Since both lateral and vertical spreading occur, there is a reduction in the velocity and temperature of the heated plume and an increase in z_L. In this early region, the changes in velocity and z_L often dominate. A review of Eq. 5.3 reveals that this will cause F_L to decrease, eventually possibly becoming 1.1 or less. Then vertical mixing will be essentially zero, and the plume will only spread laterally. This region is assumed to begin at $s = s_1$ along the plume axis. If F_j is less than 1.1, then s will correspond with the actual outfall. In this region, z_L is assumed reasonably constant due to the reduced vertical mixing. As the plume spreads laterally, the velocity will decrease and $\Delta\rho/\rho$ will approach zero. Eventually, at about $s = s_2$, the value of F_L will then rise until it once again becomes greater than 1.1. Physically, the temperature has decreased to the point at which the vertical gradient is no longer adequate to prevent mixing. This description implies

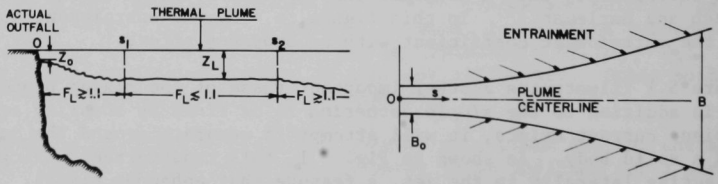

Fig. 5.3. Schematic View of Thermal Plume.[133]

that two-dimensional models (no vertical mixing) do have their place. If F_j is small, the region of initial vertical mixing is small, and such models are more applicable. In general, due to the neglect of this early mixing, the tendency is for such models to be conservative; i.e., they predict temperatures and surface areas that are too large. This tendency is especially large for lower-temperature rises, such as those occurring past $s = s_2$, where substantial vertical mixing may be neglected. These limitations apply to models such as those by Sundaram *et al.*,[133] Carter,[21] Hoopes *et al.*,[59] and Motz and Benedict.[94]

In the description above, buoyancy has been assumed to have an effect only on suppressing vertical mixing. In reality, buoyancy also tends to induce lateral spreading of the plume as it tries to "ride up" over the colder ambient waters. Stolzenbach and Harleman[131] discuss this effect, calling the region roughly corresponding to that between s_1 and s_2 the stable region. They note that the buoyant spreading laterally will cause the plume depth to continually decrease in this stable region. No one is yet certain whether this is drastically affected by existence of a strong crosscurrent.

In discussing inhibition of vertical mixing by density gradients, one should not forget that the gradient may be a naturally occurring one. For example, if the receiving body is a stratified lake, the thermocline region may act similarly to a solid bottom boundary.

The diffusion concept is based on a Fickian model for molecular diffusion of a material. The general form for the rate of such diffusive motion is

$$v_i = D_{x_i}\, dc/dx_i \ , \tag{5.5}$$

where D_{x_i} = the diffusion coefficient in the x_i direction,

c = concentration of the material under discussion,

x_i = coordinate axis of interest, and

v_i = inflow velocity.

This inflow velocity is a fictitious velocity in the same vein as the entrainment velocity introduced earlier. In the same fashion, the flow into the plume as it moved downstream could be estimated by taking this inflow velocity at a given point and multiplying it by the area across which this exchange would be taking place. Ordinarily, this area would be a plane perpendicular to the x_i axis. That is, if we are concerned with diffusion in the lateral or y direction, it would be across the plane parallel to the xz plane.

The Fickian law arises from the transport of material by purely random molecular movement, i.e., molecular diffusion. However, the use of this relation for turbulent flow is based on the assumption that transport due to turbulent velocity fluctuations can be lumped into the diffusion coefficient, D_{x_i}. The intensity of these turbulent fluctuations is expected to increase for larger vector-velocity differences between the plume and the ambient current.

There are several means for estimating values for diffusion coefficients due to natural turbulence. In lakes and oceans, the "four-thirds" law is commonly accepted. Wiegel[142] and Harleman[46] discuss this relationship, generally expressed in

$$D_{x_i} = \kappa L_s^{4/3} , \tag{5.6}$$

in which κ is a constant and L_s is the characteristic length of the phenomenon.

L_s is frequently taken as the plume width for lateral diffusion from a waste-water plume. Physically, this relation states that mixing rates get more intense as the size of the plume increases. This is because larger-scale turbulence (eddies) can attack the plume as it grows larger. Wiegel[142] notes that one can visualize this increase in diffusion rate by reviewing the separation of two particles initially close together. As the distance between these particles increases, the rate at which they separate also increases. Apparently when the particles are close together they move apart by the action of small-scale turbulence, occurring at rates small when compared to the mean flow velocity. As the distance between the particles grows, each particle may be swept up in separate larger eddies and move away from the other more rapidly. This process continues until the eddy sizes are limited by the physical bounds of the system.

In rivers, a slightly different relationship is commonly used, although the bounding scale of the physical channel still appears:

$$D_{x_i} = C_{x_i} H u_* , \tag{5.7}$$

where C_{x_i} = coefficient,

H = total river depth,

u_* = friction velocity = $\sqrt{gRS_e}$,

R = hydraulic radius (see Eq. 4.9), and

S_e = energy slope (see Eq. 4.8).

(See Refs. 99 and 100 for added information on this topic.)

There are numerous discussions of the use of the Fickian model for diffusion. Probably the simplest presentation is that by Holley,[57] which provides more insight into the occurrence of this diffusion term in the basic mass-transport equation.

2. Jet Models and Diffusion Models

The diffusion and entrainment concepts presented are means that various investigators have used to make the problem of mixing or diultion more tractable.

Models that are derived based on the entrainment mechanism are frequently called jet models. Those models based on the diffusion concept of mixing are

called diffusion models. In addition, the term "jet model" has another connotation relating to the area or the region of usefulness of the model. If the discharge occurs at an angle to the ambient flow and/or at a different velocity from the ambient velocity, then the trajectory of the heated discharge plume may vary significantly from the direction of the ambient flow. In this case, one must write a complete system of equations to describe not only the trajectory of the jet, but also the dilution that occurs along the plume. These equations would include the following: the momentum equation, often resolved into two axial components, the x and y components, and a third component if it is a three-dimensional model; the conservation-of-mass equation written along the plume; an equation expressing the conservation of heat, which may include the term for the interchange of heat energy across the air-water interface; and some geometry equations. Examples of these equations will be seen when specific models are presented later in this chapter. This system of equations must usually be solved by numerical means on the computer and results in a prediction of the trajectory of the jet, the size of the plume at any given point, both vertically and laterally, the velocity in the plume at any point, and the rate at which dilution occurs as one moves along the plume axis.

If the discharge is either parallel to the ambient fluid and/or at a much lower velocity than the ambient current, the plume will be swept immediately downstream. For this case, a diffusion model is frequently used, although it should be more properly restricted to the regions in which the heated discharge is simply following the motion of the ambient current. This latter case occurs either by having a discharge parallel to the ambient flow and at the same velocity or by going to the far-field region. In either case, the following equation[33] is the typical form of diffusion equation that must be solved:

$$\frac{\partial c}{\partial t} + u\frac{\partial c}{\partial x} + v\frac{\partial c}{\partial y} + w\frac{\partial c}{\partial z} = \frac{\partial}{\partial x}\left(D_x\frac{\partial c}{\partial x}\right) + \frac{\partial}{\partial v}\left(D_y\frac{\partial c}{\partial y}\right) + \frac{\partial}{\partial z}\left(D_z\frac{\partial c}{\partial z}\right) + \frac{h}{\rho c_p}, \tag{5.8}$$

where c is the concentration per unit mass (or, in the case of heat, the temperature rise); u, v, and w the longitudinal, lateral, and vertical velocity components at a point x, y, z at time t; D_x, D_y, and D_z, the longitudinal, lateral, and vertical diffusion coefficients at a point and for a given time; and h, an internal sink or source term giving the rate at which heat enters or leaves the unit mass such as from attenuation of short-wave radiation below the water surface.

This equation is developed in simplified form in Ref. 57. Note that this diffusion equation is only an equation for conservation of the particular property (in this case, heat) under consideration. It represents a balance between (a) the sum of the change of storage of heat in a given volume and the heat advected into that volume and (b) the sum of the heat diffused out of, and the heat lost to, the atmosphere from that same volume. The velocity field is assumed to be known and not coupled with the temperature field. In similar fashion, the continuity equation and the geometry equations are bypassed. A model based on the diffusion equation is most appropriate in the far-field

regions. There are, however, several models currently in use that try to employ this principle in the near-field region.

One concept that is important in the entrainment mechanism for mixing is that entrainment goes to zero if there is no vector difference in the velocities. Many of the models assume a constant entrainment coefficient along the length of the plume. Actually, even if the discharge occurred into a stream with the same speed and in the same direction as the discharge, there would still be mixing that would occur due to turbulent diffusion. For this reason, especially in those models assuming a constant entrainment coefficient, there is a tendency to underestimate the mixing that occurs as the jet velocity approaches the ambient velocity. This underestimation yields high temperatures and greater effected surface areas. This factor should be kept in mind for attempting to extend any jet model too far downstream.

Earlier authors have related diffusion to a type of expression based on velocity differences for free turbulent jets. Hence, where velocity differences do exist, both models are expressing the same phenomenon but in a different form. However, where vector velocity differences do not exist, one still expects mass transfer to take place due to the turbulent-velocity fluctuations in the ambient fluid. Therefore, the diffusion model should be more applicable to these regions. The entrainment model, on the other hand, would not be valid as it would imply a zero change in flow rate. If a diffusion model is fitted to laboratory or field data, which include regions of early jet mixing, the diffusion coefficients thus obtained would exceed those attributed to natural turbulent diffusion. This would be true because they would also have to include the mixing effects generated by the shearing or jet action.

In summary, if one is interested in the trajectory of the heated discharge, a system using a jet model is required. If one is interested in the far-field region or if the near-field region is such that the discharge is not significantly different from the ambient motion, then a diffusion model may be appropriate. The limitations of using a jet model in the far-field or a diffusion model in the near-field region must be understood. Additional very helpful comments on this topic can be found in Refs. 99, 100, and 104.

3. Zone of Flow Establishment

a. General. Figure 5.4 is taken essentially from Ref. 5, which contains an excellent discussion on the entrainment process. If the velocity at the orifice is assumed uniform across the orifice, then a velocity discontinuity exists between the jet and the fluid around it. "The eddies generated in this region of high shear will immediately result in a lateral mixing process which progresses both inward and outward with distance from the efflux section." (Ref. 5, pp. 640-641.) Essentially, the fluid in the jet is being decelerated, while the surrounding fluid is gathered in or entrained by the jet and hence is accelerated. As this lateral and vertical mixing into the jet occurs, the region of constant velocity in the center region of the jet continues to decrease. When mixing just penetrates to the centerline of the jet, only the centerline velocity is the same as that at the point of efflux. The velocity decreases laterally from the centerline, gradually approaching the ambient velocity, as shown in Fig. 5.4. The flow is then called "established flow." The initial transition zone needed to attain this established condition is called the "zone of flow establishment." In many parts of this report, the

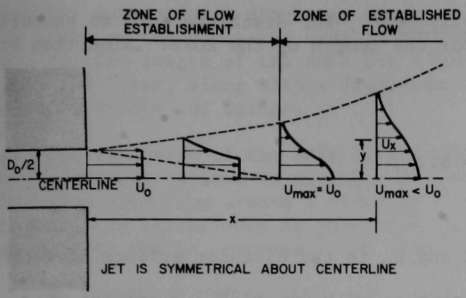

Fig. 5.4.

Definition Sketch for Zone of Flow Establishment.

designation ZOFE will be used for this zone. The end of the ZOFE is not a distinct point, inasmuch as the flow is turbulent and fluctuations exist. However, current practice treats this as a sharply defined point. This simplifies modeling considerably.

The concepts presented in this report apply equally well to submerged or surface jets of any shape -- round, slot, or other. In any case, one might well ask why the zone of flow establishment is important.

b. Similarity of Profiles. Albertson[5] and earlier workers on jets into a stagnant environment indicated that lateral velocity profiles in a jet were similar after the ZOFE was ended. This means that the shape of the distribution at each transverse section took the same mathematical form. This form was frequently found to be the Gaussian or normal-distribution curve, such that, for example,

$$\frac{U_\eta}{U} = \exp(-\eta^2/2\sigma^2) \ , \tag{5.9}$$

where U_η = velocity at distance η from the jet centerline,

U = velocity at jet centerline,

σ = standard deviation of Gaussian curve, and

η = lateral distance from jet centerline.

As will be seen later, the ability to assume similar profiles of velocities and other properties simplifies the analytical treatment of jet flows. For this reason, many jet models are only valid *from* the end of the ZOFE, as the profiles inside the ZOFE are not similar. Therefore, some means must be developed to handle the ZOFE. Most models have treated this zone in a purely empirical fashion.[38,94] Available data on the length of the zone and the angle of the jet at the end of the zone are used to provide a starting point for the model. Other recent models, including those by Hirst[54] and Stolzenbach,[129] write the appropriate equations and solve directly from the point of efflux, the ZOFE being solved for within the model. Either approach has merit, but the important thing to recognize is the need to treat the ZOFE distinctly from the zone of established flow, due to the lack of similar profiles in the former.

c. Length of Zone of Flow Establishment. For discharge into an essentially quiescent fluid, one can use Ref. 5 for the length of the ZOFE. Albertson *et al.* found that

$$\frac{s_e}{D_o} = 6.2 \ , \tag{5.10}$$

in which s_e is the length of the ZOFE and D_o is the circular orifice diameter.

Data by Reynolds[114] and also by Parker and Krenkel[100] (p. VII-33) show s_e/D_o from nine sets of data on three-dimensional jets into a stagnant environment. The lengths shown range between 5.3 and 6.6 diameters. Hence, the value $s_e = 6.2D_o$ is adequate for a round jet into a stagnant environment. Fan[38] has recommended this value also for inclined buoyant jets, assuming that buoyant forces play a minor role in these early stages of the jet.

Albertson *et al.*[5] also gave data for slot jets, indicating

$$s_e/B_o = 5.2, \tag{5.11}$$

in which B_o is the width of the slot jet. This would be an appropriate number to use for a rectangular channel discharge into a stagnant environment.

One factor shown to have a major impact on the length of the ZOFE is k, the velocity ratio. Fan[38] has discussed results obtained by Gördier,[44] Jordinson,[66] and Keffer and Baines[67] for nonbuoyant jets in a cross stream. Fan uses Gordier's data, as shown below, and assumes it is also valid for the buoyant case, finding (for a jet issuing at 90° to the main flow):

$$\beta_o = 90° - \frac{110°}{k} \tag{5.12}$$

and

$$\frac{s_e}{D_o} = 6.2e^{-3.32/k} \ , \tag{5.13}$$

in which s_e is the length of the ZOFE and β_o is the angle of jet inclination at the end of the ZOFE. Note that s_e approaches the $6.2D_o$ from Albertson's work for 1/k approaching zero.

Pratte and Baines[106] have also studied the zone of flow establishment. For k equal to 3 or 4 (typical values for a discharge canal), s_e/D_o is 3 or less. They found that for discharges into streams where k approaches 1-2,

possible values for a discharge canal on a river, the zone length would approach the order of the discharge width. Motz and Benedict[94] also present laboratory data for the length of the ZOFE for a heated surface jet. The data will be presented later, along with a discussion of their model. It follows the trends noted by Pratte and Baines.

The reduction of the ZOFE length with decreasing k illustrates the effect of the ambient current in mixing. As the ambient current moves around the jet (somewhat like flow around a circular cylinder), a vortex motion in the lateral direction is established as indicated in Fig. 5.1. This increases mixing and, among other things, decreases the length of the ZOFE.

d. Angle at End of ZOFE. The systems of equations for the various jet models must have a set of initial conditions framed at the beginning of the region, where similar profiles are assumed to exist. This means that one must know the angle the jet makes with the ambient velocity at the end of the ZOFE for those models not solving directly for the ZOFE. For surface discharges, Motz and Benedict[94] have provided laboratory data for $1.3 \leq k \leq 5.2$. This too will be presented during the discussion of their model. As an example of the results, a jet discharging initially at 90° to the ambient velocity was found to be at an angle of about 50° at the end of the ZOFE for k = 2.0. Thus, a substantial deflection of the jet can occur in the very brief ZOFE.

For submerged jets into a stagnant environment, it is usually assumed that the angle at the end of the ZOFE equals the discharge angle. This is based on the premise that buoyant forces are small in this short early region.

e. Notation at Orifice and End of ZOFE. Confusion is frequent when one reads about and/or discusses the "origin" of a heated discharge. Does this imply the more practical physical origin or the more theoretical origin of some models at the end of the ZOFE? To present some consistency in this report, the following notation will be adopted: the subscript zero plus a prime implies the physical origin; the subscript zero only implies the end of the ZOFE. For example, β_0' is the angle at the point of efflux and β_0 is the angle at the end of the ZOFE. In the numerical example cited in Sec. d above, $\beta_0' = 90°$ and $\beta_0 = 50°$. A graphical example of the use of this notation is shown in Fig. 5.5.

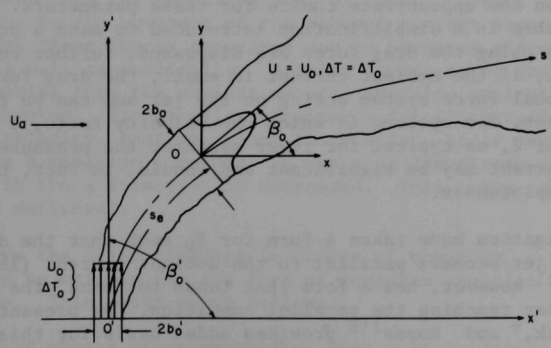

Fig. 5.5. Zone of Flow Establishment.[94]

4. Pressure Difference across Jet

If one refers again to the solid-body analogy suggested for the consideration of an ambient current flowing around the jet, it becomes obvious that an additional factor should be included. When flow occurs around the solid body, a pressure drag force is created. As the flow separates around the body, the pressure on the upstream side of the body is greater than that on the downstream side, resulting in a net force in the downstream direction. The same phenomenon can be seen to occur with jet discharges into a flowing ambient environment.

Fan[38] introduced one means of handling this pressure drag. Motz and Benedict[94] built on Fan's approach, as did Carter.[21] In this approach, the solid-body analogy is continued to write an expression for a drag force acting on the jet in the same fashion that one would write a drag-force equation for a solid body. The general form used is

$$F_d = \frac{\rho U_C^2}{2} C_d A_c \ , \tag{5.14}$$

where F_d = drag force due to pressure differences,

ρ = fluid mass density,

U_C = characteristic velocity component,

C_d = drag coefficient, and

A_c = characteristic area subjected to ambient flow.

Introduction of this formulation brings a new empirical parameter, C_d, into the picture. Unless this coefficient can be determined from basic theoretical considerations, empirical data must be gathered to evaluate and make the model useful.

Policastro and Tokar[104] discuss the forms taken by different investigators for the characteristic area and characteristic velocity. There is some difference of opinion on the appropriate choice for these parameters. Generally, however, any of them is a simplification introduced to make a problem tractable. When those models using the drag force are discussed, further comments may be made. In general, if the ambient current is small, the drag force is a small portion of the total force system acting on the jet and can be reasonably neglected. However, for systems in which the velocity ratio, $k = U_o/U_a$, might be on the order of 2, as typical for river systems, the pressure difference due to the ambient current may be significant and should, in fact, be included in the model for completeness.

Most investigators have taken a form for F_D such that the drag term goes to zero when the jet becomes parallel to the ambient current (local angle $\beta = 0$). Carter,[21] however, has a form that tends to "bend" the jet back toward the near wall after reaching the parallel condition. He presents data indicating such "bending back," and Rouse[118] provides added basis for this phenomenon. Added work is needed to define the conditions under which this "bending back" occurs. It may be a function of z_o/H, the ratio of discharge-channel depth to receiving-water depth.

5. Inclusion of Buoyancy Effects on Models

A lighter fluid discharged into a heavier receiving medium tends to ride up over the surface due to the density difference. The velocities induced by these buoyancy effects should be included in a complete model of the jet discharge action. Policastro and Tokar[104] indicate that only two current models, those by Stolzenbach and Harleman[131] and by Wada,[139] include the effects of buoyancy. Several others imply partial buoyant effects, only to the extent that they assume that buoyancy prevents vertical entrainment. As noted earlier in this chapter, vertical entrainment is a function of the local densimetric Froude number, F_L, and ceases for $F_L < 1.1$ In this report, only the Stolzenbach-Harleman model will be discussed in depth.

Stolzenbach and Harleman incorporate the effects of buoyancy into their model in the pressure-gradient terms in the equation of motion. In addition, a particular form of the velocity structure of the later convective buoyant spreading is assumed. Stolzenbach and Harleman, in addition, include the effect of buoyancy in the reduction of vertical entrainment using the results of Ellison and Turner.[37]

The current status of modeling is such that few models incorporate buoyancy effects directly. Those that do, in fact, have not yet been tested adequately to determine the sensitivity of the model to the assumptions made to incorporate these effects. Considerable work remains to be done on this aspect of the heated-discharge problem.

6. General Comments on Formulation of Momentum Equations

The momentum equation is simply a statement of Newton's second law. That is, the rate of change in momentum is equal to the sum of the forces imposed on the system. If one reviews the items about heated discharges discussed to this point, a general idea can be gained of the form these momentum equations might be expected to take for the jet models. In most current models, a momentum equation is broken into components along the major Cartesian coordinate axes (the x, y, and z axes). This is done for convenience. Briefly, several physical phenomena are contributing to the change of momentum of a heated discharge as it moves into the receiving body of water. First, there is the pressure drag due to the movement of the ambient current around the jet itself. Second, there are those forces generated due to buoyancy effects acting on the jet laterally as well as vertically. A third item causing change is the fact that the jet, moving into the ambient waters, entrains ambient fluid, which itself has a momentum. For example, consider a jet discharged initially at 90° to the ambient velocity, that is, along the y axis. As it entrains ambient fluid, which has a momentum component in the x or downstream direction, the jet's momentum in the x direction is increased. This means essentially that the jet will be deflected.

If one views the major elements in change of momentum, a qualitative expression could be written for the form of momentum equation expected for a heated discharge. This would be as follows:

$$\begin{aligned}&\text{Rate of change of momentum flux over a given distance}\\&\quad = \text{Force due to pressure drag}\\&+ \text{Force due to buoyant effects} + \text{Entrained momentum forces.}\end{aligned} \tag{5.15}$$

The momentum equations for surface discharges as well as for submerged discharges will all have this general form. Viewing the equations from this physical standpoint will avoid the initial tendency to get lost in the mass of mathematical formulations.

7. Comments on Choice of Similar Profiles

The choice of similar temperature and/or velocity profiles in transverse sections simplifies the mathematical solution of the jet problem considerably. The Gaussian profile is frequently chosen. Another profile is the so-called "tophat" or uniform profile. In this, the particular property is a constant throughout the cross section of the jet and at the edge drops immediately back to the ambient value. Morton[91] points out that the effect of assuming similar profiles and the form of the inflow velocity is to suppress analytic solution of the details of the lateral structure of the jet. Therefore, any reasonable profile shape can be assumed, for once similar profiles are assumed, any such choice suppresses detail.

The general effect of choosing different similar profiles is to introduce different constants into the basic equations. Therefore, the actual numerical value of the empirical coefficients, especially the entrainment coefficient, will be different for different similar profiles. However, especially for small ambient currents, the choice of different similar profiles will make little difference in the overall rate of temperature decrease predicted by the model. Reference 92 verifies this for a plume in a stagnant environment. However, much evidence exists implying that the Gaussian is more descriptive of the lateral profile than a "tophat" profile. This assumption is still in question, as ample evidence has not been obtained, especially in the field. For this reason, several authors feel justified in specifying a "tophat" rather than a Gaussian profile.

Some of the more interesting data on lateral profiles are by Carter[21] for jets with $k \leq 10$. He observed a roughly bell-shaped temperature profile on the offshore side of the jet centerline. On the near-shore side, the temperature decreases to some temperature between the centerline and ambient temperatures and remains constant. The velocity profiles are a mirror image of the temperature profiles. Carter has chosen, therefore, to use "tophat" profiles in his theory.

A point should be made concerning the relative rate of spreading of heat and momentum. Taylor's theory implies that heat is diffused laterally faster than is momentum. (See pp. 482-3 of Ref. 122.) Consider the effect of this on the zone of flow establishment. If the limits of this zone are based on velocity, the velocity would still equal U_o at the end of the zone of flow establishment. However, due to more rapid spreading, the temperature rise, ΔT, would be less than ΔT_o by possibly 10-15%. Fan[38] notes that the general effect of assuming that both velocity and temperature profiles spread at identical rates is to underestimate the dilution. He expects this error to be in the range of 10-15%.

8. Time of Exposure of Organisms

Exposure of organisms to elevated temperatures can be critical. The impact of a power plant on the environment must be assessed in light of its impact on

the biota. One of the most potentially useful aspects of any analytical model is to provide information on exposure time, which might be converted by biologists to useful evaluations of impact.

In considering the time of exposure of an organism once it has passed through the condenser or is entrained shortly after leaving the condenser, one should consider three separate time elements. The first is the time the organism spends in the elevated temperature in the conduit, be it open channel or pipe, leading from the condenser to the final point of discharge to the ambient receiving waters. The second time element is the time the organism spends in the ZOFE. While in this zone, the organism, if it were assumed to be on the plume centerline, would still be subjected to the temperature rise that existed in the conduit leading to the discharge point. The third time element would be the time the organism required to move from the end of the ZOFE to the given temperature rise specified by the biologist. It might frequently be of concern, for example, to determine the time it takes an organism to return to a temperature environment only 5°F above the ambient. All the computations will assume that the organism moves at the velocity of the fluid particles in the plume and that the organism is moving along the jet axis. Therefore, exposure times for areas off-axis would differ from that presented here.

In general terms, the three time elements considered above are defined by

$$T_c = \frac{L_c}{U'_c} , \tag{5.16}$$

in which T_c is the time in the conduit, L_c is the length of the conduit, and U'_c is the velocity in the conduit (usually = U_o for open channel discharges);

$$T_{ZOFE} = \frac{s_e}{U_o} , \tag{5.17}$$

in which T_{ZOFE} is the time spent in the ZOFE; and

$$T_{ZOEF} = \int_o^{s_t} \frac{ds}{U(s)} , \tag{5.18}$$

in which T_{ZOEF} is the time spent in the ZOEF until the desired temperature rise is reached, s_t is the distance to the point at which the desired temperature contour crosses the plume axis, measured from the end of the ZOFE, and U(s) is

the velocity as a function of distance along the axis, s. These can be combined to yield

$$T_t = T_c + T_{ZOFE} + T_{ZOEF} \cdot \tag{5.19}$$

Equation 5.18 will frequently have to be evaluated by numerical means concurrently with the model computer solution. This could easily be included in the computer programs of current models.

If it is preferred, however, one can determine times of exposure graphically if he has a model output of velocity as a function of distance along the jet axis. Then, plotting 1/U against s, the distance, will enable graphical integration of Eq. 5.18. Many of the models have outputs of velocity and distance in some dimensionless form. These dimensionless forms can be plotted and the graphically integrated areas multiplied by a constant to yield exposure times.

This graphical procedure can be illustrated for output from the Stolzenbach and Harleman[131] model, and the procedure will be identical for other models, except for the constants. Using the nomenclature from Ref. 131, one can state the integral for time of exposure as follows:

$$t_f = \int_0^{s_t} \frac{ds}{U} = \frac{1}{U_o} \int_0^{s_t} \frac{ds}{(U/U_o)} = \frac{\sqrt{z_o B_o/2}}{U_o} \int_0^{s_t} \frac{d\dfrac{y}{\sqrt{z_o B_o/2}}}{(U/U_o)} , \tag{5.20}$$

where z_o = depth of discharge flow channel,

B_o = width of discharge channel,

s_t = distance to desired point, and

t_f = time in ZOFE + time in ZOEF.

The right-hand integral can be evaluated by replotting U/U_o as U_o/U (the inverse) against $y/\sqrt{z_o B_o/2}$ and planimetering under this area up to the distance where the time is desired; then simply multiply by the constant $\sqrt{z_o B_o/2}/U_o$ to obtain an exposure time to s_t.

Figure 5.6 illustrates the graphical-integration technique. In the figure, for example, point 1 might represent the distance to the 10°F contour and point 2 the distance to the 5°F contour. The area needed for point 1 is that designated A_1. The area needed for point 2 is $(A_1 + A_2)$, i.e., the total area under the curve up to point 2. The obvious disadvantage to doing this by hand is the repetitive nature of the effort. That is, you must repeat the graphical evaluation for every point to which you desire the travel time. It would be easier to get the U/U_o output from the basic model and then feed it into another program (or subroutine in the main program) and let the machine do the work. When studying exposure time, one must not neglect the time spent in the discharge channel itself, or L_c/U_o.

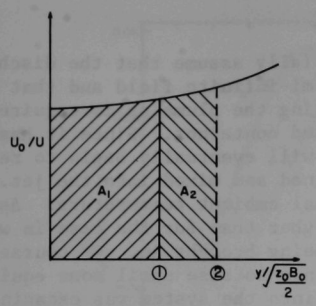

Fig. 5.6.

Schematic for Graphically Calculating Exposure Time.

9. Consideration of Surface-cooling Effects

Several of the models to be discussed include the effects of surface cooling or can be modified to include the effects of surface cooling on the heated temperature distribution. Almost all the models use an equilibrium-temperature approach. The details of this method are discussed in Chapter III, but it essentially involves a statement that the heat loss is equal to some cooling coefficient, K, times a driving force, usually the difference between the water-surface temperature and the equilibrium temperature. To use this approach, we assume the natural water temperature or the ambient water temperature is equal to the equilibrium temperature. This is, of course, not exactly true.

Edinger and Geyer[32] discuss the relationship of natural water temperature to equilibrium temperature. When the water temperature is increasing, the equilibrium temperature is greater than the water surface temperature, e.g., during the spring. When the water temperature is decreasing, the equilibrium temperature is less than the water surface temperature, e.g., during the fall months. The equilibrium temperature would be expected to nearly equal the natural water temperature when the temperature was not changing very much; this would be expected to be during the times of maximum temperatures in the summer and minimum temperatures in the winter. Since the former of these two cases is frequently considered the most critical for possible damage to biological systems, it is justified to assume that the natural water temperature equals the equilibrium temperature for application of the models.

Pritchard[109] discusses this point in reference to the time relationship of equilibrium and natural temperatures. He notes that in the spring this modeling approach tends to overestimate the heat loss from the natural water body. Since the equilibrium temperature is higher than the natural water temperature at this time of year, the actual driving force for heat loss would be less than that in the model assumption. By similar reasoning, Pritchard points out that in the fall the actual heat loss would be greater than that predicted by the model. However, Pritchard notes that mixing and the resultant dilution are the primary processes in reducing the temperature of most heated discharges presently being designed. As a result, the effect of surface cooling, especially where standards must be met, is not significant, and the exact form of the cooling approximation is less critical.

10. Accounting for Limited Dilution Water

All the models to be discussed essentially assume that the discharge either occurs into an infinite field or into a semi-infinite field and that in any event as much water is available for diluting the plume as is required. Picture, however, a jet that discharges into a closed container. Since it has no new dilution water moving into the system, it will eventually begin to re-entrain some fluid that has previously been entrained and mixed into the jet. Hence, this water will no longer be at the original ambient temperature. As a result, the plume temperature would be somewhat higher than for the case in which an infinite supply of water was continually being brought in. Of course, in the example cited, the temperature would continue to rise until some equilibrium was gained where all the heat being input into the system was escaping to the atmosphere. In a natural system, even if a stagnant current existed for a time, one would expect that ultimately some new dilution water would become available. Therefore, some means of estimating any possible re-entrainment of fluid should be considered.

Pritchard[109] has developed a simple scheme for use with his model. It seems, however, an appropriate scheme to be adapted to other models and will therefore be presented in the general section rather than in the particular discussion of Pritchard's model (Sec. V.E). Pritchard estimates this recirculation or re-entrainment, or what he calls "background temperature," in the following manner: he calculates the excess temperature that would result if the heated discharge were mixed completely with the available supply of diluting water. As an example of this, consider a discharge of 2000 cfs with an initial temperature rise, ΔT_o, of 20°F. Assume that available information indicates that the river or estuary into which the discharge is occurring has an average net flow of 50,000 cfs. Then, Pritchard would compute the background temperature to be 2,000 divided by 50,000 = 1/25 of ΔT_o, or in this case 0.8°F. Pritchard would probably suggest that this be reduced for the effect of surface cooling. In this instance, depending upon the exact design, a background temperature of 0.5 or 0.6°F might be suggested.

Calculation of the available dilution water depends on the site. For a river, the average river flow in volume per unit time would be the figure desired. For estuaries, methods exist (some of them discussed by Pritchard[108,110]) for calculating the amount of available new water from ocean sources and freshwater river flows. (These methods are discussed in Sec. V.J below. Examples of some calculations in a simple form are presented in Ref. 110.)

Figure 5.7 shows Pritchard's estimate of temperatures near the proposed Calvert Cliffs Station. The temperatures shown represent mean temperatures within successive longitudinal reaches of the estuary. The lower pair of curves illustrates the inclusion of surface cooling effects. In this figure, c and c_o represent concentrations at any point and initial concentrations of a conservative substance. The peak temperature rise adjacent to the plant site is $0.06\Delta T_o$, representing a dilution of 1/0.06 or 16.7. Since the plant flow is 5400 cfs, this represents a flow of new dilution water equal to 16.7(5400), or about 90,000 cfs. If the plant temperature rise, ΔT_o, is assumed to be 10°F, the lower curves show an excess temperature of 0.04(10) = 0.4°F. Pritchard calls this excess temperature ϕ'.

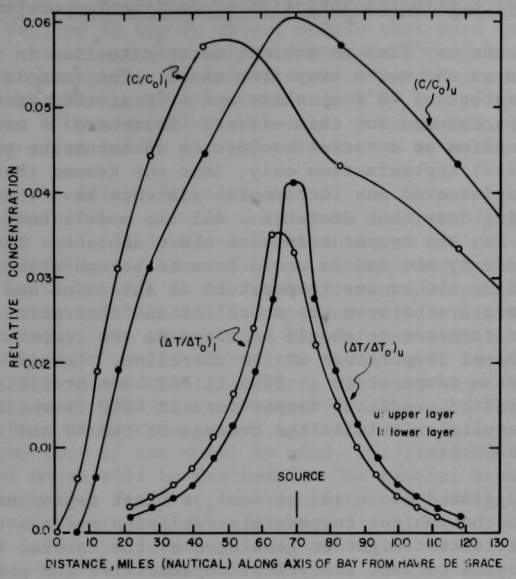

Fig. 5.7. Longitudinal Distribution in the Chesapeake Bay of the Sectional Mean Relative Concentration and Temperature Rise.[109]

For a lake, individual assessment must be made based on the site. If some geometry constraints seem to exist, some estimate may need to be made of this background temperature. Perhaps the only accurate way to get an assessment is by building a hydraulic physical model for the site. If, however, the shoreline is relatively free and large amounts of dilution water are expected to be available, it may not be necessary to make any correction to the predicted results.

Once the available dilution water and these so-called "background temperatures" have been assessed, Pritchard simply adjusts those values he has calculated from his plume model by use of

$$\Delta T' = \Delta T + \left(1 - \frac{\Delta T}{\Delta T_o}\right) \phi' , \qquad (5.21)$$

in which $\Delta T'$ is the temperature rise adjusted for background temperature and ϕ' is the background excess temperature.

Although Pritchard is the only author who has directly used this method, it would probably be applicable to other models as well.

11. Accounting for Horizontal Variation of Ambient Temperature

Occasionally one may find an ambient water situation in which the ambient temperature varies as one moves away from shore. The example cited in the Great Lakes had a temperature of 48°F on shore and 42°F at 6000 ft off shore. No current model has accounted for this effect. Pritchard[140] mentioned this problem in a discussion at a recent conference on estuarine problems. He suggested, as a first approximation only, that one assume that the water entrained into the jet over any incremental distance have the average ambient temperature existing over that distance. All the models here predict excess temperature, that is, the temperature rise above ambient. This would mean that the predictions made by the models would have to be converted to an actual temperature by taking the excess temperature at any point and adding it to the mean ambient temperature between the shoreline and that point. For the current discussion, excess temperature should be taken as the temperature rise with respect to the ambient temperature at the shoreline. Consider the example cited above. If the excess temperature at 6000 ft had been predicted by a given model to be 3°F, the adjusted predicted temperature at 6000 ft would be 3 + 45 = 48°F. The use of 45°F results as this is the average of the 48 and 42°F temperatures varying over the 6000 ft.

The method suggested above is, at best, a first approximation. No available model handles the ambient temperature variation and the subsequent additional buoyant forces that might be generated by the lateral temperature changes. This problem is beyond current analytical capabilities and probably beyond current physical-modeling capabilities. Perhaps the only saving grace is that this is not a usual situation and generally does not occur at the supposedly critical time of the year, the summer months. It is suggested that if one encounters such a case, a first-cut estimate of the type above be made. A larger than usual safety factor should be used in interpreting the results.

B. Selection of Models for Discussion

Now that some of the general features and terminology concerning models have been reviewed, some of the current models that might be used for evaluation of heated discharges will be presented. To avoid overwhelming the reader with a large number of models from which he must make a choice, we have decided to make a representative selection of the models available. Reference 104 contains considerable detail on 12 available models. No effort will be made to duplicate that work, which is extensive and well done. Policastro and Tokar are currently working on reports comparing the various models in their predictive capabilities and to field data. If these reports were available, this current report would choose different models.

Some criteria must be provided to choose the models to be presented here. First, some models should be presented for the near-field condition and some for the far-field condition. Second, to the extent possible, methods available for river, lake, and estuary conditions should be included. In many cases, these will be the same methods. For estuaries, however, two additional far-field models will be discussed. The third criterion is that the model should be one that is reasonably available and under current use. A fourth criterion is the ease of ability to use the model. Thus, for example, if the model is a highly sophisticated one requiring extensive computer usage and no computer program is publicly available, it would be useless to include it in this report.

For another criterion (probably the most critical in the final reduction of choices), it was decided to try to choose models that were representative of groups of models. As an example, the Motz-Benedict[94] model will be discussed in more detail than the models by Hoopes *et al.*[59] and Carter.[21] These models are similar in composition, and an understanding of one of them should enable a person to go into a more detailed reference, such as Ref. 104 or the individual references for the given model, and understand them as well.

The effort in the following sections will not be merely to provide technical information, but also to provide sufficient understanding of the modeling processes currently used. This should enable one to use other models, including new ones that are developed. The format to be followed to the extent possible in the following sections will be to try to present a capsule version of the model. In these reviews, the basic assumptions will be listed. In addition, the equations resulting from these basic assumptions will be listed as a matter of information. The data needed to run the models will be noted. In addition, the verification, both field and laboratory, that has been obtained for the model will be mentioned. In this context, Policastro and Tokar point out that no model has yet been adequately tested against field data. With this fact in mind and the assumptions of the model in mind, the limitations and strengths of each individual model will be discussed. The general areas of applicability, whether near field or far field or for specific cases, will be reviewed. Finally, example solutions available in the basic literature for each model will be presented. Here it is recognized that three types of information generally would be desired from a model output. One is some measure of the distance to a given temperature isotherm. A second, a frequently useful idea, is the concept of an area within a given temperature isotherm, so that one might evaluate the portion of the receiving body that is affected. Finally, biologists frequently are concerned with time of exposure of organisms. No models currently provide the time of exposure as a part of their routine output. However, as noted earlier, the formulation of this is simple. Where possible, estimates of time of exposure in the context of a numerical example will be provided from published results. Otherwise, we will simply note what additions to the solution should be included to provide this information for the investigator. This would frequently only require adding a few steps to the standard computer program for the model. For those who are continually using a number of these models on computer facilities, this would be a short expenditure of time and would provide possibly useful information for evaluation of environmental impact.

C. Stolzenbach-Harleman Model

Harleman and Stolzenbach[131] have developed a near-field jet model. Reference 129 gives an abbreviated view of the model, and Ref. 104 also reviews the model. Figure 5.8 shows the general case being considered. Stolzenbach and Harleman (p. 15) state that they are considering

> "...a horizontal surface discharge of heated water from a rectangular open channel of arbitrary width and depth into a large unstratified body of water which may be stagnant or flowing with an arbitrary distribution at right angles to the direction of discharge and which may be infinitely deep or may have a sloping bottom. The temperature and velocity distribution in the discharge are considered as functions of the discharge channel geometry, the initial velocity and temperature

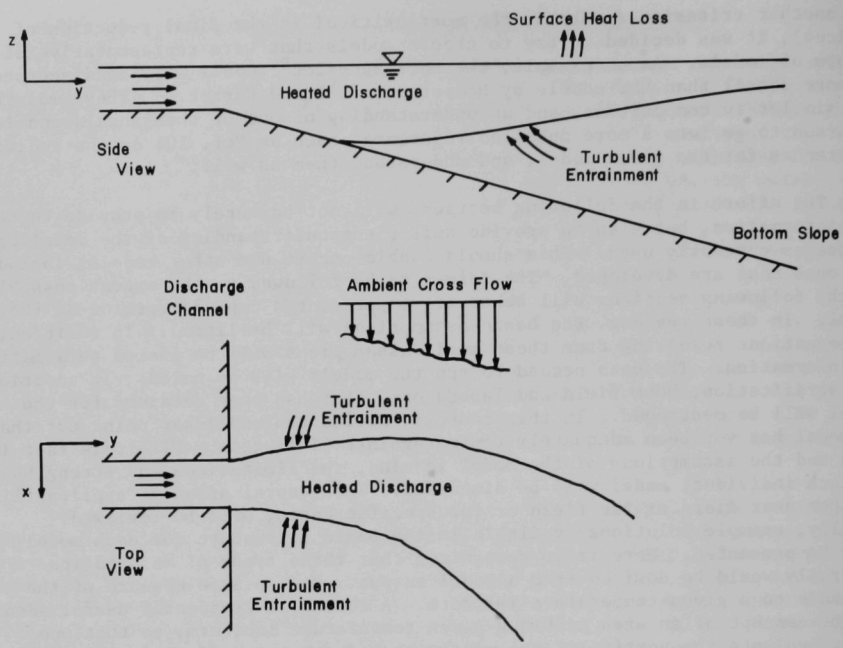

Fig. 5.8. Schematic of Heated Surface Discharge.[131]

rise, the magnitude of the ambient cross flow and bottom slope, and the surface heat transfer rate. The discharge is considered only to the point where jet-like behavior ceases and natural turbulence and convection dominate the temperature and velocity distributions."

1. Assumptions

The basic premise for development of this model lies in using available data and solutions for nonbuoyant turbulent jets as a starting point. Assuming linear jet spreading and similar profiles, the nonbuoyant case is solved to give information on lateral and vertical entrainment coefficients. In referring to the buoyant case, the linear spreading assumption is not valid. Pertinent assumptions in the model include:

(1) The similar profiles for velocity and temperature are chosen as shown. (See Fig. 5.9 for a definition sketch.)

$$f(\zeta) = (1 - \zeta^{3/2})^2 \text{ for velocity;} \tag{5.22}$$

$$t(\zeta) = \sqrt{f} = 1 - \zeta^{3/2} \text{ for temperature,} \tag{5.23}$$

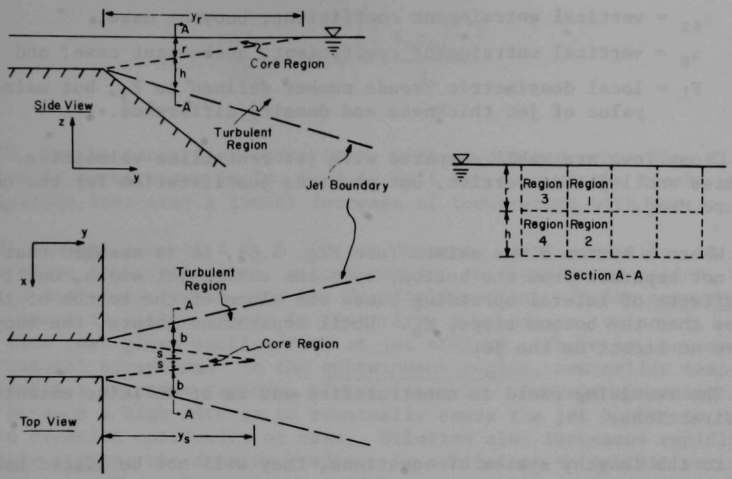

Fig. 5.9. Geometrical Characteristics of the Jet.[131]

in which ζ is the dimensionless lateral distance = the distance from the jet centerline (or the edge of the core in the core region) to the point of interest normalized by half-width of the jet. Therefore, $\zeta = 1.0$ at the edge of the jet, implying that both velocity and temperature rise go to zero at that point.

The expression f is from Abramovich's work[3] on plane, submerged, nonbuoyant jets and compares well with data for this case. The use of $t = \sqrt{f}$ is based on Taylor's theory that heat is diffused laterally faster than is momentum. Policastro and Tokar[104] note that implicit in the use of these forms are the assumptions that horizontal and vertical processes are independent and that a surface jet is half a submerged jet. They point out that these similarity functions have the added advantage over Gaussian forms of approaching zero at a finite distance, providing a definite jet boundary.

(2) The lateral entrainment function is the same in buoyant and nonbuoyant cases; i.e., the buoyant forces have no effect on horizontal entrainment.

(3) The lateral velocity due to buoyancy-induced pressure gradients (the lighter fluid "riding up" over the heavier fluid) is assumed related to the difference in buoyant and nonbuoyant spreading rates and proportional to the temperature gradient in the x-direction.

(4) Vertical entrainment is reduced as indicated by the data from Ref. 37.

$$\frac{\alpha_{sz}}{\alpha_z} = \exp(-5/F_L^2) \ , \qquad (5.24)$$

where α_{sz} = vertical entrainment coefficient, buoyant case,

α_z = vertical entrainment coefficient, nonbuoyant case, and

F_L = local densimetric Froude number defined as F_j, but using local value of jet thickness and density difference.

(5) Crossflows are small compared with jet centerline velocities. This not only implies small jet distortion, but provides justification for the neglect of pressure drag.

(6) Where a bottom slope exists (see Fig. 5.8), it is assumed that the jet will not separate from the bottom, over the entire jet width, until the buoyant effects of lateral spreading cause the slope of the bottom of the jet to be less than the bottom slope, S_b. Until separation occurs, the buoyant terms have no effect on the jet.

(7) The receiving field is nonstratified and is of infinite extent in the x and y directions.

Due to the lengthy system of equations, they will not be listed here and the reader is referred to the basic references.

2. Verification

Twenty-five laboratory runs were conducted to test the model. Ranges of parameters were:

F_j,	1.0-11.6;
z_o/B_o,	0.175-2.85;
$K/(\rho C_p U_o)$,	$1.6\text{-}10.5 \times 10^{-5}$;
S_b,	0.01-∞ (sudden dropoff);
U_{am}/U_o,	0.0-0.40;

where U_{am} is the maximum ambient velocity. (The distribution in the receiving tank was parabolic, being zero near the discharge and growing to U_{am} near the center of the tank.)

Results generally showed good agreement with theory, except where the bottom slope became significant. In this case, lateral spreading exists before separation from the bottom, a situation the model cannot handle. Therefore, the bottom-slope portion of the model should be applied carefully. The centerline temperature decrease is still predicted adequately, even in the presence of an influencing bottom slope.

There are a number of pertinent findings from the theoretical and experimental studies:

(1) A useful formula for slightly buoyant jets (F_j >15) is

$$\frac{\Delta T_c}{\Delta T_o} = 13.4 \frac{\left(\frac{1}{2} B_o z_o\right)^{1/2}}{y} , \tag{5.25}$$

where ΔT_c is the centerline temperature rise at desired centerline distance y. The value in parentheses in Eq. 5.25 is half the area of the discharge canal. This equation indicates a linear decrease of temperature with distance.

(2) Buoyant jets ($1 \leq F_j \leq 10$) are compared, most generally, in five regions along the centerline: a core region, an entrainment region, a stable region, a heat-loss region, and the far-field region. In the core region (ZOFE), there is little change in centerline temperature, velocity, or dilution, D (D = flow past given section/flow at jet efflux). There is, however, considerable lateral spreading. In the entrainment region, centerline temperatures and velocities decrease rapidly, almost linearly. Buoyant spreading laterally occurs at such a high rate as to eventually cause the jet bottom to rise in order to preserve continuity of mass. Dilution also increases rapidly. In the stable region, the density gradient is sufficient to inhibit vertical entrainment. Jet depth continues to decrease due to continuing lateral spreading, which yields very wide surface isotherms. In the heat-loss region, atmospheric heat losses finally become important due to the increase of surface area. In the far-field region, both heat loss and ambient currents are significant. If the ambient current is great enough, the far-field region may begin *before* the stable region forms. The Stolzenbach-Harleman model is not valid once the far-field region has been reached. These zones can be seen in a later example.

(3) The dilution attained by the beginning of the stable zone can be seen in Fig. 5.10. This figure allows one to make a first estimate of dilution

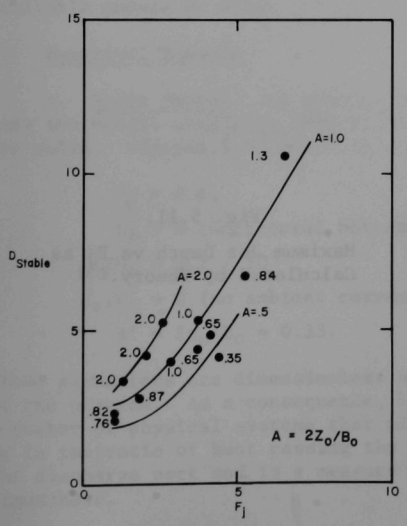

Fig. 5.10.

Dilution in the Stable Region of Buoyant Discharges.[131] (Points calculated by theoretical model.)

obtained at the end of the entrainment region and may be sufficient, for example, to ensure that more detailed calculations are unnecessary. Higher densimetric Froude numbers (due to overcoming buoyancy and allowing more vertical mixing) and high depth-width ratios (due to providing more lateral area for entrainment) yield higher dilutions. This gives some capability for suggesting improved designs.

(4) Maximum vertical jet penetration, h_{max}, increases with increasing F_j, as shown in Fig. 5.11. This again makes sense, for lower Froude numbers mean greater buoyant forces and thus more inhibition of vertical mixing.

(5) Small ambient currents (high k values) deflect the jet but do not greatly affect the temperature profile. Other authors[15] have observed this also.

(6) Bottom slopes tend to inhibit vertical entrainment for $F_j > 5$. For smaller values of F_j, no effect of the bottom is incurred.

3. Limitations and Ranges of Applicability

The model, as stated, is a near-field model only. It should be used only for small ambient velocities. No specific data are available on this; $k > 10$ probably should be a criterion for use. Stolzenbach[130] himself has stated the model was not intended for river use and should not be applied to rivers. The lack of success of the bottom-slope portion of the model apparently does not greatly affect temperature-decrease predictions. The user should still look closely at results obtained where S_b is important. As always, the model should be applied generally within the range of variables for which it has been verified. This would be especially true for the depth-width ratio of the discharge channel (maximum D/W = 2.85), as Stolzenbach and Harleman[131] (p. 130) do not feel that

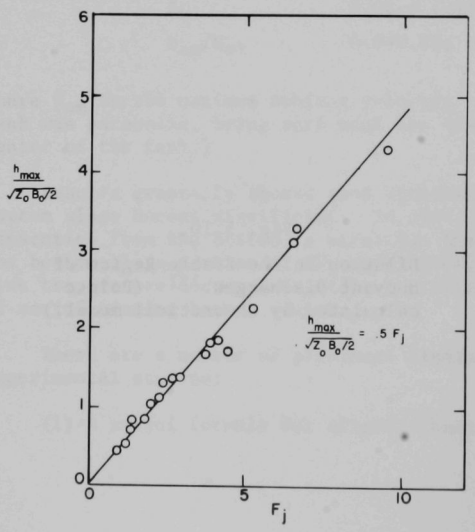

Fig. 5.11.

Maximum Jet Depth vs F_j as Calculated by Theory.[131]

the model performs as well for the larger ratios. Also, the initial discharge angle, β_o', must be near 90° for the model to be applied successfully. Otherwise, the model should be applicable to a wide range of conditions and should be very useful.

4. Data Needed

A computer program exists to solve the derived system of equation. It is currently being revised at MIT to reduce computer run time. However, once the computer program is available, this model is the easiest of the available sophisticated models to use, for the user need specify no entrainment or diffusion coefficients. Only the following physical data descriptive of the system are required:

$U_a(y)$ = values of U_a as a function of distance from shore,

F_j = initial densimetric Froude number,

S_b = bottom slope,

$A' = 2z_o/B_o$ = channel-aspect ratio,

K = surface-heat-loss coefficient,

U_o = initial jet velocity, and

β_o' = initial angle of jet with boundary of ambient region.

Other inputs to the program would generally remain constant and are not functions of the physical site being considered. (See Ref. 131 for details.)

One can still use the model for cases in which entrainment occurs on only one side by assuming that the solid-boundary restricting entrainment is the center-line of a discharge port twice the actual width. (See pp. 155-157 of Ref. 131 for further details.) This same schematization could be made with most other available models as well.

5. Numerical Example

a. Basic Output. An example of some typical results from this model will show the detail available when it is applied to cases for which its assumptions are valid. Figures 5.12 and 5.13 show results using the parameters

$F_j = 4.4$,

$S_b = 0$ (horizontal bottom),

$K/U_o = 4.2 \times 10^{-5}$,

$U_a/U_o = 0$ (no ambient current), and

$A' = 2z_o/B_o = 0.35$.

These parameters are dimensionless numbers, which is the form of their input to the program. As a consequence, the computer results could be expanded to a number of physical systems that might fit these parameters. In the figures, H_r is the ratio of heat passing the given location to the heat issuing from the discharge port and is a measure of remaining heat not yet lost to the atmosphere.

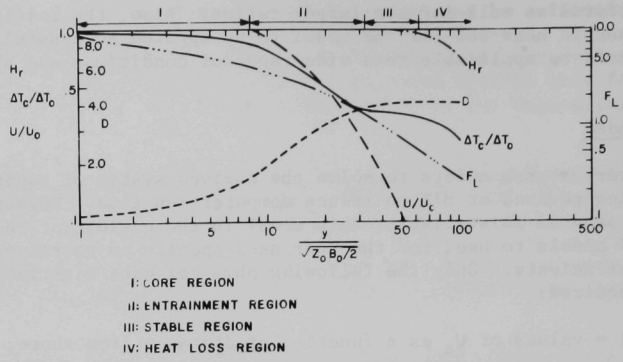

a. VARIATION OF IMPORTANT PARAMETERS ALONG JET AXIS

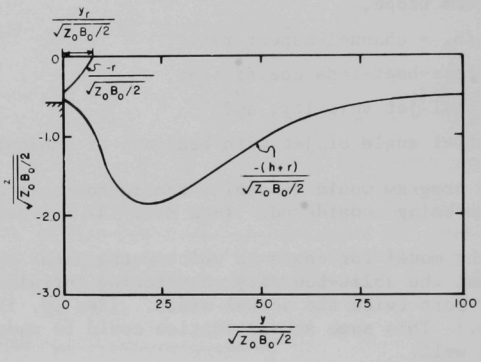

b. VERTICAL DIMENSIONS OF JET ALONG JET AXIS

Fig. 5.12. Theoretical Calculation of Jet Structure for Example.[131]

The separate regions -- core, entrainment, stable, etc. -- can be seen in the results, as well as the vertical and lateral structure. Consider the following numbers, which will also illustrate the use of Figs. 5.10 and 5.11:

z_o = 5 ft,

B_o = 28.57 ft (thus, A = 0.35),

ΔT_o = 25°F (from 65°F ambient), and

U_o = 3.35 ft/sec; this, with ΔT_o and z_o yields F_j = 4.4.

From Fig. 5.12 (or Fig. 5.10) the dilution, D, at the beginning of the stable region is about 4.0. The value of $\Delta T_c/\Delta T_o$ reaches about 0.37 at the same point, which is located at $y/\sqrt{z_o B_o/2}$ = 31. With the given conditions, this predicts a centerline temperature rise of ΔT_c = 0.37 (25.0) = 9.3°F at a distance

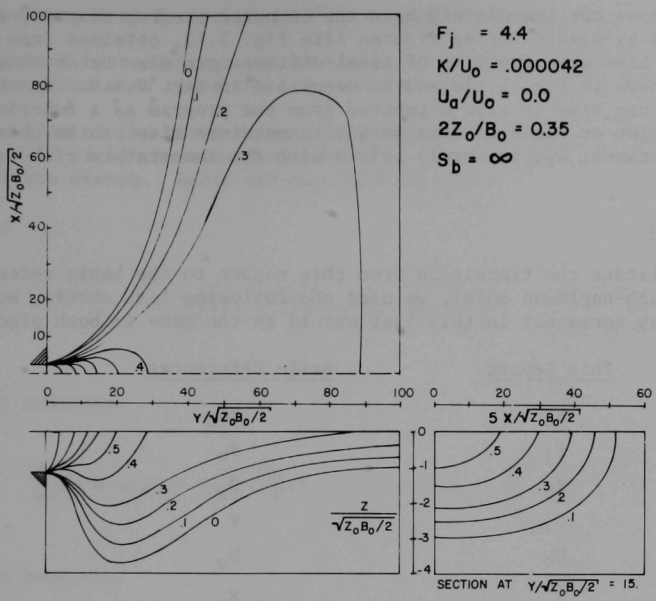

Fig. 5.13. Calculated Isotherms for Example.[131]

$y = 31\sqrt{5(28.57)/2} = 260$ ft from the jet efflux. The maximum jet depth (from Fig. 5.11 or 5.12) is approximately

(Fig. 5.11) $h_{max} = 0.5F_j\sqrt{z_o/B_o/2} = 0.5(4.4)(8.45\text{ ft}) = 18.6$ ft;

(Fig. 5.12) $h_{max} = 0.19\sqrt{z_oB_o/2} = 16.0$ ft at $y/\sqrt{z_oB_o/2} = 24$.

This case represents a fairly small plant discharge, $Q_p = 3.35(28.57)(5) = 478$ cfs, compared to many proposed plants. If a larger plant were designed so that the above dimensionless parameters still held, however, Figs. 5.12 and 5.13 would also represent the solution for that case.

b. Time of Exposure and Surface Area. The currently available program for this model does not output estimates of exposure time or surface area within a given contour. These steps can be easily added to the program since they are simple, finite-step, numerical integrations that can be performed concurrently with the solutions to the basic differential equations. The worker who plans to use this model extensively should add these steps to the program. At each given point on the centerline, the lateral distance to a given temperature contour can be found by the similarity function in Eq. 5.23. Then summing of areas can continue along the axis. For time estimates, the term ds/U can be evaluated at each new distance step and a continuous total maintained. Here, ds = incremental distance along the axis, and U = average centerline velocity over that increment. Then ds/U = time to traverse the incremental distance ds.

If one does not immediately have the computer program adapted, areas may be calculated by planimetering figures like Fig. 5.13, obtained from computer output. The time as a function of axial distance can also be obtained from the U/U_o curve shown in Fig. 5.12a and as described in Sec. V.A.8. As the centerline temperature rise is also outputted from the program as a function of distance, a plot or table of time versus temperature rise can be obtained. The time to a distance, s_t, is merely paired with the temperature rise to that point.

6. Notation

To facilitate the transition from this report to the basic references on the Stolzenbach-Harleman model, we used the following list showing equivalent notation. Any terms not in this list should be the same in both places.

This Report	Basic References
B_o	$2b_o$
F_j	F_o
S_b	S_x
U_{am}	V
U_o	U_o
y	x
z_o	h_o
β'_o	θ_o

D. Motz-Benedict Model

A two-dimensional surface jet model has been developed by Motz and Benedict. Basic references relating to the model include Refs. 15 and 93-95. In addition, Policastro and Tokar[104] discuss the model fully.

1. Assumptions

Model assumptions include the following:

a. All flows are steady, and the ambient current is uniform. The receiving fluid is infinite in extent.

b. The jet is two-dimensional; i.e., no vertical entrainment occurs.

c. Turbulent mixing into the jet can be represented by a standard entrainment mechanism using a constant coefficient of entrainment, E.

d. Changes in density along the jet axis are small compared to a reference density. Thus, inertial terms due to density gradients are negligible, and mass flux terms can be replaced by volume flux terms.

e. Similar profiles of Gaussian form are chosen for velocity and the temperature profiles.

f. Pressure drag is included using a constant drag coefficient, C_D.

g. Surface heat exchange can be expressed as some coefficient, K, times a surface area times the temperature rise existing at that area.

Integration of the basic conservation relationships over the cross section of the jet will yield the equations needed to describe the system. Figure 5.14 is a definition sketch. Basic derived equations are:

Continuity:

$$\frac{d}{ds}(Ub) = \frac{2E}{\sqrt{\pi}}(U - U_a \cos \beta) \; ; \tag{5.26}$$

x-component momentum:

$$\frac{d}{ds}(U^2 b \cos \beta) = \sqrt{2}\,\frac{2E}{\pi}(U - U_a \cos \beta)U_a + \frac{\sqrt{2}}{\sqrt{\pi}}\,\frac{C_D U_a \sin^2\beta}{2} \; , \tag{5.27}$$

y-component momentum:

$$\frac{d}{ds}(U^2 b \sin \beta) = -\frac{\sqrt{2}}{\sqrt{\pi}}\,\frac{C_D U_a \sin \beta \cos \beta}{2} \tag{5.28}$$

Temperature rise:

$$\frac{d}{ds}(U\Delta Tb) = -\sqrt{2}\,\frac{K}{\rho C_p z_o}\,\Delta Tb \; , \tag{5.29}$$

where b = half-width of jet,

ΔT = temperature rise at jet centerline,

E = entrainment coefficient,

C_D = drag coefficient,

U = jet centerline velocity,

U_a = ambient velocity,

β = angle of jet with respect to x axis,

s = distance along jet axis, and

C_p = specific heat of water.

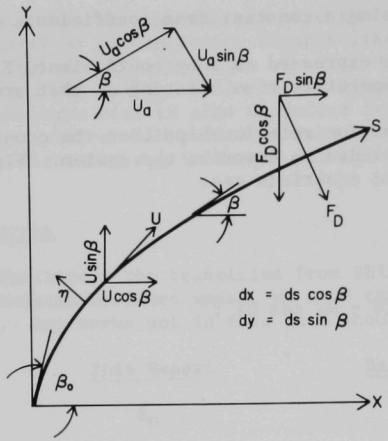

Fig. 5.14.

Definition Sketch for Motz-Benedict Model.[93]

The geometry of the jet trajectory as shown in Fig. 5.14 gives two additional equations and unknowns, or

$$\frac{dx}{ds} = \cos \beta \tag{5.30}$$

and

$$\frac{dy}{ds} = \sin \beta \ . \tag{5.31}$$

Six unknowns then exist-- ΔT, U, b, x, y, and β --all functions of s.

The Motz-Benedict model is then a two-dimensional, near-field model including surface cooling, a crosscurrent, pressure drag, and an arbitrary angle of discharge, but no lateral buoyant forces.

2. Verification

The Motz-Benedict model has been used to analyze both laboratory and field data with reasonable success. Data collected at Vanderbilt by Motz and Benedict[94] and Taimi[135] have been used. In addition, field data collected on rivers and lakes by Vanderbilt personnel and other workers have been used. Table 5.1 summarizes the results obtained. The E and C_D values are determined by fitting the data to the model.

Figure 5.15 shows the values of entrainment coefficient, E found by fitting to the sets of data shown. Note that the value of E decreases as the ambient velocity decreases, reducing the strength of the lateral vortex action in the jet. In addition, intuition indicates mixing should be less if the ambient current decreases.

Table 5.1. Values of Entrainment Coefficient

Data Source	β_o,°	F_j	$k = U_o/U_a$	W_r [a]	E
Laboratory	90	3.4-6.9	1.37-5.2	24	Avg = 0.4
Laboratory	45 & 60	3.1-6.3	1.53-5.2	24	Avg = 0.2
Widows Creek					
VU1	85	4.3	2.0	7.5	0.16
VU2	85	3.7	1.5	7.5	0.16
TVA	85	3.7	1.33	7.5	0.16
New Johnsonville	60	1.3	1.75	4	0.04
Stefan (laboratory)	--	3.7-4.1	∞	34	0.06-0.09
Vandy (laboratory)	90	4.2-7.4	3.30-∞	24	0.4-0.04
Fitch (Lake St. Croix)	60	~1.0	3.19[b]	20	0.11-0.296
Ayers (Michigan City)	90	1.2	10[b]	--	0.04
Romberg (Waukegan)	90	5.6-6.0	1.7-5.6	--	0.046-0.059

[a] *W_r = (width of ambient stream)/(width of discharge canal).*

[b] *Estimated.*

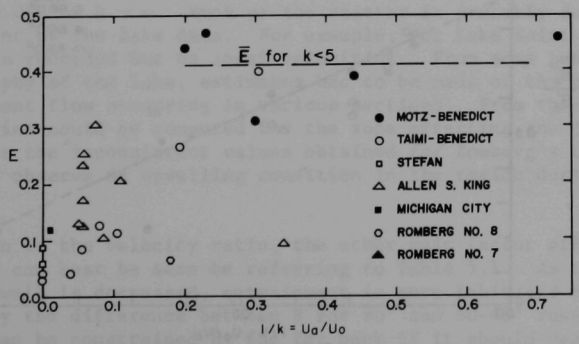

Fig. 5.15. Entrainment Coefficient as a Function of Velocity Ratio.[15]

3. Data Needed

A computer program is available for this model. The following parameters are needed to obtain temperature predictions for a given site.

Discharge features:

ΔT_o = initial temperature rise,

U_o = initial jet velocity,

B_o = initial width of rectangular canal,

U_a = ambient velocity,

K = surface cooling coefficient,

z_o = initial depth of rectangular canal or flow depth at exit if wedge exists, and

β_o' = initial angle of discharge relative to U_a.

ZOFE data:

b_o = half-width at end of ZOFE = $0.8B_o$ (from Ref. 93),

β_o = angle at end of ZOFE (obtain from Fig. 5.16), and

s_e = length of ZOFE (obtain from Fig. 5.17).

Figures 5.16 and 5.17 represent laboratory information obtained from Ref. 94.

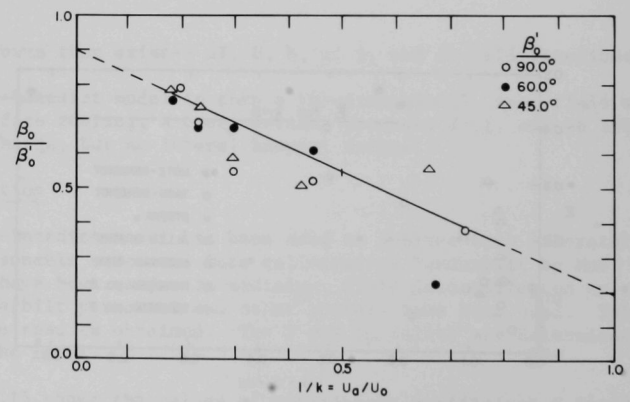

Fig. 5.16. Observed Values and Fitted Curve for Initial Angle vs Velocity Ratio.[93]

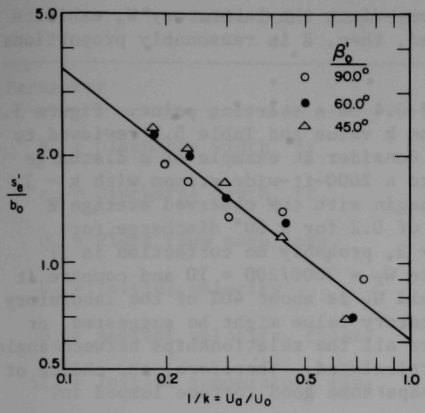

Fig. 5.17.

Observed Values and Fitted Curve for Length of Establishment Zone vs Velocity Ratio.[93]

Empirical coefficients:

C_D = drag coefficient (use as 0.5 for all cases) and

E = entrainment coefficient (obtain by review of Table 5.1 and Fig. 5.15).

The drag coefficient is chosen as 0.5, since several field studies yielded values of C_D very near 0.5. Some added comment is necessary on the value of E. Unfortunately, much of the available data omits one or more necessary parameters, most often velocity information on the canal or in the lake. In fact, only the data by Romberg *et al.*[116] for Lake Michigan provided all needed data. Other data were used where estimates could be made of needed parameters, specifically those at the Michigan City Plant on Lake Michigan[9] and the Allen S. King Plant in Minnesota on Lake Saint Croix.[42]

Although there is some scatter in Fig. 5.15, it is generally seen that for $k > 5$, the value of E for jets with unconfining geometry decreases from 0.4 down to about 0.04 for $k \to \infty$. Much of the scatter is probably due to assumptions made in treatment of the lake data. For example, for Lake Saint Croix, total ambient flow was recorded but no local velocities. From some general knowledge of the hydrography of the lake, estimates had to be made of the percentage of this total ambient flow occurring in various sections. From these estimates, average velocities could be computed for the zone affecting the jet. No reason can be given for the inconsistent values obtained for Romberg's two runs, although he did observe an upwelling condition in the region during some of his runs.

In addition to the velocity ratio, the other main factor affecting E is geometry. This can best be seen be referring to Table 5.1. As the initial angle with the wall is decreased, entrainment is more inhibited by the near bank as shown by the difference between E for 90° and 60-45° runs. In addition, the jet can be constrained by the far bank if it should reach that far. This effect can be seen in the field results as measured by E and W_r (the ratio of ambient stream width to the discharge width). Widows Creek, for example, has a W_r about 30% of the laboratory value and an E about 40% of the

laboratory value. New Johnsonville, for one-sixth the laboratory W, exhibits about 20% of the laboratory E. As expected, then, E is reasonably proportional to more restrictive geometry.

It is recommended that a maximum E of 0.4 be a starting point. Figure 5.15 should be reviewed for reduction due to the k value and Table 5.1 reviewed to indicate any reductions due to geometry. Consider an example of a discharge canal of width B_o = 200 ft discharging into a 2000-ft-wide stream with k = 3 at an initial angle $\beta_o' = 60°$. One would begin with the observed average E (see Table 5.1, laboratory value for 60°) of 0.2 for a 60° discharge for $1 \leq k \leq 5$. Figure 5.15 shows that for k = 3, probably no correction is necessary for the k value. Then, calculate W_r = 2000/200 = 10 and compare it to the laboratory W_r = 24. Since this field W_r is about 40% of the laboratory W_r, a value of E about 40-50% of the laboratory value might be suggested, or E = 0.08-0.10. More data are needed before all the relationships between angle, k, width ratio, etc., can be completely articulated. Therefore, the choice of E remains still partially an art with perhaps some good fortune lumped in.

4. Limitations and Ranges of Applicability

There are several limitations to the Motz-Benedict model. First, it allows no vertical mixing and hence underestimates early mixing. Therefore, low initial densimetric Froude numbers should exist for best results, usually $F_j \leq 5$.

Second, the model is strictly a near-field model. Due to omission of ambient turbulence and no vertical mixing, the model should not be extended too far beyond the point of about a ΔT of 3°F. Beyond this point, vertical density gradients are probably small enough to allow appreciable vertical mixing and the model would greatly underestimate further dilution.

The model seems particularly applicable to river systems where $1 \leq k \leq 5$. However, some data exist to enable its use in lake systems where k may approach ∞.

Finally, there is one major drawback to the model as a predictive tool. The results are greatly dependent on the choice of E. Although some evidence exists for selection of E, it is not sufficient to nail E down precisely. An error in E of a factor of 2 will yield an error in distances to a given isotherm, areas within an isotherm, or time of exposure of a like factor of 2. Hence, the model should be used carefully, with an awareness of its limitations. Any jet model requiring input of empirical coefficients has the same problem.

5. Numerical Example

It would be worthwhile to show one example calculation giving some idea of model output and capability. The basic references contain numerous examples including data fittings for field cases.

Consider the case described by Table 5.2.

The basic system of equations can be nondimensionalized, a computer solution then requiring specification only of k, $C_D' = C_D/4E$, and β_o, the angle at the end of the ZOFE. The results of the basic computer solution are then in dimensionless form and can be expanded to fit various physical cases depending on the values of β_o and other parameters. As calculated in an earlier section

Table 5.2. Data for Motz-Benedict Example

Parameter	*Value*
B_o = Discharge width, ft	40
z_o = Discharge depth, ft	5
Q_p = Plant flow rate, cfs	730
U_o = Initial velocity	3.65
U_a = Ambient velocity, ft/sec	0.0
ΔT_o = Initial temperature rise, °F	25.0
U_a/U_o = Reciprocal of velocity ratio	0.0
β_o' = Initial angle	90.0°
E = Entrainment coefficient	0.06
C_D = Drag coefficient	0.5
s_e = Length of ZOFE, ft	208
K = Surface cooling coefficient, Btu/ft^2-day-°F	180

in Chapter II, F_j = 4.8 for this case. Figure 5.18 presents the dimensionless temperature-decrease curve. Figure 5.19 shows isotherms. E was based on Table 5.1 and Fig. 5.15, for k approaching infinity. Table 5.3 presents the

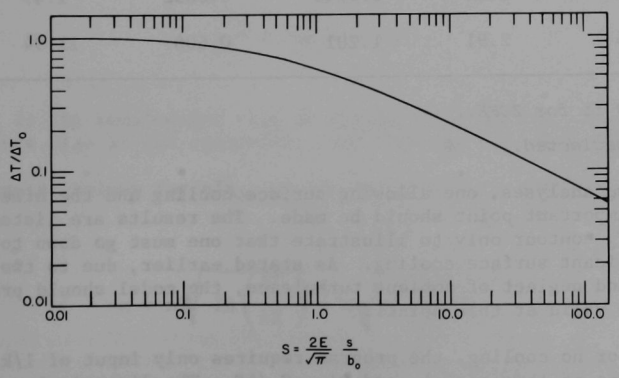

Fig. 5.18. Temperature Decrease for Motz-Benedict Example.

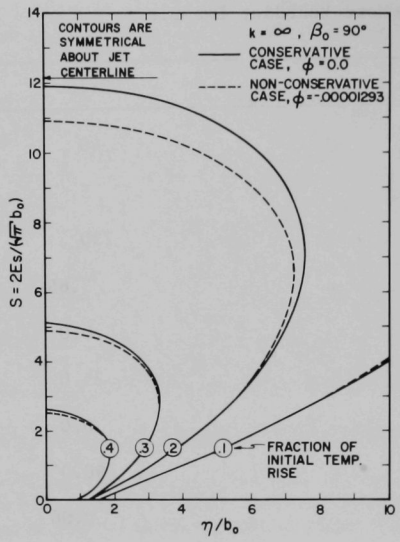

Fig. 5.19.

Isotherms for Motz-Benedict Example.

Table 5.3. Example Predictions from Motz-Benedict Model

ΔT, °F	*Distance to Contour,*[a] *mi*		*Area within Contour,*[b] *mi*^{2}		*Time to Contour, hr*	
	No Cooling	*Cooling*	*No Cooling*	*Cooling*	*No Cooling*	*Cooling*
10	0.27	0.264	0.00439	0.00427	0.173	0.164
5	1.10	1.02	0.0746	0.0652	1.47	1.29
2.5	4.46	2.91	1.201	0.608	11.94	6.30

[a]*Includes 208 ft for ZOFE.*

[b]*ZOFE areas neglected.*

results of two analyses, one allowing surface cooling and the other setting K = 0. One important point should be made. The results are listed to the 2.5°F = 0.1ΔT_o contour only to illustrate that one must go down to lower rises to get significant surface cooling. As stated earlier, due to two-dimensional assumptions and neglect of ambient turbulence, the model should probably not be considered valid at this point.

To run for no cooling, the program requires only input of 1/k, β_o' (actually sine and cosine of this angle), and $C_D' = C_D/4E$. The dimensionless results shown are then obtained. The cooling case requires that E, U_o, z_o, b_o, and K be specified.

The length of the ZOFE was chosen as $5.2B_o$ = 208 ft based on the findings of Albertson *et al.*[5] for slot jets. Since U_o = 3.65 ft/sec, the time of travel in this zone is 208/3.65 = 57 sec. No attempt will be made to include surface areas that are inside the ZOFE since the model does not yield the temperature distribution in this zone.

Some comment is needed on obtaining some of the other values. The dimensionless plot in Fig. 5.18 is plotted directly from computer output of $\Delta T/\Delta T_o$ versus S. This curve would be the same for this model for any case in which $k \to \infty$. As an example, consider the 5°F rise. From the graph, S = 11.9. Then, from the definition of S,

$$s = \frac{\sqrt{\pi}}{2E} Sb_o, \tag{5.32}$$

in which s is the distance along the axis from the end of the ZOFE, and b_o is the jet half-width at the end of the ZOFE = 0.8 B_o (see Ref. 94). Using known values, with b_o = 0.8(40) = 32 ft, we obtain

$$s = \frac{\sqrt{\pi}}{2(0.06)} (11.9)(32) = 5625 \text{ ft.}$$

Adding 208 ft to this (for the ZOFE) and converting to miles yields the value of 5833 ft = 1.10 mi in Table 5.3.

The areas and times are calculated in another computer program that uses the results of the main Runge-Kutta solution. At each incremental point on the s axis, lateral distances can be computed to any desired isotherm by use of the Gaussian relationship assumed in the model, or

$$\frac{\Delta T_\eta}{\Delta T} = \exp\left(-\eta^2/b^2\right), \tag{5.33}$$

in which ΔT_η is the temperature rise at distance η from the centerline, ΔT is the temperature rise at the centerline, and b is the jet half-width.

The computer solves for b/b_o, so the distance η to the desired contour can be found by

$$\eta = n\sqrt{-\ln\left(\frac{\Delta T_\eta}{\Delta T}\right)} = b\sqrt{\ln\left(\frac{\Delta T}{\Delta T_\eta}\right)}. \tag{5.34}$$

Then the area can be found by

$$A_c = 2 \int_0^{s_c} \eta \, ds, \tag{5.35}$$

in which A_c is the area within the desired contour and s_c is the distance at which the contour crosses the jet axis. This calculation can also be done graphically by plotting the isotherms and planimetering the areas.

The time is computed separately in a computer routine. However, the main computer Runge-Kutta solution yields values of U/U_o versus $S = (2E/\sqrt{\pi})(s/b_o)$.

It is easy to program to calculate time by numerical integration of ds/U. See Sec. V.A.8 above for details on time calculations. However, in a manner similar to that discussed there, one can obtain time estimates graphically by plotting $1/(U/U_o)$ against S, planimetering from 0 to the S desired and multiplying the planimetered area by $\sqrt{\pi}\, b_o/(2EU_o)$.

E. Pritchard's Model

Pritchard has developed a model that is classed a "complete" model. This implies that it accounts in some fashion for both near- and far-field regimes. The model also includes the effect of surface cooling. It is a model for a surface discharge from a rectangular canal at 90° to the shoreline into an essentially stagnant ambient current. The model has its basis in simple mass-, heat-, and momentum-conservation requirements. However, the basic elements of the model are drawn primarily from the author's extensive experience in analytical and physical modeling in estuaries and lakes. It is frequently difficult to find verification or support for some aspects included in the model. Nevertheless, the model is simple to apply and is claimed by Pritchard to be conservative, that is, overestimating temperatures and areas affected by this temperature. It has been widely seen in assessments of power-plant impact on receiving waters, and, therefore, it is important to understand its basic elements and be able to assess its validity.

The number of references explaining the basic model and its development is limited.[109-111] Perhaps the best source of information on this model and its development is to be found in the work by Policastro and Tokar.[104] They have synthesized the various reports and, by their discussions with Pritchard and their own analyses, have put the model in some reasonable order.

1. Model Assumptions

Several major assumptions characterize the Pritchard model. Among these are the following:

a. There is no spreading in the ZOFE, which is taken as nB_o long. The value of n is taken as 6.

b. Initial lateral jet profiles are "tophat." Profiles in this jet region and further downstream in the diffusion region are also considered "tophat"

profiles. A "tophat" profile is one in which the temperature or velocity across the width of the jet plume is constant and at the "edge" of the jet drops immediately to the ambient value of velocity or temperature. Until the jet centerline temperature has decreased to $0.2\Delta T_o$, the plume is assumed to spread linearly so that the width of b equals y/n, where n, the so-called inverse-spreading rate, is again taken as 6. This linear spreading assumption replaces the entrainment assumption made in several other jet models.

c. After the centerline temperature has decreased to $0.2\Delta T_o$, the temperatures decrease as the inverse first power of the distance. This is the same rate of decrease as that occurring due to natural diffusion from a continuous point source.

d. There is a "critical depth of mixing," z_c. This critical depth may be different for each water body and would be a function of geometry, density structure in the water body, and the natural mixing processes there.

e. The plume will mix linearly in the vertical direction until the critical depth, z_c, is obtained. Thereafter, the plume will retain a constant depth. If the initial depth is greater than z_c, the plume depth will remain constant until it reaches the far-field region.

f. If the receiving-water bottom drops off rapidly, the growth in vertical thickness of the jet measured longitudinally on the plume centerline will be taken as 0.2 ft per 100 ft. If the bottom slope of the receiving-water body is small, the method of images can be used to obtain the length required for the jet to attain a thickness of z_c.

g. One can account for the heat loss from the plume by decreasing the source strength by the amount of heat lost between the source and the given isotherm being reviewed.

h. An important assumption of the Pritchard model is that no ambient current exists. Pritchard feels this assumption is valid if $k > 10$, or the ambient current is less than 1/10 of the jet velocity, U_o.

i. Buoyancy forces are negligible.

Pritchard's approach is essentially to begin his calculations by calculating distances in plume areas for two-dimensional mixing, that is, no vertical mixing included with no surface cooling effect. Then, he makes a separate correction for any vertical mixing that has occurred and, in addition, a correction for surface cooling. Pritchard actually made many other assumptions in presenting rule-of-thumb relationships based on his empirical evidence and experience. These assumptions are not mentioned here, but will be evident as the chapter proceeds.

2. Model Equations

The assumptions given form the basis for a simplified solution to the equations of mass, heat, and momentum conservation. Figure 5.20 is a definition sketch for horizontal and vertical motion.

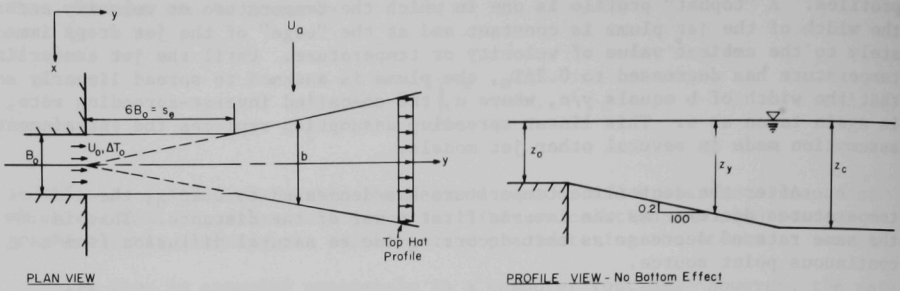

Fig. 5.20. Definition Sketch for Pritchard Model.

a. Initial Two-dimensional Distances and Contours. First, one can write the equation saying that the momentum flux past any section of the plume remains constant (and therefore equal to the momentum flux at the jet outlet). This implies a zero ambient current, for otherwise momentum would change along the plume axis.

$$\rho \int_{-b/2}^{+b/2} U^2 \, dx = \rho \, U_o{}^2 B_o \quad \text{for } y > s_e \, . \tag{5.36}$$

Similarly, for this initial solution, assuming no surface cooling, the total heat passing each section must be the same and equal to the initial heat output at the jet outlet, or

$$\rho \, c_p \int_{-b/2}^{b/2} U\Delta T \, dx = \rho \, c_p \, U_o \Delta T_o B_o \quad \text{for } y > s_e \, . \tag{5.37}$$

The velocity, U, and temperature rise, ΔT, are functions only of y for "tophat" profiles. The solutions to Eqs. 5.36 and 5.37 become

$$U = U_o \left(\frac{s_e}{y}\right)^{1/2} \tag{5.38}$$

and

$$\Delta T = \Delta T_o \left(\frac{s_e}{y}\right)^{1/2} , \tag{5.39}$$

in which $s_e = nB_o$.

The continuity principle is met by the specification of linear jet spreading, or

$$b = y/n \text{ for } y > s_e. \tag{5.40}$$

Of interest is the distance along the plume axis to the point at which a given isotherm is intersected, called $y_{\Delta T}$ here. Rearranging Eq. 5.39 gives the following expression for this distance:

$$y_{\Delta T} = nB_o \left(\frac{\Delta T_o}{\Delta T}\right)^2 . \tag{5.41}$$

This equation is assumed valid for $0.2\Delta T_o \leq \Delta T \leq \Delta T_o$. Beyond that point, Pritchard postulates a temperature decrease inversely with distance, giving

$$\frac{\Delta T}{\Delta T_o} = \frac{30B_o}{y} \quad \text{for } \Delta T \leq 0.2\ \Delta T_o . \tag{5.42}$$

As Policastro and Tokar[104] note, the term $30B_o$ appears so that Eqs. 5.39 and 5.42 will yield the same result at $\Delta T = 0.2\ \Delta T_o$. The distance to a given isotherm can be found by rearranging Eq. 5.42, or

$$y_{\Delta T} = \frac{30B_o \Delta T_o}{\Delta T} . \tag{5.43}$$

b. Areas within Isotherms. If no vertical mixing is expected, one can proceed immediately to calculate surface areas within isotherms (no surface cooling yet allowed). Pritchard has drawn on his experience and data and he has observed to provide several rules of thumb for plotting isotherms and calculating areas.

(1) The maximum width of the isotherm temperature rise ΔT is one-fourth the length of the area within the isotherm, or

$$b_m = \frac{1}{4}\, y_{\Delta T} . \tag{5.44}$$

(2) The width of the area within an isotherm increases "smoothly" from the outfall, reaching its maximum width, b_m, at one-third the area length, or $0.33y_{\Delta T}$. (The term "smoothly" is not defined any more precisely by Pritchard.)

(3) The width of the area within a given isotherm then remains constant from $y = 0.33y_{\Delta T}$ to $y = 0.75y_{\Delta T}$.

(4) The isotherm area between $y = 0.75y_{\Delta T}$ and $y = y_{\Delta T}$ is "bullet-shaped." (Again, this shape is not precisely defined.)

(5) The area within the ΔT isotherm, called $A_{\Delta T}$ here, is

$$A_{\Delta T} = 0.215\ y_{\Delta T}^2\ . \tag{5.45}$$

Figure 5.21 illustrates these rules of thumb. Such relations as these have probably created most concern about Pritchard's model. Policastro and Tokar[104] list several sources upon which Pritchard apparently drew to arrive at these rules. However, to our knowledge, there has been no publication of the rationale and data-fitting involved in arriving at these rules, and hence, no opportunity for others to evaluate their validity. Such a publication (including other items as well in a readily accessible form) would go a long way toward alleviating uneasiness concerning this model. The rules offered above certainly have the advantage of simplicity of application.

Note that if vertical mixing is to be accounted for, it must be done *before* the areas are computed.

3. Inclusion of Vertical Mixing

As mentioned in the assumptions (Sec. 1 above), Pritchard includes vertical mixing in his model in a simple fashion by allowing a linear rate of change of depth of the plume up to a depth he calls the critical depth of mixing for a given body of water. This critical depth is usually about 10 ft. Occasionally, after review of information from the various sites he has studies, Pritchard might recommend a smaller depth, for example, 6 or 8 ft for a particular site. He suggests 10 ft if no better number is available.

Pritchard considers two distinct cases for this increase of depth to reach the critical depth of mixing, z_c. First is the case in which the receiving-water-body bottom drops off so rapidly it plays no role at all. In this case, he suggests a linear change, as shown in Fig. 5.20, of 0.2 ft per 100 longitudinal feet of the plume. This means, for example, that it takes 2000 ft for the plume to increase its depth by a total of 4 ft. Once the critical depth of mixing has been attained, the plume thickness will not change in Pritchard's model.

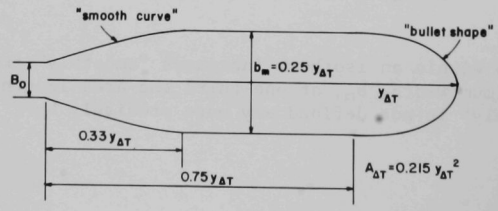

Fig. 5.21.

Pritchard's Idealized Isotherm.

The other case Pritchard considers is perhaps more typical of most discharge sites. In this case, the bottom is at a finite distance below the surface and definitely has an impact on the vertical mixing of the plume if for no other reason than the reduction of the scale of the ambient turbulence. Pritchard's method is reviewed by Policastro and Tokar[104] and thus will not be reviewed in detail here. However, he uses the method of images to place an image source above the water surface and below the lake bottom to give the effect of the reflecting boundary at the water surface and at the bottom of the water body. He then superimposes the solutions obtained by adding these image sources to the real source and arrives at the following equation for the distance, η_1, to the point where the critical depth of mixing is obtained:

$$\eta_1 = \frac{12z_o}{(1 - \sqrt{1 - z_o/z_c})^2} \tag{5.46}$$

Over this distance, η_1, the plume thickens linearly from its initial thickness, z_o, to the critical depth of mixing, z_c.

It is now necessary to adjust the temperature distribution obtained from the simple two-dimensional distribution. This will be done by assuming that, due to the increase in depth, dilution is increased in the same proportion. That is, if the depth is now 50% greater than under the two-dimensional assumption, the dilution will be 50% greater. The temperature at that point, assuming the same heat-flow through section, will be only two-thirds the temperature rise predicted under the two-dimensional assumption. This can be written as

$$\Delta\bar{T} = \frac{z_o}{z_y} \Delta T \ , \tag{5.47}$$

where z_y = plume thickness at distance y from orifice (see Fig. 5.20) and $\Delta\bar{T}$ = new average temperature over cross section. This means that at the distance, $y_{\Delta T}$, the temperature rise will now be different from that predicted by the two-dimensional model. To calculate the areas, one must find the new distances to the contours or isotherms of interest. One simple way to do this is by plotting a curve of the new temperature rises versus distance and interpolating for the isotherms of interest. This can simply be done by linear interpolations without preparing the graph. After the new values of $y_{\Delta T}$ are obtained, Eq. 5.45 can be used to calculate isotherm areas.

Therefore, the vertical-mixing adjustment is really only an adjustment due to added dilution water that is presumed to have become available because of the increasing vertical thickness of the plume. Policastro and Tokar present some cogent questions about the assumptions made in the derivation of the thickening relationship in the case for which there is a bottom at a finite depth. This analysis is completely unverified at this time and leaves some questions theoretically, even though it may give a reasonable representation of those results observed in the field.

4. Inclusion of Surface Cooling in Models

Pritchard includes the effect of surface cooling on the plume as an additional step in his analysis. Pritchard (as well as several other authors discussed in this report) has observed that surface cooling plays little role for most discharges until approximately $0.1\Delta T_o$ has been reached. Within isotherms at higher temperatures, the areas are sufficiently small so that surface cooling is negligible.

Pritchard conceptualized the effect of surface cooling by treating the loss of heat due to surface cooling as if it were an effective decrease in the strength of the source, that is, the heat existing from the jet outlet. Assuming a hypothetical case with a 20° initial rise of temperature, and consider, for example, the 10° isotherm. Some portion of the initial heat would be lost from the area inside the 10° contour. Pritchard then proceeds by a progressive summation to find the value of the effective source strength for each previously calculated isotherm (no surface cooling allowed). From this procedure, he is able to calculate the change in the isotherm area that occurs due to this effectively reduced source strength.

To carry the example further, visualize the isotherm calculated by the foregoing methods, assuming no surface cooling. Clearly, for the same conditions of discharge velocity and canal size, etc., if the total heat load rejected to the ambient water body were reduced, the 10° isotherm would not extend as far into the ambient water body. This is essentially the fashion in which Pritchard's conceptual model tries to account for surface cooling.

A qualitative equation can be writen to express Pritchard's conceptual model for a given isotherm:

Incremental area including cooling = Incremental area without cooling (5.48)
[(Source strength - Cumulative surface heat loss)/Source strength].

Notice that an equation of this form must be written for each isotherm of concern. This means that a set of simultaneous equations is derived. To quantify the relationship involved, consider the following notations to be used here:

A_n = area inside isotherm;

$(\Delta A_n)_m$ = incremental area of nth isotherm, no cooling allowed, i.e., area between nth and (n - 1)st isotherms, or $A_n - A_{n-1}$; subscript m implies mixing only.

$(\Delta A_n)_{m,c}$ = incremental area of nth isotherm, mixing (m) and cooling (c) both included;

$\Delta\overline{T}_n$ = average temperature rise between ΔT_n and ΔT_{n-1};

ΔT_n = temperature rise of nth isotherm;

$(\Delta\Gamma_n)_m$ = rate of excess heat loss between isotherms based on area calculated without cooling;

$(\Delta\Gamma_n)_{m,c}$ = rate of excess heat loss between isotherms based on area calculated including mixing *and* cooling;

Q_h = total heat-rejection rate at jet outlet.

The heat-loss rate can be expressed by

$$(\Delta\Gamma_n)_m = K\Delta\overline{T}_n(\Delta A_n)_m \tag{5.49}$$

$$(\Delta\Gamma_n)_{m,c} = K\,\overline{T}_n(\Delta A_n)_{m,c}\ , \tag{5.50}$$

in which K = surface cooling coefficient.

All those quantities with only the subscript m are already known or can be immediately calculated as in previously performed mixing-only computations. Using the notation shown, we can write Eq. 5.48 in the form

$$(\Delta A_n)_{m,c} = (\Delta A_n)_m \left[\frac{Q_h - \sum_{i=1}^{n} (\Delta\Gamma_i)_{m,c}}{Q_h}\right]. \tag{5.51}$$

The summation term on the right-hand side of Eq. 5.51 represents the heat loss from the area between the jet outlet and the given isotherm. For example, if n = 3 (the third isotherm of interest), there would be three terms of the type $(\Delta\Gamma_i)_{m,c}$.

Pritchard[107] and Policastro and Tokar[104] indicate how the simultaneous equations represented by Eq. 5.51 can be solved to arrive at the following equation, which can be used for computing the required areas:

$$(\Delta A_n)_{m,c} = (\Delta A_n)_m \left[\frac{Q_h - \sum_{i=1}^{n-1} (\Delta\Gamma_i)_{m,c}}{Q_h + (\Delta\Gamma_n)_m}\right]. \tag{5.52}$$

In this solution, use is made of

$$(\Delta\Gamma_n)_{m,c} = (\Delta\Gamma_n)_m \frac{(\Delta A_n)_{m,c}}{(\Delta A_n)_m} \tag{5.53}$$

(formed by eliminating K from Eqs. 5.49 and 5.50).

The total areas corrected for cooling can be obtained after solution by use of Eq. 5.52 by simply summing up the incremental areas, as

$$(A_n)_{m,c} = \sum_{i-1}^{n} (\Delta A_i)_{m,c} , \tag{5.54}$$

in which $(A_n)_{m,c}$ is the area inside the nth isotherm, corrected for cooling. In addition, the lengths and widths of the isotherms can be adjusted by

$$(y_{\Delta T_n})_{m,c} = (y_{\Delta T_n})_m \left[\frac{(A_n)_{m,c}}{(A_n)_m}\right]^{1/2} \tag{5.55}$$

and

$$(b_{m_n})_{m,c} = (b_{m_n})_m \left[\frac{(A_n)_{m,c}}{(A_n)_m}\right]^{1/2} . \tag{5.56}$$

A numerical example is presented later to illustrate the use of the surface cooling correction for Pritchard's model. Again, it should be noted that Policastro and Tokar[104] have presented a very rational argument against at least one phase of this surface-cooling analysis presented by Pritchard. They feel that the right-hand term in brackets in Eq. 5.51 should be squared rather than to the first power. This correction, as they note, would tend to decrease the predicted areas, hence, in this respect at least, Pritchard's model may well be conservative. This particular point of contention has not yet been resolved.

5. Time-of-exposure Calculations

Once the corrections have been made to the initial two-dimensional analysis for vertical mixing and surface cooling, one should then have distances and areas within isotherms available to him immediately. Recall Eq. 5.38, which gives the form of the velocity within the plume as a function of the distance y from the shore. Recall also the basic formulation for the time of exposure, which can be written as

$$t_{\Delta T} = \int_0^{y_{\Delta T}} \frac{dy}{U} . \tag{5.57}$$

Substituting Eq. 5.38 into Eq. 5.57 and performing the suggested integration reveals the following equation for the time to reach a given temperature contour traveling along the plume axis:

$$t_{\Delta T} = \frac{2(y_{\Delta T})^{3/2}}{3[U_o(nB_o)^{1/2}]} , \qquad (5.58)$$

in which $t_{\Delta T}$ is the time to reach the ΔT isotherm along the plume axis.

Equation 5.58 can be used to calculate directly the time of travel. As for the other equations in Pritchard's work, this is a simple calculation to perform.

6. Model Verification

The best available commentary on verification of Pritchard's model can be found in Ref. 104. Pritchard's model has not been verified extensively, at least in published information, against field or laboratory data. Large amounts of good-quality field data do not exist for the verification of any model. However, Pritchard has based his model on years of extensive experience in estuaries, lakes, and rivers. A prime benefit of his model is probably the fact that it does represent the assimilation and simplification of vast amounts of field and laboratory experience. One suspects that as added experience and information become available, they will probably be incorporated into the model. To overlook Pritchard's model because of its simplicity would be a mistake for other modelers.

Most of the comments made on verification by Policastro and Tokar concern the individual elements of the model. One such topic is the choice of the inverse-spreading ratio as 6. Review of both surface and submerged buoyant and nonbuoyant jets from a number of sources yielded this as a representative value. It seems to be relatively valid for two-dimensional mixing.

Another major feature in Pritchard's model is the inclusion of the critical depth of mixing, z_c. Pritchard has suggested that if no better information is available, z_c equals 10 ft might be an appropriate value. He arrived at this value by studying plume data from a number of different sources, especially on lakes. He found that, in most cases, excess heat is contained in a layer some 10-15 ft thick. Besides this type of information and the case that occurs when a physical bottom controls the depth of the jet, there is no real verification for the concept of a critical depth of mixing. Pritchard's method of determining the length to obtain this critical depth using a method of images solution is completely analytical and unverified in laboratory or field at this time.

Equations 5.44 and 5.45 and the rules of thumb concerning the width and area within isotherms have again been assimilated from Pritchard's field and laboratory experience. Policastro and Tokar[104] (p. 267) make the following statement: "These approximate formulas and guidelines were developed from examination of the results of plume studies at the Chesapeake Bay Institute, from model studies done for the Pilgrim Nuclear Power Station on Cape Cod Bay, and from data taken at small existing plants in the Chesapeake Bay region, such

as the Chalk Point Plant and the Chesterfield Plant on the James River. The hydraulic modeling done at Vicksburg and the experimental data obtained from the Waukegan plumes[14] were also included." In addition, Pritchard does present some comparison with field data. For example, in his Zion report,[109] he compares his model and receives reasonable agreement with data taken at the Waukegan Power Station.

In conclusion, Pritchard's model is probably no less verified than any other available model, except that he has published no generally available information on all of the data used in arriving at the model, the analyses of the data made, and the final fittings and/or modeling criteria. Much of the uneasiness that apparently exists concerning results computed with Pritchard's model would likely be alleviated by such a publication. Quite likely it would also be an extremely useful document.

Other questions have been raised as discussed already by Policastro and Tokar. For example, consider the surface cooling adjustment made by Pritchard. Policastro and Tokar, and Pritchard himself, assert that apparently if used within the restrictions already noted, Pritchard's model is a conservative model in the sense that it predicts temperatures and areas within isotherms that are larger than would ordinarily be expected. This is due to the fact that full weight is not given to vertical mixing and most of the rules of thumb that Pritchard applies have been chosen to provide an upper limit on his estimates. Since the model has not been verified extensively, however, the question of its being conservative or optimistic is unresolved. One area, for example, in which Pritchard does note that he has gotten distinctly lower temperatures than indicated is in the region very close to the jet outlet including the ZOFE. As can be seen in Fig. 5.20, Pritchard allows for no spreading and therefore no mixing in the horizontal direction in this zone. As a result, he would certainly underestimate mixing and the subsequent dilution.

Although such conservatism might be assumed, there are some aspects of the model in which conservative results might definitely not be obtained. One such example arises from Pritchard's analysis of the vertical mixing. He assumes a linear rate of spread completely independent of the density profile in the lake or the receiving-water body. If density stratification was strong, there might be much less vertical mixing than predicted by this linear rate of increase and he could conceivably overestimate the dilution by allowing too much vertical mixing. However, if the critical depth of mixing, z_c, is less than 10 ft, this limitation is probably not a likely one.

In summary, then, Pritchard's model is a simple one to use, the only data required being easily obtainable physical data. No estimate of such elements as diffusion coefficients or entrainment coefficients is necessary. The model should clearly be applied where no geometry constraints on the lateral edges of the plume are expected and where the ambient current is small; i.e., k is greater than 10. Perhaps the biggest single limitation to the model is its simplicity. Due to this feature, it cannot cover all the factors that ordinarily are expected to affect the mixing of a heated discharge. Due to his experience, Pritchard may be able to apply this model with some accuracy, even in rather unusual situations. However, guidelines for application of the model by others are not so clear, and as a result, its extension to anything other than the fairly idealized condition of its derivation should be performed

with great care. Its usefulness would primarily be for discharges into large lakes or into estuaries. River systems, especially those in which the ambient current might be important, would not be expected to be amenable to solution by Pritchard's techniques.

7. Limitations and Ranges of Applicability

Several comments should be made concerning the limitations on Pritchard's model. One is the fact that the ambient current must be less than 1/10 of the initial jet current (that is, $k > 10$). If this situation does not exist, Pritchard himself suggests the use of Carter's model. Presumably any other jet model would also suffice. If the jet effect is not accounted for and the plume is swept against the shore, the dilution water available may be so decreased that Pritchard's model would no longer be conservative but vastly underestimate the areas and distances involved.

As noted, Pritchard has not included the effect of any buoyancy terms at all. This might be especially of interest in his concept of the vertical-mixing process. He assumes that the mixing takes place in a way as to cause a linear increase in depth. Obviously, high stratification would prevent this form of mixing. In addition, his model actually assumes that mixing takes place in the vertical direction at the same rate as in the horizontal. This would be true in a nonbuoyant discharge. For a buoyant discharge, however, it would not be true. The method-of-images model that Pritchard uses to predict the distance, η_1, to the point of reaching his critical depth of mixing is unverified at this time. There is a need for additional work on this model in the vertical-mixing portion. Therefore, in any application where vertical mixing is presumed to account for an important part of the dilution, Pritchard's model probably should be applied with care.

As Policastro and Tokar point out, there is a need for a better definition of the point of transition from the jet-dilution mixing region (which Pritchard specified as that for temperature rises above $0.2\Delta T_o$) and the ambient diffusion region. Presumably, if one's only concern is in those regions for higher temperature rises, that is, above $0.2\Delta T_o$, this would not be a factor in the use of the model. However, if one is concerned with much lower temperature rises, some question might be raised as to the use of the model. In this respect, of course, this model is no different from any of the others postulated.

8. Data Needed

The parameters needed to use Pritchard's model are:

B_o = width of discharge channel,

z_o = depth of discharge channel,

U_o = initial discharge velocity,

T_n = assumed natural water temperature,

U_w = wind speed, mph,

ΔT_o = initial temperature rise,

Q_h = total heat rejection rate at jet outlet, and

z_c = critical depth of mixing.

The values of T_n and U_w are needed to evaluate K, the surface cooling coefficient, which is also a function of the temperature rise. T_n will be assumed approximately equal to the equilibrium temperature.

9. Numerical Example

a. Data. For this numerical example, a case presented by Pritchard in his study of the Zion Power Plant on Lake Michigan will be reported. For this case, the data used were

$$B_o = 24 \text{ ft},$$
$$z_o = 10 \text{ ft},$$
$$U_o = 14 \text{ ft/sec},$$
$$T_n = 70°\text{F},$$
$$U_w = 10 \text{ mph},$$
$$\Delta T_o = 20°\text{F},$$
$$Q_h = 15.0 \times 10^9 \text{ Btu/hr, and}$$
$$z_c = 10 \text{ ft}.$$

First, note that this is a very high-velocity discharge designed to encourage high initial mixing. The total plant discharge, Q_p, is (14 ft/sec)(24 ft)(10 ft) = 3360 cfs. In addition, since $z_o = z_c$, no correction for vertical mixing need be made. A numerical example of this correction will be presented for a separate case, however.

b. Lengths, Widths, Areas (No Cooling). First, calculations are made assuming only two-dimensional mixing. Equation 5.41 is used to calculate lengths of areas within isotherms in the jet region. For example, for the $\Delta T = 14°\text{F}$ contour, in the jet,

$$y_{14} = 6(24 \text{ ft})(20/14)^2 = 294 \text{ ft}. \tag{5.59}$$

For $\Delta T \leq 0.2\Delta T_o$ (or $\Delta T \leq 4°\text{F}$ in this case), Eq. 5.43 is used. Consider the $\Delta T = 2°\text{F}$ isotherm,

$$y_2 = 30(24 \text{ ft})20/2 = 7200 \text{ ft}. \tag{5.60}$$

These results are shown in Table 5.4, along with $y_{\Delta T}$ for other isotherms.

The width of the area in an isotherm is easily calculated by Pritchard's rule of thumb, Eq. 5.44. Likewise, the area within the contour is calculated by Eq. 5.45.

Table 5.4. Length, Width, and Area for Example Case, with No Cooling

Δt, °F	$Y_{\Delta T}$, ft	b_m, ft	$(A_n)_m$, ft^2	$(A_n)_m$, acres
14	2.94×10^2	0.74×10^2	1.88×10^4	0.4
12	4.02×10^2	1.01×10^2	3.50×10^4	0.8
10	5.76×10^2	1.44×10^2	7.15×10^4	1.6
8	9.00×10^2	2.25×10^2	1.75×10^5	4.0
6	1.60×10^3	4.00×10^2	5.52×10^5	12.7
5	2.30×10^3	5.75×10^2	1.14×10^6	26.2
4	3.60×10^3	9.00×10^2	2.80×10^6	64.3
3	4.81×10^3	1.20×10^3	4.98×10^6	1.14×10^2
2	7.20×10^3	1.80×10^3	1.12×10^7	2.57×10^2

For the $\Delta T = 14°F$ isotherm,

$$b_m = 0.25(294 \text{ ft}) = 74 \text{ ft and}$$
$$A_{14} = 0.215(294 \text{ ft})^2 = 1.88 \times 10^4 \text{ ft}^2.$$

For the $\Delta T = 2°F$ isotherm,

$$b_m = 0.25(7200 \text{ ft}) = 1800 \text{ ft and}$$
$$A_{14} = 0.215(7200 \text{ ft})^2 = 1.12 \times 10^7 \text{ ft}^2.$$

Again, these values are found in Table 5.4, along with intermediate values.

c. Adjustment for Surface Cooling. The initial areas calculated must now be adjusted for surface cooling. Very little heat loss occurs due to the mechanism for this case. However, the details of the procedure remain the same for other cases.

First, some discussion is needed on evaluation of K, the cooling coefficient, a topic discussed at some length in Chapter III. Pritchard does not state the source of his K values, although he presents the values in Table 5.5. It can be shown, however, that they follow closely from an extension of the equation for K, using Meyer's equation for evaporation. From Chapter III,

$$k = 15.7 + 0.26 + \frac{P_s - P_E}{T_s - T_{EQ}} (a + b\, U_w), \tag{5.61}$$

where k = surface cooling coefficient, in Btu/day-°F-ft^2,

P_s = saturation vapor pressure at water surface temperature, T_s, in mm Hg,

P_E = saturation vapor pressure at equilibrium temperature, T_{EQ}, in mm Hg,

a = constant = 73 in Meyer's equation,

b = constant = 7.3 in Meyer's equation, and

U_w = wind speed, in miles per hour.

Table 5.5. The Surface Cooling Coefficient, K (Btu-ft^2-°F-hr), as a Function of Wind Speed, Natural Surface Water Temperature, and Excess Temperature (From Ref. 109, p. 8)

U_w, mph	ΔT, °F 2	6	10	14	18
			For T_n = 40°F		
2	1.39	1.51	1.65	1.83	2.07
4	1.90	2.05	2.21	2.42	2.68
6	2.42	2.58	2.78	3.00	3.29
8	2.94	3.12	3.33	3.59	2.89
10	3.46	3.66	3.90	4.18	4.50
			For T_n = 60°F		
2	1.73	1.87	2.05	2.30	2.61
4	2.47	2.69	2.88	3.17	3.52
6	3.23	3.45	3.70	4.02	4.42
8	3.98	4.23	4.53	4.89	5.32
10	4.73	5.02	5.36	5.75	6.21
			For T_n = 80°F		
2	2.26	2.44	2.68	3.03	3.47
4	3.43	3.66	3.97	4.38	4.88
6	4.59	4.90	5.27	5.74	6.31
8	3.77	6.11	6.57	7.08	7.71
10	6.93	7.37	7.86	8.45	9.13

It is evident that K is a function of T_n (which will be called approximately equal to T_{EQ}), U_w, and ΔT. Therefore, a new K will have to be determined for each incremental area studied. Values of p_s and p_E can be obtained from standard sources such as the *Handbook of Chemistry and Physics*. In addition, Fig. 3.3 shows the relation of p to temperature. Example calculations of K

will be presented for a few incremental areas to illustrate the use of this relationship. Consider the area inside the $\Delta T = 14°F$ isotherm;

$$\Delta\overline{T}_n = \frac{20 + 14}{2} = 17°F.$$

Since $T_n \simeq T_{EQ} = 70°F$, the average temperature over this isotherm area is $70 + 17 = 87°F$.

Use of tables yields $p_s = p_{87°F} = 32.85$ mm Hg and $p_E = p_{70°F} = 18.73$ mm Hg. Using Eq. 5.61, with $T_s - T_{EQ} = 87 - 70 = 17°F$, we obtain

$$K = 15.7 + \left(0.26 + \frac{14.12}{17}\right) [73 + 7.3(10)] = 175.$$

The units used in subsequent calculations will require K to be expressed in units per hour rather than per day. Therefore, the value above would yield $K = 175/24 = 7.3$ Btu/hr-°F-ft^2. In a similar fashion, K can be computed for other isotherms. For the incremental area between the $\Delta T = 12°F$ and $\Delta T = 14°F$ isotherms, $\Delta\overline{T}_n = (14 + 12)/2 = 13°F$ and $T_s - E_Q = 13°F$. Using $p_s = 28.7$ mm Hg yields $K = 6.86$ Btu/hr-°F-ft^2. For the incremental area between the 10 and 12°F isotherms, $K = 6.77$ Btu/hr-°F-ft^2. The exact value of these numbers depends on how accurately you interpolate the vapor pressure values. However, the accuracy of a graph such as Fig. 3.3 should be sufficient.

One further note on K bears repeating from Chapter III. The expression for K is no more valid than the evaporation formula used in its development. (Discrepancies that can appear are covered in Chapter III.)

In making adjustments for surface cooling, begin the innermost isotherm listed, $\Delta T = 14°F$. This will be designated by subscript $n = 1$. For this isotherm,

$$(\Delta A_n)_m = (\Delta A_1)_m = (1.88 \times 10^4 - 0)\text{ft}^2 = 1.88 \times 10^4 \text{ ft}^2.$$

This is incremental area between the 20 and 14°F isotherms based on the no-cooling analysis. The needed areas have already been shown in Table 5.4.

Incremental heat loss can be calculated from Eq. 5.49 as

$$(\Delta\Gamma_1)_m = K_1\Delta\overline{T}_1 \ (\Delta A_1)_m$$

$$= \frac{7.3 \text{ Btu}}{\text{hr-°F-ft}^2} \frac{20 + 14}{2} \text{°F} \ (1.88 \times 10^4 \text{ ft}^2) = 2.33 \times 10^6 \text{ Btu/hr}.$$

Note that this is only $(2.33 \times 10^6/15 \times 10^9) \simeq 1/6000$ of the initial heat output, and the new incremental area including cooling can be calculated from Eq. 5.52. Since the summation (i = 1 to n - 1) goes from i = 1 to i = 0, the value is zero for this first calculation. Then,

$$(\Delta A_1)_{m,c} = (1.88 \times 10^4 \text{ ft}^2) \frac{15 \times 10^9 - 0}{15 \times 10^9 + 2.33 \times 10^6} \simeq 1.88 \times 10^4 \text{ ft}^2.$$

It can be seen that the heat lost to the atmosphere over this incremental area was such a small part of the initial source strength that no correction was even noticeable. Since the area ratio remains essentially 1.0, Eq. 5.53 shows that

$$(\Delta\Gamma_1)_{m,c} \simeq (\Delta\Gamma_1)_m = 2.33 \times 10^6 \text{ Btu/hr}.$$

Note that this number differs slightly from the 2.37×10^6 found in Table 5.6. This slight difference may be due to slight differences in reading from a graph. It certainly is not significant. Similar differences are expected in the other calculations. Equation 5.54 yields the new area inside the isotherm with cooling allowed,

$$(A_1)_{m,c} = (\Delta A_1)_{m,c} = 1.88 \times 10^4 \text{ ft}^2.$$

Table 5.6. Areas within Isotherms, for Example, with Surface Cooling Included[109]

ΔT, °F	$(A_n)_m$, ft^2	$(\Delta A_n)_{m,c}$ ft^2	$(\Delta\Gamma_n)_{m,c}$ Btu/hr	$(A_n)_{m,c}$ ft^2
14	1.88×10^4	1.88×10^4	2.37×10^6	1.88×10^4
12	3.50×10^4	1.62×10^4	1.45×10^6	3.50×10^4
10	7.15×10^4	3.65×10^4	2.66×10^6	7.15×10^4
8	1.75×10^5	1.04×10^5	6.00×10^6	1.75×10^5
6	5.52×10^5	3.76×10^5	1.64×10^7	5.51×10^5
5	1.14×10^6	5.86×10^5	1.95×10^7	1.14×10^6
4	2.80×10^6	1.65×10^6	4.42×10^7	2.79×10^6
3	4.98×10^6	2.16×10^6	4.45×10^7	4.95×10^6
2	1.12×10^7	6.13×10^6	8.86×10^7	1.11×10^7

Even though the calculations will be similar, it is perhaps worthwhile to continue the example through several more incremental areas so that treatment of the summation terms in the equations will be clear. All calculations are summarized in Table 5.6.

Consider the next incremental area (n = 2) between the 12 and 14°F isotherms,

$$(\Delta A_2)_m = A_2 - A_1 = (3.50 - 1.88)10^4 \text{ ft}^2 = 1.62 \times 10^4 \text{ ft}^2$$

$$(\Delta\Gamma_2)_m = K\Delta\overline{T}_2(\Delta A_2)_m = \frac{6.86 \text{ Btu}}{\text{hr-°F-ft}^2}\,\frac{14 + 12}{2}\,\text{°F}(1.62 \times 10^4 \text{ ft}^2)$$

$$= 1.45 \times 10^6 \text{ Btu/hr.}$$

Equation 5.52 then becomes

$$(\Delta A_2)_{m,c} = (\Delta A_2)_m \frac{Q_h - (\Delta\Gamma_1)_{m,c}}{Q_h + (\Delta\Gamma_2)_m}$$

$$= 1.62 \times 10^4 \text{ ft}^2 \frac{15 \times 10^9 - 2.33 \times 10^6}{15 \times 10^9 + 1.45 \times 10^6} \simeq 1.62 \times 10^4 \text{ ft}^2.$$

From Eq. 5.53,

$$(\Delta\Gamma_2)_{m,c} = (\Delta\Gamma_2)_m \frac{(\Delta A_2)_{m,c}}{(\Delta A_2)_m} \simeq (\Delta\Gamma_2)_m = 1.45 \times 10^6 \text{ Btu/hr.}$$

From Eq. 5.54, the new total area within the 12°F isotherm is found:

$$(A_2)_{m,c} = (\Delta A_1)_{m,c} + (\Delta A_2)_{m,c} = 1.88 \times 10^4 + 1.62 \times 10^4$$

$$= 3.50 \times 10^4 \text{ ft}^2.$$

Finally, make adjustments for the area (n = 3) between the 10 and 12°F isotherms,

$$(\Delta A_3)_m = A_3 = A_2 = (7.15 - 3.50)10^4 \text{ ft}^2 = 3.65 \times 10^4 \text{ ft}^2;$$

$$(\Delta\Gamma_3)_m = K_3\ \Delta\overline{T}_3\ (\Delta A_3)_m = \frac{6.77 \text{ Btu}}{\text{hr-°F-ft}^2}\,\frac{12 + 10}{2}\,\text{°F}(3.65 \times 10^4 \text{ ft}^2)$$

$$= 2.72 \times 10^6 \text{ Btu/hr.}$$

Then Eq. 5.52 becomes

$$(\Delta A_3)_{m,c} = (\Delta A_3)_m \frac{Q_h - (\Delta\Gamma_1)_{m,c} - (\Delta\Gamma_2)_{m,c}}{Q_h + (\Delta\Gamma_3)_m}$$

$$= (3.65 \times 10^4 \text{ ft}^2) \frac{15 \times 10^9 - 2.37 \times 10^6 - 1.45 \times 10^6}{15 \times 10^9 + 2.72 \times 10^6}$$

$$\simeq 3.65 \times 10^4 \text{ ft}^2.$$

Equation 5.54 yields the new area within the 10°F isotherm:

$$A_3 = (\Delta A_1)_{m,c} + (\Delta A_2)_{m,c} + (\Delta A_3)_{m,c}$$

$$= (1.88 + 1.62 + 3.65)10^4 \text{ ft}^2 = 7.15 \times 10^4 \text{ ft}^2.$$

Remaining calculations to complete Table 5.6 proceed in exactly the same fashion. For this case, cooling is only a small role. This does not, however, change the implementation of Pritchard's method for adjusting for cooling.

Figure 5.22 shows a plot of the final isotherms predicted for this case.

d. Time of Exposure. Continuing with the same example, times of exposure can be calculated using Eq. 5.58. If surface cooling effects had been significant, it would first be necessary to correct distances to isotherms, $y_{\Delta T}$, according to Eq. 5.55. As cooling corrections for this case were so minor, however, the distances initially calculated and shown in Table 5.4 will be used. Substitution of U_o and B_o into Eq. 5.58 gives the following equation for time as a function of distance for this case:

$$\frac{2y_{\Delta T}^{3/2}}{3[14 \text{ ft/sec } (6 \cdot 24 \text{ ft})^{1/2}]} = t_{\Delta T} = 0.00397\, y_{\Delta T}^{3/2} \text{ sec.} \qquad (5.62)$$

For example, for $\Delta T = 14°F$, $y_{\Delta T} = 294$ ft, and

$$t_{14} = 0.00397(294)^{3/2} = 20 \text{ sec}$$

For $\Delta T = 2°F$,

$$t_2 = 0.00397(7.2 \times 10^3)^{3/2} = 2440 \text{ sec} \simeq 41 \text{ min}.$$

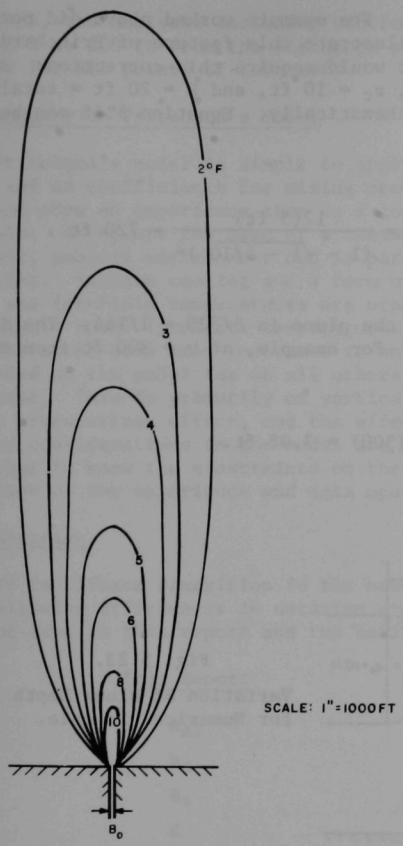

Fig. 5.22.

Predicted Isotherms for Pritchard Example.

These results imply that an organism riding with the discharge water would take 20 sec to go from $\Delta T = 20°F$ to $\Delta T = 14°F$; it would take about 41 min to go from the original 20°F rise to a rise of only 2°F. Again, time spent in the discharge canal must be added to these times.

The alert reader may notice a discrepancy appearing in the time, t_{14}, to reach the $\Delta T = 14°F$ isotherm. Even if the jet maintained its initial velocity of 14 ft/sec, it should take 294 ft/(14 ft/sec) = 21 sec to go 294 ft. The value obtained from Eq. 5.58 is only 20 sec, but it should be greater than 21 sec, since the velocity is actually decreasing along the plume. This oddity arises because Pritchard's linear-spreading model actually assumes a virtual point source at the point of jet efflux. This theoretical source spreads to the width of B_o only at the end of the ZOFE. Consequently, the theoretical relation applied from the point of jet efflux will overestimate velocities and underestimate times in the early reaches of the plume. This phenomenon should become insignificant further than $12B_o$ to $15B_o$ from the outfall.

e. Inclusion of Vertical Mixing. The example worked above did not require any vertical-mixing correction. To illustrate this feature of Pritchard's model, consider a similar example that would require this correction: $\Delta T_o = 20°F$, $B_o = 48$ ft, $z_o = 5$ ft, $U_o = 14$ ft/sec, $z_c = 10$ ft, and $H = 20$ ft = total water depth. Figure 5.23 shows this case schematically. Equation 5.46 can be used to estimate η_1:

$$\eta_1 = \frac{12 z_o}{(1 - \sqrt{1 - z_o/z_c}\,)^2} = \frac{12(5\text{ ft})}{(1 - \sqrt{1 - 5/10}\,)^2} = 720 \text{ ft} .$$

Therefore, the slope of the bottom of the plume is 5/720 = 1/144. The depth at any distance can thus be obtained. For example, at y = 300 ft from the channel,

$$z_{300} = 5.0 + \frac{1}{144}(300) = 7.08 \text{ ft.}$$

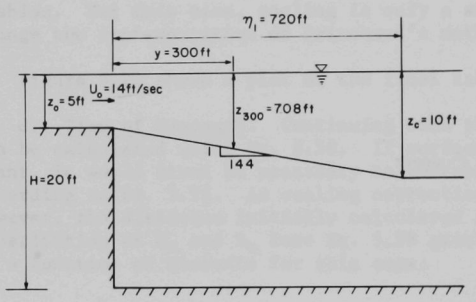

Fig. 5.23.

Variation of Plume Depth for Numerical Example.

Now, calculate the temperature at y = 300 ft point. First, Eq. 5.39 gives the temperature based on a two-dimensional analysis:

$$\Delta T_{300} = \Delta T_o \left(\frac{s_e}{y}\right)^{1/2} = 20°F \left(\frac{6.48 \text{ ft}}{300 \text{ ft}}\right)^{1/2} = 19.6°F .$$

This temperature is then adjusted to allow for the added dilution produced by vertical mixing, based on Eq. 5.47:

$$\Delta T_{300} = 19.6°F \frac{5.00}{7.08} = 13.8°F .$$

Therefore, the analysis including vertical mixing predicts a temperature rise of 13.8°F at 300 ft from the discharge point. Similar adjustments could then be made for all points of interest.

10. Summary on Pritchard's Model

Pritchard's model is simple to apply. Calculations are easily done by hand, and no coefficients for mixing need be chosen by the user. This model is based more on experience than on a complete and sophisticated theoretical analysis. It treats the case of a rectangular, surface discharge into a stagnant, ambient environment and is particularly applicable to lakes and estuaries. Surface cooling and a form of vertical mixing are included. Both near- and far-field temperatures are predicted. It is generally considered a pessimistic model (predicts temperatures and areas that are too large), although some instances have been indicated in which this may not be true. Added work is needed on the model (as on all others), and it is apparently under way at this time. This is primarily on vertical mixing, the jet-diffusion transition point, crosscurrent effect, and the effect of the bottom on vertical mixing. As many considerations in the model are rules of thumb, it is especially important to know the constraints on their application in order to gain fullest advantage of the experience and data upon which they are based.

11. Notation

To facilitate transition to the basic references on Pritchard's model, the following differences in notation are observed. Items not in this list are the same in this report and the basic references.

This Report	Basic References
$A_{\Delta T}$	A_{Θ}
b_m	$\overline{b}_{\Theta}$
B_o	b_o
K	K
s_e	ξ_v
U	u
U_o	u_o
X	y
y	ξ
$y_{\Delta T}$	ξ_{Θ}
z_y	D_{Θ}
z_c	D
ΔA_n	$\Delta A_{\overline{\Theta}_n}$
ΔT	Θ
$\Delta \overline{T}_n$	$\overline{\Theta}_n$
ΔT_o	Θ_o
$\Delta \Gamma_n$	$\Delta \Gamma_{\overline{\Theta}_n}$

F. Model by Sundaram, Easterbrook, Piech, and Rudinger

Sundaram *et al.*[133] prepared a model that treats the surface discharge of a heated waste water and is classed as a complete model, i.e., accounting for both near- and far-field effects. It is a model for the discharge from a rectangular canal at 90° to a shoreline with an ambient crosscurrent present. The model is totally two-dimensional in that no vertical mixing is accounted for. There is one major difficulty with implementation of the model. At least four empirical parameters must be evaluated from existing plume data. Thus, the model's usefulness as it stands is only for cases in which a power plant already exists and plume data have been or can be obtained. In this light, note that the initial development of this model was for a lake in the vicinity of an existing power plant. This makes the model of somewhat limited usefulness, since, if a power plant already exists, many of the conclusions on thermal effects can be derived immediately from the measurements of the plume itself. There is, however, one major reason that this model is being included here. It is the only existing readily available model that accounts for both near- and far-field effects when there is a significant ambient current. Other models, such as that by Pritchard, which account for near- and far-field effects, assume essentially no ambient current. The model will therefore be presented in the hope that use might be made of it in the future if sufficient data are reviewed to obtain some generalization of the required empirical parameters.

The model by Sundaram *et al.* also is interesting in that it treats the jet region and the diffusion or far-field region as two distinct components of mixing. These two are linked together by a particular criterion. Although there is considerable argument over the appropriateness of the criterion chosen by Sundaram *et al.*, it is nonetheless true that there is concern over finding a way to link the jet and diffusion regions. A review of one attempt at putting this feature in a model should be helpful in understanding other models that try to do similar things.

1. Model Assumptions

Sundaram *et al.* present the development of their model with important assumptions. Policastro and Tokar[104] also review the assumptions and basic elements of the model. The following assumptions were used:

a. There is no vertical mixing. The plume will be treated as two-dimensional. This implies that the initial densimetric Froude number, F_j, must be small (about 1.0).

b. Buoyancy forces are neglected except inasmuch as they may be assumed to be the factor that keeps a jet plume two-dimensional and inhibits vertical mixing.

c. The standard means of analyzing smoke-stack plumes can be used for a heated surface jet. This is essentially a two-step method. First, the height of the plume axis on the surface is calculated for any downwind distance. This would be the location of the heated-surface-plume centerline with respect to the shoreline. Then, the lateral concentration distributions at the section being studied are assumed to be identical to those resulting from a simple two-dimensional turbulent jet into a stagnant environment. Figure 5.24 shows the

general procedure. This stagnant-jet analysis will not be modified to include an ambient current.

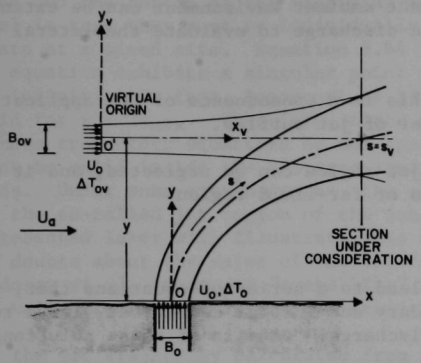

Fig. 5.24.

Two-step Method of Plume Analysis.[133]

d. Beyond some downstream distance, ambient turbulence controls the mixing processes. The criterion for locating the transition point between these regions will be the equality of the eddy-diffusion coefficient due to self-induced turbulence (jet turbulence) and the eddy-diffusion coefficient due to ambient turbulence.

e. The rate of spreading of lateral profiles of velocity and temperature is identical.

The diffusion portion of the Sundaram model is constructed almost identically to the method presented by Brooks.[19] Therefore the assumptions of that model are essentially the assumptions of the Sundaram diffusion model. These include the following.

f. Any diffusion coefficient is a function of longitudinal location only and not of the lateral location within a given cross section.

g. The local plume width will be defined as $2\sqrt{3}$ times the standard deviation of the lateral temperature distribution. Brooks defined his width in this manner so that the width would equal B_o at the origin.

h. The eddy-diffusion coefficient, K_H, can be expressed by the "four-thirds" law. That is,

$$K_H = k_H L_s^{4/3} \tag{5.63}$$

in which K_H is the eddy-diffusion coefficient, k_H is a constant, and L_s is a length scale descriptive of the mixing process. The constant k_H is apparently a function of the meteorological conditions existing above the receiving-water

body. Other assumptions made by Sundaram *et al.* include these:

i. The application of classical, two-dimensional jet theory for a free-turbulent jet issuing into a stagnant ambient environment can be extended to the initial region of a jet surface discharge to evaluate the lateral profiles of temperature and velocity.

j. The ZOFE is neglected. This is a consequence of the application of assumption i directly from the point of jet outflow.

k. Surface heat loss in the jet region can be neglected, and it will be accounted for only in the diffusion or far-field region.

2. Model Equations

The assumptions listed above lead to a series of equations that, when combined with the appropriate boundary and initial conditions, leave two solutions for the heated surface discharge. Details of these solutions are contained in the basic references.

a. Jet Mixing Region. Some method must be chosen to predict the initial trajectory of the jet as it exits from the outfall. Figure 5.24 illustrates the general situation. A virtual origin is proposed. This virtual origin represents an imaginary location, chosen so that a real jet located there would yield the plume width, velocity, and temperature observed in the real section of the jet under consideration. As one moves along the jet axis, the location of the virtual origin changes until eventually it coincides with the real jet. The virtual source is representative of the two-dimensional jet in a stagnant environment that would give the same velocity and temperature at the corresponding cross section of the real jet.

Sundaram *et al.* chose to use an empirical relation developed by Bosanquet *et al.*[16] for jet trajectory. Important trajectory equations are

$$\frac{y}{y_{max}} = 1 - \alpha \frac{y_{max}}{x} \tag{5.64}$$

and

$$\frac{y_{max}}{B_o} = \frac{\beta}{1 + \gamma\left(\frac{1}{k}\right)} k \ , \tag{5.65}$$

where y_{max} = maximum penetration of jet into cross current,

y = penetration of jet at any distance x,

$k = U_o/U_a$,

α, β, γ = empirical constants, and

x = distance from actual outfall along x axis, which concides with the shoreline.

Policastro and Tokar[104] note that the empirical coefficients denoted by α,β, and γ are assumed independent of the level of ambient turbulence. They are considered dependent upon outfall geometry and on the topography of the shoreline and the bottom of the receiving-water body. One difficulty in using the model is that they must be individually evaluated, at present, from existing plume data at a given site. Equation 5.64 is not applicable at a point, $x = 0$, for the equation exhibits a singular point for this instance such that the term goes to infinity. In fact, Bosanquet *et al.* note that Eqs. 5.64 and 5.65 are not valid for $x < 2y_{max}$. Therefore, there may be a considerable range over which these trajectory equations do not apply. The jet trajectory equations might not be valid inside the distance limits suggested by some temperature standards. Under some circumstances, the equation will not be valid for any part of the so-called jet region of the Sundaram model. A numerical example to be presented later will illustrate this discrepancy. Therefore, there are serious doubts about the value of the jet-trajectory model that has been chosen, and Sundaram *et al.* recommend "eyeballing" the point at which the equation becomes valid from a plotting of the trajectory.

On the jet trajectory calculated from Eqs. 5.64 and 5.65, Sundaram *et al.* develop relations for the temperature and velocity distributions. Numerous classical free-jet analyses and experimental data are used and assimilated to arrive at a final solution for this portion of the problem. One important assumption mentioned earlier is expressed in

$$\frac{U_\eta}{U} = \frac{\Delta T_\eta}{\Delta T} \quad . \tag{5.66}$$

This equation is applicable to the variation within a lateral cross section of the plume. This assumption differs from the findings of Taylor as discussed earlier in this chapter.

The lateral distribution of velocity resulting from the assumptions and analyses is shown in graphic form in Ref. 104, page 294. The curve is a plot of the hyperbolic secant squared, rather than the conventional Gaussian distribution. The general shape of these curves is similar, except that the hyperbolic secant curve is slightly more pointed toward the maximum value of velocity. Due to the assumption in Eq. 5.66, this also becomes the lateral profile for temperatures. The profile is shown in Fig. 5.25.

The centerline velocity decrease is taken as proportional to the inverse 1/2 power of the axial distance, or

$$\frac{U_{c_2}}{U_{c_1}} = \left(\frac{s_2'}{s_1'}\right)^{-1/2} \tag{5.67}$$

where U_{c_2} = centerline velocity at distance s_2' along axis, and

U_{c_1} = centerline velocity at distance s_1' along axis.

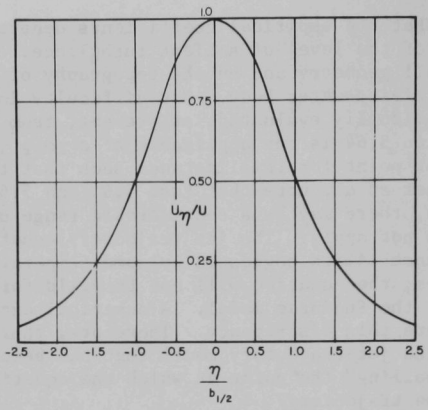

Fig. 5.25.

Velocity Distribution for Turbulent Two-dimensional Jet.

These results appear on p. 606 of Ref. 122. However, Sundaram *et al.* do not tie Eq. 5.67 specifically to a known initial point, thereby not yielding an expression for absolute values of the velocity. Hence, it will not be possible to get a time of exposure from the model.

Sundaram uses Brooks' definition[19] of b, the plume width,

$$b = 2\sqrt{3}\,\sigma\ , \tag{5.68}$$

in which σ = standard deviation of lateral temperature distribution. Simple two-dimensional theory for a jet into a stagnant environment yields a linear spreading of the plume, shown as

$$b = B_o + 0.2s\ . \tag{5.69}$$

In combination with the assumption that heat and velocity profiles spread at the same rate, Eqs. 5.69 and 5.67 directly yield the centerline temperature decay. Since jet depth remains constant in a two-dimensional model, dilution would be proportional to the width. Therefore, decrease of temperature along the jet axis becomes

$$\frac{\Delta T}{\Delta T_o} = \left(\frac{b}{b_o}\right)^{-1/2} = \left(\frac{B_o + 0.2s}{B_o}\right)^{-1/2}\ . \tag{5.70}$$

In addition, theory yields an expression for $K_{M_{jet}}$, the eddy diffusivity of the jet region:

$$K_{M_{jet}} = 0.008bU. \tag{5.71}$$

These two-dimensional jet findings are directly from works summarized in Ref. 102. Policastro and Tokar give a better review of the details of the development than does Ref. 133, which primarily lists only the results shown above.

3. Equations for Diffusion Region

This portion of the model is essentially the same as one developed by Brooks.[19] The diffusion equation for two-dimensional mixing becomes

$$U_a \frac{\partial \Delta T}{\partial x} = \frac{\partial}{\partial y}\left(K_H \frac{\partial \Delta T}{\partial y}\right) - \frac{K}{\rho C_p z_o} \Delta T \tag{5.72}$$

(Advected heat = Diffused heat - Surface heat loss),

where K_H = eddy diffusivity of receiving water.

Note that the standard xy coordinates of this current report are used. The use of ΔT in the first two terms of Eq. 5.72 is allowed, since changes in temperature are all that are needed. The development of Eq. 5.72 can be seen by visualizing an imaginary cube in the fluid. The first term is the heat advected into and out of the cube by riding along with the mean ambient current. The next term (first term on right side) represents the heat diffused into and out of the cube by the processes of turbulent fluctuations. The final term represents the loss of heat due to surface cooling. The cooling term is based on the standard assumption that the ambient water temperature equals the equilibrium temperature. This equation must be solved for some virtual source whose location is dependent on the trajectory and initial mixing of the jet region. Thus, the initial conditions are defined at the virtual source. The boundary conditions imply that ΔT approaches 0 at large distances from the plume.

The eddy diffusivity can be written, choosing the plume width, b, as a characteristic length, as

$$K_H = k_H b^{4/3} \ . \tag{5.73}$$

Brooks then solved Eq. 5.72 to yield the concentration (here temperature) in the (xy) field as

$$\Delta T(\tilde{x},\tilde{y}) = \frac{1}{2} e^{-P_2 \tilde{x}} \left(\text{erf} \frac{2\tilde{y} + 1}{4\sqrt{x'/P_1}} - \text{erf} \frac{2\tilde{y} - 1}{4\sqrt{x'/P_1}}\right), \tag{5.74}$$

where $\Delta T = \Delta T/\Delta T_{ov}$,

ΔT_{ov} = temperature rise at virtual origin,

$\tilde{x} = x/B_{ov}$,

B_{ov} = width of virtual orifice,

x,y = measured from virtual origin,

$$P_2 = \frac{KB_{ov}}{\rho C_p U_a z_o} ,$$

$$x' = \frac{P_1}{24} \left[\left(1 + \frac{8\tilde{x}}{P_1}\right)^3 - 1 \right] ,$$

$$P_1 = \frac{U_a}{k_H \, B_{ov}^{1/3}} , \text{ and}$$

erf = error function (e.g., erf = $j = \frac{2}{\sqrt{\pi}} \int_0^j e^{-t^2} dt$), which is available in most standard mathematical or statistical handbooks.

The entire two-dimensional far-field temperature field is determined from Eq. 5.74, once pertinent physical parameters and B_{ov} are evaluated. For the centerline (y = 0), Eq. 5.74 reduces to

$$\Delta\tilde{T}_c = e^{-P_2\tilde{x}} \text{ erf} \left[\frac{1.5}{\left(1 + \frac{8\tilde{x}}{P_1}\right)^3 - 1} \right]^{1/2} , \tag{5.75}$$

where $\Delta\tilde{T}_c = \Delta T_c / \Delta T_{ov}$, and

ΔT_c = centerline temperature rise.

4. Relating Near- and Far-field Solutions

a. Introduction. The key to the Sundaram plume analysis lies in linking the near- and far-field solutions. Sundaram *et al.* do this by equating eddy-diffusion coefficients for the two regions. They reason that, when the jet-induced turbulence level equals that due to ambient turbulence, the ambient turbulent field can be assumed to take over. In addition, the momentum flux from the virtual outfall should equal that from the real outfall. Thus,

$$B_{ov} \, U_{ov}^2 = B_o \, U_o^2 , \tag{5.76}$$

where U_{ov} = velocity from virtual origin. Equating the diffusion coefficients from Eqs. 5.71 and 5.73 and coupling this with Eq. 5.76 yields the following expression for the virtual source width, B_{ov}.

$$\frac{B_{ov}}{B_o} = \left(0.008 \frac{U_o}{k_H B_o^{1/3}}\right)^{1/2} . \tag{5.77}$$

One can find the end of the region of jet influence by using Eq. 5.69 to find the distance s_o along the actual jet axis at which the width of the plume from near-field theory equals the width of the virtual source calculated above. (Refer to Figure 5.24.) At this transition point, the virtual origin would lie on the physical plume. At this point, s_v from Fig. 5.24 equals s_o, which is calculated from Eq. 5.69 for $b = B_{ov}$:

$$s_o = 5(B_{ov} - B_o) \tag{5.78}$$

Finally, the value of ΔT_{ov} is needed. This will be the temperature rise on the real plume where the virtual source lies or at $s = s_o$. Equation 5.70 shows that

$$\Delta T_{ov} = \left(\frac{B_{ov}}{B_o}\right)^{-1/2} \Delta T_o . \tag{5.79}$$

The discussion here reveals that B_{ov} must be greater than B_o. Thus, the right-hand side of Eq. 5.79 must be greater than 1.0. If it is not, then the jet region is neglected, ambient turbulence is assumed to control, and the virtual source is taken at the actual discharge location, with $\Delta T_{ov} = \Delta T_o$ and $B_{ov} = B_o$.

The procedure in plume calculation using the two-step approach can be summarized briefly.

(1) Calculate B_{ov} from Eq. 5.77 and ΔT_{ov} from Eq. 5.79.

(2) Calculate s_o from Eq. 5.78. This gives the limit for jet calculations.

(3) Calculate jet trajectory from Eqs. 5.64 and 5.65.

(4) Calculate the temperature decrease along this axis by Eq. 5.70.

(5) Calculate plume widths (if desired) in the jet region by Eq. 5.69. If location of isotherms is desired, this can be calculated by using the lateral profile (sech^2 curve) shown in Fig. 5.25.

(6) Use Eq. 5.74 to calculate isotherms for diffusion region or Eq. 5.75 if only centerline temperatures are desired.

b. Time of Exposure and Surface Areas. As noted earlier, the solution chosen does not yield an estimate of time of travel along the plume. Areas within isotherms can be obtained by plotting and planimetering. Another way

to do this would be to write a simple computer program to calculate isotherm widths along the plume axis, both in near- and far-field regions and numerically to integrate to find areas by

$$A_{\Delta T} = \sum_{i=1}^{n} b \, \Delta s \, , \tag{5.80}$$

in which $A_{\Delta T}$ is the area with ΔT isotherm, and Δs is the length along the axis between points where b is calculated.

5. Verification

The model has only been applied to plumes from the Milliken Power Station on Cayuga Lake (New York). For this case Sundaram *et al.* found the parameters for Eqs. 5.64 and 5.65 to be $\alpha = 0.2$, $\beta = 9.0$, and $\gamma = 0$. Values of k_H were found by matching measured centerline temperature decreases with Eq. 5.75. The values of k_H varied from about 0.3×10^{-3} to 1.8×10^{-3} $ft^{2/3}/sec$ and were strongly a function of wind speed. Higher wind speed yielded a higher k_H, which is reasonable in terms of the turbulence created by wind-generated currents in the water.

The model did a reasonable job when fitted to the Milliken data. It has not, however, been applied to any laboratory or other field data and therefore remains essentially unverified. There is no empirical evidence on surface plumes to guide in the selection of α, β, and γ.

6. Limitations and Ranges of Applicability

With this model, as with others, there are several limiting features in its use. One major assumption is that the plume is two-dimensional. For this reason, the use of the Sundaram model should be restricted to two-dimensional cases, either by virtue of the bottom barrier or by virtue of a low densimetric Froude number approaching 1.0. Any use of this model for Froude numbers F_j greater than 10 may greatly overestimate the temperatures within a given isotherm due to neglect of early vertical mixing. This is the same restriction noted on the Motz-Benedict model.[94]

A second major feature of the model concerns the transition from jet mixing to diffusion regions. To this time, the criterion that the eddy-diffusion coefficients of these two regions will be equal at the transition point has not been verified as valid. The location of the transition point is critical in reviewing the results obtained from the diffusion portion of the model, since the results may differ considerably, depending on the assumed location of the transition point.

A major question concerning the use of the model arises from the need to specify three empirical coefficients for the jet-mixing-region model. In addition, the value of k_H must be specified from meterological conditions at the site. The three empirical parameters for the jet model, as outlined in Ref. 133, must be evaluated from existing plume data at the site. A review of plume data existing at sites that have some similar conditions might enable one to predict

the trajectory by using the model for a site where there was no plant. However, if one must depend upon a plant already built, then the model's predictive capabilities are limited. However, a review of existing data and appropriate fittings might make the three empirical coefficients more capable of being generalized to other sites.

The model at hand was developed for one case under a special contract and, as of this time, apparently has not been generalized to other sites. Policastro and Tokar are continuing work at Argonne National Laboratory to test values of this model and approach. The ZOFE is essentially neglected in the model, because the jet formulas developed are applied immediately from the point of the outfall. This would presumably not be a major factor in the far-field region. In the region very near the outfall, however, results might be expected to be less adequate.

Despite the limitations of this model, it has some aspects that commend it. First, it is the only model, except possibly for some very recent ones, that combines both near- anf far-field effects for a discharge into a strong ambient current. Second, it has made an analytical attempt at tying together the near- and far-field regions rather than choosing, for example, some arbitrary temperature rise as chosen by Pritchard. As discussed previously, there are some severe limitations on the ability to predict jet trajectory in the near-field region. If one can make a reasonable assessment or estimate of the empirical coefficients required for the model, then the model can be applied for a range of cases. It is designed to handle a surface discharge from a rectangular channel at 90° to the flowing ambient current and to predict profiles in both near- and far-field regions. Its best use would probably be in lakes. However, there seems to be no reason it could not be used in a river or estuary analysis of heated discharges. However, if this model is used in such situations, it would have to be with care, for it has not been applied to any data from such sources.

One shortcoming of the model lies in the difficulty in predicting time of exposure, as noted in the discussion of the change of the centerline velocity along the plume axis. At present, the form of the equation is such as to make its use difficult for integration to determine such a time. In addition, results for plume areas would probably have to be obtained by graphical means, except for the far-field areas. One would have to neglect those higher-rise contours occurring very near the outfall, however, where they are not encompassed within the model.

7. Data Needed

To produce predictive results for heat discharged into a particular site, several inputs are needed to the equation system discussed. Among these are the following parameters:

B_o = initial outfall width,

z_o = initial outfall depth,

U_a = ambient velocity,

U_o = initial jet velocity,

ΔT_o = initial temperature rise,

K = surface cooling coefficient,

k_H = constant of proportionality for eddy diffusivity, and

α, β, γ = empirical coefficients to be used in jet trajectory predictions.

All the information is standard information that should be available for proposed discharges, except for the four empirical coefficients which must be evaluated. Sundaram *et al.*[133] give values of k_H for six different environmental conditions at Lake Cayuga. A review of these values might enable a choice if the site under consideration had similar environmental conditions at the cricical time. Sundaram *et al.* have evaluated the value of the parameters of α, β, and γ for the jet model for only one case. However, if one could generalize the type of geometry and limited receiving-body conditions at a site, he could possibly find some data, either from smoke plumes or from similar plume receiving bodies, that would enable him to evaluate α, β, and γ. This has not yet been done in a general sense.

8. Numerical Example

For purposes of presenting a numerical example, consider numbers similar to those used in Ref. 133:

B_o = 100 ft,

z_o = 10 ft,

Q_p = 1200 cfs,

U_o = 1.2 ft/sec,

K = 282 Btu/ft^2-°F-day,

ΔT_o = 15°F,

U_a = 0.248 ft/sec,

k_H = 1.0×10^{-3} ft$^{2/3}$/sec,

α = 0.2,

β = 9.0, and

γ = 0.0.

First, the characteristics of the virtual source are calculated using Eqs. 5.77-5.79:

$$B_{ov} = \left[0.008 \frac{U_o}{k_H B_o^{1/3}}\right]^{1.2} B_o$$

$$= \left[\frac{0.008(1.2 \text{ ft/sec})}{1 \times 10^{-3} \text{ ft}^{2/3}/\text{sec } (100 \text{ ft})^{1/3}}\right]^{1.2} (100 \text{ ft}) = 238 \text{ ft.}$$

Then, $s_o = 5(B_{ov} - B_o) = 5(238 - 100)\text{ft}$

$= 690$ ft (along jet axis) and

$$\Delta T_{ov} = \left(\frac{B_{ov}}{B_o}\right)^{-1/2} \Delta T_o = \left(\frac{238}{100}\right)^{-1/2} (15°F) = 9.7°F.$$

The following calculations of constants can then be made. From the definitions in Eq. 5.74,

$$P_1 = \frac{U_a}{k_H B_{ov}{}^{1/3}} = \frac{0.248 \text{ ft/sec}}{(1.0 \times 10^{-3} \text{ ft}^{2/3}/\text{sec})(238 \text{ ft})^{1/3}} = 40;$$

$$P_2 = \frac{K\, B_{ov}}{\rho C_p U_a z_o} = \frac{(282 \text{ Btu/ft}^2\text{-°F-day})(238 \text{ ft})(1 \text{ day}/86{,}400 \text{ sec})}{(62.4 \text{ lb}_m/\text{ft}^3)(1 \text{ Btu/lb}_m\text{-°F})(0.248 \text{ ft/sec})(10 \text{ ft})} = 5 \times 10^{-3}.$$

To continue the centerline temperature predictions past the location of the virtual origin, turn to Eq. 5.75. Consider, for example, the temperature at a point 1000 ft along the plume axis or 1000 - 690 = 310 ft from the virtual source. Then,

$$\tilde{x} = \frac{x}{B_{ov}} = \frac{310}{238} = 1.302.$$

Then, from Eq. 5.75,

$$\Delta T_c = e^{-(5\times10^{-3})(1.302)} \operatorname{erf}\left[\frac{1.5}{\left(1 + \frac{8}{40}\,1.302\right)^3 - 1}\right]^{1/2}$$

$$= e^{-6.5\times10^{-3}} \operatorname{erf}(1.22) = 0.910 .$$

Thus, $\Delta T_c = 0.910\Delta T_{ov} = 0.910(9.7°F) = 8.8°F$. Therefore, the temperature rise at 1000 ft along the jet axis is predicted to be 8.8°F. Calculation of a number of other points in the diffusion region and also in the jet region enables one to plot a complete centerline temperature profile as shown in Fig. 5.26. The jet-region decrease is calculated from Eq. 5.70. For example, for s = 500 ft,

$$\Delta T_{500} = \left[\frac{100 + 0.2(500)}{100}\right]^{-1/2} (15°F) = 10.6°F.$$

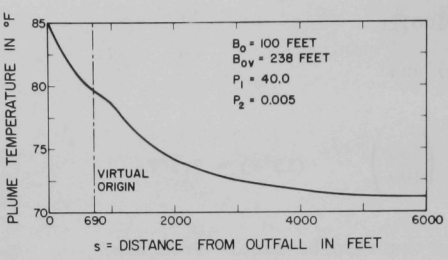

Fig. 5.26.

Decay of Temperature along Plume Centerline for Lake Surface Temperature = 70°F and Discharge Temperature = 85°F.

Figure 5.26 has a slight break in the region of transition of the two models that is not totally unexpected inasmuch as the jet-entrainment mechanism has suddenly been replaced by a diffusion-mixing mechanism. In some of their figures, Sundaram *et al.* apparently smoothed out any such breaks when plotting their curves.

The user may well desire information on plume location and isotherm areas. For the problem at hand, the jet trajectory can be calculated using Eqs. 5.64 and 5.65. Equation 5.65, with the given α, β, and γ, becomes

$$\frac{y_{max}}{B_o} = 9k. \tag{5.81}$$

Since $k = U_o/U_a = 1.20/0.248 = 4.84$ and $B_o = 100$ ft, $y_{max} = 9(100 \text{ ft})(4.84) = 4360$ ft. Then, Eq. 5.64 takes the following form for this case:

$$y = 4360 \text{ ft}\left(1 - 0.2\,\frac{4360 \text{ ft}}{x}\right). \tag{5.82}$$

Bosanquet *et al.*[16] state that Eq. 5.82 is only valid for $x > 2y_{max}$, or >8720 ft in this instance. This is obviously well past the end of the so-called jet region (s_o = 690 ft). For this case, essentially similar to those from Ref. 133, the jet-trajectory formula is not valid at all. Hence, no isotherms can be plotted for this region. However, widths can be calculated and translated to isotherms by the sech^2 curve of Fig. 5.25. This discrepancy in the jet region is disturbing, especially because α, β, and γ were evaluated from data at a plant on the same lake.

Equation 5.74 can be used to obtain isotherms for the diffusion region. Sundaram *et al.* present the isotherms shown in Fig. 5.27, plotted in the dimensionless form. Areas inside these contours could easily be obtained by use of a planimeter. The results shown in Fig. 5.27 were for a slightly different set of parameters than were used for the preceding portion of the numerical example. Hence, Fig. 5.27 is shown only to present the type of results obtained from Eq. 5.74.

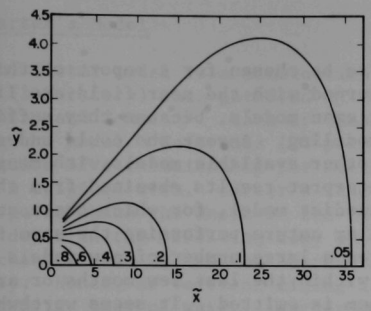

Fig. 5.27.

Isotherms in Diffusion Zone by Sundaram *et al.* Model.[133]

G. Conclusions

1. Discussion

The Sundaram model has a number of shortcomings as a predictive tool. No guidance has been given for choice of α, β, and γ for the initial jet trajectory. An example problem worked here indicated some possible real difficulties with transferring information on these values. In short, at this moment, it is not very useful as a predictive tool.

There are two good reasons for including this model. First, it is the only presently generally recognized model that treats both near- and far-field regions for a strong ambient current. Second, and closely related, the model tries to find a rational basis for a transition from a jet-controlled region to the ambient-controlled region. There is considerable interest in doing this with other models. Therefore the Sundaram model provides some insight into this coupling procedure, providing a better understanding of other such models.

2. Notation

To facilitate transition from this report to the basic reference, the following equivalence of notation is given. This is more difficult here, as Ref. 133 frequently uses the same symbol with two or more meanings redefining it.

This Report	Basic Reference
B_o	b_o
s	x (axial distance)
U_a	u_a
U_o	u_o
y_{max}	$h_{e_{max}}$
y	h_e
z_o	d
ΔT	T

H. Other Near-field Models

Some limiting number of models had to be chosen for a report of this nature. As a result, those models primarily concerned with the near field are limited to the Motz-Benedict and Stolzenbach-Harleman models, because they sufficiently demonstrated the basic elements of the modeling. Anyone who could understand either of these models could then go to other available models with many of the same elements and use them as well or interpret results obtained from them. This is especially true with the Motz-Benedict model, for which there are two other generally available models of similar nature performing the same functions. In addition, Policastro and Tokar[104] noted a large number of new models being developed. Many of these have appeared within the last few months or are being written at this time, and coverage of them is omitted. It seems worthwhile, however, to discuss briefly the Carter[21] and Zeller *et al.*[148] models. Because of the similarity of many features of these two models to the Motz-Benedict model, comments will be restricted to major differences and to general findings of the authors about heated discharges. These two models are especially being mentioned because there is a dearth of models treating the case of a jet discharge into a strong ambient current. This situation, although not the important one in lakes, for example, may be important in estuaries and rivers.

1. Hoopes-Zeller-Rohlich Model

One of the earlier surface-jet models developed was by Hoopes *et al.* of the University of Wisconsin. Several basic references to this model including those by Zeller *et al.*,[148] Hoopes,[59] and Zeller.[147] Further, the results obtained by these authors were a major factor in the form of solution chosen by the developers of the Motz-Benedict model.[94]

The model considers a surface discharge from a rectangular channel with no vertical mixing and an ambient current. In addition, the effect of wind stress on the plume is considered. An entrainment mechanism is postulated for mixing, Gaussian lateral profiles are chosen for velocity and temperature, and an approach similar to the Motz-Benedict model yields several equations to be solved by numerical techniques. The trajectory of the plume, the centerline temperature and velocity, and the width of the plume are all functions of the distance. Although time of exposure and area within contours are not standard parts of the output, they can be obtained in the same fashion as obtained from the results from the Motz-Benedict model. The model has been applied to an extensive series of field data taken from Lake Monona, Wisconsin. There are two basic differences in the assumptions used in developing the model. First, pressure drag is not included. Second, the entrainment mechanism postulated uses the centerline velocity only, rather than using the difference of the centerline velocity and some ambient component. This latter assumption is only valid if the discharge plume is at an angle of 90° to the ambient current or if the ambient current is much smaller than the jet velocity. The neglect of pressure drag is only appropriate if the ambient velocity is small. Hence, even though the model does include an ambient crosscurrent, application to a case with a very strong crosscurrent should proceed with care.

With these limitations in mind, the model can be applied to essentially the same range of problems as the Motz-Benedict model with essentially the same constraints. An entrainment coefficient must be chosen for use with the model. Details of the model can be found in the basic references and in Ref. 104.

2. Carter's Model

The Carter model is a combination of theoretical considerations and experimental (laboratory) data gathered by Carter, as outlined by Carter[21] and by Policastro and Tokar.[104] Both of these works should be reviewed when implementing the model. Reference 104 points out a slight algebraic error in integration of a relationship for determining the centerline trajectory in Carter's original work. Carter's study is for a purely two-dimensional discharge in which the depth of the flow in the discharge channel is the same as the depth in the receiving body of water. The receiving body is a rectangular channel with an ambient current at 90° to the initial jet-discharge velocity. Hence, no vertical mixing is allowed, due to the solid bottom of the receiving body of water. Carter has made several important findings in his experimental studies. He is continuing these studies, and his model is expected to be updated soon. The results from his continuing investigations should represent a worthwhile contribution to the literature.

Carter considers the jet plume only up to the point when it reaches its maximum penetration into the ambient current. Within the limits of the measurements that Carter took, for values of the velocity ratio k between 1 and 10, he found that the temperature decrease along the centerline was independent of the velocity ratio and could be expressed by

$$\frac{\Delta T}{\Delta T_o} = \left(\frac{s}{B_o}\right)^{-1/4} , \qquad (5.83)$$

where s = distance along jet axis. This equation from Ref. 21 is valid for the ZOEF. Carter uses this equation as part of his theoretical model.

Carter also defines a drag coefficient, including the mechanism of pressure drag in his model. He has observed generally a very rapid bending over of the plume as it issues into the receiving body of water. He has, in fact, observed one phenomenon not reported by other investigators. Even for flume widths as great as 120 times the width of the discharge slot, he has observed a bending back of the jet. That is, rather than bending until it is parallel to the ambient current and then keeping that path, the plume tends to return to the near shore. A general relationship between this phenomenon and the width of the discharge flume and the velocity ratio k is not yet established. When this bending back is compared to the works of other authors, the relative depth (the relationship of the depth of the discharge to the depth of the receiving body) may play a role.

Carter observed some interesting relationships in the lateral profiles found in the heated plume. He made measurements that indicate that the profiles are not similar within the plume. For example, he observed a roughly bell-shaped temperature profile laterally on the side of the plume away from the near shore. However, on the near shore-side of the plume, he observed a continual decrease of the temperature until it reached some temperature intermediate between the ambient and the centerline temperature, at which it remained constant. He therefore chose in his remaining analyses to consider a tophat profile rather than some more sophisticated version. As noted earlier

by Morton,[91] however, once a form has been chosen for a lateral profile, the specific nature of that form is not too important. The simple choice of any similar form has removed from the analytical technique the ability to predict lateral structure within the plume. Carter's findings are extremely significant in the study of these plumes.

There are some differences in Carter's analyses from those conducted by other authors. One specific one is Carter's essential elimination of the continuity equation by assuming that, once the ZOFE has been passed, the velocity is everywhere (within the plume and outside) equal to the ambient current. His justification for this is his observation visually that the plume is rapidly bent over. However, this is a point of very real contention with the model. Inclusion of this simplification creates one additional problem. Carter feels that the simplification involved here does not justify calculation of any plume widths or isotherm widths from his model. As a result, it is not possible from Carter's model to obtain sizes or areas within isotherms. This is a point of interest to people charged with evaluting thermal discharges. In addition, this assumption means that the capability for a more accurate prediction of the time of exposure of organisms is removed. Since the velocity has been assumed equal to the ambient velocity everywhere, the only estimate of time would be the distance traveled divided by the ambient current. This would be an upper limit on the time of exposure. For more accurate estimates, however, one would have to include the fact that the velocity in the earlier portions of the plume is greater and that the time of exposure would be less than that estimated by this maximum time. For some measures, this upper limit might be adequate.

In summary, then, Carter has established some important laboratory information on heated discharges. His model has, to best knowledge, not been verified against field data. However, it should be applicable to many instances of flow in rivers or estuaries. The assumption that the velocity is equal to the ambient everywhere in the ZOEF may even mean that the model would be best adapted to lower values of the velocity ratio. The use of the model should be undertaken along with the comments in Ref. 104.

The use of Carter's model is simple and the errors mentioned in Ref. 104, when corrected, should make no major differences in its application. The model has been used by Pritchard in combination with his own model. He uses the Carter model in the early regions of the discharge to establish the point at which the jet has reached the maximum penetration into the ambient current and has turned to become parallel to the ambient current. From that point on, he treats the decay in the same fashion that he treats an initial discharge with his own model. Policastro and Tokar[104] (p. 64) have outlined this procedure.

I. Other Far-field Models

The only steady-state far-field models discussed in detail are the far-field portions that exist in the model by Sundaram *et al.*[133] and by Pritchard. Both of these also have a near-field region at the beginning of the jet. One reason that no more detail concerning the far field has been offered at this time is that many of the major concerns are expected to be in the near field. This is where high temperature rises will exist. In addition, standards are becoming more stringent. Therefore, people using surface discharges would probably be tending more and more to discharges designed for very high rates of early mixing, thereby reducing the region of effect.

There still may be a desire to make some computations for what would be known as the far field. However, once one has reached the point of 1 or 2°F above ambient, the difficulties in modeling are extreme. Natural variations are frequently much greater than this. As a result, using steady-state diffusion, efforts to model the changes in a very complex real system are quite strained. Reference 104 outlines in detail a number of far-field models including those by Wada,[139] Edinger and Polk,[33] Csanady,[27] Kolesar and Sonnichsen,[74] and Wnek.[144] One noticeable thing about these models is that one must specify something that may be called by different names, such as an eddy diffusivity, a diffusion coefficient, or an eddy-thermal diffusivity. Moreover, a diffusion coefficient by any other name is still a diffusion coefficient. That is, these are coefficients designed to express something about the intensity of mixing that arises due to turbulence in the receiving-water body. The difficulty in adequately defining these diffusion coefficients under ordinary conditions is significant. The "4/3" law has done a reasonably adequate job, particularly in large bodies of water. However, information on the values of these coefficients in stratified waters and in the vicinity of heated discharges is very weak. As a result, the models are extremely sensitive to the choice of these coefficients. If the coefficients are off by a factor of 10 or more (which at the present state of knowledge is not at all impossible), the areas predicted may be off by a similar factor. Of course, if one has particular knowledge of a given locale he may be able to make a better choice of diffusion coefficient. Nevertheless, the state of the art is still such that there is much difficulty in defining the parameters needed for the models.

An additional point related to most proposed discharges is that even if a far-field model is needed, there should be some means of accounting for what is expected to be a relatively high degree of initial mixing. Both the Pritchard and Sundaram models attempt to do this. Pritchard chooses a simple arbitrary cutoff point between his models. Sundaram uses a slightly more sophisticated, though probably no more verifiable, means of making this transition. The limits of the regions of jet mixing and diffusion mixing are not well defined at this point.

Of the models mentioned, the Edinger and Polk[33] model is probably the easiest to use once a diffusion coefficient is chosen. One can immediately calculate areas within isotherms and the shapes of these isotherms. These are for discharges on the shoreline into a moving ambient current. Most of the other models involve considerably more effort, although they frequently include other factors.

In summary, then, the basic approach of this report with reference to the far-field model has been this: If there is an extensive effect on the far-field region, the power plant is probably too big for the given receiving body or the discharge structure is ill-designed. For this reason, less detailed emphasis has been placed on far-field analyses. It seems relatively unlikely that a discharge will meet temperature criteria, as being presently established, and at the same time have an extensive influence in the far-field region. However, anyone wishing to make estimates of the far-field case should review the models outlined in Ref. 104 and refer to the basic references on those models. In addition, he might review Refs. 99 and 100 for information on calculation of diffusion coefficients, at least under strained conditions.

J. Surface Discharges--Transient Conditions

All models discussed to this point have predicted temperatures for assumed steady-state conditions. That is, the discharge of heated water, the ambient water velocity, meteorological parameters, and all other parameters in the system are considered not to vary with time. In natural systems, the components of the atmosphere and the receiving-water body are especially liable to be continually changing with time. Also, the heated water discharge might vary in terms of total heat rejected or flow rate. However, in many instances, a constant water is run at a constant flow rate from the given power plant, regardless of the number of units operating at the time.

Any physical receiving body of water may be subjected to transient or time-varying conditions. This would include rivers, lakes, and estuaries. For lakes, no present treatment is available, short of building a physical hydraulic model to study the reaction of a heated discharge at a given site in an unsteady-flow environment. Most of the attention here will be centered on rivers and estuaries to which some previous analytical attention has been devoted.

In rivers, unsteady flows may develop due to the operating schedule of hydroelectric or other dams. One example of this is the proposed Browns Ferry Plant in the TVA system (and all other TVA plants). At the Browns Ferry site, conditions are such that one may obtain flow reversal; i.e., flow is going upstream. This situation complicates matters considerably. For this site, a diffuser structure was chosen, and TVA is running extensive model studies on this diffuser.

Estuaries have been divided into many different types. A general definition is given in Ref. 107. Considerable general discussion of estuaries is given in Ref. 77. Additional comments on the mixing characteristics of estuaries appear in Ref. 126. In an estuary, the transient conditions are dominated by the tidal flows. There may be other transient conditions due to varying degrees of fresh-water inflow from tributary streams as well.

A general summary of existing knowledge on discharges into receiving waters subject to transient conditions could be made by saying that there is no presently available technique for handling the near-field case in the transient state. There are some approaches for studying the far-field temperature distribution analytically. In this light, a section on thermal discharges presented results only from steady-state solutions for far-field cases and few new analytical techniques. This is indicative of the state of analysis in transient conditions.

This section will discuss both the near- and far-field case. In the near-field case, some guidance will be given for applying current models to make a best estimate of temperature effects. In the far-field case, two models will be discussed and a number of other available models mentioned. The emphasis will be less detailed, primarily because the far-field problem is not only less well defined but is also probably not so much the area of concern for evaluating thermal impact. In this vein, note, however, that the two far-field methods presented will give a means of assessing the possible lack of dilution water in the near-field region, which might cause temperatures to be greater than those predicted. Hence, these models might contribute a valuable adjustment to prediction from steady-state models.

1. Near-field Models

As stated already, no techniques are available for the direct analysis of a heated discharge in the near-field region into a transient current. As a result, the technique has primarily been to choose some sort of critical condition and to apply a steady-state model to this system. Although the title of this section refers to surface discharges, the general statements made here would also be applicable to heated discharges from submerged structures. The critical condition selected could be evaluated by taking a number of different situations, making separate analyses, and comparing the results. Frequently for lake discharges the stagnant water condition is accepted as being the worst condition. If the ambient current is generally fairly small, this is probably not a bad assumption, inasmuch as one would wish to take the case for which the smallest amount of dilution water was available. There are, however, some conditions for which this might not be the worst case. For example, consider the existence of a strong longshore current, which pushes the heated plume up against the shoreline. In this event, extremely long plumes may develop, simply because no dilution water is available on one side of the jet due to the inhibiting shoreline. The same statement could be made for rivers or estuaries. Therefore, if the possibility of the plume being pushed against the shoreline does exist, it might be well to consider this the worst case and analyze the discharge by the standard steady-state procedures. If there is a question as to what the worst condition is, application of the appropriate models should be made for a number of different values of, for example, ambient velocity.

There are obviously limitations to the method proposed here. Treating the discharge as a steady-state discharge overlooks mixing that may occur due to the unsteady flow that exists. As a result, if the worst condition has been chosen for the steady-state analysis, it may yield a conservative result. For example, consider the assumption of zero tidal velocity for making predictions. The plume for such a case would probably never fully develop, because the period of zero (or very close to zero) tidal velocity would be very short. It is perhaps much more likely that those plumes in the up or downstream direction (depending upon the tide direction) will have the opportunity to fully develop. Conservative results are fine, if the predictions indicate that there will be temperature rises that will be acceptable and appear to cause no impact on the environment. On the other hand, consider a case for which the predictions imply an undesirable temperature rise. In this case, the only means probably available to demonstrate a lower rise than predicted by steady-state models would be the building and operation of a physical hydraulic model for the system at hand. Because of the uncertainty of the applications of steady-state models to transient systems, one must interpret each such application of any model and the results obtained from that model with real care.

In short, no methods exist for analysis of the temperature distribution resulting from a heated discharge into a transient ambient environment. There are some approximations that can be made to allow an analysis by standard steady-state means. Extreme care should be taken in such applications, and interpretations of results should be thorough. If care is taken, however, a conservative estimate of the temperature effects can probably be found for many cases.

2. Far-field Estimates

a. Introduction. Estuaries can be divided into a number of different classes. Those two treated most frequently in the models are the partially mixed estuary and the completely mixed or homogeneous estuary. In the latter system, tidal action is strong enough so that all substances are mixed completely laterally and vertically within any given reach of the estuary. This means, for example, that no stratification is caused by salinity, temperature, or other matter. In the partially mixed estuary, there is some vertical structure. One may conceptualize this type of estuary as being a two-layered system in which the salinity is greater in the bottom layer. If the salinity difference becomes great enough, mixing between the upper and lower layers may be limited entirely. The more general case is one in which some vertical interchange is permitted. Rivers could take the same form. There may be rivers in which stratification exists due to temperature or perhaps sediment-laden streams on the bottom. The simpler case is the fully mixed river.

b. Segmented Model for Partially Mixed Estuary. Pritchard[108] developed a simplified model for the partially mixed estuary. Figure 5.28 is a schematic of this segmentation. In this model, Pritchard treats the net nontidal flows in the partially mixed estuary. Due to the fresh-water inflow which proceeds toward the ocean from the upper end of the estuary, a net nontidal flow exists in both the upper and lower layers. This fresh-water inflow causes additional material to mix from the lower layer into the upper layer, causing a net nontidal flow toward the ocean in the upper layer; to conserve mass, there is a net flow away from the ocean in the lower layer. Pritchard[110,111] has used this model himself to estimate the amount of available dilution water. An example of this application to the Calvert Cliff site was given in Sec. V.A.10.

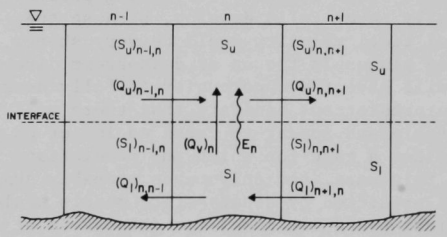

Fig. 5.28.

Segmented Model for Partially Mixed Estuary.

Pritchard[108] gives details of this approach, an outline of which is presented here. In the following, the subscript u will imply upper layer; while the subscript l will denote lower layer. Subscripts of the form k,j will indicate values of the parameter at the boundary between segments k and j. As examples, $(Q_u)_{n,n+1}$ is the flow in the upper layer *across* the boundary from section n to section n + 1; $(S_u)_{n-1,n}$ is the salinity *at* the boundary between segments n - 1 and n. The term $(S_v)_n$ is the salinity at the boundary between upper and lower layers in section n. Then, a steady-state salt balance can be written for the upper layer of segment n as

$$(Q_u)_{n-1,n}\,(S_u)_{n-1,n} + (S_v)_n + E_n\,[(S_l)_n - (S_u)_n] = (Q_u)_{n,n+1}\,(S_u)_{n,n+1} \tag{5.84}$$

in which E_n = vertical-exchange coefficient in the nth segment where this coefficient is essentially a diffusion coefficient times a length, since it describes the salt movement assumed proportional to the salinity gradient, as in molecular diffusion. In Eq. 5.84, the first term represents the salt transferred in to the nth segment by flow from the (n - 1)st segment. The second term indicates the salt mixed vertically upwards into the upper layer by tidal mixing, etc. The third term represents the salt transferred by diffusion. These first three terms give the total salt inflow. The right-hand side shows the flow of salt out of section n into the adjacent section (n + 1). Since this is assumed steady state, the salt concentration is not changing. Thus, salt in must equal salt out, and Eq. 5.84 is complete.

Simple conservation of water mass for segment n is expressed as (water in = water out for steady state):

$$(Q_u)_{n-1,n} + (Q_v)_n + \Delta R' = (Q_u)_{n,n+1}\ , \tag{5.85}$$

where $\Delta R'$ is the change of fresh-water inflow rate.

In addition, $R' + Q_l = Q_u$ for any section, where R' = fresh-water inflow. This is, simply, that the total net flow to the sea must equal the fresh-water flows ($R' = Q_u - Q_l$), which will occur in the upper layer, since these fresh-water flows are lighter. If one assumes that salinities in the layers are inversely proportional to flow, or dilution water, then $S_l/S_u = Q_u/Q_l$, and these equations can be written for any segment:

$$Q_u = R'\frac{S_l}{S_l - S_u} \tag{5.86}$$

and

$$Q_l = R'\frac{S_u}{S_l - S_u}\ . \tag{5.87}$$

To use these equations to evaluate flows, one must know the observed fresh-water inflows and salinity variations. Estimates of R' must come from hydrologic techniques based on tributary stream flows and surface and groundwater runoff. Salinities must be measured. If this information is available, Q_u and Q_l can be computed for every segment by Eqs. 5.86 and 5.87; then vertical flows, Q_v, can be computed from Eq. 5.85; finally, values of the exchange coefficient, E_n,

can be obtained from Eq. 5.84. Salt has then become a conservative tracer to define mixing patterns within the estuary. For example, consider a section at which the fresh-water inflow, R', has been determined to be 40,000 cfs, and the salinity values for upper and lower layers are 10.0 and 12.5 parts per thousand, respectively. Then,

$$Q_u = R'\frac{S_1}{S_1 - S_u} = 40{,}000 \text{ cfs } \frac{12.5}{12.5 - 10.0} = 200{,}000 \text{ cfs}$$

and

$$Q_1 = R'\frac{S_u}{S_1 - S_u} = 40{,}000 \text{ cfs } \frac{10}{12.5 - 10.0} = 160{,}000 \text{ cfs.}$$

If the fresh-water inflow at the next downstream station were R' = 42,000 cfs (includes added fresh water from surface runoff), S_u = 10.2, and S_1 = 12.7, then Q_u = 213,360 cfs and Q_1 = 171,360 cfs, with $\Delta R'$ = 2000. From Eq. 5.85 the vertical flow between the two sections becomes

$$(Q_v)_n = (Q_u)_{n,n+1} - (Q_u)_{n-1,n} - \Delta R' = 213{,}360 - 171{,}360 - 2{,}000 = 40{,}000 \text{ cfs .}$$

Pritchard then uses the flows and coefficients so found to study expected concentrations of a pollutant introduced into the upper layer of segment k. The assumption is made that the pollutant is mixed completely throughout this layer in segment k. Therefore, results from the model may be tainted if this condition is greatly violated. A multiport diffuser across the estuary will come nearest to meeting this criterion. A discharge keeping the plume mostly against one bank would probably not yield such good results with this method.

Conservation of pollutant equations can be written for each segment, expressing the steady-state requirement that the mass of pollutant going into the segment must equal the mass of pollutant leaving the segment. For the upper layer, using C as pollutant concentration, one obtains

$$(Q_u)_{n-1,n}\frac{(C_u)_{n-1} + (C_u)_n}{2} + (Q_v)_n\frac{(C_u)_n + (C_1)_n}{2} + q_{p,n} + E_n\left[(C_1)_n - (C_u)_n\right] = (Q_u)_{n,n+1}\frac{(C_u)_n + (C_u)_{n+1}}{2}, \tag{5.88}$$

in which $q_{p,n}$ = pollutant discharge into nth segment.

For the lower layer, the conservation requirement yields

$$(Q_l)_{n+1,n} \frac{(C_l)_{n+1,n} + (C_l)_n}{2} = (Q_l)_{n,n-1} \frac{(C_l)_n + (C_l)_{n-1}}{2} + (Q_v)_n \frac{(C_l)_n + (C_u)_n}{2} + E_n \left[(C_l)_n - (C_u)_n\right] . \tag{5.89}$$

Both equations use concentrations on the boundaries between two segments (or upper/lower layer) as the average between the two segments. In Pritchard's discussion, the value of q_p is zero in all but segment k; there is, however, no reason the model could not be applied to cases for which effluents were discharged into more than one segment. In addition, discharges could occur into the lower layer, whereupon a term q_p would be added on the left side of Eq. 5.89.

If the estuary is broken into M sections longitudinally, the Eqs. 5.88 and 5.89 yield 2M simultaneous equations. Boundary conditions are as follows:

(1) The concentration will approach zero upstream, as does the salinity, since the pollutant will not move further than the salt.

(2) Pollutant concentration at the ocean in the lower layer is zero.

These equations can be written in a matrix form and solved by matrix inversion; for this problem, however, a much easier means of solution, known as the Thomas algorithm, is detailed in Ref. 61. Pritchard[109] solved these for the Calvert Cliffs and Chalk Point sites to determine dilution water available at the site.

As it stands now, this model is primarily useful for assessing far-field effects and flushing action. For either case, some correction to the results should be included for surface cooling. In fact, another term could be included in Eq. 5.88 to account for this. The model assumes that flushing action is primarily a function of the net nontidal motion generated by fresh-water inflows; hence the problem is reduced to a steady-state problem. Tidal action in this process is assumed accounted for by vertical flows and the exchange coefficient. The near-field analysis must still continue as noted earlier, with a steady-state plume analysis, but this model may help make gross adjustments to such predictions if available dilution water is limited. In addition, such a simplified model could be helpful in evaluating additive impact of more than one plant on the estuary by including a q_p in more than one segment in Eq. 5.88.

This model would not be directly applicable to rivers, since no convenient conservative tracer, such as salt, exists. There are, however, models that do treat the stratified river problem, such as those in Refs. 65 and 141 and others. These are all far-field models and do not add too much to the near-field solutions. Due to the generally less extreme river-flow reversals, information on available dilution water can generally be obtained directly from river-flow data from such sources as the United States Geological Survey.

3. Time-varying Model for Homogeneous Estuary

One-dimensional models have been developed for the time-varying motion in a homogeneous estuary. This means that substances are mixed fully in the lateral and vertical directions in reaches of the estuary. The channel is then divided for numerical-solution purposes into a number of longitudinal segments. This is similar to the Pritchard model developed above, except that there is only one layer, which is fully mixed vertically. The basic equation for transport of a substance or a property in such a medium is

$$\frac{\partial c}{\partial t} + U_i \frac{\partial c}{\partial x} = D_L \frac{\partial^2 c}{\partial x^2} - \frac{Kc}{\rho C_p H} , \qquad (5.90)$$

in which c = concentration of property or substance of interest, U_i = instantaneous velocity, t = time, D_L = longitudinal dispersion coefficient, and H = total depth of estuary. This is actually a simplified version of the more general equation as discussed by Harleman.[47-49] The nature of this conservation equation can be seen by reviewing the individual terms. The first term represents the increase of concentration of the material within the given section with time. The second term represents the transport of material into and out of the section by the average instantaneous current, U_i, across the estuary. The first term on the right-hand side represents the material dispersed into the section by virtue of moving at some velocity other than the mean velocity. The last term is a decay term, which, in the case of heat, would be the loss of heat to the atmosphere across the air-water interface.

The solution to this equation is representative of far-field conditions in the estuary. The assumption is again made that the heated discharge is completely mixed into the estuary section adjacent to the discharge. A multiport submerged diffuser would be most likely to give such a nearly uniform condition. On the other hand, the case of a discharge that hung against the shore might not be a good place to apply this model. Equation 5.90 would be valid not only for estuaries but also for rivers. One difference is that in rivers the value of the dispersion term is likely to be negligible. In estuaries, on the other hand, the dispersion term may be substantial because, when the tide reverses, concentration gradients may be extreme in certain parts of the estuary. However, studies by Harleman *et al.*[51] and Lee and Harleman[77] indicate that, once the basic dispersion term is included, significant changes of it by as much as an order of magnitude have little impact on the predicted concentrations. Lee and Harleman, based on work by Holley *et al.*,[58] suggest the following equation for estimating the dispersion coefficient:

$$D_L = 100 n U_{max} R^{5/6} , \qquad (5.91)$$

in which D_L is in feet squared per second, n is Manning's roughness coefficient, U_{max} is the maximum tidal velocity and R the hydraulic radius, in feet. The velocity U appearing in Eq. 5.90 represents the instantaneous velocity. Information on this may be obtained by measurement in the actual field site. However, numerous programs are also available that will calculate the velocity and depth

in an estuary or river as a function of time and the controlling boundary conditions.

Several solutions have been performed for Eq. 5.90 by expressing the equation as a finite-difference expression at a number of sections within the estuary or river. For example, a computer solution is available in Ref. 77. To run this program the needed information is the estuary geometry; the tidal features, that is, the variation of depth and velocity with time; the information about the fresh water flow; and the roughness characteristics of the estuary. Manning's n in Eq. 5.91 is the roughness coefficient appearing in Manning's equation for velocity. Information on this parameter appears in Refs. 12 and 25. The solution by Lee and Harleman is for the concentration of any general substance with a decay term appropriate to that substance. For the case at hand, temperature is of interest. To reiterate for emphasis, the heated discharge is assumed to be mixed fully in the section adjacent to the plant discharge. This can be expressed by the following equation, noting that the total heat rejected from the plant would be mixed completely into the fresh water flow past the plant:

$$Q_h = \Delta T_o \rho C_p A_R U_f \ , \tag{5.92}$$

in which Q_h is the total heat rejected by the plant, A_R is the cross-section area of estuary, and U_f is the fresh-water flow velocity. To illustrate this beginning point, consider the plant for which $Q_h = 5 \times 10^9$ Btu/hr, which is equal to 1.39×10^6 Btu/sec. Consider that the estuary has a 60-ft depth and a 2000-ft width, yielding a cross-sectional area of $60 \times 2000 = 120{,}000$ ft^2. Assume a fresh-water inflow past this point of 24,000 cfs. Combined with the cross-section area, this yields $U_f = 24{,}000/120{,}000 = 0.2$ fps. Inserting these terms into Eq. 5.92 yields

$$\Delta T_o = \frac{1.39 \times 10^6 \text{ Btu/hr}}{(62.4 \text{ lb}_m/\text{ft}^3)(1 \text{ Btu/lb}_m\text{-°F})(1.2 \times 10^5 \text{ ft}^2)(0.2 \text{ ft/sec})} = 0.93°\text{F} \ .$$

The computer output from the program would then be in terms of $\Delta T/\Delta T_o$ and would decrease from this mixed temperature in the section adjacent to the plant.

Estuaries have been used in these discussions. However, this model should also be applicable to rivers if the geometry and the unsteady features of the flow can be defined. If far-field effects are of interest and one has a river or vertically mixed estuary, this one-dimensional approach would be a good way to handle the problem, perhaps by obtaining the Lee and Harleman[77] program. This one-dimensional approach is also another way of assessing the total dilution water available at a given site. In addition, just as for Pritchard's two-layer segmented model discussed earlier, this one-dimensional model gives the capability of reviewing the effects of multiple sources. One could include several heat sources along an estuary and see what interactions there might be from plants even relatively far apart.

4. Other Finite-difference Models

In the last several years, many finite-difference models have appeared for the one-dimensional problem discussed above and for two-dimensional problems that may occur in an estuary or an embayment. These two-dimensional problems here refer to variations in the x and y directions. Predictions from these models frequently include the depth and velocity as a function of location in the bay.

Several of these lateral models have also combined the hydrodynamic equations with the equations for dispersion of a pollutant and have attempted to treat various water-quality parameters in this fashion. Some attention has recently been given to the problem of thermal plumes in such models. One difficulty immediately arises when attempting to account for buoyancy effects from the heated plume, as the models assume. The models available until about 1970 are summarized in Ref. 140.

Due to the finite size of steps required in the computer program and present limitation on computer size, the finite-difference solutions of equations, by necessity, mean that little definition in the immediate vicinity of the discharge will be possible. Therefore, any finite-difference models now being discussed would have to be considered essentially far-field rather than near-field models. An example of this approach consists of a model prepared by Tracor.[137,138] Buoyancy effects were neglected in the model. As an example of its application, Ward and Espey[140] note the results obtained by using a 500- by 500-ft computational grid. If one has a criterion on the temperature mixing zone that is on the order of 1000 ft, he cannot expect to obtain acceptable results from such a model. If, however, his interest is in the broad-scale effects of this discharge on the entire bay (in this case, the Galveston Bay), such a model might be a good means for obtaining estimates. No details will be provided on this model or the others that might be adapted to thermal discharges, simply because they are too complex for this discussion. In addition, many of the models have available computer programs with sufficient documentation to enable their use. Anyone having an interest in reviewing or using some of these models should refer to Refs. 20, 41, 96, 98. 124 and 132. Reference 41 is based on models developed by Leendertse and Gritton.[80-83]

K. Surface Discharges--Conclusions

The emphasis in this report has been placed on near-field discharges since this appears to be the area of primary interest in terms of thermal impact on the environment. The far-field case has not been completely omitted, however. A review of the rationale for selection of the models seems appropriate. This section was written as both a learning device and a workbook for some of the available models. It would have been inappropriate to include complete descriptions and examples from every other available model. Rather it was decided to take a smaller number of models encompassing the basic elements available and unique to near-field models. Hopefully, one who understands the four models presented in this section can interpret somewhat more detailed literature about any other discharge-analysis scheme. This will be particularly important, since people reviewing proposed projects may see a continuing flood of new models on the market. In some instances, they will just be repeats. In any event, the models chosen were taken with an eye toward instructing rather than restricting the reader to the use of only those models discussed here. As an

example, we feel that anyone understanding the entrainment mechanisms used in some of the jet models will have no trouble transferring this understanding to a similar jet model. By the same token, anyone understanding the surface-cooling mechanisms introduced into one model should have little trouble understanding the use of a similar mechanism in another model or the limitation of that assumption.

1. Three-dimensional Models and Vertical Mixing

It should be initially stated that no complete three-dimensional model is available. "Complete" in this sense means a model that will handle all cases. The most nearly theoretically complete three-dimensional model is the one prepared by Stolzenbach and Harleman.[131] The primary limitation on this model's usage is the fact that it is not considered valid for high ambient currents. A restriction could be stated that the model should be used for $k \geq 10$, where $k = U_o/U_a$, or the ratio of jet velocity to ambient velocity. It is certainly the only near-field model available for any time that incorporates vertical mixing in a rational scheme into the analysis. Many of the others either use a simplified scheme or neglect vertical mixing altogether. Pritchard's model uses a simple linear growth rate of the plume for vertical mixing. His model, too, is limited to $k > 10$. Thus, none of the models presented here include effects of both vertical mixing and a strong ambient current. At present, then, the presence of a strong ambient current may require a two-dimensional model. The neglect of vertical mixing generally is expected to give conservative results, that is, higher predicted temperatures and larger surface areas affected. In lakes or coastal environments or in some very wide estuaries where the ambient current is small, the use of the Stolzenbach model might have the best theoretical base. However, Pritchard's model should not be neglected for this use, for it is based on extensive experience and is probably the easiest model to apply of all those discussed. Neglect of vertical mixing would not be a problem in an environment such as Lake Michigan, where many of the shoreline sites are shallow for a considerable distance. In this event, the Stolzenbach model should have no real advantage over these other models, except that one does not need to specify any coefficient for the Stolzenbach model.

2. Effect of Velocity Ratio

It has been noted that the Stolzenbach-Harleman and Pritchard models are not considered valid for high ambient currents. In these instances it is suggested that a model such as those by Motz and Benedict,[94] Carter,[21] or Hoopes *et al.*[59,148] be used. In addition, if appropriate information is gained on the necessary parameters, other models such as the Sundaram model might be used for river or estuary discharges where there is a significant ambient current. Significant in this sense means that the value of k is somewhat less than 10. Conceivably, if the k value was low and approaching 1.0, some of the far-field models discussed by Policastro and Tokar[104] might be used in the analysis of the plume. Currently designed discharge systems will probably not use this as a means of discharge, however. A plume that is swept up against the bank immediately by a high ambient current is likely to spend a long time hugging the bank and travel a considerable distance with small temperature decrease.

Table 5.7 presents a brief view of the applicability of the near-field models discussed in this report, summarizing comments on k and vertical mixing.

Any three-dimensional model can also handle two-dimensional cases by simply not allowing plume depth to change.

Table 5.7. Near-field Model Applicability

	Steady State[a]		
	Two-dimensional	*Three-dimensional*	*Transient*
$1 < k < 5$	MB, C, H, S	None	
$5 < k < 10$	MB, C, H, S, KDS[b]	KDS[b]	None[c]
$10 < k$	P, KDS, MB, C, H, S	P, KDS	

[a]*C = Carter, H = Hoopes et al., KDS = Stolzenbach-Harleman, MB = Motz-Benedict, P = Pritchard, and S = Sundaram et al.*

[b]*Uncertain in this range.*

[c]*Must use steady-state assumption.*

3. Situations Not Covered by Current Near-field Models

Table 5.7 shows that no three-dimensional model exists for discharge into a strong ambient current ($k < 5$).

Several other factors are generally not included in any model of the near field. The first is transient conditions. There is simply no model for a near-field discharge into a time-varying condition. Second, there is generally no handling of geometry effects, except by empirical means. That is, if the plume runs into the near or far bank, about all that can presently be done by most models is to estimate the effect and proceed by, for example, reducing the entrainment coefficient. In addition, little has been done in the area of treating unequal entrainment on the two sides of a discharge into a strong ambient current. At present, there are no adequately tested means of connecting the region of jet mixing to the region in which mixing is controlled by ambient turbulence. In this light, note that those models classed primarily as near-field (or jet) models neglect any form of ambient mixing, although those that obtain values of empirical parameters by fitting probably include a certain degree of ambient turbulence in those coefficients. In the same vein, models classed as far-field or diffusion models neglect any form of initial jet mixing. The present technique has been generally to apply a jet model, choose a criterion for transition, and apply a diffusion model from that transition point onward. Much more work is needed in this area.

4. Far-field Estuary Models

If the discharge mechanism is such that the heated water is reasonably well mixed into the river or estuary water in the immediate vicinity of the plant discharge, there are far-field techniques with one-dimensional and

simplified two-dimensional schemes that will reveal something about the far-field distribution with some confidence. There is still no real gauge, however, of exactly how complete this mixing must be to provide reasonable results from these models. Discussion at a recent conference on estuaries[140] indicates a real ability to treat even estuaries such as the Delaware Estuary as one-dimensional. Therefore, these one-dimensional models at least must be able to accept a reasonable degree on nonuniformity and still produce valid results. If it is assumed that there is not sufficient mixing within the nearby section to begin the far-field problem by methods such as those of Lee and Harleman[71] or Pritchard,[108] some better techniques must be developed.

5. Model Verification

When the question of verification arises, it becomes plain that few of the models have been fitted against sufficient data from a variety of sites and circumstances ro provide definitive statements about their validity. In this light, the upcoming reports by Policastro and Tokar comparing the results predicted by the models for varieties of situations should be extremely useful. Little data are available on such items as time of exposure of organisms. There are frequently insufficient data on many of the important parameters in any set of field data taken. Fortunately, much of the data presently being taken are being treated with more care and the appropriate parameters measured. It is hopeful that information will especially be obtained on the region very near the jet discharge.

6. Model Implementation and Interpretation of Results

To analyze a proposed or existing heated discharge, one must first define needed input parameters for his model. Many of these parameters are simple geometric features of the discharge structure and receiving-water body, as well as expected condenser-cooling-water flows and temperature rises. In addition, some flow must be assumed in the receiving-water body. Usually, some expected critical condition is chosen, such as stagnant conditions or a low flow of some given frequency of occurrence. The latter may be specified by some water-quality control agencies.

Most of the models presently available require the specification of some sort of entrainment coefficient, drag coefficient, or other empirical parameters. This is a drawback in the use of any such model as a predictive tool. The state of the art presently is such that considerably more work needs to be done to make these models usable by the general user. By this it is meant that many of the models can probably yield reasonable results if used in familiar situations. However, for the model to be a useful predictive tool for all users, the difficulty of obtaining these coefficients must be reduced.

To aid in model selection, the models discussed in this report are briefly characterized in Table 5.8.

It can be concluded that a number of models are available to treat the near-field case. Each has some limitations; each has some strengths. No single model will handle every possible case.

Each site and condition must be treated individually. A careful review of all the parameters at a site must be made in order to choose an appropriate

model for the analysis to be made. Results should be interpreted at this time with conservatism. If one is told that he must meet a particular temperature standard by 1000 ft from the discharge and the predictive model reveals that he has reached it at 950 ft, it might be well for him to evaluate the results very closely. The application of any of the models outside the range of parameters for which they have been verified should imply a factor of safety on intepretation of the results. This is done not only so that the environment may be protected, but also so that the investigator might sleep better at night. These statements add up to saying that model results should not be treated as exact. They should be treated as representative of the results to be obtained with a particular discharge and interpreted in light of the verification of the model and existing knowledge of the site.

The designer intending to sell a particular discharge design for a power plant should remember the following: Try to design your discharge so that you can analyze it. A discharge structure designed with some unusual shape or condition or designed to discharge so that no analysis is possible only complicates the matter. For example, someone feeling real confidence in the Stolzenbach model on a lake site might take the approach of designing a high-velocity discharge that would remove the concern of possible high ambient current. He could apply the Stolzenbach model without any concern over that limitation.

In this way, one may assume that the analysis yields reasonable results.

Table 5.8. Characteristics of Models

	Valid for k					*Field*		*Computer*		*Pressure*	*Coefficients*
	1-5	*5-10*	*< 10*	*2-D*	*3-D*	*Near*	*Far*	*Program*	*Transient*	*Drag*	*Needed*
Carter	Y	Y	Y	Y	N	Y	N	N	N	Y	1
Hoopes *et al.*	Y	Y	Y	Y	N	Y	N	Y[a]	N	N	1
Motz-Benedict	Y	Y	Y	Y	N	Y	N	Y[a]	N	Y	2
Pritchard	N	?	Y	Y	Y	Y	Y	N	N	N	0
Stolzenbach-Harleman	N	?	Y	Y	Y	Y	N	Y[b]	N	N	0
Sundaram *et al.*	Y	Y	Y	Y	Y	Y	Y	N	N	Y[c]	4
Lee-Harleman	–	–	–	–	N	N	Y	Y[b]	Y	–	1[d]
Pritchard (Segmented)	–	–	–	–	N	N	Y	?	Y[e]	–	0

[a]*Available from authors.*
[b]*Available in a publication.*
[c]*Through use of smoke-plume trajectory equations.*
[d]*Manning's "n."*
[e]*Uses net nontidal flows.*

VI. SINGLE-PORT SUBMERGED DISCHARGES

The most popular means of disposing of heated water has been to discharge it to a receiving-water body through a surface channel. This method is the simplest and least expensive means of discharge. However, more stringent thermal standards in recent years have brought more interest in the use of submerged discharges. Although costs for construction and pipes make this a generally more expensive alternative, submerged discharges may allow higher initial dilutions, thus enabling standards to be met.

Many factors bearing on submerged discharges have been discussed in some detail in earlier chapters and will not be repeated here. The reader is especially referred to Chapter V (Secs. A.1, A.3, A.4, A.6-8, A.10, and J). In addition, considerable material in Chapter II relates to submerged discharges. Such topics include the effect of ambient stratification, the ambient velocity, the effect of F_j, the densimetric Froude number of the discharge, and especially the effect of boundary influences (both bottom and free surface) on jet behavior. Both the latter boundaries tend to inhibit mixing and are especially important for shallow-water discharges. All the models to be presented in this chapter are infinite-field models; that is, they are derived neglecting any such boundary influences. Therefore, one must exercise caution when interpreting model predictions near a boundary. In this current chapter, familiarity with material in these sections of Chapters II and V will be assumed. In the same manner, sufficient detail will be developed in this chapter to form an adequate background for Chapter VII.

It is worth discussing the approach taken in this chapter. Several models are presented to handle both round and slot jet discharges into a variety of environments. The conceptual makeup of all of these models is identical. The differences between models lie in details of such things as the precise form chosen for similar profiles or the terms to be omitted or included for specific cases. A general development will be presented showing the rationale for the equation system common to all the models. For subsequent models, sufficient detail will only be given to enable the use of the model for some examples. This is especially true where models must be solved on the computer. The reader will be referred to the basic references for detailed developments of individual models.

In this chapter, discussion centers on two initial jet shapes--the round orifice and the slot. For each shape, available knowledge is reviewed for discharges into both stagnant environments and flowing receiving bodies. The important effect of ambient density structure is included by discussing receiving environments that are uniform, linearly stratified, or arbitrarily stratified. Uniform bodies of water are those whose density is the same from top to bottom. Linearly stratified media are those whose density increases at a constant rate with depth from top to bottom. This means that density plotted against depth in the receiving body would yield a straight line. Arbitrarily stratified waters can have any variation of density with depth. Figures 2.2 and 2.4 are examples of these density structures.

A. Theory and Application of Submerged Jets

1. Introduction

Historically, the approach to the solution of a submerged-jet discharge of a waste of interest (heated waters, sewage, and brine waste) involved the solution of equations of continuity, motion, energy, and geometry. The two basic approaches used are differential analysis and integral analysis. The differential approach involves solving the general partial-differential equation of motion and heat diffusion to arrive at velocity and temperature (or concentration) distribution. Integral analysis assumes that a specific form of the lateral variation in the heated plume of both concentration (or heat) and velocity distributions exists. Integral equations of conservation of mass, momentum, etc., are written. This is the form of analysis used in those models of Chapter V for which similar lateral profiles are chosen. The term "integral equation" here simply means that the basic equations have been integrated over the cross section of the plume to reduce all unknowns so that they are only functions of location along the plume centerline. All the models discussed in this chapter are based on integral techniques.

The solution of waste-discharge problems can be divided into classes according to applicability. Three general classes are recognized according to ambient-velocity considerations, density structure of receiving body (due to thermal or salinity differences), and type of discharge structure. The ambient-velocity field can be considered as stagnant (no ambient current), having uniform ambient current, or being subject to transient velocities due to tidal variations. Stratification may be due to temperature or salinity variations in the receiving bodies of water. The outfall structure may consist of a slot jet or a round jet. In addition, consideration must be given to jet interference that reduces the dilution if a series of slots or round jets is used as a diffusion structure. This latter problem is treated in Chapter VII.

Hence, the choice of model will depend largely on answering the following questions:

a. What are the velocities in the receiving body of water?
b. What type of discharge structure is used?
c. What does the density profile of the receiving body look like?

In addition to the above information, the following information is needed to evaluate the discharge.

a. What is the critical ambient flow with which one must be concerned? Also, what are the associated depths?
b. What do the cross-sectional profiles look like if the discharge is into a river?
c. What are the critical discharge rates of heated waste water?

2. Jets in General

Fan,[38] Fan and Brooks,[39] Hirst,[54] Abraham,[2] Morton *et al.*[92] and many other investigators have studied submerged jets. Many solutions of the problem of heated-waste-water discharges of the previous investigators, however, have been limited to specific applications. Fan and Brooks presented solutions for buoyant

jets in a stagnant environment with a uniform density or linearly stratified. Also, Fan presented a solution for a round, buoyant jet in a flowing, uniform environment. Applying Fan's plume analysis, Baca[11] developed a round, buoyant jet model that describes thermal-plume behavior in three space dimensions, discharging at arbitrary angles to a crossflow. Hirst presented a model of round, turbulent jets, discharged into flowing stratified environments. Hirst's model is the most general in that it allows the discharge to be arbitrarily injected at any angle.

3. Axis of Reference

Figure 6.1 represents the axis of reference being used in this report. The x axis is in the direction or parallel to the ambient velocity, the z axis represents the vertical direction and is thus parallel to the buoyancy force, and the y axis is perpendicular to both the x and z axes and will represent some lateral axis. For example, if the discharge is into a river, the x axis will be in the direction of ambient flow, the y axis will represent the lateral location across the width of the river, and the z axis will represent the depth of the river. In addition, the s axis is located on the centerline of the jet. Also, two variables, r and ϕ, are used to represent the location in some plane A, which is perpendicular to the jet axis at some location, s. The variable r represents the radial distance from the centerline; ϕ represents the angular rotation of the radial coordinate r.

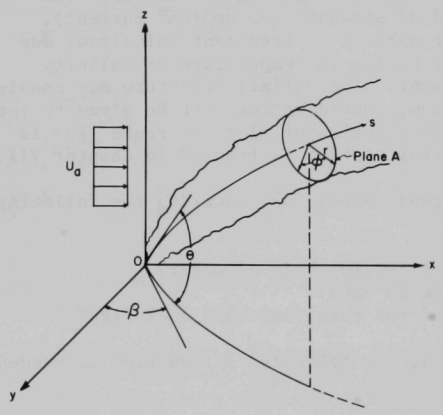

Fig. 6.1.

Schematic Diagram of Reference Axis.

The main difference in the ranges of applicability for the models developed by Fan and by Hirst may be more readily seen by a brief example. Consider the bottom and left-hand edges of this page to represent the x and y axes, respectively, of the reference system. Hence, the page will form the xy plane of the system. Then, the z axis would be perpendicular to the page and coming out of it at the lower left-hand corner; θ represents the angle that a tangent to the s axis makes with the xy plane; β represents the angle that the projection of the s axis on the xy plane makes with the y axis. Hence, in Fan's model, the value of β is always 90° and θ may vary, so that the discharge is always in the plane bounded by the x and z axes. Physically, this means that the y coordinate of the jet axis is constant. However, in Hirst's model, the jet may

be injected at any arbitrary value of β and θ, and the location of the jet axis will be related to all three coordinate axes.

4. General Assumptions for Submerged Jet Models

The general assumptions used in the development of this model were outlined by Fan.[38] These assumptions hold true for all models presented in this chapter:

a. Flows are steady.
b. The fluids are incompressible.
c. Variations of fluid density throughout the flow field are small compared with the reference density chosen. The variation of density can be neglected in considering inertia terms, but it must be included in gravity terms. Since the variation in density is assumed small, this leads to the approximation that the conservation of mass flux can be replaced by the conservation of volume flux.
d. Within the range of variation, the density of the fluid is assumed to be a linear function of salt concentration or heat content above the reference level. This is a reasonable assumption for temperatures between about 60 and 100°F.
e. Flow in both the jet and ambient fluids is fully turbulent, as exhibited by high values of the Reynolds numbers, Re_j and Re_a. Transport by molecular motion is then negligible.
f. Pressure is hydrostatic throughout the flow field.
g. Curvature of the trajectory of the jet is small. In other words, the ratio of the local characteristic width of the jet to the radius of curvature is small. The effect of curvature can be neglected.
h. The velocity profiles are similar at all cross sections normal to the jet trajectory. When similarity is assumed, that means that all profiles can be described with the same mathematical function. For example, Morton *et al.*[92] assume similarity for the velocity profiles and assume the distribution is "tophat"; i.e., the velocity profile is uniform in a particular plane of the jet. The most commonly chosen similar profile is the Gaussian, or bell-shaped, curve. Similarity is also presumed for profiles of buoyancy and concentration of any tracer. Fan[38] presents evidence to support the assumption of similarity in concentration profiles taken in the vertical direction. This physically implies a unimodal or Gaussian distribution. The assumption of similar profiles facilitates the integration of the equations that describe the jets. However, if experience indicates that some profile other than Gaussian exists, it should be used in the integration of the equations. Typical specific forms of the profiles are given in the next two sections.

The analysis applies only to the ZOEF, where all the profiles are fully developed. ZOFE and ZOEF were discussed in Chapter V, and their importance to practical application of submerged jets is presented in Sec. F.1, K.2.a, Q.1, and Q.2 of this chapter.

5. Entrainment in Submerged Jets

Morton *et al.* first proposed an entrainment mechanism to account for the dilution and spreading of jets. They reasoned that the rate of entrainment of fluid at any height is proportional to a characteristic velocity at that height. The physical environment (stagnant versus flowing environment) into

which the jet issues will determine the form the characteristic velocity will take. When a stream of fluid comes into contact with another stream at an angle or at a different velocity, eddies (added turbulence) are generated. These eddies cause the transfer of matter into the jet. This transfer of matter can be characterized by velocities proportional to the relative velocities of the two streams. Fan[38] uses the following equation to relate the rate of change of volumetric flux to the entrainment of fluid from the ambient environment:

$$\frac{dQ}{ds} = 2\pi b\alpha \left|\vec{U}_j - \vec{U}_a\right|, \tag{6.1}$$

where Q = volumetric flux,

α = coefficient of entrainment,

U_j = velocity of jet at the centerline,

U_a = ambient velocity, and

b = a characteristic length described by Eq. 6.4 (p. 188).

The velocity difference is a vector difference, meaning that the angle is included. Physically, Eq. 6.1 means that ambient fluid is gathered into the jet at a rate proportional to the difference in jet and ambient velocities. The proportionality constant is called the coefficient of entrainment, α. Further detail on the entrainment concept appears in Chapter V.

For a simple jet, the coefficient, α, is assumed constant. Albertson *et al.*[5] find the value of $\alpha = 0.057$. A simple *jet* is one in which the momentum forces are much larger than the buoyancy force or there are not any buoyancy forces to consider. A simple *plume* is characterized by a turbulent flow pattern generated by a continuous source of buoyancy, e.g., a smoke cloud from a fire. Rouse *et al.*[117] found that α was constant and equal to 0.082 for such simple plumes.

Hirst considers the entrainment relationship to consist of three different parameters based upon observations by Morton *et al.*,[92] Fan,[38] Fox,[43] and Hoult *et al.*[60] Hirst reasons that the entrainment function should depend on the following factors:

a. Local mean flow conditions within the jet, U_j and b.
b. Local buoyancy within the jet, as defined by F_L, the local densimetric Froude number.
c. Velocity ratio, $k = U_o/U_a$.
d. Initial jet orientation, β_o' and Θ_o'.
e. Ambient turbulence.

Hirst uses data from previously published reports to choose the best values of entrainment coefficients. The following equation is developed to include as many of the factors outlined above as possible, based on an optimum fit to available data:

$$E_r = \left(0.057 + \frac{0.97 \sin \beta}{F_L^2}\right) \left[b|U_j - U_a| + 9.0U_a b \sqrt{1 - (\sin \beta_* \cos \Theta)^2}\right], \tag{6.2}$$

where E_r = rate at which ambient fluid is entrained,

F_L = local densimetric Froude number, defined as

$$F_L = \frac{U_j}{\sqrt{g(\Delta\rho/\rho_o)b}}, \tag{6.3}$$

U_j = local jet centerline velocity,

$\Delta\rho = \rho_a - \rho$,

ρ_a = ambient density,

$\beta_* = 90° - \beta$,

ρ = jet centerline density,

ρ_o = reference density,

g = gravitational acceleration, and

b = characteristic length defined by Eq. 6.4.

The physical implications of Eq. 6.2 should be reviewed. Consider the fairly typical case in which $\beta = 90°$. For this case, the value of the square root in Eq. 6.2 becomes 1.0. Therefore, the angle Θ shows up in only one term. As Θ nears zero, sin Θ approaches zero, thereby indicating decreased entrainment. This corresponds to the jet becoming parallel to the ambient velocity, thereby reducing the "disturbance" and hence the generated turbulence. As the local densimetric Froude number, F_L, increases, entrainment also decreases. This differs from the situation with surface discharges discussed in Chapter 2, where entrainment increased with increasing F_j. However, in a submerged discharge, the velocity, and hence the mixing, can be increased by buoyant forces acting to push the heated plume toward the surface. Many of the data sets used by Hirst in developing Eq. 6.2 are for $\Theta_o' = 90°$ (in the vertical direction). Higher values of F_L imply lower values of $\Delta\rho$, or a lesser influence of buoyancy. Lesser buoyancy causes the jet to rise through the ambient fluid with a smaller velocity, decreasing mixing. Equation 6.2, like 6.1, indicates greater mixing for greater vector velocity differences.

Recall that in a surface jet, the ambient current is assumed to generate a lateral circulation in the jet, as shown in Fig. 5.1. A similar phenomenon is experienced for submerged jets. Figure 6.2 is a simplified view of a cross section through a jet, showing counterrotating vortices. Those vortices are formed as the ambient fluid flows past the edges of the jet and tends to pull the jet fluid in the direction of ambient flow. This section shape is frequently called a "horseshoe" shape. Fan[38] observes this "horseshoe" pattern in experimental studies. He finds that the concentration profile in the lateral

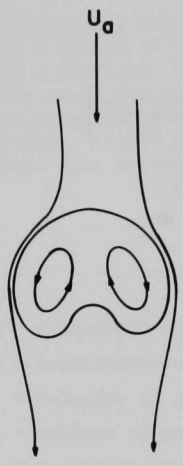

Fig. 6.2.

Schematic of a Simplified Section of a Jet with Counterrotating Vortices.

direction is bimodal, i.e., two regions with a maximum concentration. However, the vertical concentration profile shows only one maximum, and it can be approximated with a Gaussian distribution. Hence, the assumption of an axisymmetric jet with a Gaussian distribution of velocity or concentration profiles is a simplification and is reflected in the values of α used for the given model. Platten and Keffer[103] include an additional entrainment coefficient to account for the entrainment due to the counterrotating vortices, and this is the origin of the last term in Eq. 6.2. Therefore, an increase in U_a should result in increased mixing by vortex action.

Equation 6.2 does not account for one item Hirst considers important, ambient turbulence. On the other hand, Davis[29] believes that this item is not important for a vertical jet. The omission of the ambient turbulence term is, however, a major drawback when using the Hirst model for coflowing discharges under some conditions. This aspect is discussed in Sec. VI.L below. Coflowing simply means that the initial jet discharge is exactly parallel to U_a.

The entrainment mechanisms discussed here do not account for the presence of any bottom or free-surface boundary. Due to limitation of the water available for entrainment, any such boundary will inhibit entrainment. Therefore, caution is urged in using models based on these entrainment mechanisms. All predictions must be checked for reasonableness. Especially in shallow water (submergence less than about 10 diameters), the free surface may play a major role in jet behavior.

6. Typical Similar Profile--Velocity, Buoyancy and Tracer

The velocity profiles are assumed to be similar and of Gaussian form above the ambient velocity component, $U_a \cos\Theta \sin\beta$, as shown in (the velocities used are shown in Fig. 6.3)

$$u^*(s,r,\phi) = U_a \cos\Theta \sin\beta + u(s) \exp(-r^2/b^2), \qquad (6.4)$$

where

$u^*(s,r,\phi)$ = local jet velocity,

U_a = ambient uniform velocity,

$u(s)$ = jet centerline velocity at s, and

b = characteristic length.

This assumption is used by Baca[10] and Hirst.[54] The initial velocity of the jet, relative to a stationary body, is the jet velocity as it is discharged from the jet port of the diffuser, plus the component of the ambient velocity parallel to the jet axis. Figure 6.3 illustrates the physical meaning of Eq. 6.4 and the assumption of similar velocity profiles. Sections A-A and B-B are representative sections along the s axis. The uniform segment at each section is the component of ambient velocity, which exists whether a jet is discharged or not. The bell-shaped segment is the jet-induced component of velocity.

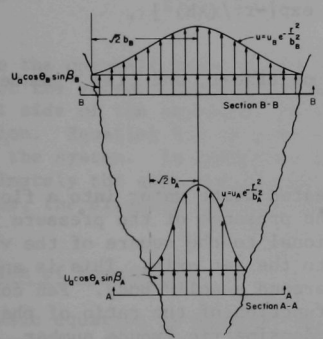

Fig. 6.3.

Typical Jet Cross Section for a Discharge into a Flowing, Ambient, Environment.

Fan defines the half-jet width as $\sqrt{2}\,\sigma$. Morton *et al.*[92] define b as the distance from the axis of symmetry to points at which the local velocity and local buoyancy values are 1/e of those values on the centerline of the jet. They note that this length is characteristic of the normal distribution profile and can easily be used for purposes of calculations. In addition, they state that this does not correspond with the radius observed in experiments, but is proportional to it. Hence, if b is defined as the characteristic length with some value, then insertion of this value into Eq. 6.4 yields a ratio of local jet velocity to centerline jet velocity as 1/e if the jet is discharged into a stagnant environment.

The buoyancy profiles are also frequently assumed to be Gaussian. In general, the equation for the buoyancy profiles in a linearly stratified environment is

$$\frac{\rho_a^*(s,r,\phi) - \rho^*(s,r,\phi)}{\rho_o} = \frac{\rho_a(s) - \rho(s)}{\rho_o} \exp\,[-r^2/(\lambda b)^2], \qquad (6.5)$$

where λb = the characteristic length of the profiles,

ρ_a^* = local ambient density,

ρ^* = local density within a jet,

ρ_o = reference density taken as $\rho_a(0)$, and

ρ = density along the jet axis.

The quantity λ^2 is the turbulent Schmidt number and is assumed constant. Fan uses $\lambda = 1.16$ for a round, buoyant jet in a stagnant environment and $\lambda = 1.0$ for a round, buoyant jet in a flowing environment. The significance of the value of λ is that it relates the growth of the concentration or density profiles to the growth of the velocity profiles. Hirst states that λ is a measure of the relative spreading of concentration and velocity profiles. Further comments on relative spreading rates appear in Sec. V.A.7. Profiles of a certain tracer concentration are also assumed similar and Gaussian:

$$c^*(r,s,\phi) = c(s) \exp[-r^2/(\lambda b)^2] \ , \tag{6.6}$$

in which $c^*(r,s,\phi)$ = local concentration of tracer, and $c(s)$ = centerline concentration of jet.

7. Pressure Drag

When considering the discharge of heated waste water into a flowing environment, Fan[38] reasons that the effect of the presence of the pressure field can be lumped into a gross drag term proportional to the square of the velocity component of the oncoming stream normal to the jet axis. This is analogous to the drag force created by fluid flow around a solid body. Fan considered C_d, the gross drag coefficient, to be a function of the ratio of the jet velocity to ambient velocity, k, and the densimetric Froude number, F_j. Abraham[2] considers $C_d = 0.3$ for all cases.

B. Development of the General Equations for a Round, Buoyant Jet

The equations for the discharge of a round, buoyant jet into a linearly stratified flowing environment will be developed here. The purpose of showing the development is to illustrate the rather simple basis for the models to be discussed. One loses sight of the fundamental physical laws at work when a system of several lengthy, complex differential equations is thrust at him. The equations are therefore presented as an aid to going into any of the basic references on the models to be discussed (or similar models) and understanding their developments. In fact, the final form of the equations developed in this section is secondary to this understanding. Later applications to different systems will also aid in comprehension. For example, if the jet is discharged into a stagnant environment, then $U_a = 0$. This will greatly simplify the development of the equations. The basic approach applied by Fan,[38] Fan and Brooks,[39] Morton *et al.*[92] and Baca[11] will be used.

1. Equation of Continuity

One basic relationship to be satisfied is that of continuity, or conservation of mass. The flow rate past one section of the jet must equal the flow

rate past an earlier section plus the fluid entrained by the jet between those sections. The flow rate, Q, past a given cross section is

$$Q = \int_A u^* \, dA, \tag{6.7}$$

in which $\int A$ implies an integral or summation over the entire cross section of the jet. The entrainment rate can be expressed by Eq. 6.1. The Gaussian profile shown in Eq. 6.4 enables evaluation of the integral in Eq. 6.7. This expression for Q can then be substituted into Eq. 6.1, which (after dividing by π) results in

$$\frac{d}{ds}[b^2(2U_a \cos\theta \sin\beta + u)] = 2\alpha b(U_a^2 \sin^2\theta \sin^2\beta + u^2)^{1/2}. \tag{6.8}$$

The term to the one-half power on the right side of the equation is merely the expansion of the vector-velocity difference $|\vec{U}_j - \vec{U}_a|$. The term in brackets on the left side of the equation, if multiplied by π, is equal to Q past the given section. Equation 6.8 is then merely an expression imposing conservation of mass on the system. In addition, the assumption is made that the densities are approximately the same and the mass flux can be approximated by the volumetric flux. Hence, the dilution can be found by dividing by the initial value of Q, namely Q_o.

2. Equation of Momentum

The basic equation of momentum has historically been written as F = ma, where F represents the forces acting on a body, m is the mass of the object subjected to the forces, and a is the acceleration of the object. However, the more basic equation is written as $\Sigma F = d\,mv/dt$, where mv represents the momentum of the object. Physically, this means that the sum of the imposed forces equals the rate of change of momentum. The imposed forces on a submerged jet consist of pressure and buoyancy forces. In addition, for a jet gathering fluid from its surrounding environment, there will be a change of momentum due to the entrained fluid. Hence, the equations of momentum are written to account for the rate of change in momentum due to the imposed forces plus entrained ambient fluid. The approach taken here is to write the expression in terms of the three Cartesian directions: x, y, and z.

In general, a jet discharged into a flowing stream will be deflected in the same direction as the flow. Fan adopts the premise that a jet into a flowing environment is deflected in the direction of flow for two reasons. First, the pressure drag already mentioned tends to deflect the jet somewhat as if it were a solid body. Second, the jet is entraining ambient fluid, which has a momentum in a direction other than along the jet centerline. For example, consider a jet discharged along the z axis and into an ambient velocity parallel to the x axis. The initially vertical jet will entrain ambient fluid having an x-momentum component and will be deflected in the x direction. In this development, reference to Fig. 6.4 will aid in visualizing the force and entrained-momentum components. The drag force can be taken[38] as

$$F_D = \frac{C_d}{2} \rho_a \underbrace{U_a^2 \sin^2 \theta \sin^2 \beta}_{\substack{\text{velocity}\\ \text{component}\\ \text{squared}}} \underbrace{(2\sqrt{2}\, b)}_{\substack{\text{area}\\ \text{per}\\ \text{length}}}, \tag{6.9}$$

in which C_d is the gross drag coefficient.

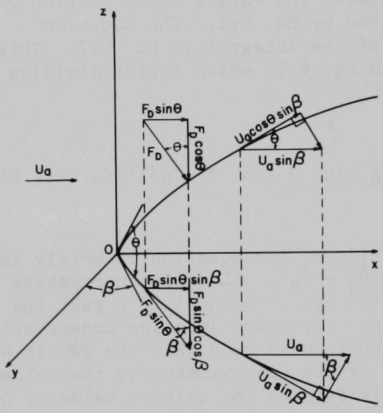

Fig. 6.4.

Schematic Diagram of Ambient-velocity and Drag-force Components.

a. <u>y momentum</u>. Since the x axis was chosen to be in direction of the flow of ambient fluid, the only force acting on the jet will be a component of drag force, F_D, and there will be no entrained momentum component. Hence, the equation of y momentum is

$$\underbrace{\frac{d}{ds} \int_A \rho^* u^* (u^* \cos\theta \cos\beta) dA}_{\substack{\text{Rate of change of}\\ \text{y momentum}}} = \underbrace{F_D \sin\theta \cos\beta}_{\substack{\text{Drag-force}\\ \text{component in}\\ \text{y direction}}} . \tag{6.10}$$

In this equation and others to follow, the superscript * implies the value of that parameter at *any* point in the jet cross section, while the nonsuperscript parameter implies the value on the jet centerline. For example, ρ^* is the density at any point in the section (defined by the Gaussian curve) and ρ is the centerline density. Use of the assumed Gaussian profiles for velocity and density and letting $\rho^* \simeq \rho_a \simeq \rho_o$ give

$$\frac{d}{ds}\left[\frac{b^2}{2} \cos\theta \cos\beta (2U_a \cos\theta \sin\beta + u)^2\right] = \frac{C_d}{\pi} \sqrt{2}\, b\, U_a^2 \sin^3\theta \sin^2\beta \cos\beta . \tag{6.11}$$

b. x momentum. The momentum forces to consider in the x direction include the change in momentum due to the entrained ambient fluid and the drag force component in the x direction:

$$\frac{d}{ds}\int_A \rho\, {}^*u^*(u^*\cos\theta\,\sin\beta)dA$$
$$= \rho_a\, 2\pi\alpha b\, U_a|\vec{U}_j - \vec{U}_a| + F_D \sin\theta\,\sin\beta\,. \tag{6.12}$$

Using the assumed similar profiles yields

$$\underbrace{\frac{d}{ds}\left[\frac{b^2}{2}\cos\theta\,\sin\beta(2U_a\cos\theta\,\sin\beta + u)^2\right]}_{\text{momentum}}$$
$$= \underbrace{2\alpha b\, U_a(U_a^2\sin^2\theta\,\sin^2\beta + u^2)^{1/2}}_{\text{entrainment}} + \underbrace{\frac{C_d}{\pi}\sqrt{2}\, b\, U_a^2\sin^3\theta\,\sin^3\beta}_{\text{drag force}}\,. \tag{6.13}$$

c. z momentum. In the vertical direction, z, the change in momentum is due to the buoyancy flux or the density difference between the jet density and the ambient density. In addition, the drag force will have a vertical component. This is not limited to heated discharges or to instances in which the waste is lighter than the receiving ambient fluid. It may also apply to discharges that are heavier than the receiving ambient waters, e.g., brine wastes. Anderson[8] conducted a laboratory investigation using Fan's model to predict the dilutions and trajectories of negatively buoyant jets in a flowing stream and found that Fan's model will predict the dilution and trajectory for a negatively buoyant jet into a flowing uniform environment.

$$\underbrace{\frac{d}{ds}\int_A \rho^* u^*(u^*\sin\theta)dA}_{\text{z momentum}} = \underbrace{\int_A g(\rho_a^* - \rho^*)dA}_{\text{buoyancy}} - \underbrace{F_D\cos\theta}_{\text{drag force}}. \tag{6.14}$$

Substituting Eqs. 6.4, 6.5, and 6.9 into Eq. 6.14 yields

$$\frac{d}{ds}\left[\frac{b^2}{2}\sin\theta(2U_a\cos\theta\,\sin\beta + u)^2\right] =$$
$$g\lambda^2 b^2\,\frac{\rho_a - \rho}{\rho_o} - \frac{C_d}{\pi}\sqrt{2}\, b\, U_a^2\sin^2\theta\,\cos\theta\,\sin^2\beta\,. \tag{6.15}$$

The simplification is made by letting $\rho_a^* = \rho_o$, where ρ_o is some reference density usually taken as the ambient density at the discharge port.

Therefore, Eqs. 6.11, 6.13, and 6.15 are the three component expressions of Newton's second law, F = ma. Their complex appearance should not hide that fact.

3. Density Deficiency

A general expression can be written for the conservation of the density flux of a jet discharged into a flowing linearly stratified environment. The buoyancy flux (relative to the reference density ρ_o) is no longer constant, because of the entrainment along the buoyant jet's edge. The rate of change of heat (or salt-deficiency) flux through a cross section of the plume equals the amount of heat or salt entrained from the ambient fluid. This physical fact can be written as

$$\frac{d}{ds}\int_A u^*(\rho_o - \rho^*)dA = \alpha b\,|\vec{U}_j - \vec{U}_a|\int_o^{2\pi}[\rho_o - \rho_a^*(s,b,\phi)]d\phi\ . \quad (6.16)$$

Using assumed similarity profiles, the equation for the density deficiency yields

$$\frac{d}{ds}\left[b^2[(1+\lambda^2)U_a\cos\theta\sin\beta + u](\rho_a - \rho)\right] = \frac{1+\lambda^2}{\lambda^2}b^2(2U_a\cos\theta\sin\beta + u)\frac{d\rho_a}{ds}\ . \quad (6.17)$$

4. Continuity of Tracer

The general expression will be written to conserve the tracer in the jet (salt, temperature, or whatever). Conservation of tracer requires that the rate of change of tracer flux along the jet axis must equal zero. That is,

$$\frac{d}{ds}\int_A c^*u^*dA = 0. \quad (6.18)$$

Use of the assumed similarity relations for tracer and velocity enables evaluation of Eq. 6.18 and its direct integration to yield

$$b^2[(1+\lambda^2)U_a\cos\theta\sin\beta + u]c = \text{constant}. \quad (6.19)$$

If the discharge consists of salt water and is discharged into an estuary with a salinity gradient, Eq. 6.19 will not apply. Hirst's model[54] does, however, account for the discharge into an environment with a salinity gradient.

5. Geometric Relationships

In addition to the equations already developed, three geometric relationships exist, namely,

$$\frac{dx}{ds} = \cos\theta \sin\beta, \tag{6.20}$$

$$\frac{dy}{ds} = \cos\theta \cos\beta, \tag{6.21}$$

and

$$\frac{dz}{ds} = \sin\theta. \tag{6.22}$$

This yields nine first-order, ordinary differential equations (Eqs. 6.8, 6.11, 6.13, 6.15, 6.17, 6.19, 6.20, 6.21, and 6.22) with nine unknowns: u, b, c, $(\rho_a - \rho)$, θ, β, x, y, and z. When these equations are finally used in a specific occasion, the boundary conditions allow one to simplify the equations and arrive at those commonly reported by other authors. In addition, a closer look at the Hirst model will be made when the case of a round buoyant jet discharged into a flowing, stratified environment is studied. Hirst's model applies equally well to discharges into a stagnant environment.

6. Conclusions

A typical nine-equation system has been developed for submerged jets. Three equations arise from Newton's second law; three from conservation of mass, density deficiency, and tracer; and three from simple geometry relationships. The reader should understand the physical bases for the equations, rather than the detailed formulation. The detailed formulation may be important in understanding the basic references on given models. An understanding of the formulations will not, however, be necessary for a reading of the remaining sections on submerged discharges.

C. Round, Buoyant Jets in a Stagnant Environment

A jet may be discharged into a stagnant body of water that has a uniform, linear, or some arbitrary density profile. In most models that include ambient stratification, a linear profile is used for mathematical simplification. In a uniform environment, the jet is initially deflected upward because of the vertical momentum due to the action of the buoyant force. As the jet rises, its width increases and it entrains ambient fluid. In the linearly stratified environment, the density of the ambient fluid decreases with height from the discharge point. Consequently, the jet will entrain ambient fluid that could be equal to or less than the density of the jet. Hence, the jet will eventually become heavier than the ambient fluid. The jet will reach a point of neutral buoyancy (local jet density and ambient density are equal), but may continue past this point due to remaining vertical momentum flux. As the jet continues

past the point of neutral buoyancy, the jet becomes heavier and tends to sink. Figure 2.4 illustrates this point. The point at which the vertical momentum flux vanishes is called the terminal point (z_t, x_t). The jet half-width at the terminal location is w_t. Figure 6.5 represents a round jet in a uniform environment and a linearly stratified environment.

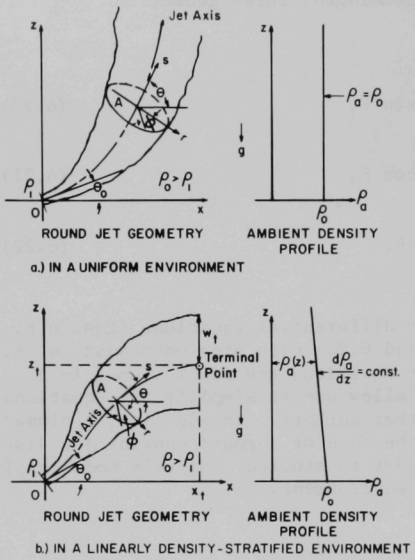

Fig. 6.5.

Schematic Diagrams of Round, Buoyant Jet Problems Studied.[39]

In a stagnant environment, a basic consideration is that the ambient velocity equal 0. Hence, the x and y axes can be interchanged without any loss of generality. In addition, the angle β will be constant and equal to 90°. However, θ will be a variable along the jet axis, with an initial value of θ_o' at the orifice and θ_o at the end of the ZOFE. Two separate cases are discussed for stagnant discharges: a uniform receiving environment and a linearly stratified receiving environment. The basic equations are frequently made dimensionless to help make the solutions applicable to a broader range of cases. Where needed, important normalized (dimensionless) parameters are introduced.

D. Round, Buoyant Jets in a Stagnant Uniform Environment

1. Basic Equations

The discharge of heated waste water into a uniform environment implies that $\rho_a = \rho_o$ = constant and that $d\rho_a/ds = 0$. This factor, coupled with $U_a = 0$, reduces the basic equations for this case.

Fan and Brooks[39] present the equations in dimensionless form so that one solution may be scaled to fit any number of situations. There are essentially seven equations to be solved. The set of parameters, u, c, $(\rho_o - \rho)$, θ, b, x, and z, can be determined by solving the system of simultaneous first-order

ordinary differential equations. This is simple enough for a uniform or linearly stratified case. Figures 6.6 and 6.7 illustrate the solution of the equations for a round, buoyant jet discharged horizontally into a stagnant, uniform environment. As noted by Ditmars,[30] if the density profile is not linear, each case must be solved individually. This should present no problem, however. Ditmars has a computer program to solve the case of an arbitrarily stratified stagnant environment.

2. Normalization of Governing Parameters

a. Introduction. The parameters Fan uses as normalizing parameters to interpret Figs. 6.6 and 6.7 are as follows. The volume flux parameter, μ, for a round buoyant jet in a stagnant uniform environment is simply a ratio of the volume flux (ub^2) to the initial volume flux or discharge ($U_o b_o^2$) of the jet at the end of ZOFE; i.e.,

$$\mu = ub^2/(U_o b_o^2). \tag{6.23}$$

Another important measure of jet development is the momentum flux, expressed generally as u^2b^2. A dimensionless parameter, m, is introduced to give the ratio of the momentum flux past any section to some normalizing momentum flux value at the end of the ZOFE:

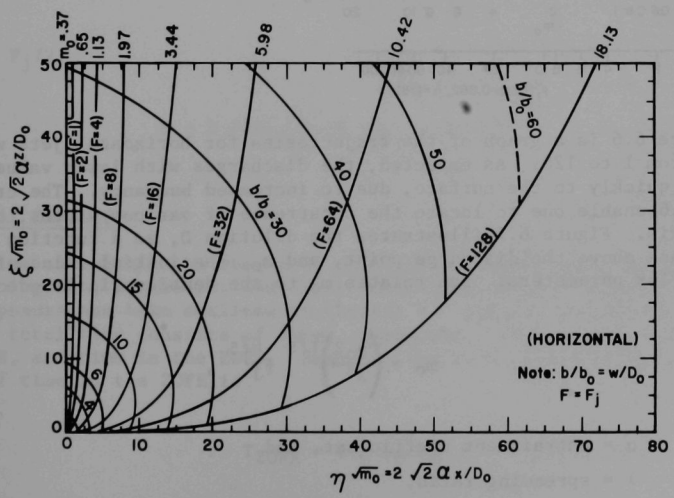

Fig. 6.6. Trajectories and Half-width b/b_o of Round, Buoyant Jets in a Stagnant Uniform Ambient Fluid: $\Theta_o' = 0°$, Based on $\alpha = 0.082$.[39]

$$m = \left[\frac{g\lambda^2 U_o^3 b_o^6 (\rho_o - \rho_1)}{4\sqrt{2}\ \alpha\rho_o}\right]^{-2/5} \frac{u^2 b^2}{2} \ . \tag{6.24}$$

Dimensionless coordinates are also introduced, but they are not needed for the current discussion.

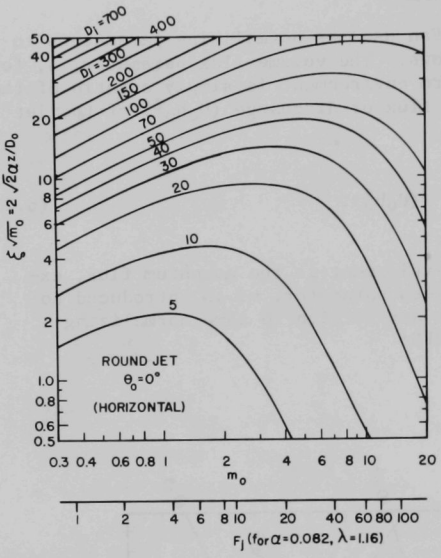

Fig. 6.7

Dilution of Round, Buoyant Jets in Stagnant, Uniform Environment: $\Theta_o' = 0°$.[39]

Figure 6.6 is a graph of the trajectories for horizontal jets with F_j varying from 1 to 128. As expected, the discharges with lower values of F_j rise more quickly to the surface, due to increased buoyancy. The cross lines in Fig. 6.6 enable one to locate the occurrence of various widths, b, along the jet axis. Figure 6.7 illustrates the dilution D, as a function of z, the distance above the discharge point, and m_o, the initial value of the momentum flux parameters. Fan relates m_o to the densimetric Froude number by

$$m_o = \left(\frac{2\alpha^2}{\lambda^4}\right)^{1/5} F_j^{4/5} \ , \tag{6.25}$$

where α = entrainment coefficient, and

λ = spreading ratio.

To facilitate its solution, the equation system must be given a set of boundary conditions. In this case, the values of u, b, ρ, θ, c, x, and z take on the values they have at the end of the ZOFE, namely U_o, b_o, ρ_1, θ_o, c_o, x_e, and z_e. Frequently, for convenience, x_e and z_e are used as zero inside the

numerical-integration computer program. The equations are integrated with respect to s, the axial distance, beginning at s = 0; b_o may be solved in terms of D_o, the initial jet diameter, by equating the momentum at the orifice to the momentum at the end of the ZOFE. This yields

$$b_o = \frac{D_o}{\sqrt{2}} . \tag{6.26}$$

Hence, to solve the above equations for a real physical situation, the needed input values are (a) the initial jet velocity U_o, (b) the initial jet diameter D_o (orifice diameter), (c) the initial concentration c_o or ΔT_o, (d) the initial density of a jet at ρ_1, (e) the initial density of ambient fluid at jet discharge, θ_o. Figures 6.6 and 6.7 represent the jet trajectories, jet half-width, and jet dilution for a buoyant, round jet issued horizontally.

b. Cederwall's Solution. Cederwall[22] presents solutions for horizontal jet diffusion into a stagnant, uniform environment. The equation can be used to give a quick estimate and comparison with the previous techniques discussed. Figure 6.8 presents comparative theoretical solutions for the prediction of the dilution at various depths. The dilution, D, is a function of the jet densimetric Froude number and of the submergence of the discharge z/D_o. For $z/D_o < F_j/2$,

$$D = 0.54\ F_j[z/(D_oF_j)]^{7/16}. \tag{6.27}$$

For $z/D_o > F_j/2$,

$$D = 0.54F_j\left(0.38\ \frac{z}{D_oF_j} + 0.66\right)^{5/3}. \tag{6.28}$$

3. Time of Exposure

The time an organism is subjected to a given temperature rise is of concern to many biologists, engineers, and other environmentalists. Computation of time of exposure has been outlined in Chapter V. Similar procedures are used here. The total time consists of three components: time in the conduit, time in the ZOFE, and time in the ZOEF. Based on the work of Albertson *et al.*,[5] an estimate of time in the ZOFE is

$$T_{ZOFE} = 6.2\ D_o/U_o\ , \tag{6.29}$$

where T_{ZOFE} = time in the ZOFE,

D_o = orifice diameter, and

U_o = initial jet discharge velocity.

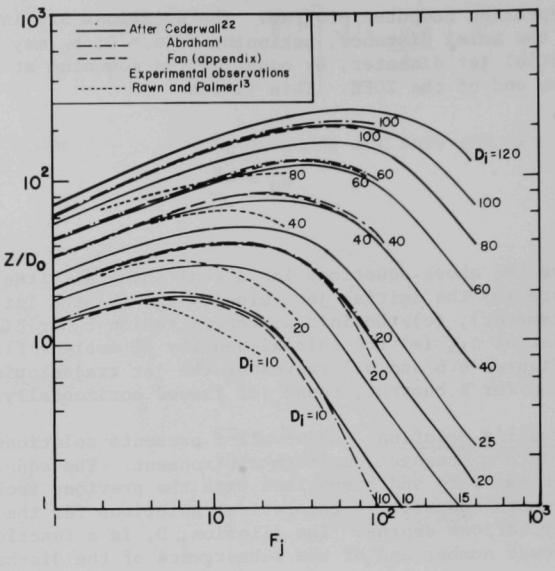

Fig. 6.8. Theoretical Solutions of Dilution, D_i, for Horizontal, Buoyant Jet in Stagnant Receiving Water of Uniform Density.[22]

The value of T_{ZOEF} may be solved in terms of the dimensionless parameters as shown in

$$T_{ZOEF} = \frac{m_o^{3/2} D_o}{2\sqrt{2}\ \alpha U_o} \int_o^{\zeta_c} \frac{\mu}{m}\, d\zeta\ , \tag{6.30}$$

in which ζ_c is the dimensionless jet distance (along the axis) of concern. An example of a similar equation developed for submerged jets in a cross flow will be used later and will illustrate this application. Hence,

$$T_t = \frac{D_o}{U_o}\left[L_c/D_o + 6.2 + \frac{m_o^{3/2}}{2\sqrt{2}\ \alpha}\int_o^{\zeta_c} \frac{\mu}{m}\, d\zeta\right], \tag{6.31}$$

in which L_c is the length of the conduit.

E. Discharge of a Round, Buoyant Jet into a Stagnant, Linearly Stratified Environment

1. Basic Equations

In a linearly density-stratified environment, $d\rho_a/ds \neq 0$. Hence, the z-momentum and density-deficiency equations used for the uniform environment must be changed. Other equations remain the same. The initial conditions are the same as those for the equations for a uniform environment. However, Fan introduces a new set of dimensionless parameters to use his graphs.

2. Fan and Brooks' Solution

Fan and Brooks[39] nondimensionalize the basic equations, solve them numerically, and present representative results in graphical form. They introduce three dimensionless parameters: the volume-flux parameter, μ; momentum-flux parameter, m; and a buoyancy-flux parameter. These parameters represent the rate of growth of the appropriate flux as one proceeds along the jet. Growth of the volume-flux parameter, for example, implies dilution of the jet, as more fluid is flowing in the jet due to entrainment.

There are three relevant parameters for the solution of a round, buoyant jet discharged into a linearly stratified environment: μ_o, m_o, and Θ_o. These represent the jet flow rate, jet momentum flux, and jet angle at the end of the ZOFE. Means of calculating μ_o and m_o from jet characteristics such as F_j, etc., are introduced and used in an example in Sec. VI.F.2.a below. The parameters (μ, m, η, ξ, and δ) will all be defined at that point. Use of the results shown in Figs. 6.9-6.11 are also illustrated in that example. Fan and Brooks present Figs. 6.9-6.11 to illustrate the influence of the initial angle of discharge on the terminal jet height, ξ_t, terminal horizontal coordinate, η_t, and terminal volume-flux parameter, μ_t, as a function of μ_o and m_o. Several such figures are available in Fan and Brooks. For situations that are not covered by Fan and Brooks, the nondimensional equations are available and can be numerically integrated.

3. Ditmars' Solution

Ditmars[30] presents another form of the equations by Fan and Brooks in terms of the variables u, b, c, $\rho_a - \rho$, x, z, and Θ. Ditmars' computer program allows one to use any gravitationally stable density profile. However, the density profile must be divided at any number of arbitrarily selected points (that best fit the actual profile) and calculated as linear between those points. In a sense, an arbitrary density profile is approximated by a series of linear density profiles. An example worked by Ditmars to illustrate this is shown in Fig. 6.12, where the real density profile consists of three linearly varying profiles. Ditmars' solution is applicable also to simple momentum jets ($\rho_a - \rho = 0$) and jets discharged into a uniform environment ($d\rho_a/dz = 0$). However, as noted by Ditmars, these equations are not valid for the simple plume ($U_o = 0$), which requires that the initial momentum flux be equal to zero.

4. SYMJET and PLUME Models

PLUME is a model developed by Baumgartner *et al.*[13a] and capable of treating plume behavior in an arbitrarily density-stratified ambient fluid. Any jet

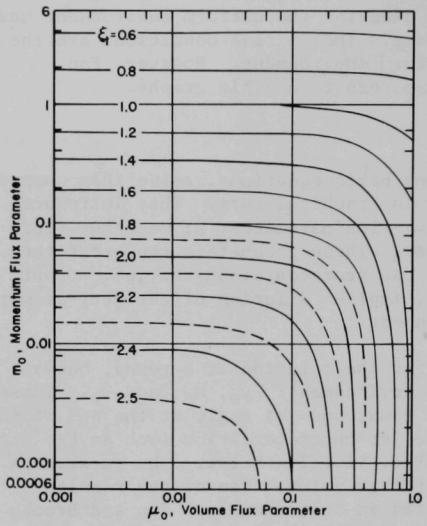

Fig. 6.9

Terminal Height of Rise ξ_t for Horizontal, Round, Buoyant Jets ($\Theta' = 0°$) in a Linearly Density-stratified Environment.[39]

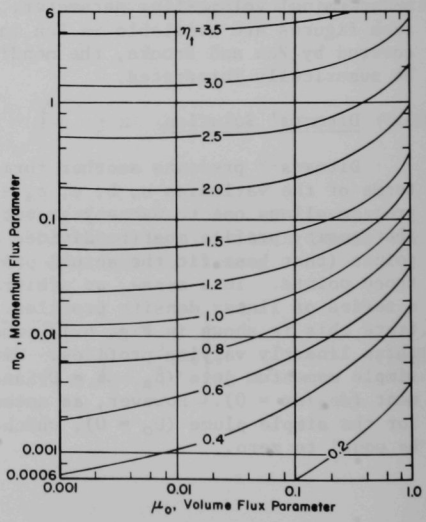

Fig. 6.10.

Terminal Horizontal Coordinate η_t for Horizontal, Round, Buoyant Jets ($\Theta_o' = 0°$) in a Linearly Density-stratified Environment.[39]

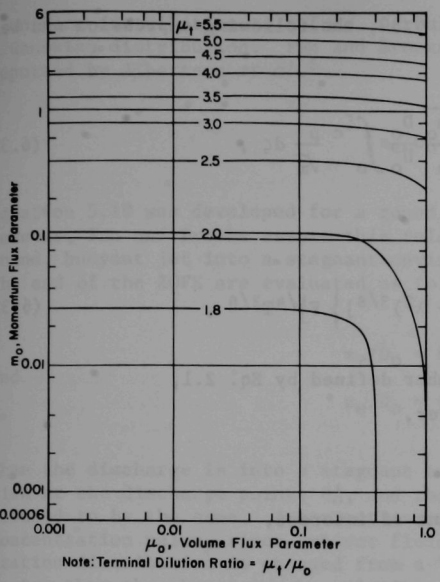

Fig. 6.11.

Terminal Volume-flux Parameter μ_t for Horizontal, Round, Buoyant Jets ($\Theta_o' = 0°$).[39]

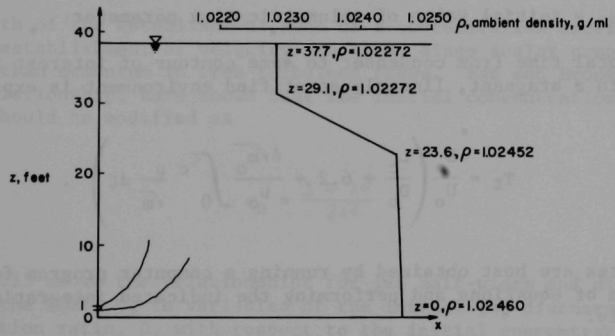

Fig. 6.12. Density Profile for Ditmar's Example Problem.[30]

angle can be handled. A model developed by Trent and Welty,[138a] called SYMJET, solves the equations of mass, momentum, and energy transport by finite-difference techniques. Axisymmetric jets discharging vertically into a stagnant, stratified ambient fluid are treated. Both PLUME and SYMJET are worthy of review.

5. Time of Exposure

The approach in Sec. VI.D.3 for a uniform environment can be used here.

With the method used to derive Eq. 6.30, the following expression can be obtained for the time in the ZOEF:

$$T_{ZOEF} = \delta \frac{\sqrt{m_o}}{\mu_o} \frac{D_o}{U_o} \int_o^{\xi_c} \frac{\mu}{\sqrt{m}} d\zeta \ , \tag{6.32}$$

where δ = scale factor defined by

$$\delta = \left\{ \sqrt{\lambda} / [2\sqrt{\alpha}(1 + \lambda^2)^{3/8}] \right\} F_j^{1/4} T^{3/8} \ , \tag{6.33}$$

F_j = densimetric Froude number defined by Eq. 2.1,

T = stratification parameter,

$$T = \frac{\rho_o - \rho_1}{-D_o \, d\rho_a/dz}$$

ρ_o = ambient density at point of interest,

ρ_1 = initial jet density,

m_o = initial value of momentum-flux parameter, and

μ_o = initial value of volumetric-flux parameter.

Hence, the total time from condenser to some contour of interest for a heated discharge into a stagnant, linearly stratified environment is expressed in

$$T_t = \frac{D_o}{U_o} \left(\frac{L_c}{D_o} + 6.2 + \frac{\delta\sqrt{m_o}}{\mu_o} \int_0^{\zeta_c} \frac{\mu}{\sqrt{m}} d\zeta \right) \ . \tag{6.35}$$

These estimates are best obtained by running a computer program for solution of the system of equations and performing the indicated integration in Eq. 6.35 simultaneously.

In reviewing Eq. 6.34, note that T describes the extent of stratification. At the one extreme, if the environment has a uniform density, $d\rho_a/dz = 0$, implying that T approaches infinity. As the stratification becomes stronger, T will decrease.

F. Round, Buoyant Jets in a Stagnant Environment--Application to a Practical Problem

1. Round, Buoyant, Jet into a Stagnant, Uniform Environment

When the jet theory of heated waste discharges is applied to a practical problem, the region of ZOFE as previously described is the region immediately beyond the diffuser in which the mean flow profile undergoes a transition from

a uniform distribution to a free, turbulent distribution, often something like a Gaussian distribution. Fan and Brooks[39] use values of the length of the ZOFE reported by Albertson *et al.*[5]

$$s_e/D_o = 6.2 \tag{5.10}$$

Equation 5.10 was developed for a round, nonbuoyant jet, discharged horizontally; however, Fan and Brooks assume this relationship will also apply to an inclined, round, buoyant jet into a stagnant environment. The coordinates x_e and z_e at the end of the ZOFE are evaluated as follows:

$$x_e/D_o = 6.2 \cos \theta_o' \tag{6.36}$$

and

$$z_e/D_o = 6.2 \sin \theta_o' \ . \tag{6.37}$$

When the discharge is into a stagnant environment, the initial angle of inclination at the discharge point, θ_o', and the angle at the end of the ZOFE, θ_o, are assumed to be the same. A correction must also be made to the centerline concentration value, since ambient fluid is being entrained while the concentration distribution is changed from a "tophat" to the Gaussian distribution faster than the change in the velocity profiles.

The length of the establishment zone of a concentration profile is shorter than for the establishment of velocity profiles, since scalar properties diffuse more rapidly than momentum in free turbulent flows. Fan and Brooks, using the continuity relationship, have shown that the initial concentration of the tracer in the ZOFE should be modified as

$$c_o = \frac{1 + \lambda^2}{2\lambda^2} \ . \tag{6.38}$$

Figure 6.13 shows the relationships for jet half-width and dilution at the beginning of the ZOEF, 0, to variables at the initial jet discharge structure, 0'. The dilution ratio, D, with respect to the initial concentrations at the discharge point 0', is

$$D = \frac{2\lambda^2}{1 + \lambda^2} D_i = \frac{2\lambda^2}{1 + \lambda^2} \mu \ , \tag{6.39}$$

in which D_i = unadjusted dilution.

All that is needed to solve a practical problem is to know what values of α and λ to use. Fan suggests values of $\alpha = 0.082$ and $\lambda = 1.16$ based on results obtained from Rouse *et al.*[117] However, $\alpha = 0.083$ was obtained from data on a simple plume. Cederwall[22] contends that the entrainment coefficient should vary as the local densimetric Froude number, F_L, defined by Eq. 6.3

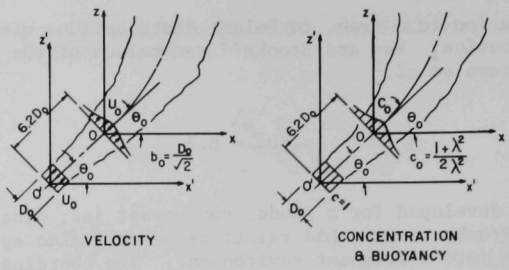

Fig. 6.13. ZOFE for an Inclined, Round, Buoyant, Jet.[39]

changes. Hirst[54] adopted the same approach, as shown in Eq. 6.2. However, Fan[38] presents experimental results that verify the use of $\alpha = 0.082$ for a round, buoyant jet discharged into a stagnant, stratified environment. For a simple jet ($m_o = \infty$, $F_j = \infty$), Fan and Brooks[39] suggest the best choice of $\alpha = 0.057$, based on the results of Albertson *et al.*[5] Hence, the substitution of $\alpha = 0.082$ and $\lambda = 1.16$ into Eqs. 6.25 and 6.39 yields

$$D = 1.15\ D_i = 1.15\ \mu \tag{6.40}$$

and

$$m_o = 0.374\ F_j^{4/5}\ . \tag{6.41}$$

In addition, the physical x and z coordinates can be related to the dimensionless parameters by

$$x/D_o = 4.32\eta\sqrt{m_o} \tag{6.42}$$

and

$$z/D_o = 4.32\xi\sqrt{m_o}\ . \tag{6.43}$$

For a practical example, consider a thermal discharge, 160 ft below the surface of a lake, discharged horizontally from a single, round port. This is a deeply submerged discharge, but the techniques applied here will be the same for less deeply submerged discharges. Consider the critical condition in the lake as occurring when the average velocity of the lake is zero. The temperature of the lake is 59°F, and the temperature rise across the condensers is 18°F. Therefore, the temperature of the heated waste waters is 77°F. The power plant is a 1000-MW plant with an operational efficiency of $\varepsilon = 33\%$. The diameter of the discharge port is 16 ft. What is the temperature of the jet as it reaches the surface?

To solve this problem, seven steps must be followed. In most cases, however, the engineer will have sufficient information so that he can begin with step three.

(1) Values of $\alpha = 0.082$ and $\lambda = 1.16$ will be used to evaluate this discharge. Also, θ_o will be 0°. The total heat rejected to the receiving body of water can be calculated from

$$H_{rejected} = H_{plant}\left(\frac{100}{\varepsilon} - 1\right) , \tag{6.44}$$

where

$H_{rejected}$ = heat rejected by plant,

H_{plant} = rated capacity of plant, and

ε = operational efficiency of plant, percent.

Hence, the heat rejected by the plant is

$$H_{rejected} = 1000 \text{ MW}\left(\frac{100}{33} - 1\right) \simeq 2000 \text{ MW} .$$

Converting this to Btu/hr yields

$$H_{rejected} = 2000 \text{ MW} \times 3.41 \times 10^6 \text{ Btu/MW-hr} \simeq 6.8 \times 10^9 \text{ Btu/hr} .$$

(2) The required flow rate of the heated discharge, Q_p, can be calculated to give an 18°F rise, by using

$$H_{rejected} = \rho_o C_p Q_p (\Delta T) , \tag{6.45}$$

where ρ_o = ambient density at the discharge port,

C_p = specific heat capacity of water, approximately 1.0 Btu/lb_m-°F,

Q_p = flow rate of discharge, cfs, and

ΔT = the difference in discharge temperature and the ambient temperature at the discharge port, °F.

Therefore,

$$Q = (6.8 \times 10^9)/[(0.99913)(62.4)(1.0)(18)(3600)] \simeq 1700 \text{ cfs} ,$$

where $\rho_o = 0.9913$ for 59°F. Thus, 1700 cfs is the flow needed to yield the initial temperature rise specified.

(3) The initial velocity of the discharge can be calculated using the continuity relationship expressed by

$$Q = U_o A_p \ , \tag{6.46}$$

where U_o = initial jet discharge velocity, and

A_p = area of discharge port, ft^2.

This leads to

$$U_o = 1700/[\pi(16)^2/4] = 8.5 \text{ fps} \ .$$

(4) To enter the Figs. 6.6 and 6.7, m_o must be evaluated. The densimetric Froude number, F_j, can be calculated using Eq. 2.1:

$$F_j = \frac{U_o}{\sqrt{\frac{\rho_o - \rho_1}{\rho_o} gD_o}} = \frac{8.5}{\sqrt{(0.00206)(32.2)(16)}} = 8.3 \ ,$$

where ρ_1 = 0.99707 for 77°F and

ρ_o = 0.9913 for 59°F.

Using Eq. 6.41, we can calculate m_o:

$$m_o = 0.374F^{4/5} = (0.374)(5.45) = 2.0 \ .$$

(5) Since the diameter of the jet orifice is known to be 16 ft, the components of the length of the ZOFE can now be calculated using Eqs. 6.36 and 6.37:

$$x_e = (6.2)(16 \text{ ft})(\cos 0°) = 99 \text{ ft};$$

$$z_e = (6.2)(16 \text{ ft})(\sin 0°) = 0 \text{ ft} \ .$$

Since the depth of the jet submergence is 160 ft, the vertical distance from the end of the ZOFE to the surface will be 160 ft.

(6) Using Eq. 6.43, we can calculate the ordinate for Figs. 6.6 and 6.7:

$$\xi\sqrt{m_o} = (0.232)(160/16) = 2.32 \ .$$

Now enter Fig. 6.7 and use m_o = 2.0 and $\xi\sqrt{m_o}$ = 2.32 to find the dilution at the surface,

$$D_i \simeq 6 \ .$$

To calculate the corresponding dilution with reference to the discharge port, use Eq. 6.40:

$$D = 1.15\ D_i = 1.15(6) \simeq 6.9 \ .$$

(7) Since the concentration of tracer is assumed to be a linear function of heat or salt content, the temperature rise at the surface can be calculated using

$$\Delta T_{surface} = \Delta T/D = 18/6.9 \simeq 2.6°F \ . \qquad (6.47)$$

Then the centerline temperature of the jet when it reaches the surface will be 61.6°F.

Two other important considerations are (1) the horizontal distance between the discharge port and the centerline when the jet surfaces, and (2) the jet width at the surface. Using Fig. 6.6 and remembering that $\xi\sqrt{m_o} = 2.32$, $m_o = 2.0$, and $F_j = 8.3$, we can find the value of $\eta\sqrt{m_o} \simeq 4$ and $b/b_o \simeq 5$. Then, from Eq. 6.42,

$$x = (4.32)(\eta\sqrt{m_o})D_o = (4.32)(4)(16) = 278 \text{ ft} \ .$$

Therefore, the total distance is 278 + 99 = 377 ft from the discharge structure. The width of the jet can be calculated as follows:

$$\frac{b}{b_o} = \frac{w}{D_o} \ .$$

By substitution, the width is found to be 80 ft, as follows:

$$w = (5)(16) = 80 \text{ ft} \ .$$

Now for comparison of models to predict the dilution, use the equations developed by Cederwall.[22] To use Eqs. 6.27 and 6.28, first calculate

$$z/D_o = 160/16 = 10.0$$

and

$$0.5F_j = (0.5)(8.3) = 4.15 \ .$$

Use Eq. 6.28, since $z/D_o > 0.5\ F_j$. Hence,

$$D = 0.54(8.3)\left(0.38 \times \frac{10.0}{8.3} + 0.66\right)^{5/3} = 5.5 \simeq 6\ .$$

Reading from Fig. 6.8 yields $D < 10$. Had Cederwall's model included an adjustment for the ZOFE, the two models might have given more similar results.

2. Round, Buoyant Jets into a Stagnant, Stratified Environment

a. Fan and Brooks Solution. For a linearly stratified environment, a parameter, T, called the stratification parameter, is introduced in Eq. 6.34. Hence, the inclined-buoyant-jet problem in a linearly stratified environment is dependent or characterized by three parameters, F_j, T, and θ_o. Parameters m_o and μ_o are related to F_j and T as follows:

$$m_o = \frac{(1 + \lambda^2)F_j^2}{4\lambda^4 T} \tag{6.47}$$

and

$$\mu_o = \frac{(1 + \lambda^2)^{5/8}F_j^{1/4}}{2\alpha^{1/2}\lambda^{3/2}T^{5/8}}\ . \tag{6.48}$$

Fan uses the scale factor defined by Eq. 6.33 to relate the nondimensional vertical and horizontal distance to the x/D_o and z/D_o values:

$$\frac{x}{D_o} = \delta\eta \tag{6.49}$$

and

$$\frac{z}{D_o} = \delta\xi\ . \tag{6.50}$$

The scale factor, δ, relates the coordinates distances on the jet trajectory to T, the stratification parameter and F_j, the densimetric Froude number.

The relationship for a ZOEF is the same as for a jet into a uniform environment. Using $\alpha = 0.082$ and $\lambda = 1.16$ and substituting into the appropriate equations, the relevant parameters m_o and μ_o are related to F and T as follows:

$$D = 1.15\mu/\mu_o\ , \tag{6.51}$$

$$m_o = 0.324F^2/T\ , \tag{6.52}$$

$$\mu_o = 2.38F^{1/4}/T^{5/8}\ , \tag{6.53}$$

and

$$\delta = 1.37F^{1/4}T^{3/8}\ . \tag{6.54}$$

The dimensionless jet half-width, $\tilde{w}$, is defined by

$$\tilde{w} = w/\delta D_o \tag{6.55}$$

and

$$\tilde{w} = 0.232\mu/h_o^{1/4} , \tag{6.56}$$

where h_o = initial horizontal momentum flux component, $m_o \cos^2 \theta_o$. At the terminal point (indicated by subscript t),

$$D_t = 1.15\mu_t/\mu_o \tag{6.57}$$

and

$$\tilde{w} = 0.232\mu_t/h_o^{1/4} . \tag{6.58}$$

For a practical example, consider the discharge in the previous example, except that this time the discharge is into a stratified environment. Consider the surface temperature of the water to be 73.5°F.

$$T_{surface} = 73.5°F, \ \rho_s = 0.99755 \text{ at } z = 160 \text{ ft};$$

$$T_o = 59°F, \ \rho_o = 0.99913 \text{ at } z = 0 \text{ ft}.$$

In this case, there are nine steps to follow:

(1) Calculate the slope of the normalized density profile.

$$-\frac{1}{\rho_o}\frac{d\rho_a}{dz} = -\frac{0.99755 - 0.99913}{0.99913(160 - 0)} \simeq 1 \times 10^{-5} \text{ ft}^{-1} .$$

(2) Recalling the following physical variables of the discharge:

$$\theta_o = 0° ,$$

$$D_o = 16 \text{ ft} ,$$

and

$$U_o = 8.5 \text{ fps} .$$

Allow F_j = 8.3 and T as calculated using Eq. 6.34:

$$T = \frac{\rho_o - \rho_1}{D_o\left(-\frac{d\rho_a}{dz}\right)} = \frac{0.00206}{16(0.99913)(10^{-5})} = 12.9 .$$

(3) From Eqs. 6.52-6.54, the values of m_o, μ_o, and δ can be calculated:

$$m_o = 0.324F_j^2/T = 0.324(8.3)^2/12.9 = 1.73 ,$$

$$\mu_o = 2.38F_j^{1/4}/T^{5/8} = 2.38(1.7)/(4.95) = 0.82,$$

$$\delta = 1.37F_j^{1/4}T^{3/8} = 1.37(1.7)(2.61) = 6.1 ,$$

and

$$h_o = m_o \cos^2 \theta_o = 1.73 .$$

(4) Using the calculated values of m_o and μ_o, enter Figs. 6.9-6.11 to solve for ξ_t, η_t, and μ_t, respectively.

(5) The terminal height of rise is $\xi_t = 0.8$. From Eq. 6.50,

$$z_t = D_o\delta\xi_t = 16(6.05)(0.8) = 78 \text{ ft} .$$

(6) The vertical distance from discharge port is $z_t + 6.2(D_o) \sin \theta_o = 78$ f

(7) The terminal horizontal coordinate is $\eta_t = 2.4$. From Eq. 6.49,

$$x_t = D_o\delta\eta_t = 16(6.1)(2.4) = 234 \text{ ft} .$$

(8) The horizontal distance from the discharge port is $x_t + 6.2\ D_o \cos \theta_o = 333$ ft.

(9) Since the terminal dilution is $\mu_t = 3.8$, the dilution with respect to the discharge can be calculated by Eq. 6.57, as follows:

$$D_t = 1.15(3.8)/(0.82) = 5.3 .$$

To determine if the jet remains submerged, the jet-terminal half-width can be calculated using Eq. 6.58:

$$\tilde{w}_t = 0.232\mu_t/h_o^{1/4} = 0.232(3.8)/(1.73)^{1/4} = 0.77$$

and

$$w_t = \delta\tilde{w}_tD_o = 6.1(0.77)(16) = 75 \text{ ft} .$$

The outer edge of the jet is located at a distance of 78 + 75 = 153 ft from the discharge port. Hence, the jet will remain submerged, since 153 ft is less than 160 ft.

The dilution of the jet discharged into the stagnant linearly stratified environment is less than the dilution of a jet discharged into a stagnant,

uniform environment. This is not hard to understand since the terminal height of the jet into the stratified environment is less than the submergence of the discharge or, essentially, the jet does not travel as far in the stratified medium. Physically, the ability to entrain the ambient fluid is less. In addition, as the jet into a stratified environment approaches its terminal height, it is beginning to entrain fluid near its own density.

b. Hirst's Model. Hirst's model,[54] as well as that by Fan and Brooks, can be used to predict the dilution and trajectory of buoyant jets into stagnant uniform or stratified environments. Hirst has a computer program and input instructions that are available upon request and will not be discussed here. However, the analysis of the example problem is conducted to compare the results obtained by the methods of Fan and Brooks,[39] Hirst,[54] and Cederwall.[22] The pertinent parameters for comparison are dilution ratio, jet trajectory, and terminal locations, depending on which application is made. Hirst's model predicts the decay of the temperature ratio ($\Delta T/\Delta T_o$) in Fig. 6.14 for a buoyant-jet discharge into a uniform environment. T_a is the uniform ambient temperature, and T_o is the initial temperature of the jet discharge. For the case of the example, $T_a = 59°F$ and $T_o = 77°F$. The example problem is solved by computer. The dilution, D, at the surface, using Hirst's model, is 6.5. Hirst's model includes considerations of the ZOFE inside the computer program, and thus no corrections need to be made to the computer program, and thus no corrections need to be made to the computer output. Therefore, the dilution is with respect to the discharge location. The vertical distance is 160 ft from the discharge, and the horizontal distance is 256 ft from the discharge to the point where the jet strikes surface. The length of the jet axis from the discharge port is 323 ft. The jet trajectory is shown in Fig. 6.15. Only the terminal location of the jet's trajectory predicted by Fan and Brooks is shown. One reason the jet axis is shorter for Hirst's prediction than for Fan and Brooks' prediction is the value of the entrainment coefficient. Hirst[54] notes that predictions obtained for a value of $\alpha = 0.082$ provide excellent agreement with experimental trajectories. Recall that $\alpha = 0.082$ is the value suggested by Fan and Brooks. For a stagnant environment, Hirst's value of α reduces to 0.057, the value for a simple, nonbuoyant, round jet. (See Eq. 6.2.) Hence, the choice of which model to use for a round, buoyant jet must be tempered with an examination of the physical system involved. If the jet is a buoyant jet into a stagnant, uniform environment, the Fan-Brooks model matches experimental results best. If the jet is a simple, round jet ($F = \infty$, $m_o = \infty$), then the use of $\alpha = 0.057$, or Hirst's model, is recommended.

For a round, buoyant jet into a stagnant, stratified environment, Hirst's model predicts the terminal location to occur 82 ft vertically and 274 ft horizontally from the discharge port. The jet length is 290 ft from the discharge port. This compares to the predicted values from the Fan-Brooks model as $x_t' = 331$ ft and $z_t' = 78$ ft. From Hirst's model, the dilution at the terminal height with respect to the discharge port is 3.3, versus the 5.3 obtained from the Fan-Brooks model. This difference is again due to the value of entrainment coefficient used. Figure 6.15 shows the predicted jet trajectory using Hirst's model. The terminal location predicted by the Fan-Brooks model is also shown. Table 6.1 compares the predicted results.

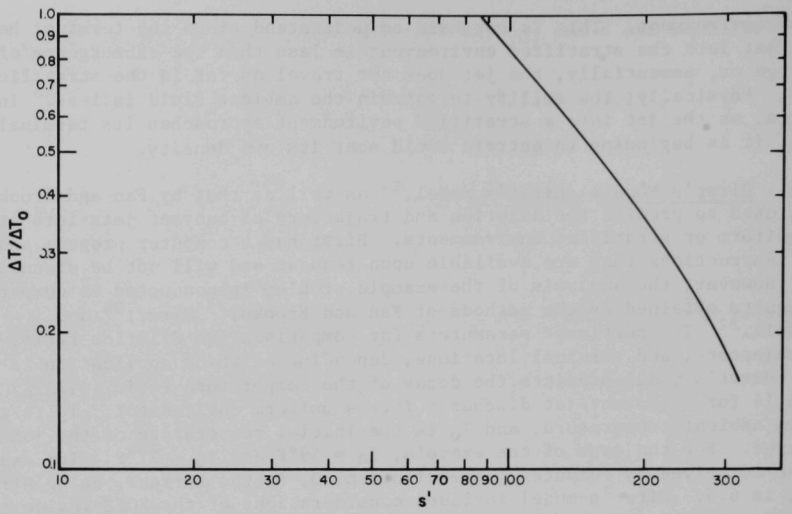

Fig. 6.14. Predicted Temperature Decrease for Example Problem Using Hirst's Model (stagnant environment).

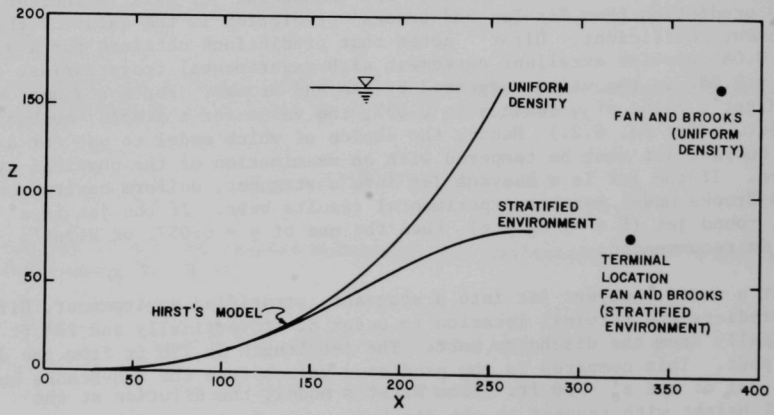

Fig. 6.15. Comparison of the Predicted Jet Trajectories for Stagnant-environment Numerical Example.

Table 6.1. Comparison of Predicted Values for Example Problem of Round, Buoyant Jet Using Fan and Brooks, Cederwall, and Hirst

	Fan and Brooks[39]	*Cederwall*[22]	*Hirst*[54]
Uniform Environment			
Dilution, D	6.9	5.5	6.5
Vertical location, ft	160	160	160
Horizontal location, ft	377	N/A	256
Stratified			
Dilution, D	5.3	N/A	3.3
Jet terminal length, ft	-	N/A	290
Vertical terminal length, ft	78	N/A	82
Horizontal terminal length, ft	333	N/A	274

N/A means not applicable.

G. Round Jets into Stagnant Environments--Summary and Conclusions

Three techniques have been reviewed to predict the dilution and trajectory of buoyant round jets into a stagnant environment. The model by Fan and Brooks[39] will predict the dilution and trajectory for an inclined round, buoyant jet into a stagnant uniform or stratified environment. The model will accept jets injected at various angles to the flow. Figures are presented here to describe the dilution, trajectory, and half-width for a jet discharged horizontally. However, Fan and Brooks present other theoretical predictions for initial angles of discharge of 15, 30, 45, and 90°. Fan[38] presents experimental verification of the model for the horizontal discharge of round, buoyant jets in a uniform environment for ranges of F_j from 10 to 130.

Cederwall presents an equation for the prediction of the dilution of a horizontally discharged, buoyant, round jet into a uniform environment. The results predicted by the Fan-Brooks model and Cederwall's equation are comparable, as illustrated in Fig. 6.8.

If a case exists for an arbitrary injection angle not covered in the figures presented by Fan and Brooks, the equations may be integrated numerically, e.g., using the program written by Ditmars,[30] by applying the appropriate initial conditions. Fan[38] presents experimental verification for the discharge of an inclined round, buoyant jet into a stagnant, stratified environment. The data presented are for various angles of discharge from 0 to 90°. The jet densimetric Froude number, F_j, varies from 9 to 57. In addition, the following

equation is presented for the dilution of a simple, nonbuoyant jet ($F_j = \infty$) and is experimentally verified:

$$D_i = 0.185\ x'/D_o\ . \tag{6.59}$$

Hirst's model can also be used for inclined round, buoyant jets in a uniform or stratified environment. However, as noted by Hirst,[54] the dilutions predicted by his model are less than those from the experimental data and Fan and Brooks' predictions. Hirst attributes this to the difference in entrainment coefficients where $\alpha = 0.082$ in the Fan-Brooks model and 0.057 in Hirst's model. This is also apparent in the example problem. For a higher entrainment coefficient, the jet concentration tracer (heat, in this example) will be diluted much faster. Consequently, the jet will stay submerged longer. For smaller entrainment coefficients, the buoyancy forces will be larger (relative to the model with a higher entrainment coefficient) in the initial reaches of the jet. This is also brought out in the comparison of the predicted dilutions. For Hirst's model, the surface dilution or terminal dilution was smaller than that predicted by Fan and Brooks' model. Shirazi and Davis[123] have completed analyses of jets into stagnant environments for a range of F_j between 1 and 600. Davis[29] feels that Hirst's model is applicable for a jet in a stagnant environment at all angles of discharge. However, Fan and Brooks' model does give better predictions, and Hirst's predictions do lag the experimental data due to the difference in entrainment coefficients. It is therefore recommended that the Fan and Brooks model be used for buoyant jets into both stratified and nonstratified stagnant environments. For uniform environments, the Cederwall equation gives an excellent estimate of surface dilutions.

H. Discharge of a Round, Buoyant Jet into a Flowing Stream

Fan,[38] Abraham,[2] and Hirst[54] have presented solutions that analyze a round, buoyant jet discharged into a flowing stream. Hirst's model is the most general in that it will allow the discharge to be injected at an arbitrary angle with respect to the direction of flow. Also, the model can be used in a flowing, stratified environment. However, to date, there exist no field data for the discharge of a round, buoyant jet into a flowing, stratified environment. Baca[10] presents an extension of Fan's model, which introduces the ability to inject the discharge at any arbitrary angle. Shirazi and Davis[123] state that the Hirst model is not applicable for all situations and must be used judiciously. Hirst's model is discussed in Sec. VI.J below. The equations presented earlier in Sec. VI.B include the option of discharging into a flowing, stratified environment. However, there has been no attempt to verify these equations with field data.

The utilization of the equations developed in this section depend upon the values of α and λ used. Fan considers the values of $\lambda = 1.0$ for the discharge of a round, buoyant jet into a uniform, flowing environment. Hirst uses a value of $\lambda = 1.16$. Fan also allows α to vary with the velocity ratio, k, and jet densimetric Froude number, F_j. Hirst allows the entrainment function, E_r, to vary along the jet axis as a function of the local jet densimetric Froude number, F_L, as shown in Eq. 6.2. In Abraham's model, the solution of the equations involves the combination of two entrainment coefficients. First, in the region close to the discharge, momentum is assumed to

dominate buoyancy effects, and α is taken as 0.057 (the entrainment coefficient for a simple nonbuoyant jet). Where the axis of the jet is nearly parallel to the direction of the ambient flow, α is taken as 0.5 (the entrainment coefficient for a cylindrical thermal).[115] Fan's approach will be discussed first.

I. Discharge of a Round, Buoyant Jet in a Flowing, Uniform Environment

1. General Equations--Fan's Model

For the discharge into a flowing, uniform environment, $U_a \neq 0$. The equations developed by Fan consider β to be constant and equal to 90°. Also, since the discharge is into a uniform environment, $d\rho_a/ds = 0$ and $\rho_a = \rho_o$ = constant. The basic equations are modified as required. (See Ref. 38 for details.)

The developments yield seven equations with seven unknowns: u, c, b, Θ, $(\rho_o - \rho)$, x, and z. Two equations are integrated directly, leaving five first-order ordinary differential equations to be integrated numerically. These equations may be integrated using any available numerical-integration computer program, such as a Runge-Kutta or Hamming's modified predictor-corrector program. These are both in the IBM 360 Scientific Subroutine Package and are readily available.

Conditions at the end of the establishment zone must be specified to obtain a solution. This includes the velocity, width, ambient density, angle, and temperature rise. The angle, Θ_o, is no longer the initial angle of discharge at the discharge port due to the deflection caused by the oncoming stream. Reference is made to the previous discussion (in Chapter V) to the reduced angle at the end of the ZOFE. The initial jet half-width at the end of the ZOFE is designated b_o. Equating the buoyancy flux at the orifice to that at the end of the ZOFE, b_o can be related to D_o by

$$b_o = D_o\sqrt{k/2k'} \ , \tag{6.60}$$

in which $k = (u_o + U_a \cos \Theta_o)/U_a$ and $k' = k + \cos \Theta_o$.

Fan presents normalized, dimensionless equations to solve the case of a round, buoyant jet in flowing, uniform-density environments. Figures 6.16 and 6.17 demonstrate the effect of the cross stream on the trajectory and dilution ratios. The value of $r_{0.5}$ is the radial distance from the jet centerline at which $\Delta T/\Delta T_c = 0.5$ and is based upon a Gaussian distribution; ΔT_c is the centerline temperature rise. Hence, $r_{0.5}$ is equal to 0.833b. The larger the value of k, the more the jet will behave as if it is discharged into a stagnant environment. However, for small k, the jet is swept downstream and the dilution is reduced. Physically, for small k, the crossflow velocity, U_a, is approaching the discharge velocity, U_o. From Eq. 6.1, the rate of dilution is proportional to the vectorial velocity differences. When the jet is introduced into a stream whose velocity is about the same value as the jet velocity, the initial angle of discharge undergoes a severe reduction. Hence, the jet approaches the co-flowing case. Therefore, the difference in the vectorial velocity is small. This difference is reflected in the smaller dilution ratios for smaller k values. Also, Fan has shown that this result is accentuated as the densimetric Froude

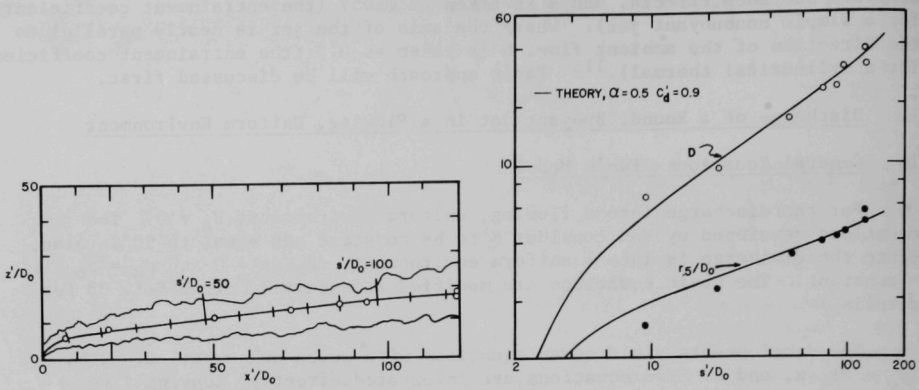

Fig. 6.16. Comparison of Observed and Theoretical Trajectory, Half-widths, $r_{0.5}/D_o$, and Centerline Dilution Ratios, D, of a Buoyant Jet in a Uniform Cross Stream: $F_j = 20$ and $k = 4$.[38]

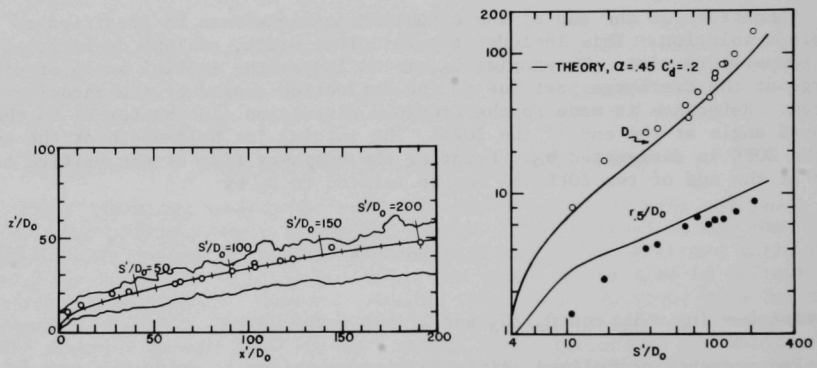

Fig. 6.17. Comparison of Observed and Theoretical Trajectory, Half-widths, $r_{0.5}/D_o$, and Centerline Dilution Ratios, D, of a Buoyant Jet in a Uniform Cross Stream: $F_j = 20$ and $k = 8$.[38]

number increases and the buoyancy effect decreases. For the same values of k, a jet with a high densimetric Froude number will be swept downstream more, and diluted less, than jets with a lower densimetric Froude number. This is because buoyancy forces in the latter case tend to cause the jet to rise more rapidly, increasing the vector-velocity difference and, in turn, the dilution. The total effect of buoyancy on the discharge may be tempered by the total depth of submergence of the discharge. If the discharge is shallow, the plume may strike the surface before significant buoyance-induced mixing occurs. In such shallow water discharges (say submergence less than about 10 diameters), care must be taken in application of any of the infinite-field models, such as the Fan model being discussed here.

To use Fan's equation for a practical problem, values of α and C_d must be available for a particular combination of k and F_j. Figure 6.18 presents the values for α and C_d' as a function of k and F_j; C_d' is defined by

$$C_d' = \left(C_d\sqrt{2}\right)/\alpha\pi \ . \tag{6.61}$$

These values of α and C_d' have been experimentally verified for values of k from 4 to 16 and values of F_j from 10 to 80. This is a practical limitation, since all cases of heated-jet discharges are not constrained to fall within these ranges.

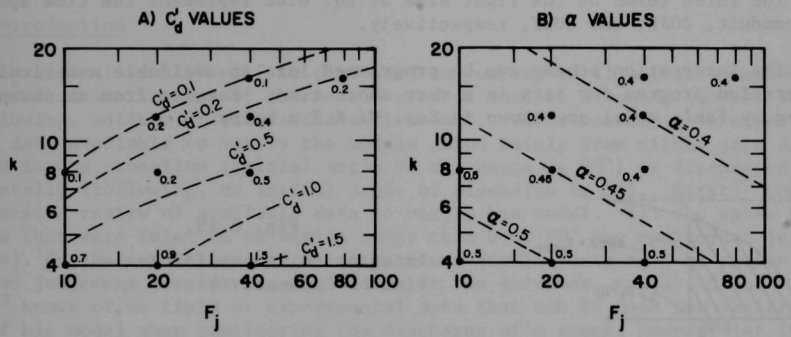

Fig. 6.18. Variations of the Entrainment Coefficient, α, and the Reduced Drag Coefficient, C_d', for Buoyant Jets in Uniform Cross Stream for a 90° Discharge.[38]

2. Abraham's Model

Abraham[2] presents a set of equations that are somewhat different from those used by Fan. Since Abraham uses a different entrainment relationship, the equations of continuity and x momentum are changed. The rest of Fan's equations remain the same. The starting point for the integration is now at the discharge port rather than at the end of the ZOFE.

To use Abraham's equations, all that is needed is to specify the velocity ratio, k, and densimetric Froude number, F_j, since the values of α and C_d are constant. Abraham's model compares well with the experimental data for the limited number of cases he shows. All these cases use data from Fan.[38]

3. Time of Exposure

The technique developed previously is again used to evaluate the length of time an organism is subjected to temperatures greater than some temperature standard of concern. With Eq. 5.19, the time can be evaluated. Figure 6.19 is a representative sketch of the integration process. Therefore, the

following equation will give the time of travel from the condensers to a particular distance on the jet axis of interest:

$$T_t = \frac{L_c}{u_o} + \frac{s_e}{U_o} + \frac{kD_o}{U_o} \int_0^{S_c/D_o} \frac{d(s/D_o)}{(U/U_a)} , \qquad (6.62)$$

in which s_c is the axial distance to the point of interest, and L_c is the conduit length.

The three terms on the right side of Eq. 6.62 represent the time spent in the conduit, ZOFE, and ZOEF, respectively.

The integration scheme can be programmed into an available numerical-integration program for jets in a very short time. Results from an example worked by Fan's model are shown in Sec. VI.K.2.a below.

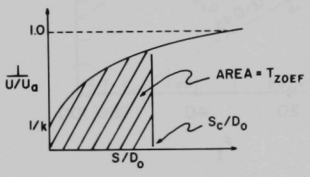

Fig. 6.19.

Integration Scheme for Evaluating Time of Exposure.

J. Discharge of a Round, Buoyant Jet in a Flowing, Stratified Environment

1. Introduction

Hirst[54] developed a general mathematical model that will evaluate each case previously presented and is supposed to be completely general. Even though there is still some question as to the validity of its use for all cases, it is still the only model developed that will mathematically describe the discharge of a round, buoyant jet into a *stratified*, flowing environment. Hirst does apply his model to previously reported data from numerous investigators and finds a reasonably good fit of his theoretical model to reported results. Data include that for jets into stagnant, uniform or stratified environments and jets into flowing, uniform environments. In addition, his model takes into account stratification due to concentration of substance (salinity stratification), as well as stratification due to temperature difference. However, according to Hirst,[55] no field data exist to verify this application.

2. General Equations

Hirst develops his basic equations from the Navier-Stokes equation. However, a velocity and concentration profile must be assumed, and the equation developed is similar to the equations developed using the integral technique outlined by Morton *et al.*[92] Two unique characteristics of Hirst's model are that it allows the jet to be discharged at any arbitrary angle to the

crossflow (therefore Θ_o' and β_o' can both be any value), and that the definition of the entrainment function described in Eq. 6.2 is different from the entrainment relationship used by Fan. Also, the equations developed by Hirst reveal certain terms involving the turbulence and radius of curvature that do not appear in other methods. The entrainment function includes the effects of internal turbulence, buoyancy, and crossflow. This new equation contains four coefficients, only one of which had to be determined empirically by fitting the predictions to the data.[54] A computer program available from Hirst includes four outputs: the dilution ratio, the jet trajectory, the jet half-width values, and the time of exposure.

K. Round, Buoyant Jets in a Flowing Environment--Application to a Practical Problem

1. Introduction

A practical problem will be discussed and worked to illustrate some of the practical limitations of the models used to analyze a round, buoyant jet in a flowing, uniform or stratified environment. Unfortunately, the experimental data available to verify the models arise mainly from either jets discharged into a crossflow (initial angle of discharge is 90°) or discharged horizontally (coflowing, or initial angle of discharge is 0°). Hirst[54] conducts an extensive review of available data to verify his model. All the cases he reviews that were injected at angles other than 0 or 90° are nonbuoyant jets ($F_j = \infty$).[103] Hence, values of the entrainment coefficients must be chosen based on judgement considering the values at the extremes, namely, 0 and 90°. Hirst[55] knows of no field or experimental data that can be used for verification of his model when considering the discharge of a round, buoyant jet into a flowing, stratified environment. Hence, the problem of choosing appropriate entrainment coefficients soon becomes apparent for some intermediate angle of discharge. However, the summary section will elucidate some of these limitations, and recommendations will be made concerning best approximations.

2. Round Buoyant Jet in a Flowing, Uniform Environment

Consider the previous example of a round, buoyant jet discharged into a stagnant, uniform environment. For this example, consider the receiving stream to have a uniform ambient current of 2 fps. In a real situation, the value of U_a may have to be obtained using some low flow criterion coupled with cross-sectional data if the discharge is into a river. If the discharge is into a lake or estuary, then some type of velocity profiles are needed to determine a uniform ambient current.

Recall the values of the pertinent parameters:

$\Theta_o' = 0°$,

$u_o = 8.5$ fps,

$U_o = u_o + U_a \cos \Theta_o = 8.5 + 2 = 10.5$ fps,

$D_o = 16$ ft,

$T_o = 77°F$ with $\rho_1 = 0.99707$, and

$T_a = 59°F$ with $\rho_o = \rho_a = 0.99913$.

a. Fan's Model. The first treatment of this problem will be made using Fan's model[38] for a round, buoyant jet discharged into a flowing, uniform environment. Using the definition referred to in Eq. 6.60,

$$k = \frac{U_o}{U_a} = \frac{u_o + U_a \cos \Theta_o}{U_a} = \frac{10.5}{2} = 5.25 \ .$$

In this case, Θ_o is considered to be the same as Θ_o'. This is an oversimplification, for the buoyancy flux of the jet will undoubtedly cause the potential core (ZOFE) to be deflected upward. However, if the approximation of a simple jet is made due to the initial momentum of the jet, the real situation can be approximated by considering no change in the initial angle of discharge. Fan presents data for the reduction of the initial angle of discharge (as a function of k) when the discharge is at 90°. However, no data exist for any other angle of discharge. Hence, for this example, assume that the relationships in Eqs. 6.36 and 6.37 exist.

The only remaining parameters to be chosen are α and C_d. As previously stated, the values of α and C_d are functions of k and F_j; F_j is calculated according to Eq. 2.1:

$$F_j = \frac{U_o}{\sqrt{\frac{\Delta\rho}{\rho} g D_o}} = \frac{10.5}{\sqrt{(0.00206)(32.2)(16)}} = 10.2 \ .$$

The values in Fig. 6.18 are for a 90° discharge of a round, buoyant jet into uniform, flowing streams. The values of $\alpha = 0.5$ and $C_d' = 0.45$ would be chosen for a 90° discharge. However, for a horizontal, coflowing jet, the initial vectorial velocity difference would be less. If the jet is bounded on one side (i.e., the jet discharge port is located on the bottom of the river, then the ability to entrain fluid from the underside would be limited until the jet clears or lifts off the bottom. Some reduction in the entrainment coefficient could be made (e.g., reducing it by one-half), rather than reintegrating the equation for only one-half the area. Therefore, for the purpose of illustration, choose a value of $\alpha = 0.10$. Since pressure forces are not changed, C_d should remain the same. Fan contains no data with which to select C_d' for the coflowing case; $C_d' = 0.45$ will therefore be used here.

Thus, the pertinent parameters for the numerical integration of Fan's model are: $F_j = 10.2$, $k = 5.25$, $\Theta_o = 0°$, $\alpha = 0.1$, and $C_d' = 0.45$.

The temperature-decay curve is shown in Fig. 6.20. Using Fan's model with $\alpha = 0.1$ and $C_d' = 0.45$, the dilution at the surface is 9.2. Using Eqs. 6.36 and 6.37, the x and z length of the ZOFE can be calculated:

$$x_e = 6.2(16)\cos 0° = 99.2 \text{ ft} \ ;$$

$$z_e = 6.2(16)\sin 0° = 0 \text{ ft} \ .$$

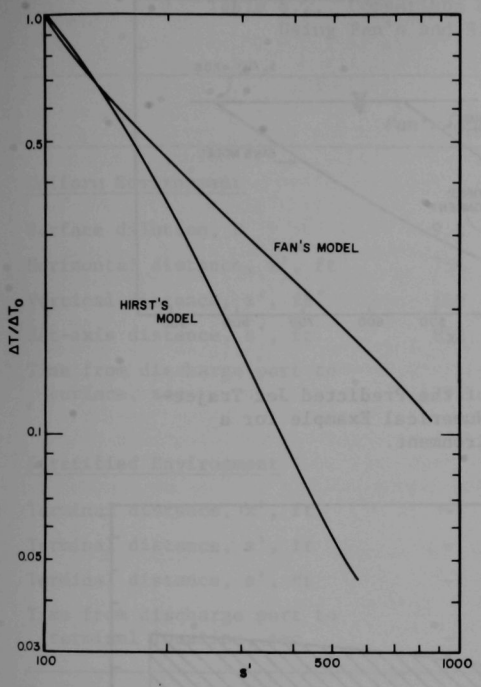

Fig. 6.20.

Comparison of the Predicted Temperature Decrease for Numerical Example for a Flowing Environment.

The vertical distance from the discharge port is 160 ft; the horizontal distance from the discharge port to the surface location is 657 + 99 = 756 ft; the length along the jet axis is 852 ft. The jet trajectory is shown in Fig. 6.21. The time an organism would remain in the ZOEF until it reaches the surface is shown in Fig. 6.22. The area under the curve is the time, which is 182 sec. Since the time in the ZOFE is about 9 sec, the total time from the discharge port to the surface is 191 sec.

b. Hirst's Model. Using Hirst's model for comparison, the dilution at the surface is 22.2. The temperature-decay curve is shown in Fig. 6.20. Hirst's computer program relates everything to the discharge port. The terminal vertical coordinate is 160 ft from the discharge port. The horizontal distance from the discharge port is 544 ft. The length of the jet axis is 569 ft at the surface. The time it would take an organism to travel from the jet discharge port to the surface is 141 sec. The jet trajectory is shown in Fig. 6.21.

The only model available that can evaluate the discharge of a round, buoyant jet into a flowing, stratified environment is Hirst's model. Consider the surface temperature for the example problem to be 73.5°F and the ambient temperature at the distance port to be 59°F. Using these values, the normalized density profile is about 10^{-5} ft^{-1}.

From Eq. 6.34, the stratification parameter, T, is calculated to be 12.9. The terminal location of the jet is calculated. The vertical distance from the

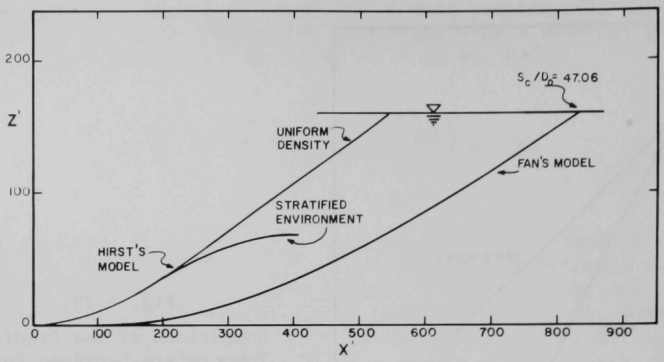

Fig. 6.21. Comparison of the Predicted Jet Trajectories for Numerical Example for a Flowing Environment.

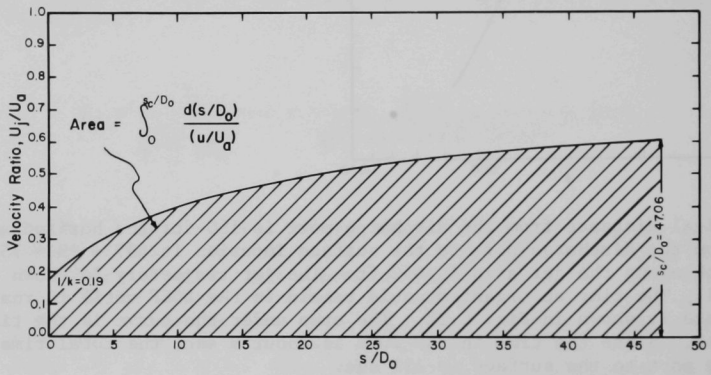

Fig. 6.22. Graphical Integration for the Time of Exposure Using Fan's Model.

discharge port is 66.5 ft; the horizontal distance from the discharge port is 403 ft; and the jet-axis length is 409 ft. The jet trajectory is shown in Fig. 6.21. The time to reach the terminal height is 80 sec. Table 6.2 compares the results from the various model applications.

There is a large discrepancy between the results from Fan's model and Hirst's model. This is the point that was intended. These models cannot be used without understanding how that parameters are obtained. For example, Fan's values of α and C_d' were obtained for a 90° discharge, or a crossflow case. The problem described here, however, is for a horizontal discharge, or a coflowing case. Hence, there is really no way that one can actually determine the value of the entrainment coefficient in this case. All one can say

Table 6.2. Comparison of Predicted Results Using Fan's and Hirst's Models

	Fan's Model	*Hirst's Model*	*Shirazi's Equations*[a]
Uniform Environment			
Surface dilution, D	9.2	22.2	15.0
Horizontal distance, x', ft	756	544	-
Vertical distance, z', ft	160	160	160
Jet-axis distance, s', ft	852	569	1340
Time from discharge port to surface, sec	191	141	-
Stratified Environment			
Terminal distance, x', ft	-	403	-
Terminal distance, z', ft	-	66.5	-
Terminal distance, s', ft	-	409	-
Time from discharge port to terminal location, sec	-	80	-

[a]*See Appendix A.*

is that the entrainment coefficient should be smaller. Additional experimental evidence is needed to clarify this point. This illustrates again the danger of extrapolating model usage outside the range of its verification.

L. Round Jets into a Flowing Environment--Summary and Conclusions

Two models have been discussed to predict the dilution and trajectory of a round, buoyant jet in a flowing environment. However, the limitations of the models themselves plus the paucity of experimental verification restrict their applicability.

The uses of the coefficients presented by Fan in Fig. 6.18 are limited to a range of k from 4 to 16 and F_j from 10 to 80 for a jet discharged at 90° to the flow. Therefore, the validity of results for any conditions outside this range may be open to question. However, within this range of parameters and for a 90° discharge, the model results are valid. Abraham[2] has modified Fan's model, using a constant drag coefficient, $C_d = 0.3$, for all cases. In addition, the entrainment mechanism is changed, eliminating the need to specify a value for the entrainment coefficient. The model shows good agreement with the sets of Fan's data that Abraham shows. Due to the simplified model use (no coefficients to specify), the reader is encouraged to review Ref. 2.

Hirst verified his model by fitting it to numerous investigators' results. For a 90° discharge, the model seems to work well. Shirazi and Davis[123] note that Hirst's model predicts completely opposite trends when compared to experimental data taken by McQuivey *et al.*[90] for a coflowing jet, the ambient turbulence plays an important role in the dilution, whereas the interaction of the jet with the ambient fluid is important to achieve dilution for a 90° discharge. Hirst's model does include ambient turbulence terms in the theoretical derivation, but they are dropped before reaching the final equations. As Hirst's model exists now, Davis says that the model blows up for $F_j \approx 1$. However, for the analysis of a coflowing jet, the results are valid for $F_j < 10$. Compared to data, there is a 10-15% error in the predictions for values of F_j between 10 and 50. The ability to match laboratory data gets progressively worse for values of $F_j > 50$. At high densimetric Froude numbers, there is as much as 300% error. Shirazi and Davis add some empirical terms to account for ambient turbulence for a coflowing jet. The terms added do not affect the solution for a 90° discharge. The terms are obtained by matching theory to data for both extremes (90 and 0° discharge). The data used are for k from 0.5 to 6 for the coflowing case, and from 2 to 16 for the crossflow case. Results agree at the end points (0 and 90°) for other angles of discharge for k from 2 to 4. Reference 123 should be a real asset for those making analyses of submerged discharges, for it will in many cases obviate the use of a computer solution.

For horizontal discharges, the initial version[54] of Hirst's model is best used for F_j greater than 1 but less than 10, and for velocity ratios, k, less than 16. If the velocity ratio gets much greater than 16, then the analysis using the Fan and Brooks model[39] for a jet into a stagnant environment will be applicable. However, with the modification to include the ambient turbulence terms, the ability of Hirst's model to predict the jet characteristics is improved for all values of F_j.[29]

However, the scant experimental data for injections at angles other than 90 and 0° make the analysis for such angles difficult. Geometry constraints are also difficult to include. Even so, a judgment can be made based upon the physical conditions of the receiving body. For example, if the ability of the jet to entrain ambient fluid is hindered by some boundary, then the entrainment coefficient should be adjusted. Also, if a mathermatical-model analysis cannot yield satisfactory results, then a physical model may have to be constructed and the temperature field determined from such a model.

Table 6.3 summarizes modeling capabilities for submerged jets in flowing, ambient environments.

M. Buoyant, Slot Jets

In many instances, heated waste waters are discharged from a rectangular slot. In other instances, the discharge may be from a multiport diffuser consisting of circular discharge ports. If the ports are located sufficiently close to each other, the discharge structure may be treated as a slot discharge due to the interference of each jet with its neighboring jets. The merging of the many small jets of a multiple-port diffuser often produces an effective line or slot source of heated waters a short distance away from the diffuser structure.[31] Numerous investigators have studies buoyant jets (Fan and Brooks,[39] Koh and Fan,[73] Cederwall and Brooks,[23] and Sotil[128]). Historically, the

Table 6.3. Modeling Capabilities in Flowing Environments

Case	*Model to Use*	*Verification*
$\theta_o' = 90°$, $10 < F_j < 80$, $4 < k < 16$	Fan[38]	Good
$\theta_o' = 0°$, $1 < F_j < 10$,[a] $k < 16$	Hirst[54,b]	Good
$\theta_o' = 0°$, $F_j > 50$, $k < 16$	Hirst,[54,b] including ambient turbulence	Good
$\theta_o' = 0°$, $k > 16$	Fan and Brooks[39,c] (approximately stagnant)	Good
Stratified, flowing environment; $k < 16$	Hirst[54]	None
Stratified, flowing environment; $k > 16$	Fan and Brooks[39]	Good
Transient conditions	None	None

[a]*Can be extended to $F_j = 50$ with about 15% error.*

[b]*Use of Shirazi equations may yield better results; see Appendix A.*

[c]*Use of Koh-Fan[73] model including effects of ZOFE may be preferable; see Appendix B.*

equations developed are the ones to analyze a buoyant, slot jet in a stagnant uniform or stratified environment. Hence, the equations here will reflect this paucity of information to analyze the more practical case of a discharge into a flowing environment.

N. Buoyant, Slot Jets into a Stagnant Environment--General Equations

The general assumptions outlined in Sec. VI.A on round jets apply also to slot jets. One difference is that the slot jet is analyzed as a two-dimensional flow problem rather than an axisymmetric problem as for a round jet. Figure 6.23 reflects this difference, where s is again the jet axis and n is the coordinate normal to the jet axis at some s location. The entrainment or change in volume flux can be written as shown in Eq. 6.1. However, for a stagnant environment, $U_a = 0$; therefore, $|U_j - U_a| = U_j$ or u, where u is the characteristic velocity along the jet axis. In addition, $2\pi b$ in Eq. 6.1 for round jets should be replaced by $2L_*$, where L_* is the total jet width. Consequently, the entrainment is proportional to the characteristic jet velocity times the area. For slot jets, the flow rate is commonly written in terms of discharge per unit length (cfs/ft).

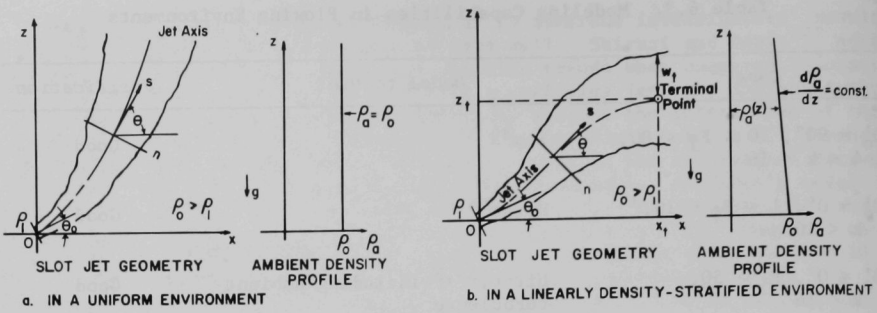

Fig. 6.23. Schematic Diagrams of Slot-buoyant-jet Problems Studied.[39]

The approach used in Sec. VI.B on round jets can be used here for the development of buoyant, slot jets. The equations of continuity, momentum, density deficiency, and concentration of tracer, and two geometric equations can be written. (See the basic references for details). There are seven first-order ordinary differential equations to solve for the seven unknowns: u, b, c, $(\rho_a - \rho)$, θ, x, and z. Two equations can be integrated directly, leaving only five general equations to be numerically integrated. The numerical integration must begin with the values of the unknowns at the end of the ZOFE.

0. A Buoyant, Slot Jet in a Stagnant, Uniform Environment

For the discharge of a buoyant, slot jet into a uniform environment, $d\rho_a/ds = 0$ (or the density gradient is equal to zero) and $\rho_a = \rho_o$ = constant. The equation set is therefore simplified.

1. Fan and Brooks

Fan and Brooks[39] normalize the governing equations to obtain generalized solutions and perform various numerical integrations for a range of parameters, as illustrated by Figs. 6.24 and 6.25, which represent the jet trajectory, jet half-width, and dilution ratios for a horizontal, buoyant, slot jet in terms of dimensionless parameters. The initial value of b_o can be obtained by applying the momentum relation between cross sections 0 and 0' to give

$$b_o = \sqrt{\frac{2}{\pi}}\, B_o \,, \tag{6.63}$$

where b_o = jet half-width at end of ZOFE and

B_o = jet width at orifice.

A volume-flux parameter, μ, and a momentum-flux parameter, m, are introduced as for round jets, with similar meaning. The initial value of m $(= m_o)$ is needed and can be found from

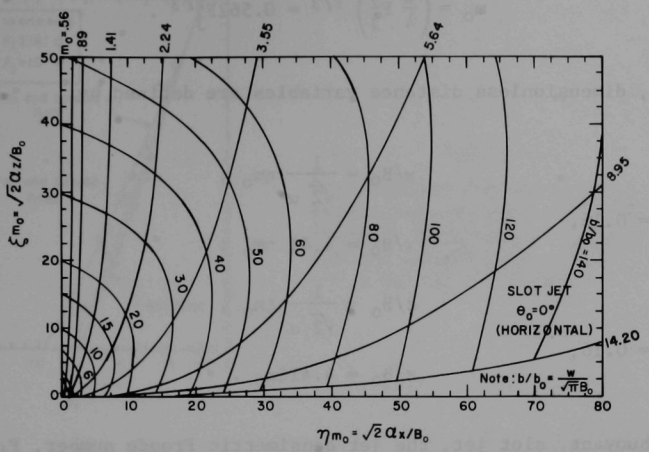

Fig. 6.24. Trajectories and Half-widths, b/b_o, for Slot, Buoyant Jets in a Stagnant, Uniform Environment: $\Theta_o' = 0°$.[39]

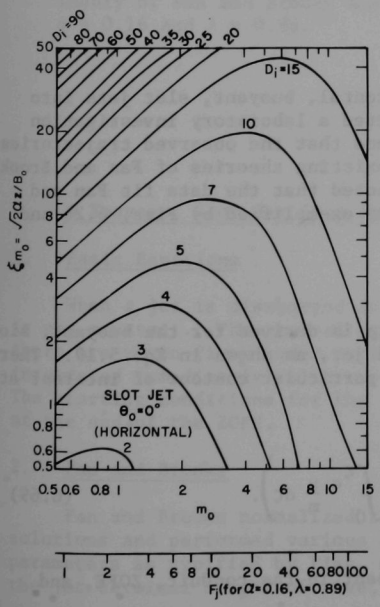

Fig. 6.25.

Dilution of Slot, Buoyant Jets in Stagnant, Uniform Environment: $\Theta_o' = 0°$.[39]

$$m_o = \left(\frac{\alpha}{\lambda} F_j^2\right)^{1/3} = 0.562 F_j^{2/3} . \tag{6.64}$$

In addition, dimensionless distance variables are defined by

$$x/B_o = \frac{1}{\sqrt{2}\,\alpha} \eta m_o , \tag{6.65}$$

and, for $\alpha = 0.16$,

$$x/B_o = 4.41\ \eta m_o ; \tag{6.66}$$

$$z/B_o = \frac{1}{\sqrt{2}\,\alpha} \xi m_o , \tag{6.67}$$

and, for $\alpha = 0.16$,

$$z/B_o = 4.41 \xi m_o . \tag{6.68}$$

For a buoyant, slot jet, the jet densimetric Froude number, F_j, must be redefined. The diameter, D_o, must be replaced by the jet slot width, B_o, leading to

$$F_j = \frac{U_o}{\sqrt{g \frac{\Delta\rho}{\rho_o} B_o}} .$$

2. Cederwall and Brooks

Cederwall and Brooks[23] investigated horizontal, buoyant, slot jets into stagnant or flowing environments. They conducted a laboratory investigation for various densimetric Froude numbers and found that the observed trajectories and dilutions are in good agreement with the existing theories of Fan and Brooks[39] and Abraham.[1] However, Cederwall and Brooks noted that the data fit Fan and Brooks' theory better than Abraham's theory, as exemplified by Figs. 6.26 and 6.27.

3. Time of Exposure

The time-temperature exposure relationship is derived for the buoyant, slot jet in the same manner as for a buoyant, round jet, as shown in Eq. 5.19. Therefore, the total time from the condensers to a particular contour of interest at an axial distance, ζ_c, is given by

$$T_t = \frac{B_o}{U_o}\left(\frac{L_c}{B_o} + 5.2 + \frac{m_o^{\ 2}}{\sqrt{2}\,\alpha} \int_0^{\zeta_c} \frac{\mu}{m}\, d\zeta\right). \tag{6.69}$$

The three terms on the right represent time spent in the conduit, ZOFE, and ZOEF, respectively.

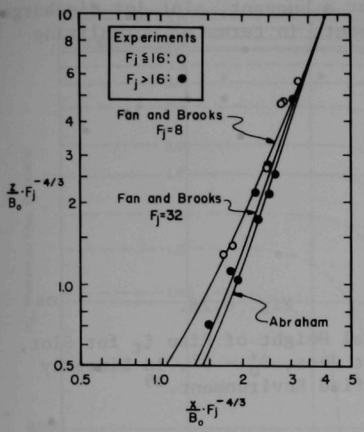

Fig. 6.26.

Experimental Jet Trajectory for a Horizontal, Buoyant, Slot Jet in Stagnant Environment, Compared with Fan and Brooks Theory Based on $\alpha = 0.16$ and $\lambda = 0.89$.[23]

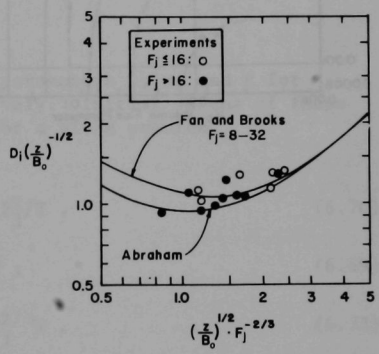

Fig. 6.27.

Experimental Centerline Dilution for a Horizontal, Buoyant, Slot Jet in Stagnant Environment, Compared with Theory of Fan and Brooks Based on $\alpha = 0.16$ and $\lambda = 0.89$.[23]

P. A Buoyant, Slot Jet in a Stagnant, Stratified Environment

1. Basic Equations

When a jet is discharged into a stratified environment, $d\rho_a/ds \neq 0$ and ρ_a is not constant. The general equations discussed earlier are applicable. Thus, there are seven first-order ordinary differential equations (two of which were integrated immediately) with seven unknowns: u, b, c, θ, $(\rho_a - \rho)$, x, and z. The starting conditions for the solution are the values of these seven variables at the end of the ZOFE.

2. Fan and Brooks

Fan and Brooks normalized the governing equations to obtain generalized solutions and performed various numerical integrations for a range of normalized parameters as typified by Figs. 6.28-6.30. These figures are illustrative of the jet terminal height of rise, ξ_t; jet terminal horizontal coordinate, η_t,

and jet terminal volume-flux parameter, μ_t, for a buoyant, slot jet discharged horizontally in a linearly stratified environment, in terms of normalizing parameters.

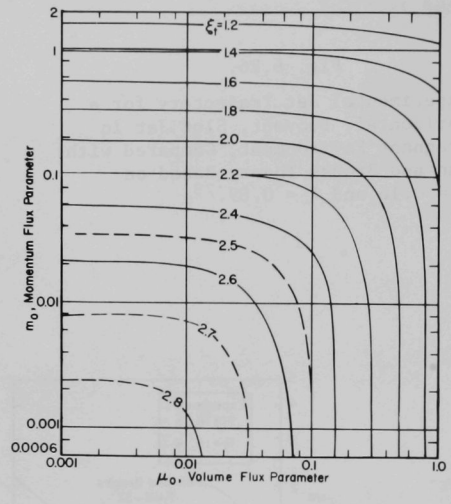

Fig. 6.28.

Terminal Height of Rise ξ_t for Slot, Buoyant Jets, $\Theta_o' = 0°$, in Linearly Stratified Environment.[39]

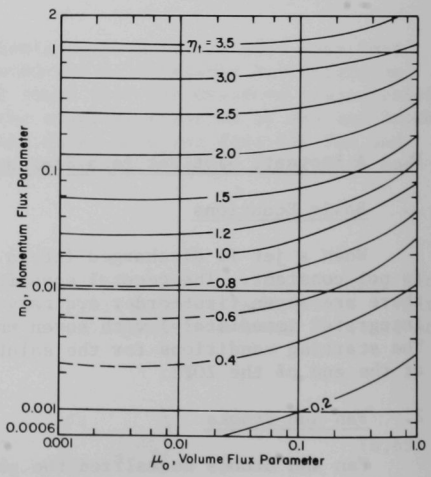

Fig. 6.29.

Terminal Horizontal Coordinate η_t for Slot, Buoyant Jets, $\Theta_o' = 0°$, in a Linearly Stratified Environment.[39]

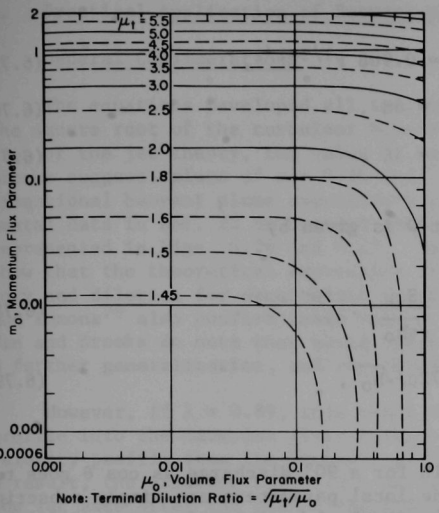

Fig. 6.30.

Terminal Volume Flux Parameter μ_t for Slot, Buoyant Jets, $\Theta_o' = 0°$, in Linearly Stratified Environment.[39]

Fan and Brooks introduced dimensionless parameters μ, m, and β for volume, momentum, and buoyancy flux, respectively. Initial values of these parameters are needed to enter their graphs for a given problem.

$$m_o = \left[\frac{\sqrt{2(1+\lambda^2)}}{4\lambda^2}\right] F_j^2/T \ , \tag{6.70}$$

and, for $\lambda = 0.89$,

$$m_o = 0.600 F_j^2/T \ ; \tag{6.69}$$

$$\mu_o = \left[\frac{\sqrt{2(1+\lambda^2)}}{4\lambda^{4/3}\alpha^{2/3}}\right] F_j^{2/3} T \ , \tag{6.72}$$

and, for $\lambda = 0.89$ and $\alpha = 0.16$,

$$\mu_o = 1.89 F_j^{2/3}/T, \tag{6.73}$$

in which T is defined by Eq. 6.34 with D_o replaced by B_o.

Fan and Brooks define a scale factor, δ, which scales the normalized values of ζ, η, and ξ to dimensionless values of s/B_o, x/B_o, and z/B_o. The scale factor δ is defined in the following equation as a function of the governing parameters m_o and μ_o or F_j and T:

$$\delta = \frac{1}{2^{3/2}\alpha} \frac{m_o^{1/2}}{\mu_o} = \frac{\lambda^{1/3}}{2^{3/4}\alpha^{1/3}(1+\lambda^2)^{1/4}} F_j^{1/3} T^{1/2}. \tag{6.74}$$

For $\alpha = 0.16$ and $\lambda = 0.89$,

$$\delta = 2.21\ m_o^{1/2}/\mu_o = 0.908\ F^{1/3}T^{1/2}, \tag{6.75}$$

$$x/B_o = \delta\eta\ , \tag{6.76}$$

and

$$z/B_o = \delta\xi\ . \tag{6.77}$$

The dimensionless half-width of the jet $\tilde{w}$ is given by

$$\tilde{w} = \frac{8\alpha\mu}{\sqrt{\pi h_o}}\ . \tag{6.78}$$

For $\alpha = 0.16$,

$$\tilde{w} = 0.72\mu/\sqrt{h_o}\ , \tag{6.79}$$

where $h_o = m_o \cos^2\theta$.

Equations 6.78 and 6.79 are invalid for a 90° discharge as $\cos\theta$ goes to zero. At the terminal location, all the local parameters are simply subscripted with a "t" as shown and evaluated at the terminal position (e.g., μ_t and $\tilde{w}_t$).

The set of normalized equations are presented in Ref. 39. Solutions are obtained by numerical integration of the equations, and the governing parameters are μ_o, m_o, and θ_o. A set of graphs of jet trajectory, jet half-width, and dilution can be generated for any combination of these three dimensionless parameters.

3. Time of Exposure

The time an organism will be subjected to temperature rises grater than some level can be evaluated as before by integrating the incremental distance divided by the velocity of the jet at that point. Then the total time from the condensers to the particular s location of interest is given by

$$T_t = \frac{B_o}{U_o}\left[\frac{L_c}{B_o} + 5.2 + \frac{m_o}{2\sqrt{2}\ \alpha\ \mu_o^{3/2}}\int_0^{\zeta_c}\sqrt{\frac{\mu}{m}}\,d\zeta\right]. \tag{6.80}$$

As before, the three components in Eq. 6.80 represent time spent in the conduit, ZOFE, and ZOEF. The expression for the time of travel in the discharge structure is really some detention time. Thus, for an irregular structure, consider the detention time, rather than L_c/U_o. This is frequently a rather large portion of the total time.

Q. Practical Application of Buoyant-slot-jet Models

1. General Considerations

The equations developed all include the coefficient of entrainment, α, and the square root of the turbulent Schmidt number, λ. Before practical application of the jet theory, the value or values of α and λ must be known. Fan and Brooks suggest values of $\alpha = 0.16$ and $\lambda = 0.89$, based upon results on two-dimentionsl buoyant plume experiments by Rouse *et al.*[117] Refer to the experimental data in Ref. 23 on buoyant jets in a stagnant, uniform environment represented in Figs. 6.26 and 6.27. These data (based on F_j from 13 to 25) show that the theoretical expression of Fan and Brooks does predict the trajectory and dilution for densimetric Froude numbers (F_j) between 8 and 32. Lee and Emmons[78] also confirm these values in their study of line fires. However, Fan and Brooks do note that using these values in a stratified environment is a further generalization, and experimental verification is needed.

However, if $\lambda = 0.89$, this means that the development of the concentration profile into the Gaussian distribution lags behind the development of the velocity profile from its "tophat" profile to the Gaussian distribution. As a result, the dilution ratio, $D = c_o/c$, will equal 1 for some distance along the jet axis after the end of the ZOFE has been reached. The dilution with respect to the discharge point 0' can then be obtained by considering the continuity relation for the tracer and written as

$$D = (c_o/c)\sqrt{\frac{2\lambda^2}{1+\lambda^2}} = \mu\sqrt{\frac{2\lambda^2}{1+\lambda^2}} \quad \text{for } \mu\sqrt{\frac{2\lambda^2}{1+\lambda^2}} > 1$$

and (6.81)

$$D = 1 \text{ for } \mu\sqrt{\frac{2\lambda^2}{1+\lambda^2}} < 1 \ .$$

If $\lambda = 0.89$, Eq. 6.81 reduces to

$$D = 0.94\ \mu \text{ for } \mu > 1.06 \ ;$$

and (6.82)

$$D = 1 \text{ for } \mu < 1.06 \ .$$

2. Buoyant, Slot Jets in a Stagnant, Uniform Environment

For values of $\alpha = 0.16$ and $\lambda = 0.89$, the dilution with respect to the discharge location 0' is given by Eq. 6.82. The problem of a buoyant, slot jet in a stagnant, uniform environment is governed by the initial values of m_o and θ_o. Practically, the densimetric Froude number, F_j, characterizes a buoyant jet. Equation 6.64 shows the relation of m_o to F_j. To locate any local variable, all distances must include the length of the ZOFE. Fan and Brooks consider dimensionless distances (designated by a prime) with respect to the discharge port 0' to be given by the following equations and illustrated in Fig. 6.31:

$$x'/B_o = x/B_o + 5.2 \cos \theta_o \tag{6.83}$$

and

$$z'/B_o = z/B_o + 5.2 \sin \theta_o . \tag{6.84}$$

Also, the dimensionless distances, x/B_o and z/B_o, can be evaluated in terms of the normalized parameter by evaluating Eqs. 6.65 and 6.67.

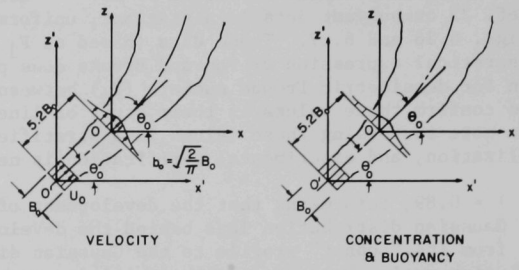

Fig. 6.31. ZOFE for an Inclined, Slot, Buoyant Jet.[39]

3. Numerical Example--Stagnant, Uniform Environment

A thermal power plant is horizontally discharging 1000 cfs through 10 slot jets, whose dimensions are 2 × 15 ft, into a stagnant environment. The centerline of the slot is 100 ft below the water surface and 50 ft above the bottom of the receiving body. The temperature of the receiving water is 59°F and uniform throughout. There is an 18°F rise across the condensers. Analyze the jet, and determine the jet's characteristics at the surface.

The temperature of the receiving water is 59°F with a density of 0.99913. The temperature of the discharge is 77°F with a density of 0.99707. First, the densimetric Froude number must be calculated.

Recall that Q = 1000 cfs. Therefore, Q through one port is 100 cfs. Hence, the discharge velocity is calculated by

$$U_o = Q/A = 100/(2 \times 15) = 3.33 \text{ fps}$$

and

$$F_j = \frac{U_o}{\sqrt{\frac{\Delta\rho}{\rho} gB_o}} = \frac{3.33}{\sqrt{0.00206(32.2)(2)}} = 9.13 .$$

Then, calculate m_o using Eq. 6.64:

$$m_o = 0.562 \, F_j^{2/3} = 2.51 .$$

Next, calculate the ordinate (representative of the surface, at 23 ft) for Fig. 6.25 using Eq. 6.68:

$$\xi m_o = \frac{1}{4.41} z/B_o = \frac{100}{4.41(2)} = 11.34 \ .$$

Enter Fig. 6.25 to obtain the surface dilution, D_i, with respect to the end of the ZOFE:

$$D_i \simeq 8 \ .$$

Hence, using Eq. 6.82, the dilution with respect to the discharge port is

$$D = 0.94D_i = 0.94(8) \simeq 7.5 \ .$$

Therefore, the temperature rise above the ambient temperature can be evaluated in

$$\frac{\Delta T_o}{\Delta T_{surface}} = D \ , \tag{6.85}$$

so that

$$\Delta T_{surface} = \frac{\Delta T_o}{D} = \frac{18°F}{7.5} = 2.4°F \ .$$

It follows that the temperature at the surface wil be 59 + 2.4 = 61.4°F.

Now, what are the jet characteristics at the surface? Enter Fig. 6.24 with a value of $\xi m_o = 11.34$ and $m_o = 2.51$ to find that $\eta m_o \simeq 10.5$ and $b/b_o \simeq 21$. From Eqs. 6.66 and 6.83, x'/B_o can be calculated:

$$x'/B_o = x/B_o + 5.2 \cos \theta \ ;$$

$$x'/B_o = 4.41\eta m_o + 5.2 = 4.41(10.5) + 5.2 = 51.5 \ .$$

Hence, $x' = 51.5(2) = 103.0$ ft. From the following equation, the nominal jet half-width can be calculated:

$$w = \frac{b}{b_o} \sqrt{\pi} \ B_o \ , \tag{6.86}$$

or

$$w \simeq 21\sqrt{\pi} \ (2) \simeq 74.4 \text{ ft} \ .$$

The dilution at the surface is about 7.5. This yields a surface temperature of 61.4 °F. Practically, the jet centerline is 103 ft horizontally and 100 ft vertically from the discharge port with a nominal jet half-width of about 74 ft. However, if the slots are located sufficiently close to each other, the surface dilution will be reduced. This will be covered in discussions on jet interference and lateral spreading in Chapter VII.

4. Buoyant, Slot Jets in a Stagnant, Stratified Environment

General considerations for this case are similar to those for a slot jet into a stagnant, uniform environment. The dilution reduction relative to the discharge port is expressed in Eq. 6.81 for the uniform case. For the stratified case, c_o/c is defined by

$$\frac{c_o}{c} = \sqrt{\frac{\mu}{\mu_o}} , \tag{6.87}$$

The following equation expresses the dilution ratio as a function of the volumetric-flux parameter, μ, and initial volumetric-flux parameter, μ_o:

$$D = \sqrt{\frac{2\lambda^2}{1 + \lambda^2} \frac{\mu}{\mu_o}} = \sqrt{\frac{2\lambda^2}{1 + \lambda^2}} D_i , \tag{6.88}$$

where $D_i = \sqrt{\mu/\mu_o}$.

If $\lambda = 0.89$ and $\alpha = 0.16$,

$$D = 0.94\sqrt{\mu/\mu_o} = 0.94\ D_i \text{ for } D_i > 1.06 \tag{6.89}$$

and

$$D = D_i = 1 \text{ for } \sqrt{\mu/\mu_o} < 1.06 .$$

In addition to the densimetric Froude number, F_j, the stratification parameter, T, is used to define the characteristics of a buoyant, slot jet into a stagnant environment. The parameter T is defined by Eq. 6.34, with D_o replaced by B_o. The solution of the governing equations depends upon the specification of the initial values of m, μ, and θ.

Consider the previous example of a buoyant, slot jet discharged into a stagnant, stratified environment. The temperature at the discharge port is again 59°F with $\rho_o = 0.99913$, and the temperature at the surface is 73.5°F with $\rho_s = 0.99755$. What is the terminal dilution, and will the jet remain submerged? The jet temperature is again 77°F with $\rho_1 = 0.99707$.

Recall from the previous example that $F_j = 9.13$ and $\theta_o = 0°$.

The remaining parameter, T, the stratification parameter, must be calculated. If

$$-\frac{1}{\rho_o}\frac{d\rho_a}{dz} = -\frac{0.99755 - 0.99913}{100} = 1.58 \times 10^{-5}\ \text{ft}^{-1} ,$$

then

$$T = \frac{\rho_o - \rho_1}{B_o(-d\rho_a/dz)} = \frac{0.00206}{2(1.58 \times 10^{-5})} = 65.2 .$$

Now, the governing parameters, m_o and μ_o, can be calculated from Eqs. 6.71 and 6.73 respectively, so that the appropriate figure may be entered:

$$m_o = 0.600F^2/T = 0.600(9.13)^2/65.2 \simeq 0.77$$

and

$$\mu_o = 1.89F^{2/3}/T = 1.89(9.13)^{2/3}/65.2 \simeq 0.127 .$$

Using the values of $m_o \simeq 0.77$ and $\mu_o \simeq 0.127$, enter Fig. 6.28-6.30 for a slot jet discharged horizontally. From Fig. 6.28, read the value of the jet terminal height of rise, $\xi_t = 1.45$; from Fig. 6.29, read the jet terminal horizontal coordinate, $\eta_t = 3.0$; and from Fig. 6.30, obtain the jet terminal volume-flux parameter, $\mu_t = 3.7$.

From Eq. 6.89, the terminal dilution, D_t, with respect to the discharge port is

$$D_t = 0.94\sqrt{\frac{\mu_t}{\mu_o}} = 0.94\sqrt{\frac{3.7}{0.127}} = 5.4 .$$

Calculate the jet terminal height of rise from Eq. 6.77. The vertical length of the ZOFE is zero. The scale factor, δ, can be calculated from Eq. 6.75 to give

$$\delta = 0.908\ F^{1/3}T^{1/2} = (0.908)(9.13)^{1/3}(65.2)^{1/2} \simeq 15.35 .$$

From Eq. 6.77, the jet terminal height of rise is calculated to be 44.5 ft, or about 55 ft below the surface and 95 ft above the bottom:

$$z_t = \delta\xi_t\ B_o = 15.35(1.45)(2.0) = 44.5\ \text{ft} .$$

In evaluating whether the jet remains submerged, we should calculate the jet width. Fan and Brooks[39] discuss this problem. They note that if the jet

is nearly vertical at the top ($\eta_t << \xi_t$), the maximum vertical penetration of the jet is simply z_t, because the core of the jet penetrates to the highest level and the peripheral regions fan out before reaching the top. However, if the jet has appreciable horizontal momentum at its terminal height of rise ($\eta_t \geq \xi_t$), the jet will appear as in Fig. 6.23b, and the maximum vertical extent of the jet is more nearly $z_t + w_t$, where w_t is the terminal half-width of the jet. Fan and Brooks note that further research is needed to more completely define this situation.

In the current case, $\eta_t > \xi_t$, and the maximum vertical extent is more nearly $z_t + w_t$. The initial length parameter, b_o, at the end of the ZOFE can be found by equating the momentum flux at the jet orifice to that at the end of the ZOFE assuming the buoyancy force to be negligible in that small distance. Fan and Brooks show this to be

$$b_o = \sqrt{\frac{2}{\pi}}\, B_o \ .$$

By the definition of the jet half-width $w = \sqrt{2}\, b$, the value of w at the end of the ZOFE is

$$w_o = \sqrt{2}\, b_o = \frac{2\, B_o}{\sqrt{\pi}}$$

Equation 6.79 shows that $\tilde{w}_t/\tilde{w}_o$, which also equals w_t/w_o, is equal to μ_t/μ_o. Therefore,

$$w_t = w_o \frac{\mu_t}{\mu_o} = \frac{2\, B_o}{\sqrt{\pi}} \frac{\mu_t}{\mu_o} = \frac{2(2.0)}{\sqrt{\pi}} \frac{3.7}{0.127} = 65.7 \text{ ft} \ .$$

Since the terminal height is 95 ft above the bottom, no interference with the bottom is expected. However, $z_t + w_t = 65.7 + 44.5 \simeq 110$ ft, which is slightly greater than the total submergence, which is 100 ft. Therefore, some surface interference is expected, and the plume will appear at the surface. This means that the dilution calculated will be slightly high, as it assumes the availability of infinite quantities of dilution water. The effect in this case may be slight ($110 \approx 100$), but it should be considered for all cases.

R. Slot Jets--Conclusions

The presentation in this section has considered slot jets into a stagnant environment. Several limitations should be recalled on the use of the equations and figures presented here. First, the values produced by the equations have been verified by Cederwall and Brooks[23] for ranges of the densimetric Froude number, F_j, between 13 and 25. Figures 6.26 and 6.27 indicate that the equations

are probably valid for F_j from about 8 to 32. Both the trajectory and the dilution are reasonably well treated by the models. Cederwall and Brooks, in addition, have some qualitative information on slot jets into a flowing environment. However, findings in this area are not as extensive and do not yet make it possible to make as accurate predictions for the flowing-environment case. Although this section discusses the discharge of a slot jet into a stratified environment, there is a real question as to the use of the model, the values of the entrainment coefficient, and Schmidt numbers since no experimental verification exists for this case. To summarize, if one has a buoyant, slot jet for densimetric Froude numbers between 8 and 32 issuing into a stagnant environment, the methods here probably will yield good results. Outside this range, however, although some reasonable *extrapolation* might be possible if judgment is applied, real care should be taken in interpreting such predictions.

S. Surface Layers from Submerged Jets

If a submerged jet reaches the surface of the receiving body of water, it may spread out into a layer over a portion of the surface. In fact, if the jet still has considerable momentum remaining when it reaches the surface, it will not only boil up at the sruface but will have sufficient energy to move horizontally with considerable velocity. This remaining field could be of interest in determining the additional stratification caused by the heated discharge, and in making some sort of assessment of the volume of the receiving waters affected by a given temperature rise. Unfortunately, there presently is no adequate work to define the spread of the field, i.e., what surface area is affected by the surface layer. Some work has been done on this in observation of the fields of sewage from ocean outfalls. Rawn and Palmer[113] conducted an extensive series of experiments in the ocean. They used small-scale diffuser orifices, which they supported in the water, and took many measurements of dilution of the plume and the layer thickness formed on the surface. The observations they made indicated that the average layer thickness was approximately 1/12 of the plume length measured along the axis of the jet from jet orifice to the water surface. Therefore, if the length along the plume axis to the water surface was 240 ft, for example, this simple rule of thumb would predict a surface layer about 20 ft thick. It is not unreasonable to assume that this surface layer might be reasonably well mixed vertically due to wind waves. In addition to their modeling experiments in the ocean, Rawn and Palmer measured the thickness of the sewage fields at the Los Angeles and Long Beach outfalls and receivied good agreement with the 1/12 rule of thumb.

Thickness of the layer might be of only academic interest. If the plume has received sufficient dilution when it reaches the surface, so that the temperatures are not at an excessive level, then it may be unnecessary to make any further calculations to determine exactly where the heated water goes from that point. If, on the other hand, the dilution is insufficient and the plume, on reaching the water surface, still has an excessive temperature to be removed, the problem is made more difficult. At present, there are no analytical techniques to treat this problem. As noted earlier, the surface layer may spread out with some velocity. If this is the case, it may be mixing laterally, although the strong stratification may prevent much vertical mixing from occurring. Certainly there would be additional mixing due to the ambient turbulence. However, if a given submerged discharge does not meet the criteria set by the appropriate regulatory agency by the time the jet reaches the surface, physical-model studies will probably be required to ensure that the

criteria are met within a reasonable length from the point of reaching the surface. To those charged with designing submerged ports, it seems a good suggestion to design them so as to attain the necessary dilution before reaching the surface of the water. This prevents problems due to lack of analytical ability.

T. Estuarine Conditions

One of the basic considerations listed for the analysis of a buoyant discharge is the velocity field of the receiving ambient fluid. The ambient velocity field can be considered to have no ambient current (stagnant), uniform ambient current, or transient velocity patterns, e.g., those due to tidal influences or peaking-power operations. Previous sections of this chapter cover the stagnant and uniform-velocity fields. The time-varying velocity pattern due to tides or peaking power operations is a real situation and must be considered when evaluating the thermal impact on the environment.

Unfortunately, no existing models allow for the inclusion of a time-varying velocity field. Some judgment is needed to aid in evaluating the discharge characteristics. Typically, the evaluation can be made at conditions of no tide as a worst condition. Hence, the buoyant jet in a stagnant environment would apply. For these problems, one uses either Fan's model or Hirst's model, depending upon the jet and discharge characteristics. Another condition in a real situation is the discharge of the buoyant waste in a direction opposite to the direction of flow of the receiving body of water. Platten and Keffer[103] investigated this case for an air-in-air jet for velocity ratios of 4, 6, and 8. They found that the greatest deflection rate occurs for initial discharge angles, Θ_0', of 105° as described in Fig. 2.1. The rate of deflection decreased as the angle of discharge increased from 120 to 135°. Hirst's and Fan's models can be used to predict the dilution and jet trajectory for these cases. The predicted results will be questionable, since (1) evidence has shown the rate of deflection of the jet decreases as the angle of discharge approaches 180°, and (2) many of the model assumptions (for example, similar profiles) are violated for 180° discharges. In addition, little information exists on values of entrainment coefficients for such cases. Therefore, this case may yield the highest temperature rises, as indicated by Harleman *et al.*,[50] but current models cannot handle it. (See Chapter VII for work on submerged, multiport diffusers directed against the ambient current.)

The tidal fluctuations may be discharges of concern for reasons other than just time-varying velocity patterns. As a heated discharge is made into an estuary, the amount of available dilution water will be changing. Some schemes have been suggested for adjusting predicted temperatures by accounting for limitations on the amount of new dilution water. One such method by Pritchard[110] is outlined in Chapter V.

Chapter V also discusses a one-dimensional estuary model designed to model far-field (ambient processes controlling) dispersion of heat. This method is also applicable to submerged discharges. Assuming that the heat discharged from the discharge port(s) becomes uniformly mixed (laterally and vertically) with the receiving water reasonably close to the discharge point, this model treats ultimate removal of the heating by flushing or surface cooling. (Further details are available in Chapter III.)

In short, no completely time-varying model exists for near-field temperature predictions. Present analysis is simply steady-state, with some assumed critical ambient condition chosen and held steady. This may underestimate some mixing. At present, it is advised to apply this gross steady-state analysis. If dilutions seem satisfactory, you may be justified in assuming conservation in the results. If such predictions yield temperatures at or above acceptable levels, the only recourse for better evaluation is a physical model of the system or a redesign of the discharge system, if this can be done.

U. Single-port Submerged Jets--Summary and Recommendations

The discussions in this chapter have treated submerged, round jets and submerged, slot jets. Ambient environments have been considered as stagnant or flowing, and uniform or stratified. A number of models have been discussed. The reader is referred to concluding sections offered at the end of main sections in this chapter. Models recommended for various cases, along with ranges of variables limiting model use, are summarized in Table 6.4. This table should enable the reader to quickly see how to handle his problem. He can then turn to the appropriate section in this chapter for details.

A final warning on the effect of free surface and bottom boundaries should be issued. First, calculation of surface conditions must consider any surface layer that may form. As this surface layer (or the surface itself) is neared, entrainment becomes inhibited. One should probably make his predictions based on calculations ending a few feet from the bottom of the surface layer. These steps will help avoid overestimation of the dilution. A similar precaution is recommended near any bottom boundary.

Table. 6.4. Applicability of Submerged, Single-port Models

Condition	Θ_o'	k	F_j	*Recommended Model*[a]	*Verification*
Stagnant, uniform environment; round jet.	Any	∞	10-130	Fan & Brooks[39,b]	Good for 0°
	0	∞	10-130	Fan & Brooks[39,b]	
				Cederwall[22]	Good
Stagnant, stratified environment; round jet.	Any	∞	9-57	Fan & Brooks[39] (Linearly stratified)	For several angles.
	Any	∞	Any	Ditmars[30] (Arbitrary stratification)	Slight
Flowing, uniform environment; round jet.	90°	4-16		Fan[38]	Good
	0°	<16		Hirst[54,c]	Good
	0°	>16		Fan & Brooks[39,b]	Good
	See Table 6.3 for other information.				
Flowing, stratified environment; round jet.	Any	Any	Any	Hirst[54]	None
	Any	>16	9-57	Fan & Brooks[39] (Approximately stagnant)	Good for several angles.
Stagnant, uniform environment; slot jet.	Any	∞	8-32	Fan & Brooks[39]	Best for 0°
Stagnant, stratified environment; slot jet.	Any	∞	8-32	Fan & Brooks[39]	None
Transient	Any	Any	Any	None[d]	None

[a]*Reference 123 covers many of these cases in graphical form.*

[b]*Use of Koh-Fan model[73] with ZOFE modification may be preferred; see Appendix B.*

[c]*Use of Shirazi equations may yield better results; see Appendix A.*

[d]*Except by use of steady-state approximation.*

VII. SUBMERGED, MULTIPORT DIFFUSERS

Chapter VI includes the theory and application of single submerged jets with both round and slot shapes. It is becoming popular to try to distribute the heated water to the receiving body by means of a series of submerged ports. If all these ports issue from the same main pipe or structure, the unit is classed as a submerged, multiport diffuser. If the ports are spaced far enough apart so that the plumes from the separate ports do not interact with one another before reaching the water surface, then the methods of Chapter VI are directly applicable for analysis for each individual port.

A. Jet Interference

Figure 7.1 illustrates two ways in which jets from a multiport diffuser can interact. Consider Fig. 7.1a. Jets issuing from the several ports entrain fluid and spread laterally. Eventually, if the port spacing, W, is small enough compared to submergence, z, the plumes will overlap and be competing for the same entrainment water. In fact, there will be no other water to be entrained between the plumes. Rather, only water from above and below the plumes can be entrained. This is much like a slot jet, so it is frequently assumed that the port discharges act as single jets until they interact. Thereafter, they can be treated as slot jets.

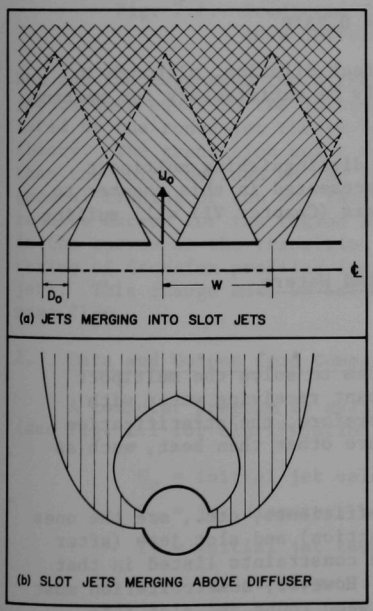

Fig. 7.1.

Two Ways in Which Jets from a Multiport Diffuser Can Interact.

More frequently seen today are diffuser designs calling for ports in alternating directions. One port points downstream, the next upstream, the next downstream, and so on. Liseth[86,87] has studied this case for deep submergence of the diffuser. Figure 7.1b illustrates his observations of the tendency for plumes from the opposite sides of the diffuser to merge into a single plume above the diffuser. Again, once this merger occurs, the dilution rate of the rising plume is decreased, as the plume surface area across which mixing can occur is reduced.

Most multiport diffuser systems discharge in the horizontal direction to maximize the distance of travel, and hence, the dilution, before the plume reaches the surface. In fact, of the models to be discussed here, only the model by Koh and Fan[73] allows for a nonhorizontal discharge. Example output from their model for several different horizontally discharging diffusers clearly indicates the effect of jet interference. Delaying jet interference by increasing W or decreasing D_o causes the jet to be sent upward more. Due to more early entrainment when interaction is delayed, the local densimetric Froude number, F_L, is more quickly reduced. This occurs because, in the initial jet regions, decay of velocity is greater than decrease of the term $\sqrt{g(\Delta\rho/\rho)D_L}$, in which D_L = local jet dimension. A lower value of F_L implies more importance of buoyancy forces, and hence, more of a tendency to rise. For the cases in Fig. 7.2, $\Delta T_o = 89.2 - 77 = 12.2°F$. The temperature rises remaining at the surface (z = 100 ft) were predicted as follows for three of the cases:

$W = 5$ ft, $D_o = 0.25$ ft: $\Delta T = 0.11°F$;

$W = 10$ ft, $D_o = 0.50$ ft: $\Delta T = 0.17°F$;

$W = 5$ ft, $D_o = 0.50$ ft: $\Delta T = 0.23°F$.

Therefore, the delayed interaction does affect dilution, although in this case, any of the alternatives would probably be satisfactory for meeting standards.

Interaction is clearly one of the features distinguishing multiport diffusers from single ports. Criteria will be presented in this chapter to enable one to decide whether a single-jet analysis (Chapter VI) will suffice or whether a multiport analysis is called for.

B. Diffusers in Stagnant, Arbitrarily Stratified Waters

1. Model Formulation

Koh and Fan have developed a computer program to solve the multiport diffuser (all ports same direction) into a stagnant receiving water with arbitrary temperature and density profiles. Therefore, the stratification in the receiving body could be due to some feature other than heat, such as salinity.

The equations, assumptions, entrainment coefficients, etc., are the ones found in Chapter VI on round jets (before interaction) and slot jets (after interaction). They are therefore subject to the constraints listed in that chapter and will not be discussed further here. However, some criterion must be chosen for selecting the transition point between round and slot jets.

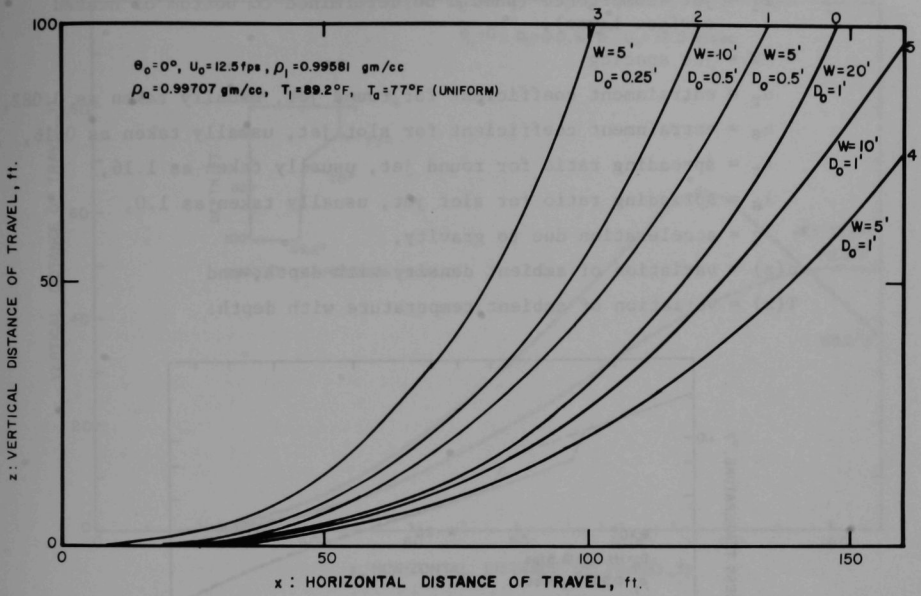

Fig. 7.2. Predicted Trajectories of Multiple, Buoyant Jets in a Uniform Environment.[73]

Koh and Fan suggested two different criteria: (1) when the width of the round jet becomes equal to the initial jet spacing, W; (2) when entrainment as calculated by the round-jet theory becomes equal to that calculated by the slot-jet theory. The transition point defined by the latter criterion occurs later than the point defined on the basis of width. Figure 7.3 illustrates the general finding of Koh and Fan that the two criteria gave essentially identical results except for the region between the two transitions. The discontinuity in the curves at the transition points occurs due to the sudden change from a series of Gaussian profiles (series of round jets) to a single profile (slot jet). This change must be accomplished with conservation of momentum and mass flow.

2. Data and Output from Computer Program

A computer program is available in Ref. 73. Basic data needed include (see Fig. 2.1 for clarification of terms):

U_o = initial jet velocity,

D_o = jet diameter,

T_1 = initial jet temperature,

ρ_1 = jet density

Θ_o' = jet discharge angle,

z_1 = jet submergence (should be determined to bottom of heated surface layer),

W = jet spacing

α_r = entrainment coefficient for round jet, usually taken as 0.082,

α_s = entrainment coefficient for slot jet, usually taken as 0.16,

λ_r = spreading ratio for round jet, usually taken as 1.16,

λ_s = spreading ratio for slot jet, usually taken as 1.0,

g = acceleration due to gravity,

$\rho(z)$ = variation of ambient density with depth, and

$T(z)$ = variation of ambient temperature with depth.

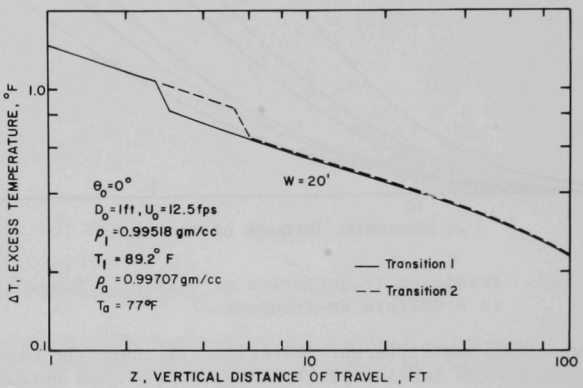

Fig. 7.3. Predicted Jet Centerline Excess Temperature of Multiple Buoyant Jets in Uniform Environment.[73]

Output from the program includes jet trajectory, jet width, dilution, temperature, density, and temperature rise, all as functions of location. Figure 7.4 shows results from application of the program to two particular discharges into a stratified environment. Neither plume reaches the water surface.

The computer output does not make a ready estimate of time of exposure possible, since velocities are not reported. However, the computer program can be modified easily to produce velocities and times. Velocities are easily computed from the dimensionless variables solved for in the program. These can then be graphically or numerically integrated as discussed in Chapters V and VI.

3. Model Applicability and Usefulness

This model has not been verified experimentally, except insofar as the separate expressions for round and slot jets have been verified as discussed

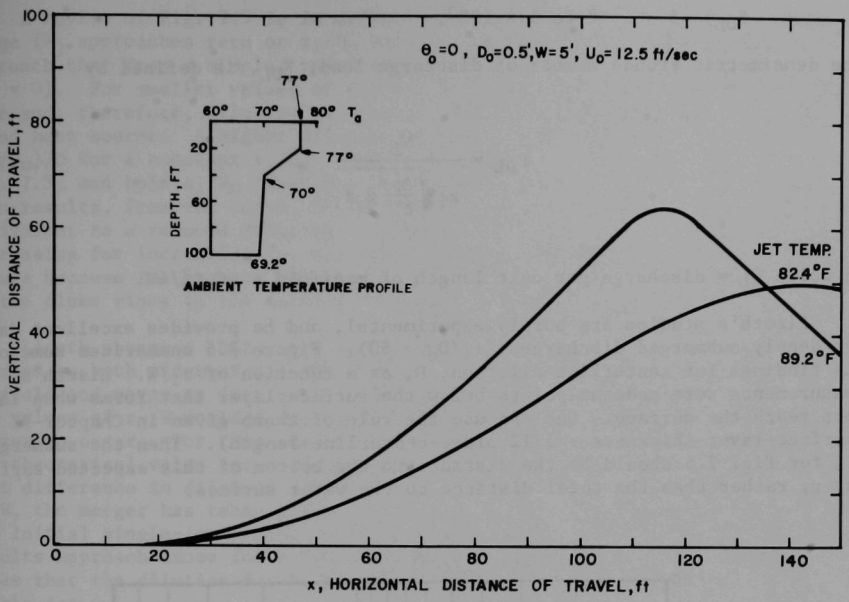

Fig. 7.4. Predicted Trajectories of Multiple, Buoyant Jets in a Stratified Environment.[73]

in Chapter VI. Based on these verifications, one can use the model with some confidence. It was noted in Chapter VI that the use of 0.16 as an entrainment coefficient had not been verified. Thus, application of the Koh-Fan model for stratified conditions might be undertaken with more care. It is, however, the only present model for a multiport diffuser discharging into a stratified environment. The restriction to a stagnant condition may not be too critical, since most diffuser velocities are much greater than expected ambient velocities.

C. Deeply Submerged Diffusers in a Stagnant Environment

1. Experimental Findings

Liseth[86,87] conducted an extensive series of laboratory experiments on diffusers, both with all ports in the same direction (unidirectional) and with ports alternating in direction. Only results for alternating ports are discussed here. Ranges of parameters in his work include:

z_1/D_o: 52-222,

z_1/W: 0-80,

F_j: 10-61,

$(z/D_o)/F_j$: 2-20, and

F_{DL}: 5×1^{-5} to 5×10^{-3}.

The densimetric Froude number of discharge load, F_{DL}, is defined by

$$F_{DL} = \frac{Q_L}{z_1 \sqrt{\frac{\Delta\rho}{\rho} g z_1}} , \tag{7.1}$$

in which Q_L = discharge per unit length of manifold = $\pi U_o D_o^2/4W$.

Liseth's studies are purely experimental, and he provides excellent data for deeply submerged discharges ($z_1/D_o > 50$). Figure 7.5 summarizes some of his findings for centerline dilution, D, as a function of z_1/W. Liseth's measurements were made at points below the surface layer that forms when the jets reach the surface. One can use the rule of thumb given in Chapter VI (surface-layer thickness = 1/12 plume-centerline length). Then the submergence, z_1, for Fig. 7.5 should be the distance to the bottom of this expected surface layer, rather than the total distance to the water surface.

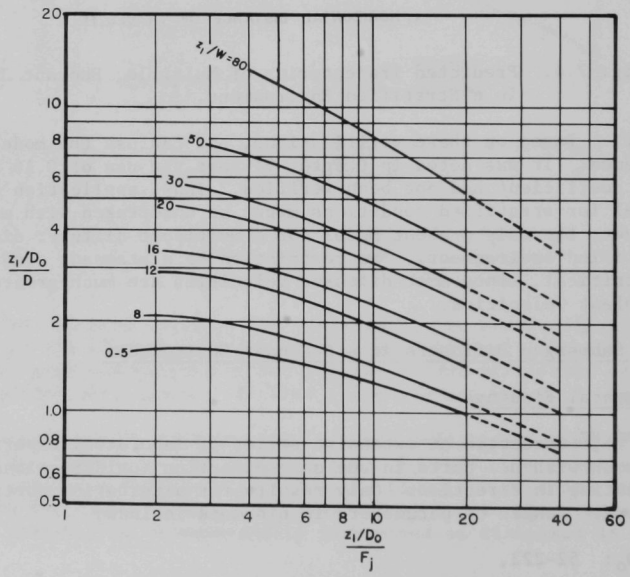

Fig. 7.5. Minimum Dilution along the Center of Merging Buoyant Jets from a Manifold in Stagnant Receiving Water of Uniform Density.[86]

A review of Fig. 7.5 is in order. As the parameter $(z_1/D_o)/F_j$ becomes large (F_j approaches zero or z_1/D_o becomes large), the dilution should approach that from a simple, round source of heat only with no momentum ($F_j = 0$). For smaller values of $(z_1/D_o)/F_j$, momentum plays a more important role and, therefore, dilution is greater than that predicted for a simple, round heat source. A higher dilution will be reflected in lower values of $(z_1/D_o)/D$ for a constant z_1/D_o. Consider a curve of constant z_1/W in Fig. 7.5, and hold z_1/D_o constant. As F_j increases, $(z_1/D_o)/F_j$ decreases. This results, from the curve, in an increase in the term $(z_1/D_o)/D$, which is equivalent to a reduced dilution. Essentially, then, Fig. 7.5 shows dilution decreasing for increasing F_j, all other factors being held constant. This occurs because the greater buoyancy (lower F_j) causes greater plume velocities as the plume rises to the surface, thereby increasing mixing.

Liseth observed that, in a deeply submerged diffuser, jets initially discharged to both sides of the diffuser are gradually forced back toward the manifold and merge to form a two-dimensional plume rising above the manifold. Low values of z_1/W would indicate that the depth was insufficient to allow this merger to occur. For this reason, the bottom curve in Fig. 7.5 approaches the theoretical value for a single jet, and for $z_1/W < 5$, there is no significant difference in dilution for that from a single jet. For high values of z_1/W, the merger has taken place long enough before reaching that height that the initial single-jet region is only a small part of the total. Thus, the results approach those for a two-dimensional buoyant slot plume. Liseth notes that the dilution for $z_1/W = 80$ is only 10-20% of that attained by a single jet.

Liseth has also developed the following relationship to approximately describe his data on the height at which the plumes merge:

$$\frac{z_m}{W} \simeq F_j \ , \tag{7.2}$$

in which z_m is the height at which the merger occurs, W is the port spacing, and F_j is the initial jet densimetric Froude number. It is logical that this merger point would rise with an increase in F_j. A higher F_j causes the initial jet to move farther away from the port before being swept upwards by buoyancy. It would then take a greater height for these plumes to interact and merge.

Liseth observes that for a given F_j and F_{DL}, a port spacing, z_1/W, between 5 and 10 will yield the highest dilution, D.

2. Numerical Example

Consider the following problem:

z_1 = depth to bottom of surface layer (here = 70 ft),

D_o = initial jet diameter = 1.0 ft,

F_j = 10,

W = jet spacing = 5 ft, and

$\Delta T_o = 20°F$.

What is ΔT at elevation z_1? Then,

$$\frac{z_1/D_o}{F_j} = \frac{70/1}{10} = 7.0$$

and

$$\frac{z_1}{W} = \frac{70}{5} = 14 \ .$$

From Fig. 7.5, these two values yield, with interpolation,

$$\frac{z_1/D_o}{D} = 2.4 \ .$$

Thus, $D = (70/1)/2.4 = 29.2$, and $\Delta T_{70} = 20°F/29.2 = 0.69°F$.

If the port spacing were increased to 15 ft, then $z_1/W = 70/15 = 4.67$. Figure 7.5 yields $(z_1/D_o)/D = 1.4$, $D = (70/1)/1.4 = 50$, and $\Delta T_{70} = 20°F/50 = 0.4°$ There is then a greater dilution attained with greater spacing. Of course, this greater spacing also implies a greater cost for the diffuser due to increased length. The designer must seek some balance.

D. Multiport Diffusers in a Shallow, Flowing Environment

Frequently, diffusers may be placed in relatively shallow waters. For this discussion, shallow will be defined as z_1/D_o less than 20. Recall that Liseth worked in the range of z_1/D_o from 52 to 222. Harleman *et al.*[50] studied, both analytically and with physical models, diffusers in a shallow receiving body. Their findings are significant for such shallow environments.

1. Experimental and Analytical Findings

Harleman *et al.* observed that for such shallow conditions, the heated discharge tends to mix completely both laterally and vertically. The maximum surface temperature is nearly equal to the fully mixed temperature. They note that this temperature is not dependent upon F_j, z_1/H, or the angle of the ports, Θ_o', for small angles. For ports discharging into a stagnant environment, the following expression is developed and verified as an *upper limit* on the dilution:

$$D = 1.3\sqrt{\frac{WH}{D_o^2}} \ , \qquad (7.3)$$

where D = dilution = $\Delta T_o/\Delta T_{surface}$,

W = port spacing,

H = receiving-water depth, and

D_o = port diameter.

If the water truly is stagnant and no new water is being moved into the region near the diffuser, there is bound to be some reentrainment of water. Therefore, the actual dilution for such a case is probably considerably less than given by Eq. 7.3.

Harleman *et al.* found that ports discharging perpendicularly to the ambient current always experience reentrainment of the heated waters. For ports discharging parallel to the ambient current, reentrainment will occur for low ambient currents, U_a, regardless of the discharge orientation -- all ports upstream, all ports downstream, or all ports alternating in direction. In fact, an effective blockage of dilution water to the diffuser occurs when the ports are directed upstream against a weak ambient current. In this case, a large eddy forms near the diffuser and (Ref. 50, pp. 64-66) "...the heated flow is circulated within this restricted eddy area resulting in temperature rises increasing with time until some equilibrium condition is reached. Dilutions are worse than predicted by the ratio of cross flow to diffuser flow." Some experiments were conducted for a time-varying ambient crosscurrent. In this case, due to reentrainment, maximum temperature rises occur at the time of minimum ambient current. The exact magnitude of the temperature rise depends on the precise form of time variation and the diffuser details. In general, the maximum temperature rise under these conditions can be decreased by increasing W, the port spacing.

For discharges parallel to an ambient current, Harleman *et al.* developed some simplified theoretical relations for the dilution. They wrote an energy equation equating external energy input to energy losses due to expansion and contraction of the flow field and bottom friction. Empirical coefficients in the derived equations were evaluated from experiments. The following equations apply:

For ports all directed with ambient current,

$$D = \left[\left(\frac{4U_a WH}{\pi U_o D_o^2}\right)^2 + \left(\frac{8WH}{5\pi D_o^2}\right)\right]^{1/2} ; \qquad (7.4)$$

for ports all directed against the current,

$$D = \left[\left(\frac{4U_a WH}{\pi U_o D_o^2}\right)^2 - \left(\frac{8WH}{3\pi D_o^2}\right)\right]^{1/2} , \qquad (7.5)$$

for ports alternately directed,

$$D = \frac{4U_a WH}{\pi U_o D_o^2} . \tag{7.6}$$

Note that Eq. 7.6 is merely the dilution due to complete mixing, since it represents the ratio of the ambient flow over one diffuser port ($U_a WH$) to the flow from a single diffuser port ($\pi U_o D_o^2/4$). Equation 7.5 is only valid for positive values under the square-root sign. In fact, one criterion for the blockage of dilution flow mentioned earlier is the equality of the two terms under the square-root sign in Eq. 7.5. If these two terms become equal, blockage and subsequent higher temperature rises are expected.

The reader is referred to Ref. 50 for excellent experimental result that graphically help in understanding the mechanisms of mixing for shallow-water diffusers.

These conclusions were drawn based on the following ranges of parameters:

W/H: 0.641-3.00,

D_o/H: 0.057-0.161,

F_j: 10.4-115.8, and

z_2/H: 0.187-0.465.

2. Numerical Example

Consider the following case: U_a = 0.5 ft/sec, U_o = 12 ft/sec, H = 17 ft, W = 64 ft, D_o = 1.5 ft, and ΔT_o = 20°F. If the ports are in alternating directions, Eq. 7.6 applies, so that

$$D = \frac{4(0.5)(64)(17)}{12\pi(1.5)^2} = 25.7 .$$

Then

$$\Delta T_{surf} = \Delta T_o/25.7 = 20/25.7 = 0.8°F .$$

If the ports were all in the same direction as the ambient current, Eq. 7.4 becomes

$$D = \left[\left(\frac{4(0.5)(64)(17)}{12\pi(1.5)^2}\right)^2 + \frac{8(64)(17)}{5\pi(1.5)^2}\right]^{1/2} = 30.1 .$$

Then

$$\Delta T_{surf} = 20/30.1 = 0.66°F .$$

Use of Eq. 7.5 is the equivalent of treating the same problem for a reversal of tide. The opposing direction of flow reduces the dilution.

E. Multiport Diffusers into Stagnant, Intermediate Depths

1. Experimental Findings

Larsen and Hecker[76] have presented results for multiport discharges into a stagnant environment. The study is completely experimental. Ranges of parameters studied included the following:

Set 1: F_j = 20 all runs; z_1/D_o = 10, 20, 30; W/D_o = 4-28; h/D_o = 27, 37, 47.

Set 2: z_1/D_o = 20 (all runs); h/D_o = 37 (all runs); W/D_o = 10 (all runs); F_j = 8-25.

Notice that $H/D_o = z_1/D_o + 17$, since the ports were located $17D_o$ above the bottom of the receiving tank. Based on the values of H/D_o, this is classed as an intermediate depth. Liseth[87] studied the range of H/D_o above 50; Harleman *et al.*[50] studied shallow diffusers, H/D_o between 6 and 18.

An important note should be listed concerning the H/D_o values shown for the Larsen and Hecker data. These values, as indicated, include 17 diameters below the experimental discharge ports. However, standard diffuser designs have ports located usually only 2-4 diameters above the bottom. The submergence z_1/D_o is therefore a more meaningful parameter for their data, as it shows the relative distance from diffuser port to water surface, the distance over which mixing occurs. For the most part, the 17 diameters below the ports in Larsen and Hecker's work really do not effectively increase the submergence.

In the studies by Larsen and Hecker, dilutions were determined by actual temperature measurements on the water surface, rather than below the surface layer as Liseth did. Single-jet studies were also made, and the dilutions for the variety of port configurations were compared to those for a single jet. This gives some measure of jet interference. For F_j = constant = 20, Larsen and Hecker find minimum single-jet dilutions of 12.4, 19.7, and 29.3 for z_1/D_o = 10, 20, and 30, respectively. For z_1/D_o = constant = 20 (H/D_o = 37), dilution increased from 14.8 for F_j = 8 to 21.7 at F_j = 23.5. Therefore, dilution can be seen to increase with increasing depth (longer distance of travel, hence more dilution, before reaching surface), and also with increasing Froude number (again caused by longer travel distance).

Figures 7.6 and 7.7 show some of the significant experimental findings by Larsen and Hecker. In these figures, D_m is the surface dilution for multiple ports and D_s is the surface dilution for a single jet. Therefore, if D_m/D_s = 1.0, the jet spacing is such that the jets do not interact before reaching the surface. It is interesting to compare results in Figs. 7.6 and 7.7 with the work done by Liseth and Harleman *et al.* First, notice in Fig. 7.7 that dilution for the multiport diffuser is a function of F_j for H/D_o from 27 to 47. For Larsen and Hecker's work, $H/D_o = z_1/D_o + 17$. The work of Harleman *et al.* implies that dilution is not a function of F_j. However, the Harleman study was for much more shallow receiving bodies (H/D_o = 6 to 18). Free surface and bottom boundary influences are more dominant in such shallow

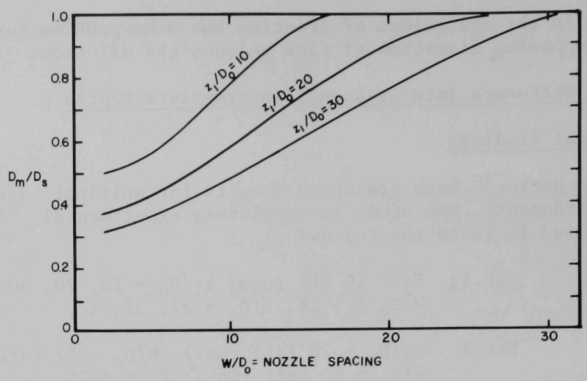

Fig. 7.6. Jet Interference vs Nozzle Spacing and Submergence at Froude Number $F_j = 20$.[76]

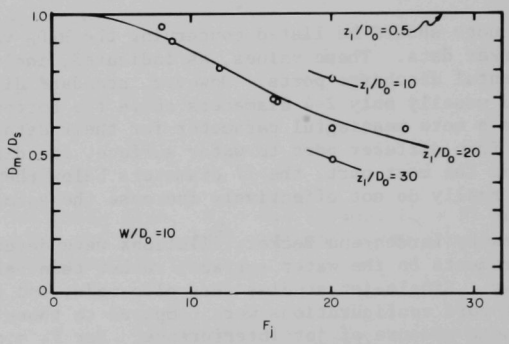

Fig. 7.7. Jet Interference vs Froude Number at Spacing $W/D_o = 10$.[76]

bodies, enhancing the prospect of complete mixing. In addition, Harleman *et al.* observed stratification (incomplete mixing) for F_j as low as about 15. Note that the two dilution values ($z_1/D_o = 20$) for $F_j = 20$ and 25 in Fig. 7.7 are almost identical. The difference in the Larsen-Hecker and Harleman *et al.* results can then be attributed to two factors: (1) different ranges of H/D_o, and (2) different ranges of F_j (most of the Harleman *et al.* runs were for $F_j > 20$). This difference points out the danger inherent in using results outside their range of verification.

Liseth reports findings that alternating port discharges behave like single jets (no interaction) if z_1/W is less than 5. Note that W is the spacing between any two ports; therefore, the spacing between any two ports

on the same side of the diffuser is 2W. Larsen and Hecker's results can be converted to z_1/W by dividing z_1/D_o by W/D_o. In Fig. 7.6, for Froude number, $F_j = 20$, notice the intersection of the three curves with the $D_m/D_s = 1.0$ line. For $z_1/D_o = 10$, 20, and 30, the critical values of z_1/W are 0.6, 0.75, and 1.0, respectively. This means that for any values of z_1/W greater than these values, the jets will interact before reaching the surface and will not behave as single jets. These results contradict those of Liseth, who specified $z_1/W = 5$ as the critical value. Larsen and Hecker suggest that one difference is that their measurements are made at the surface, while Liseth makes his measurements below the heated surface layer. Additionally, Liseth's studies are in the range of $(z_1/D_o)/F_j = 2$ to 20. Larsen and Hecker vary this parameter from 0.5 to 2.5, or essentially below the range of Liseth's work. A review of Liseth's work reveals that, for the range of parameters he uses, dilutions are essentially identical for $z_1/W = 5$ and $z_1/W = 0$. The latter is the case of a single port. A review of Larsen and Hecker's results in Fig. 7.7 reveals that the single-jet case is approached as $(z_1/D_o)/F_j$ increases. Consider, for example, $z_1/D_o = 20$ and $F_j = 8$ [implies $(z_1/D_o)/F_j = 2.5$]. The dilution is about 95% of that for a single jet. Therefore, the major difference between the results of Liseth and those of Larsen and Hecker seems to lie in the ranges of $(z_1/D_o)/F_j$. This parameter is a measure of the relative depth compared to the mixing strength of the jets. It would be well then to use the work of Liseth and of Larsen and Hecker as complementary information, employing the results only within the ranges of parameters for which they are developed.

2. Numerical Example

To use the results of Larsen and Hecker as shown in Figs. 7.6 and 7.7, the dilution for a single jet must be estimated. This can be done using any of the models suggested in Chapter VI. In addition, results from Rawn *et al.** are available, as well as some information presented by Larsen and Hecker themselves. consider the following example:

$z_1 = 30$ ft,

$D_o = 1.5$ ft,

$U_o = 6$ ft/sec,

$U_a = 0$,

$W = 15$ ft,

$\Delta T_o = 18°F$ (from 59 to 77 °F),

$\rho_a = 0.99913$ for 59°F, and

$\rho_o = 0.99707$ for 77°F.

First, F_j must be calculated as

$$F_j = \frac{U_o}{\sqrt{g \frac{\Delta\rho}{\rho} D_o}} = \frac{6}{\sqrt{32.2(0.00206)(1.5)}} = 19 .$$

*A. M. Rawn, F. R. Bowerman, and N. H. Brooks, *Diffusers for Disposal of Sewage in Sea Water*, J. Sanit. Eng. Div., Am. Soc. Civil Eng. 86(SA2), 65-106 (1960).

For $z_1/D_o = 30/1.5 = 20$, Larsen and Hecker indicate a surface dilution of $D_s = 19.1$ for $F_j = 19$ for a single jet. Figure 7.7 can be used for $W/D_o = 15/1.5 = 10$ and $F_j = 19$ to find $D_m = 0.65D_s = 0.65(19) = 12.3$ The actual predicted surface temperature rise, ΔT_s, is then

$$\Delta T_s = 18/12.3 = 1.46°F .$$

F. Conclusions -- Multiport Diffusers

Multiport, submerged-diffuser discharges of heated water are becoming more popular. Several sets of experimental data have been presented along with a computer model, to aid in evaluating such discharge schemes. At the outset, one can discern some areas in which no work has been done. First, there is no model for discharge into an ambient current parallel to the main-diffuser-pipe axis. These two cases are very complex. As with surface discharges, short of going to physical models, transient conditions are handled only by application of steady-state models to selected critical conditions. Table 7.1 summarizes regions of applicability of the models discussed here.

Table 7.1. Applicability of Submerged-multiport-diffuser Information

Feature	*Stagnant Ambient*	*Flowing Ambient*
Deeply submerged ($H/D_o > 50$)	Liseth; Koh and Fan	None
Intermediate submergence ($30 < H/D_o < 50$)	Larsen and Hecker; Koh and Fan	None
Shallow submergence ($H/D_o < 20$)	Harleman *et al.*; Koh and Fan	Harleman *et al.*
Stratified receiving waters	Koh and Fan	None
Alternating ports	Liseth	Harleman *et al.*
Transient	None[a]	None[a]

[a]*Except by application of steady-state approximation.*

All the studies shown, except Koh and Fan,[73] represent experimental studies, with some analysis. The Koh and Fan model has not been verified in total. It is especially uncertain that the model can be adequately applied in shallow waters, where the free surface may have a real impact on mixing conditions. None of the results shown in this chapter should be applied outside the range for which they are verified. Table 7.2 summarizes the ranges of some pertinent parameters. The reader is referred to the basic references for details of what combinations were run within the ranges noted.

Table 7.2. Ranges of Parameters for Studies Reported

Parameter	*Liseth*[86]	*Larsen and Hecker*[76]	*Harleman et al.*[50]
H/D_o	52-222	27-47	6-18
F_j	10-61	8-25	10-115
W/D_o	1.7-168	4-28	5-40
H/W	0-80	1.3-9.3	0.3-1.6
$(z_1/D_o)/F_j$	2-20	0.5-2.5	0.06-1.8

The biggest breakpoints in Table 7.2 occur in those parameters that indicate relative depth of submergence. Liseth's results apply to deeply submerged diffusers; the Larsen-Hecker results are for intermediate submergence; and the work by Harleman *et al.* covers shallow-water diffusers.

One piece of important work on submerged diffusers (and single-port submerged discharges) is Ref. 123. It is a compilation of 180 graphs showing the solutions to a wide variety of submerged jet problems. It is based on the Fan,[38] Hirst,[54] and Koh and Fan[73] models. The ranges of parameters it covers are

F_j: 1-600,

Θ_o': 0-90°, and

k: 0.5-16.

Stratification of the receiving waters, submergence of the discharge, and port spacing are also varied. Not all combinations of the parameters listed exist. The publication has been prepared with care to avoid extrapolation outside the range of verifying data. This publication should be a helpful tool and will, for many cases, negate the need for a computer to operate the Koh and Fan model.

VIII. COOLING PONDS

A. Introduction

The objective of this chapter is to discuss some of the present methods used in predicting cooling-pond performance. As will become evident, the accuracy of these methods depends primarily on empirical values such as equilibrium temperature, cooling coefficients, and mixing coefficients. Another limiting criterion is the assumption of steady-state conditions, which are assumed, to varying degrees, by all the methods discussed. Therefore, these predictive methods for cooling-pond performance should always be accompanied with an awareness of their limited accuracy. As a general rule, a difference of less than 3°F between actual effluent temperatures and predicted effluent temperatures is considered excellent, and differences as large as 3-5°F are acceptable.

The models in this chapter are arranged in an order chosen to help the reader in his understanding. Initially, the hydraulic classification of cooling ponds is discussed. The next section presents the Edinger-Geyer model, which uses the equilibrium-temperature concept to analyze idealized ponds. Section D presents the Thackston-Parker model, which provides a convenient method for estimating the performance of a pond. Section E presents the more detailed Littleton model. Use of this model allows one to make a more comprehensive analysis and to investigate the transient nature of a cooling pond. Sections F and G discuss an entrance entrainment model and one developed by Edinger. These models remove the idealized hydraulic restrictions present in the first three models and thus consider modeling real ponds. Next, the problem of evaluating the water loss due to elevated temperatures is discussed. Then a section on deep-reservoir modeling is presented. Finally, a concluding section provides a general overview of the tools for cooling-pond analysis presented in this chapter.

B. Hydraulic Classification of Cooling Ponds

The hydraulic characteristics of cooling ponds represent the area of least understanding. Although widespread work has been conducted regarding predictive techniques for the cooling capacity of a cooling pond, predictive techniques to describe the hydraulic action of a pond are nonexistent. Predictive technique, as used in this chapter, refers to a technique to completely describe the actual physical performance without constructing a physical model or running field tests on the prototype. Keeping in mind this definition of predictive technique and particularly the nonexistence of such hydraulic techniques, the following are offered as possible hydraulic classifications of ponds.

1. Completely Mixed Ponds

One assumption that can be made concerning the hydraulic nature of a pond is that it is completely mixed. To be completely mixed, a slug of water entering a pond would be immediately mixed uniformly throughout the pond. For a specific time, a completely mixed pond would have the following characteristics:

a. $T_p \neq fn(x)$;

b. $T_{EFF} = T_p$; (8.1)

c. $T_{EQ} - T_P$ = cooling driving force = $C_1 \neq fn(x)$.

In Eq. 8.1, x is the distance from pond intake to some point of interest, T_p is the pond temperature, T_{EFF} is the effluent temperature, T_{EQ} is the equilibrium temperature, and C_1 is some constant. Equation 8.1c deals with the cooling rate of a pond and is one method of simplifying the heat-budget equation as discussed in Chapter III.

The hydraulic characteristics of a completely mixed, continuous-flow pond can best be physically described by an example. Assume that one has a conservative dye--"conservative" meaning that dilution is the only mechanism available to reduce its concentration. Heated water is an example of a non-conservative element, because both dilution and loss of heat to the atmosphere tend to reduce the temperature. Further assume that a single slug of this dye is instantaneously injected into the intake of the pond. A graphical representation of this input is shown in Fig. 8.1a. The value C_o in Fig. 8.1a is the concentration that would be present if an equal amount of dye was uniformly mixed throughout a batch (or non-continuous flow) tank of a volume equal to that of the pond. Thus, the input to the completely mixed pond would be a spike occurring at time t equal to zero, the area under the spike in Fig. 8.1a being proportional to the amount of dye injected. In keeping with the definition of a completely mixed, continuous-flow pond, the instant the slug of dye entered the pond it would be equally distributed throughout the pond. Therefore, to measure the concentration at the effluent, one would measure a concentration equal to C_0 at time t = 0. At some time increment later, the effluent concentration would be less than the value C_0. This reduction occurs because, as a given volume of water that contains dye leaves in the effluent, an equal reduction in pond and effluent concentration results. Figure 8.1b is a plot of effluent concentration versus time for the process just discussed. The curve in Fig. 8.1b is exponential in form. Additional information on the subject of flow-through curves appears in Ref. 84.

The main disadvantage of this type of flow regime is the constant driving force expressed in Eq. 8.1c. In keeping with the definition of a completely mixed pond, the hot water entering the pond is immediately mixed with cooler pond water, reducing the cooling driving force. Consequently, the maximum driving force is a weighted average of the two temperatures.

Completely mixed conditions are common in waste-treatment facilities where small flow-through times exist and high degrees of turbulence or mixing are prevalent. In cooling ponds, however, large flow-through time with low turbulence is a common situation. Therefore, very few ponds, if any, could be classed as completely mixed.

2. Plug-flow Ponds

A second type of hydraulic-flow regime is plug flow. Under plug-flow conditions, a slug of water would enter a pond and retain its identity

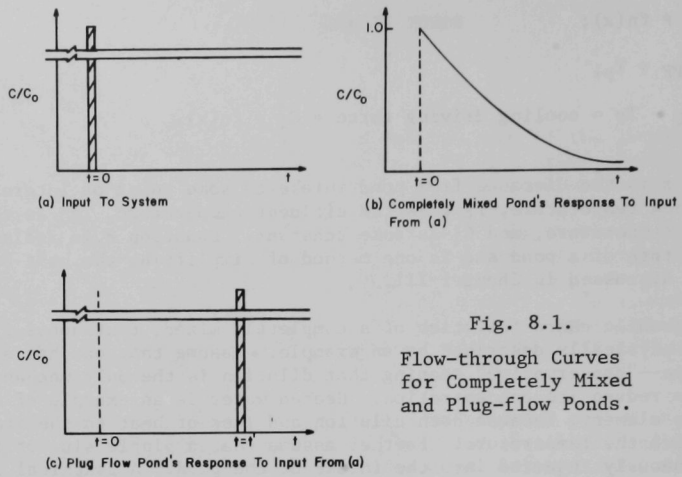

Fig. 8.1.

Flow-through Curves for Completely Mixed and Plug-flow Ponds.

throughout its complete journey, not mixing with any foreign water. For a specific time, a plug-flow pond would have the following characteristics:

a. $T_p = fn(X)$;

b. $T_{EFF} = T_p$ at $X = L$; (8.2)

c. $T_{EQ} - T_p$ = driving force = $fn(X)$;

where L is the distance from intake to outlet of a pond.

To help understand the hydraulic characteristics of a continuous-plug-flow pond, assume that the input spike represented in Fig. 8.1a is now injected into this type of pond. Under plug-flow conditions, the slug would retain its identity and arrive at the effluent intact. The time of arrival at the effluent is called the detention time, t', and is equal to the rate of flow through the pond divided by the volume of the pond.

A main advantage of plug flow can be seen in the driving-force term expressed in Eq. 8.2c. In keeping with the definition of plug flow, the hotter water entering the pond would *not* mix with any cooler water. Consequently, the maximum driving force for cooling would be retained at all locations throughout the pond.

Thackston and Parker[136] discuss some physical characteristics of a plug-flow pond. Of major importance is the long, slender, channellike shape that aids plug-flow conditions. Outlet and intake at opposite ends, and narrow widths (to decrease wind mixing) also aid in inducing plug-flow conditions. Concerning depth, Thackston and Parker state that shallow depth and a low flow rate to reduce vertical velocity gradients are physical characteristics that promote plug-flow conditions.

3. Actual Ponds

The two classifications mentioned above are the two extremes. The active region of actual ponds, that portion of the pond that is actually part of the flow regime, will be a combination of the two extreme conditions. An example of active versus dead areas can be found in a square pond. In such a pond, the center portion is part of the flow regime while the corners would be dead regions where small flows occur.

An often-made assumption is that the performance of a cooling pond will fall somewhere between that of a completely mixed pond and that of a plug-flow pond of the same volume and surface area. This assumption is only true, however, if the active region of the actual pond is more or less equal to that of the completely mixed and plug-flow ponds. In most ponds, especially in those where the water's edge is determined by a natural contour, the actual performance of the pond may be below the so-called conservative performance of a completely mixed pond. One reason for this poor performance of actual ponds is often that flow-through calculations are based on the total volume instead of the volume of the active region. Such miscalculations result in gross overestimates of the flow-through time and, consequently, of the performance. Methods for estimating a pond's actual performance are discussed in Secs. G and H of this chapter.

In assessing active and dead regions, Ryan[119] notes that density currents in the pond may play a major role in moving heated water into some of the backwaters, embayments, etc., which would ordinarily be passive (inactive) regions. He cites some examples of this effect, but he notes that it may be necessary to build a physical model to fully assess this effect.

Cooling-pond analysis can be extended to other bodies of water if these bodies satisfy certain hydraulic conditions. The dissipation of excess heat from a cooling pond is basically a surface phenomenon. This is because most cooling ponds are shallow bodies of water taking advantage of the far more rapid cooling ability of surface cooling versus the slower cooling ability of conductive heat losses obtained at the walls of the pond. Therefore, most cooling-pond models assume no temperature gradient in the vertical or horizontal direction. Realization of these assumptions limits cooling-pond models to regions of a body of water that satisfy these assumptions.

A cooling-pond model could be applicable to a deep reservoir during a period of strong stratification, at which time all the excess heat would be contained within the upper layer, or epilimnion, of the lake. In most cases, the epilimnion satisfies all the criteria for cooling ponds mentioned above and thus can be treated as a cooling pond. Once strong stratification has been determined, the active and dead regions of flow of the epilimnion must still be analyzed.

Several other features of actual ponds are important in pond performance. Ryan[119] presents the best currently available review of these factors. Some of the more important ones will be mentioned here. For example, if one considers a pond as part of a closed system (intake and outlet on same body of water), then the inlet should be designed to take water from the bottom of the ponds. Such deep withdrawals will minimize possible short-circuiting of the hot water and also provide the coolest possible water to the condensers.

This deep withdrawal can be accomplished by (1) building the intake pipe or other structure out into some deeper part of the pond, or (2) providing a deep skimmer wall at the inlet-channel entrance so that only deeper waters are withdrawn.

Another important physical factor for any pond is wind. Ryan notes several effects of wind, but perhaps the major one is the ability to enhance or inhibit short-circuiting. As a general guideline, a pond should be designed so that the prevailing wind during the summer blows from the inlet toward the outlet. This will help prevent short-circuiting, causing the heated water to be slowed in its movement toward the intake.

Entrance mixing, which can be closely controlled by design of the outlet channel, plays an important role in determining the temperature at which most of the heat transfer to the atmosphere takes place. This feature is discussed more fully later in this chapter. In addition to consideration of winds, the inlet and outlet must be carefully placed so that short-circuiting is made more difficult by geometry. In addition to natural geometric constraints, it may be more desirable to provide some man-made boundaries to produce flow patterns maximizing the surface area of the heated discharge exposed to heat exchange with the atmosphere. This can be done by building dikes inside the cooling pond (usually done by merely pushing up some soil). (See Ref. 119 for a discussion of some possible schemes.)

The pond depth is another important parameter, inasmuch as it contributes to the determination of whether the pond will be stratified. In general, then, the designer should seek out all available information that will help describe the behavior of the pond. Such knowledge of the system should result in better designs.

4. Pond Optimization

Although topography and climate play a major role in determining pond performance, the designer does have available to him several options that can lead to enhanced cooling. Variation of intake and outfall location and flow rate has already been mentioned as a possibility. For example, a lower-velocity surface discharge will yield a lower initial dilution than a high-velocity discharge, therefore leaving higher surface temperatures for dissipation to the atmosphere.

In making an economic analysis to choose an optimum pond size, Ryan notes that the following must be considered: land cost, reduction in plant capacity due to back pressure, cost of makeup water, effect of discharge temperature, and temperature rise across the condenser. Hogan *et al.*[56] perform an analysis of this sort, although they neglect the cost of makeup water. Here the designer can begin to make tradeoffs. Do the added benefits offset the costs for doing such things as internal diking to help the flow pattern or designing a better outlet? A careful analysis can lead to a pond design that not only performs its role as a cooling agent but that at least approaches economic efficiency.

References 70, 88, and 119 contain additional discussion of the hydraulic characteristics of actual ponds.

C. Equilibrium-temperature Model for Cooling Ponds

The operating mode of a pond influences its performance. The two basic types of operation are recirculation and once-through cooling. Recirculation ponds are those whose effluent waters are returned directly to the condenser intakes. Thus, a recirculation pond forms a closed system with the power plant. In once-through cooling, however, the condensers take their water from a body of water other than the cooling pond. Under once-through operation the pond serves as a buffer to prevent the waters receiving its effluent from being damaged. These two types of operation will be discussed separately here.

1. Once-through Cooling Ponds

This model is a direct application of the Edinger-Geyer[32] equilibrium-temperature representation discussed in Chapter III. The following assumptions are made:

a. A steady-state condition prevails. This means that the flow into the pond, the cooling coefficient, and the equilibrium temperature are not a function of time and that the pond's temperature, which these parameters determine, is constant with time.

b. The only source of mass input to the system is the pond intake, and the only source of mass leaving the system is the pond effluent. Under this assumption, terms such as evaporation and seepage terms and minor sources of inflow and outflow are considered negligible. Thus, this assumption eliminates the necessity for a complete mass balance and requires only a heat balance of major terms.

Use of the steady-state assumption means that the heat in minus the heat out of the pond must equal the heat dissipated by the pond. Thus, under steady-state conditions, the following equation can be derived for a once-through pond:

$$\rho C_p q_p (T_{IN} - T_{EFF}) = KA(T_p - T_{EQ}) \ , \tag{8.3}$$

in which T_{IN} is the intake temperature of the pond, K is the cooling coefficient, A is the area of the pond, ρ is the density of the pond water, C_p is the coefficient of heat for the pond water, q_p is the intake flow of the pond, T_{EFF} is the pond effluent temperature, and T_{EQ} is the pond equilibrium temperature.

Letting $r_1 = KA/(\rho C_p q_p)$ reduces Eq. 8.3 to

$$T_{IN} - T_p = r_1(T_p - T_{EQ}) \ . \tag{8.4}$$

Since $T_p = T_{EFF}$ in a completely mixed pond, Eq. 8.4 can be rearranged to give

$$\frac{T_{EFF} - T_{EQ}}{T_{IN} - T_{EQ}} = \frac{1}{r_1 + 1} \ . \tag{8.5}$$

Using the same approach for a plug-flow pond results in

$$\frac{T_{EFF} - T_{EQ}}{T_{IN} - T_{EQ}} = \exp(-r_1) \ . \tag{8.6}$$

Equations 8.5 and 8.6 allow one to compare the relative efficiencies of the two types of ponds. Equating these two equations gives

$$\frac{\left(T_{EFF} - T_{EQ}\right)_{CM}}{\left(T_{EFF} - T_{EQ}\right)_{PLUG}} = \frac{\exp(r_1)}{1 + r_1} \tag{8.7}$$

Table 8.1 gives the ratio of the area of a completely mixed pond to that of a plug-flow pond for the same value of the left-hand term in Eqs. 8.5 and 8.6. As can be observed in the table, when the required amount of cooling is small (when the left sides of Eqs. 8.5 and 8.6 are close to unity), there is little difference between the two ponds. However, as the demand for cooling is increased, the plug-flow pond becomes more advantageous.

Table 8.1. Comparison of Completely Mixed and Plug-flow Ponds

Temperature-excess Ratio, $(T_{EFF} - T_{EQ})/(T_{IN} - T_{EQ})$	*Ratio of Areas,* A_{CM}/A_{PLUG}
0.8	1.12
0.7	1.20
0.6	1.30
0.5	1.44
0.4	1.64
0.3	1.95
0.2	2.47
0.1	3.87

As an example, assume the same meteorological data used in the examples from Chapter III. In addition, the following data are given:

Power-plant size = 1000 MW;

Plant flow = 1350 cfs = 11.6×10^7 ft^3/day;

Temperature rise through condensers = 15°F;

Pond depth = 15 ft;

Surface areas of pond = 800 acres = 3.485×10^7 ft^2;

1500 acres = 6.534×10^7 ft^2;

2200 acres = 9.583×10^7 ft^2;

Initial uniform pond temperature = 72°F.

Some of the data above are not necessary for this example; however, the data will be used for other examples in this chapter, and it is felt having them all present at one location will aid in understanding the examples.

The initial step in the Edinger-Geyer solution is to calculate r_1:

$$r_1 = \frac{KA}{\rho C_p q_p} .$$

As was noted in Chapter III, there are three evaporation formulas that lead to three different T_{EQ} and K values. Using only the two extreme values of K and T_{EQ} and the three pond areas, one gets six different values of r_1. As an initial step, consider only the 800-acre pond; the upper limit K, K = 167 Btu/ft^2-day-°F; and the upper limit T_{EQ}, T_{EQ} = 82.1°F. Therefore,

$$r_1 = \frac{(167 \text{ Btu/ft}^2\text{-day-°F})(3.485 \times 10^7 \text{ ft}^2)}{(62.4 \text{ lb}_m\text{/ft}^3)(1 \text{ Btu/lb}_m\text{-°F})(11.86 \times 10^7 \text{ ft}^3\text{/day})} = 0.788 .$$

Assuming that the condenser water intake is at equilibrium temperature allows one to calculate the inflow temperature to the pond as

$$T_{IN} = T_{EQ} + \Delta T_C = 82.1 + 15.0 = 97.1°\text{F} .$$

Therefore, the effluent temperature for a completely mixed pond is

$$T_{EFF} = \frac{T_{IN} + r_1 T_{EQ}}{r_1 + 1} = \frac{97.1 + 0.788(82.1)}{1.788} = 90.4°\text{F} .$$

The effluent temperature for a plug-flow pond is

$$T_{EFF} = T_{EQ} + e^{-r_1}(T_{IN} - T_{EQ}) = 82.1 + e^{-0.788}(97.1 - 82.1)$$
$$= 88.9°F \ .$$

Table 8.2 summarizes the results of using both upper and lower values of K and T_{EQ}, plus the effect of pond area for completely mixed and plug-flow ponds with once-through cooling.

Table 8.2. Results from Example Problem for Once-through Cooling

	T_{EFF}, °F			
	Completely Mixed		*Plug Flow*	
Area, acres	*Upper Limit*	*Lower Limit*	*Upper Limit*	*Lower Limit*
800	90.4	99.6	88.9	99.0
1500	88.3	97.6	85.5	95.8
2200	86.8	96.0	83.8	93.7

Note: Upper limit = K = 167 Btu/ft^2-day-°F, T_{EQ} = 82.1°F.
Lower limit = K = 98 Btu/ft^2-day-°F, T_{EQ} = 89.5°F.

These values are plotted in Fig. 8.9, which is introduced later (p. 288) to illustrate all the methods of calculations.

2. Recirculating Cooling Ponds

The heat into a recirculating cooling pond is equal to the heat added to the cooling water by the power plant, Q_h, and is equal to

$$Q_h = \rho C_p q_p (T_{IN} - T_{EFF}) \ , \tag{8.8}$$

in which T_{IN} is not only the input temperature of the pond but also the exit temperature from the condensers, T_{EFF} is not only the effluent temperature of the pond but also the intake temperature of the condensers, and $T_{IN} - T_{EFF} = \Delta T_c$ and is the condenser temperature rise at flow rate q_p. Substituting Q_h in place of the "heat-in" portion of Eq. 8.3 results in the following equation for a completely mixed pond:

$$T_{EFF} = \text{temperature of condenser intake} = \frac{Q_h}{KA} + T_{EQ} \ . \tag{8.9}$$

Using the same approach for a plug-flow pond results in

$$\frac{T_{EFF} - T_{EQ}}{\Delta T_c} = \frac{\exp(-r_1)}{1 - \exp(-r_1)} . \tag{8.10}$$

As an example, assume the same data as used in the once-through, completely mixed cooling-pond example. Therefore,

$$Q_h = \rho C_p q_p \Delta T_c$$

$$= (62.4\ lb_m/ft^3)(1\ Btu/lb_m\text{-}°F)(11.86 \times 10^7/ft^3/day)(15°F)$$

$$= 11.1 \times 10^{10}\ Btu/day .$$

Considering the 800-acre pond at the upper limit of T_{EQ} and K gives

$$T_{EFF} = \frac{Q_h}{KA} + T_{EQ} = \frac{11.1 \times 10^{10}}{167(3.485 \times 10^7)} + 82.1 = 101.2°F .$$

Thus the steady-state effluent temperature for the 800-acre pond is 101.2°F for a closed cycle and 90.4°F for once-through cooling.

Considering the data above, but applying it to an 800-acre, recirculating plug-flow pond, results in

$$r_1 = 0.788 ,$$

$$\frac{T_{EFF} - T_{EQ}}{\Delta T_c} = \frac{\exp(-r_1)}{1 - \exp(-r_1)} = 0.833 ,$$

and

$$T_{EFF} = (0.833)(15°F) + 82.1 = 94.6°F .$$

Table 8.3 summarizes the results of using both upper and lower values of K and T_{EQ} from Chapter III, plus the effect of pond area for recirculating ponds. (These values are plotted in Fig. 8.9.)

D. First Trial Model for Cooling Ponds

Thackston and Parker[136] presented a method for calculating a general, first-trial estimate of a cooling pond's performance for any location in the United States. They compiled weather data from 88 locations within the United States. The final form of their data consisted of average monthly

Table 8.3. Results from Example Problem for Recirculating

	T_{EFF}, °F			
	Completely Mixed		*Plug Flow*	
Area, acres	*Upper Limit*	*Lower Limit*	*Upper Limit*	*Lower Limit*
800	101.2	122.1	94.6	115.0
1500	92.3	106.8	86.6	100.5
2200	89.0	101.3	84.0	95.4

values for the required parameters for their heat-budget equation (see Chapter III). They also compiled the extreme monthly values for these input parameters. For the average monthly values, the values for a particular parameter are merely averaged for a particular month for the entire historical record. From this historical record of monthly averages, the worst 10% are picked and averaged to derive the extreme values for each parameter.

With these average and extreme values, the average and extreme equilibrium temperature and exchange coefficient can be calculated for each month of the year (see Fig. 8.2). Thackston and Parker also included a plot of plant temperature rise versus month of the year for three different completely mixed ponds (see Figs. 8.2c and d). To arrive at these plots, they assumed that each pond was receiving the heat load from a 1000-MW power plant operating at 38% efficiency. They then used the Edinger-Geyer equation for a completely mixed pond to calculate the effluent temperature in terms of the plant temperature rise (the °F above the equilibrium temperature of the pond's effluent water, assuming that the power-plant intake is receiving water at the equilibrium temperature).

Based on Figs. 8.2a and b, one can calculate the necessary pond size to obtain a predetermined plant temperature rise at or near any of the 88 locations. The following example demonstrates the solution to this type of problem.

> Example: What size pond would be required so that the maximum plant temperature rise will not exceed 7°F under normal conditions? The plant is located in Nashville, Tennessee, and is loaded by a 1000-MW power plant operating at an efficiency of 38%. The initial step is to plot plant temperature rise versus pond surface area (see Fig. 8.3). To create this plot, one reads values of plant temperature rise for each month for the three ponds sizes calculated in Fig. 8.2c. A contour for each month can be created by connecting a line of best fit through these three points. Once Fig. 8.3 is drawn, one enters the plot at the predetermined plant temperature rise and reads across, until the 7° line intercepts a month contour line. He then reads down to the necessary area. In this example, the months of January,

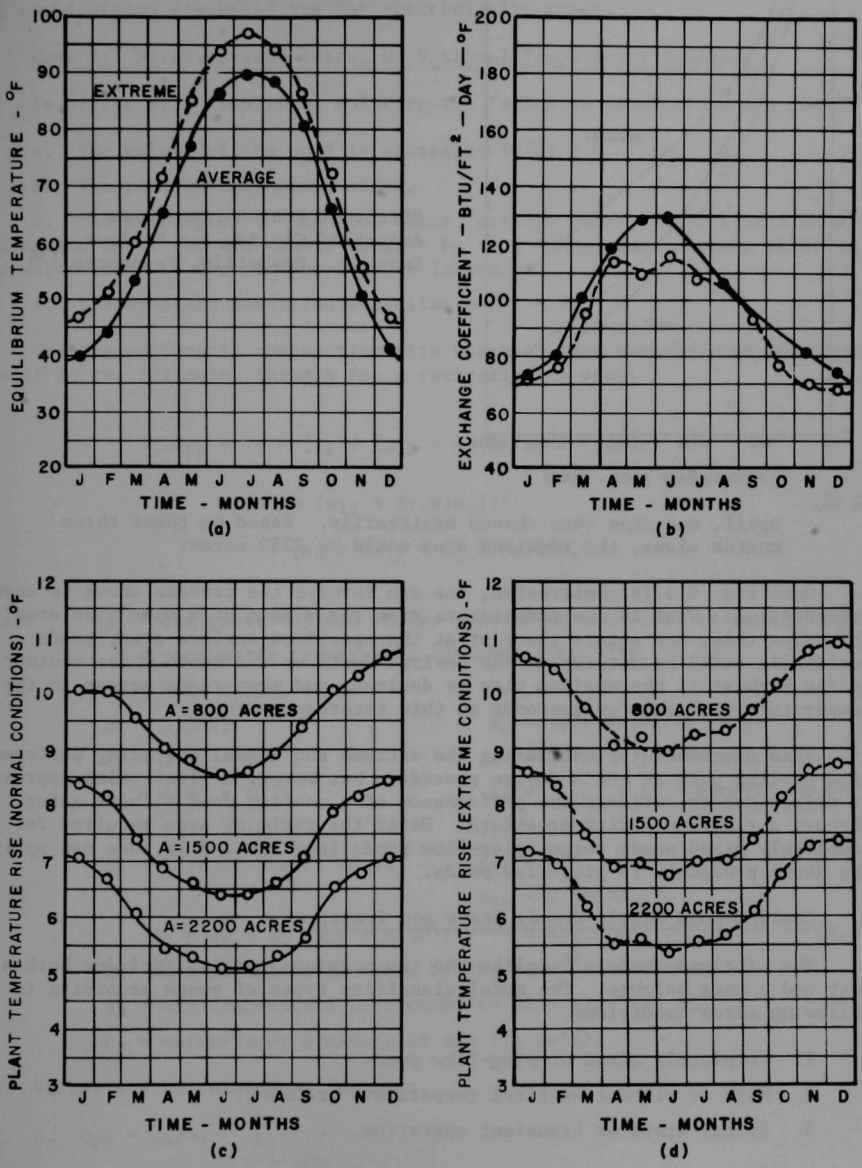

Fig. 8.2. Results for Nashville, Tennessee.[136]

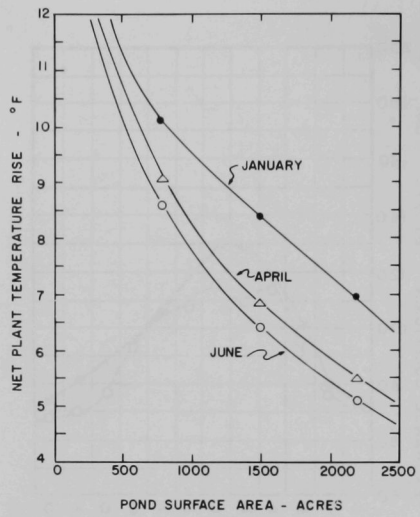

Fig. 8.3.

Effect of Pond Surface Area on Amount of Cooling for Various Seasons: Nashville, Tennessee.[136]

April, and June were chosen arbitrarily. Based on these three months alone, the required area would be 2250 acres.

Once Fig. 8.3 is constructed, one can reverse the process above to answer the question: What is the temperature rise for a pond of a specified area? To answer this, one enters the plot at the specified surface area, reads vertically until he intercepts the desired month or the month whose contour is the highest if the maximum rise is desired, and then reads across to the temperature rise that corresponds to this intercept point.

This procedure for estimating the extreme and normal operating performance of a cooling pond is not a design procedure but merely a first-trial approach. It allows one to estimate the performance of a cooling pond without going through a rigorous design procedure. Using the ratio of area required for completely mixed ponds versus plug-flow ponds (see Table 8.1), one can apply the above procedure to plug-flow ponds.

E. Cooling-pond Model--Steady State and Transient

The Littleton model,[56] unlike the two previous models, includes both a heat and a mass balance. The model classifies types of ponds according to the following three conditions:

1. Completely mixed or plug-flow pond.
2. With or without vertical temperature gradient.
3. Steady-state or transient operation.

There are eight possible combinations of these three conditions. These combinations will be discussed in order. Very little mathematical derivation

will be included. However, a complete derivation is included in Ref. 56. All the combinations discussed are for recirculating ponds.

1. Case I: Mixed, Steady State, No Vertical Temperature Gradient

To arrive at a simplified solution the following assumptions are made:

a. The volume of the pond is constant; $\partial V/\partial t = 0$.

b. The pond is completely mixed.

c. The enthalpies of the pond water, seepage water, precipitated water, and makeup water are all equal; $h_{POND} = h_s = h_p = h_{mu}$, where makeup water is the water added to the pond to replace losses.

d. Steady-state condition prevails; $\partial\theta/\partial t = 0$.

The assumptions in conjunction with the heat- and mass-balance equations result in the following formula for a recirculating pond:

$$Q_{pp} + f_1 = [a_6 + (a_{12} + a_{13}W)(a_2 + a_{14})]\theta + [a_7 + (a_{12} + a_{13}W)a_3]\theta^2 + [a_8 + (a_{12} + a_{13}W)a_4]\theta^3 , \quad (8.11)$$

where Q_{pp} = the waste thermal energy imposed on the pond, in Btu/ft^2-day,

θ = pond-water temperature referenced to 32°F, in °F,

W = wind speed, in mph,

$a_1 = 0.089$, $a_6 = 19.176$ Btu/ft^2-day-°F,

$a_2 = 3.50 \times 10^{-3}$, $a_7 = 5.850 \times 10^{-2}$ Btu/ft^2-day-°F^2,

$a_3 = 5.68 \times 10^{-6}$, $a_8 = 7.923 \times 10^{-5}$ Btu/ft^2-day-°F^3,

$a_4 = 1.13 \times 10^{-6}$, $a_{12} = 3730$,

$a_5 = 2358.74$ Btu/ft^2-day, $a_{13} = 373$,

$a_{14} = 0.00473$,

$$f_1 = Q_N - a_5 (a_{12} + a_{13}W)(a_1 - \theta_a a_{14} - P_a) , \quad (8.12)$$

Q_N = net radiation absorbed by the pond, Btu/ft^2-day,

θ_a = air temperature referenced to 32°F (in °F), and

P_a = water-vapor pressure in air (in psia).

Values are calculated as follows:

a. $Q_{pp} = Q_h/A$,

where Q_h = plant heat load, Btu/day, a known value, and

A = surface area of pond, ft^2, a known value.

b. $Q_N = (Q_s - Q_{sr}) + (Q_a - Q_{ar})$,

where Q_s = solar radiation, Btu/ft^2-day, obtained from Weather Bureau data,

Q_{sr} = reflected solar radiation = $R_{sr}\ Q_s$, where $0.04 \leq R_{sr} \leq 0.12$ (therefore use $R_{sr} = 0.07$),

Q_a = atmospheric radiation = $3.98(T_a + 460)^4(C_B + 0.223\sqrt{P_a})$,

(These terms are explained fully in Chapter III.)

T_a = temperature of air, °F, and

Q_{ar} = reflected atmospheric radiation = $0.03(Q_a)$.

c. $\theta_a = T_a(\text{dry}) - 32°F$.

d. W = wind speed, in mph, from Weather Bureau data.

Once these four values are computed, one can calculate the value of the left side of Eq. 8.11. To aid in arriving at a solution, Eq. 8.11 is plotted for different values of $(a_{12} + a_{13}W)$ in Fig. 8.4. One enters Fig. 8.4 at the proper $(f_1 + Q_{pp})$ value, reading upward until one intercepts the proper $(a_{12} + a_{13}W)$ contour, then reading across to the value of T_{EQ}.

Equation 8.11, while numerous in terms, expresses a simple relationship. To visualize this relationship, assume that Q_{pp} is zero; this would be the condition with no power plant in the closed system. The resulting equation is the Littleton model's simplified version of the heat-budget equation (Eq. 3.29)

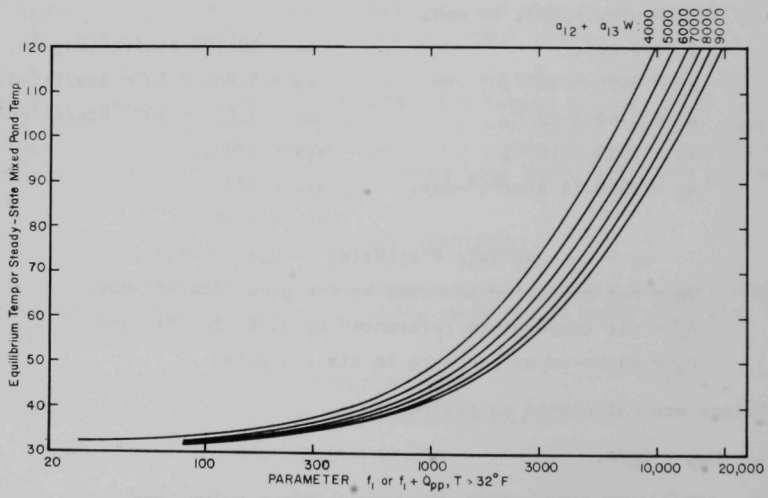

Fig. 8.4. f_1 vs. Equilibrium Temperature or Steady-state Mixed Pond Temperature.[56]

shown in Chapter III. Some additional terms (via a complete mass balance of the pond) are included, such as seepage and precipitation, that were not included in the previously discussed heat-budget equation. Inspection of this reduced form of Eq. 8.11 reveals that all the terms in the right-hand side are the heat-budget terms, which are a function of the water-surface temperature. The only remaining term, f_1, appears on the left side and represents all the terms in the heat-budget equation that are not a function of the water-surface temperature. In this reduced form, θ then represents the equilibrium temperature (referenced to 32°F). This temperature will be higher than the equilibrium temperature, since more heat is being added to the pond, as this is the temperature the pond would approach if all heat inputs and outputs were only those from natural sources. Returning Q_{pp} to the left side changes the connotation of θ to that of the steady-state pond temperature, T_{SS}, of a closed system that includes a power plant. To help understand this method, the following example, which assumes the same meteorological data from heat-budget examples and the pond data for the Edinger-Geyer example, is provided for the 800-acre pond:

$$Q_{pp} = \frac{\rho C_p q_p \Delta T_c}{A}$$

$$= \frac{(62.4\ \text{lb/ft}^3)(1\ \text{Btu/lb-°F})(11.66 \times 10^7\ \text{ft}^3/\text{day}\ (15°\text{F})}{3.485 \times 10^7\ \text{ft}^2}$$

$$= 3130\ \text{Btu/ft}^2\text{-day};$$

$f_1 = 5475$, from T_{EQ} calculation in Chapter III.

Therefore,

$$f_2 = f_1 + Q_{pp} = 5475 + 3130 = 8605\ \text{Btu/ft}^2\text{-day}\ .$$

From Fig. 8.4 at $f_2 = 8605$ and $a_{12} + a_{13}W = 6190$, find $T_{EFF} = 98.0°F$.

Using the same procedure for the 1500- and 2200-acre pond gives $T_{EFF} = 92.0$ and 89.0°F, respectively. These results are plotted in Fig. 8.9 (presented after other examples have been computed).

2. Case II: Mixed Pond, Steady State with Vertical Temperature Gradient

The temperature θ in Eq. 8.11 is the pond temperature. It appears in the equation, however, because it is the surface temperature, and the air-water heat exchange is assumed to be a surface phenomenon. Therefore, if θ is interpreted as the surface temperature, the pond could have any vertical temperature structure and would not have to be mixed vertically. Hogan *et al.*[56] discussed the example of a linear temperature profile, as shown in Fig. 8.5. For this case, consider the bulk average temperature, θ, occurring at middepth. Then,

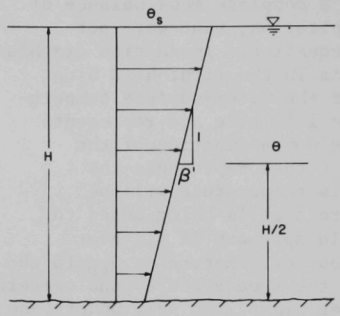

Fig. 8.5.
Linear Temperature Profile.

$$\theta = \theta_s - \beta'(H/2) \tag{8.13}$$

or

$$\theta_s = \bar{\theta} + \beta'(H/2) \ . \tag{8.14}$$

Therefore, with θ (= θ_s) obtained from Eq. 8.11, the temperature at any pond depth can be obtained. The gradient does not have to be linear. Whatever the shape of the profile, θ will still be the surface temperature. This could be important in assessing vertical location of the withdrawal for the pond. Heavy withdrawal from lower layers would decrease (and possibly eliminate) the gradient. Hogan *et al.* indicated that a review of available data showed that β is generally less than 1.0°F/ft. This is true even for extreme cases where deliberate attempts are made to float a hot layer onto the pond.

3. Case III: Mixed Pond, Transient Operation, No Vertical Temperature Gradient

a. Equations. Consider now the case in which certain parameters are changed with time. In this instance, visualize a pond initially operating at some steady-state temperature. Then, the inflow temperature is increased and continued at the new temperature. Clearly, the pond will have to adjust, as the heat in no longer equals heat out; there will be a change in the pond's heat content and therefore a change in pond temperature. This will continue with time until a new equilibrium is approached.

Removal of Assumption d of Case I, $\partial\theta/\partial t = 0$, results in Eq. 8.11 becoming

$$\begin{aligned} \rho C_p(V/A)\ d\theta/dt = {} & [Q_{pp} + f_1] - [a_6 + (a_{12} + a_{13}W)(a_2 + a_{14})]\theta \\ & - [a_7 + (a_{12} + a_{13}W)a_3]\theta^2 \\ & - [a_8 + (a_{12} + a_{13}W)a_4]\theta^3 \ , \end{aligned} \tag{8.15}$$

where C_p = specific heat capacity of water, 1 Btu/lb_m-°F;

ρ = mass density of water, 62.4 lb_m/ft^3;

V = volume of water in pond, ft^3;

A = surface area of pond, ft^2; and

t = time.

Replace all θ's in Eq. 8.11 with the steady-state temperature, θ_{ss}, at which the given mixed pond will operate referenced to 32°F. Substituting the right side of this equation for $(Q_{pp} - f_1)$ in Eq. 8.15 gives

$$\frac{d\theta}{dt} = \frac{1}{\rho C_p(V/A)} \Big\{ [a_6 + (a_{12} + a_{13}W)(a_2 + a_{14})](\theta_{ss} - \theta) + [a_7 + (a_{12} + a_{13}W)a_3](\theta_{ss}^2 - \theta^2) + [a_8 + (a_{12} + a_{13}W)a_4](\theta_{ss}^3 - \theta^3) \Big\} . \tag{8.16}$$

Multiplying Eq. 8.16 by dt and numerically integrating gives

$$\int_{\substack{\theta=\Theta \\ @t=0}}^{\theta} d\theta = \int_{t=0}^{t} (\text{right side of Eq. 8.16})\, dt . \tag{8.17}$$

Equation 8.17 therefore represents an equation of θ versus t for a recirculating pond. To eliminate the necessity of numerically integrating Eq. 8.17 for each solution, a plot of θ versus f_2 for a certain value of steady-state temperature, T_{ss}, is presented. Figure 8.6 is an example of such a plot, where

$$f_2 = f_{2_i} + \frac{1}{\rho C_p(V/A)} ,$$

in which f_{2_i} is the initial value at f_2 at time zero. The value f_2 is used as the abscissa in Fig. 8.6 instead of $t/[\rho C_p(V/A)]$ because these plots will be used for plug flow also, in which case the definition of f_2 will change.

Equation 8.17 is an expanded heat-balance equation like Eq. 8.11, except that Eq. 8.17 has a time-dependent term, $t/[\rho C_p(V/A)]$. This is the term representing the rate of change of heat stored in the pond. Because of this time-dependent term, an initial pond temperature, θ, must be known so that an initial value for f_2 can be determined. This initial f_2 value can be visualized as being equal to $t'/[\rho C_p(V/A)]$, where t' is the time required for the pond to arrive at its present temperature from some fictitious temperature at time zero. Once f_{2_i} is determined, the term $t/[\rho C_p(V/A)]$ is added to it until the heat-budgeted terms on the right side of Eq. 8.17 equal zero which corresponds to $\Delta\theta = 0$, or the steady-state condition.

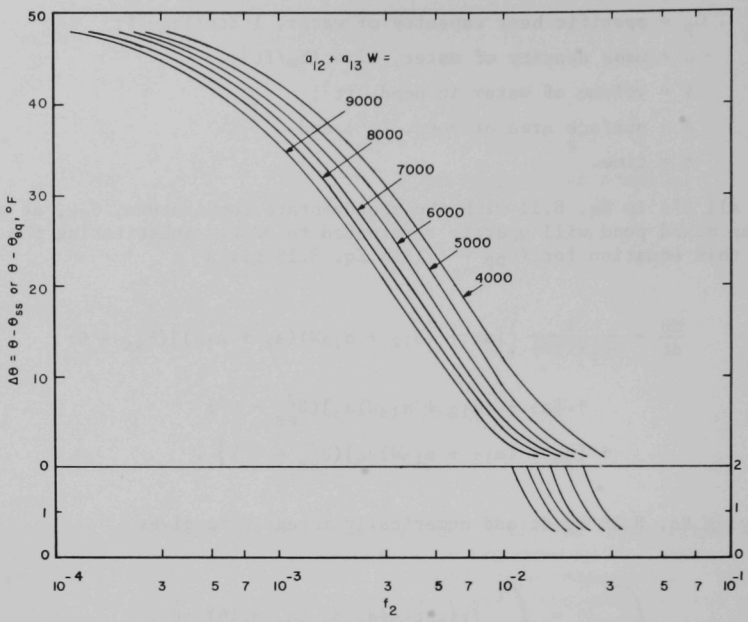

Fig. 8.6. f_2 vs. $\Delta\Theta$ for Equilibrium Temperature of 80°F.[56]

Proceed as follows:

1. Calculate θ_{ss}, using the method described in Case I.

2. Calculate the initial value of $(\theta_{ss} - \theta)$, where θ is the uniform pond temperature at t = 0.

3. From Fig. 8.6, at $\Delta\theta = (\theta_{ss} - \theta)$ and $(a_{12} + a_{13}W)$, find f_2 initial.

4. Calculate the pond temperature for any time by adding f_2 initial and $t/[\rho C_p(V/A)]$ and returning to Fig. 8.6 for a new $\Delta\theta = (\theta_{ss} - \theta_t)$.

b. Example of Case III. For an illustration of the procedure outlined, assume the same conditions as Case I and consider the 800-acre pond. First, initial values and pertinent constants must be calculated.

Initial value of $T_{ss} - T_{IN} = 98.0 - 72.0 = 26.0°F = \Delta\theta$.

Initial f_2 value:

Using Fig. 8.6 at $\Delta\theta = 26.0°F$ and $a_{12} + a_{13}W$

$= 6190$, find $f_{2_i} = 2.8 \times 10^{-3}$.

$$\frac{t}{\rho C_p(V/A)} = \frac{t\ (\text{days})}{(62.4\ \text{lb/ft}^3)(1\ \text{Btu/lb-°F})\dfrac{(A \times 15\ \text{ft})}{A}} = \frac{t\ (\text{days})}{936\ \text{Btu/ft}^2\text{-°F}}\ .$$

Calculations are tabulated in Table 8.4.

Table 8.4. Calculations for Transient Example

t, *days*	$\frac{t}{\rho C_p(V/A)}$	f_{2t}	$\Delta\theta$,[a] °F	$T_{POND} = T_{EFF} = T_{ss} - \Delta\theta$
2	2.14×10^{-3}	4.94×10^{-3}	17.0	81.0
4	4.27×10^{-3}	7.07×10^{-3}	11.5	86.5
6	6.41×10^{-3}	9.21×10^{-3}	7.5	90.5
8	8.55×10^{-3}	11.35×10^{-3}	5.0	93.0
10	10.70×10^{-3}	13.50×10^{-3}	3.0	95.0
15	16.05×10^{-3}	18.85×10^{-3}	1.1	96.9
20	21.4×10^{-3}	24.20×10^{-3}	0.4	97.6
25	26.7×10^{-3}	24.50×10^{-3}	0.0	98.0

[a]*From Figure 8.6.*

The calculations show that the constant-input conditions given would require 25 days for the pond to reach steady state. If, during this 25-day period, some value of input data changed, for example, the value Q_{pp}, then the pond temperature for future calculations would be the value at that time and not the steady-state value. Results are plotted in Fig. 8.7.

4. Case IV: Mixed Pond, Transient Operation, with a Specified Linear Vertical Temperature Gradient

Using the same relationships as in Case II and substituting θ_s in place of θ in Eq. 8.17, one can use the same procedure previously outlined under Case III to work this type of problem.

5. Case V: Plug-flow Pond, Steady State, No Vertical Temperature Gradient

a. Equation Development. In the derivation of a formula for plug-flow ponds, the following assumptions are made:

1) The volume of the pond is constant: $\partial V/\partial t = 0$.

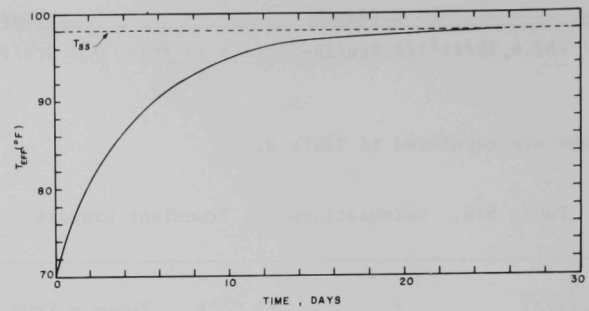

Fig. 8.7. Transient Pond Temperature for 800-acre Completely Mixed Pond.

2) The pond water, seepage water, precipitated water, and makeup water have the same enthalpy.

3) Steady-state condition prevails: $\partial\theta/\partial t = 0$.

These assumptions, in conjunction with the heat- and mass-balance equations, result in

$$\frac{d\theta}{dA} = \frac{\Delta T_c}{Q_h}\Big\{f_1 - [a_6 + (a_{12} + a_{13}W)(a_2 + a_{14})]\theta - [a_7 + (a_{12} + a_{13}W)a_3]\theta^2 - [a_8 + (a_{12} + a_{13}W)a_4]\theta^3\Big\}, \tag{8.18}$$

where ΔT_c is the temperature rise experienced by the cooling water as it passes through the condenser (in steady-state conditions, ΔT_c must also equal the temperature drop through the pond), and Q_h is the waste thermal energy from plant to pond, Btu/day.

Equation 8.18 is derived by considering a slug of condenser discharge water as it travels through the pond and writing an energy balance for this slug. Since there is no other water mixing with this slug for plug flow, the only mechanism for change of heat content in the slug ($d\theta/dt$) is loss to the atmosphere. Also, additional heat input from the plant will not affect the slug; hence, the Q_{pp} term of Eq. 8.15 does not appear in Eq. 8.18. By convention, plug-flow equations are frequently written in terms of the area swept out by a slug in a given time, rather than the time itself. The substitution $dt = HdA/q_p$ enables Eq. 8.18 to be written in terms of A. With this substitution and $\rho C_p q_p = Q_h/\Delta T_c$, Eqs. 8.15 and 8.18 are identical except for the Q_{pp} term in the former. This is correct because Q_{pp} represents the plant heat being continuously added to each fluid parcel due to the complete mixing.

Solving for the θ corresponding to equilibrium, θ_{EQ}, in Eq. 8.11 by letting $Q_{pp} = 0$, and substituting this expression into Eq. 8.18, gives

$$\frac{d\theta}{dA} = \frac{-\Delta T_c}{Q_h} \left\{ [a_6 + (a_{12} + a_{13}W)(a_2 + a_{14})](\theta - \theta_{EQ}) \right.$$

$$+ [a_7 + (a_{12} + a_{13}W)a_3]\left(\theta^2 - \theta_{EQ}^2\right) \tag{8.19}$$

$$\left. + [a_8 + (a_{12} + a_{13}W)a_4]\left(\theta^3 - \theta_{EQ}^3\right) \right\} .$$

Multiplying Eq. 8.19 by dA and numerically integrating gives the following result for a recirculating pond:

$$\int_{\substack{\theta=\Theta \\ @A=0}}^{\theta} d\theta = \int_{A=0}^{A} (\text{right side of Eq. 8.19})\ dA . \tag{8.20}$$

By letting $f_2 = \Delta T_c dA/Q_h$, one can use Fig. 8.6.

The reader is encouraged to visualize what Eqs. 8.19 and 8.20 represent. Equation 8.19 is a more convenient form of Eq. 8.18. Equation 8.20 then numerically integrates, i.e., sums the heat loss that the slug suffers as it passes through various incremental areas of the pond. The number of differential volumes the water has passed through is expressed in terms of the summation of their surface area.

b. Problems that Can Be Solved. Within Case V, two possible problems exist.

1) Given that the temperature leaving the pond is equal to the equilibrium temperature plus the approach, find the pond area that satisfies this condition. The approach is the temperature difference between T_{EQ} and T_{EFF} for a closed system.

2) Given A, Q_h, and the meteorological conditions, find the approach. This is a trial-and-error solution.

To work problem 1) above, one would complete the following steps:

a. Calculate T_{EQ} by the Case I solution.

b. Calculate $T_c = T_{EQ}$ + Approach, where T_c is the temperature of the water entering the condensers.

c. At the hot end of the pond, the following relationship holds:

$$(\theta - \theta_{EQ})_{initial} = (T_c + \Delta T_c) - T_{EQ} , \tag{8.21}$$

where ΔT_c is the temperature rise across the condensers and θ is the temperature of the pond water. From Fig. 8.6, one can find f_{2i}. The value of f_{2i} is somewhat similar to that discussed in Case III, but here f_{2i} represents the area required to arrive at this condition from some fictitious initial condition.

d. At the cold end of the pond, the following relationship holds:

$$\theta - \theta_{EQ} = T_c - T_{EQ} = \text{Approach} \ . \tag{8.22}$$

From Fig. 8.6, one can find f_{2f}.

e. Having the f_2 values at each end one now has an area term that satisfies the approach given initially. Direct calculation of the area uses the relationship $A = (f_{2f} - f_{2i})Q_h/\Delta T_c$.

To solve problem 2, one needs to find two points along the $(a_{12} + a_{13}W)$ line in Fig. 8.6 such that $(f_{2f} - f_{2i})$ would equal the expression $A\Delta T_c/Q_h$ and

$$(\theta - \theta_{EQ})_f - (\theta - \theta_{EQ})_i = \Delta T_c \ .$$

The initial step would be to calculate $(f_{2f} - f_{2i}) = \Delta f$ from the information given. Then by trial and error, one moves this value of Δf until the differences between the two $(\theta - \theta_{EQ})$'s are equal to the given ΔT_c. A singular solution is possible because there is only one steady-state condition where the difference in the two area terms, Δf, will allow the pond to reject the right amount of heat to give the ΔT_c temperature drop across the pond.

c. Example for Case V. An example of each of the two types of problems will be worked.

1) Type 1 Example. To illustrate this type of problem, assume the same conditions as in the Case I example and find the area of plug flow necessary to give the same approach as an 800-acre completely mixed pond.

$$T_{EQ} = 82.3°F, \text{ and } T_{EFF} = 98.0°F \ .$$

$$\therefore \text{Approach} = T_{EFF} - T_{EQ} = 98.0 - 82.3 = 15.7°F \ .$$

$$T_c = T_{EQ} + \text{Approach} = 82.3 + 15.7 = 98.0°F = T_{EFF} \ .$$

Hot End

$$(\theta - \theta_{EQ})_i = (T_c + \Delta T_c) - T_{EQ}$$

$$= (98.0 + 15) - 82.3 = 30.7°F \ .$$

From Fig. 8.6 at $(\theta - \theta_{EQ})_i = 30.7$ and $a_{12} + a_{13}W = 6190$, find $f_{2i} = 2.1 \times 10^{-3}$.

Cold End

$$(\theta - \theta_{EQ})_f = T_c - T_{EQ} = \text{Approach} = 15.7°F .$$

From Fig. 8.6 at $(\theta - \theta_{EQ})_f = 15.7$ and $a_{12} + a_{13}W = 6190$, find $f_{2f} = 5.6 \times 10^{-3}$.

$$Qh = \rho C_p \Delta T_c q_p = 62.4(1)(15)(11.66 \times 10^7) = 10{,}900 \times 10^7 \text{ Btu/day} .$$

$$A = (f_{2_f} - f_{2i}) \frac{Q_h}{\Delta T_c}$$

$$= (5.6 \times 10^{-3} - 2.1 \times 10^{-3}) \frac{10.9 \times 10^{10}}{15} = 2.54 \times 10^7 \text{ ft}^2 = 583 \text{ acres} .$$

Thus, the transition from a completely mixed pond to a plug-flow pond reduces the area required from 800 to 583 acres.

2) Type 2 Example. To illustrate this type of problem, assume the same conditions as for Case I and find the effluent temperature for a plug-flow pond of 800 acres.

$$\Delta T_c = \text{range} = \Delta\Theta = 15°F ;$$

$$f_{2f} - f_{2i} = \frac{A\Delta T_c}{H_p} = \frac{(3.485 \times 10^7 \text{ ft}^2)15°F}{10{,}900 \times 10^7 \text{ Btu/day}} = 4.8 \times 10^{-3} .$$

From Fig. 8.6 and a trial-and-error solution, the results are

$$f_{2f} = 7.75 \times 10^{-3} .$$

Therefore,

$$\Delta\Theta_f = 10.0°F ,$$

and

$$T_{EFF} \simeq 82.3 + 10 = 92.3°F .$$

And,

$$f_{2i} = 2.95 \times 10^{-3} .$$

Therefore,

$$\Delta\Theta_i \simeq 25.1°F ,$$

and

$$T_{IN} \simeq 82.3 + 25.1 = 107.4°F \ .$$

For the 1500-acre pond, $T_{EFF} \simeq 87.1°F$ and $T_{IN} \simeq 102.8°F$.

For the 2200-acre pond, $T_{EFF} \simeq 83.1°F$ and $T_{IN} \simeq 98.3°F$.

The results for all three ponds are plotted in Fig. 8.9, the overall comparison graph.

6. Case VI: Plug-flow Pond, Steady State, with a Specified Linear Vertical Temperature Gradient

Again, as in Case II, solve for Θ_s using the relationships used there. Then substitute Θ_s in place of Θ in Eq. 8.20, and follow the solutions presented in Case V.

7. Case VII: Plug Flow, Transient, No Vertical Gradient

a. Equation Development. The transient nature of a pond is of interest when the period of constant input conditions never allows the pond to arrive at steady-state operation. To arrive at a solution, one must therefore know the temperature distribution along the pond at the time when some input value changes. The heat balance for a slug of water in this case is identical to Eq. 8.18. The transient solution is outlined in the steps below:

1) Determine the pond input temperature at time zero.

2) Calculate the theoretical flow-through time, t_r, using the relationship

$$t_r = \frac{V\rho C_p \Delta T_c}{Q_h} \ . \tag{8.23}$$

If a series of input values is being considered, plots of T_{EQ}, t_r, and $(a_{12} + a_{13}W)$ versus time should be made.

3) At the hot end, one can write

$$(\Theta - \Theta_{EQ})_i = T_{IN} - T_{EQ} \ . \tag{8.24}$$

where T_{IN} is the temperature of the water entering the pond. From Fig. 8.6 at $(\Theta - \Theta_{EQ})_i$ and $(a_{12} + a_{13}W)$, find f_{2i}.

Using

$$f_{2t} = f_{2i} + \frac{t}{\rho C_p (V/A)} \tag{8.25}$$

and Fig. 8.6, one can find $(\Theta - \Theta_{EQ})_t$ for any time downstream or for any location by writing

$$\Delta A = A \frac{t_f - t_i}{t_r} , \tag{8.26}$$

where t_i is the time the slug of water entered the pond, t_f is the time of flow downstream to point f, and ΔA is the amount of the pond's area traversed by the slug. Therefore, $\Delta A/A$ relates the fraction of the total length the slug has traversed at the time under consideration.

4) Two situations could arise at this point. First, the slug fails to arrive at the cold end of the pond before meteorological values change. In this situation, one treats the remaining portion of the pond as a separate pond and repeats steps 1-3 using the slug temperature at the time the meteorological values changed as the input temperature to the remaining portion of the pond. Second, the slug arrives at the hot end of the pond. In this situation, one adds ΔT_c to the cold end temperature; this simulates going through the condensers in this closed system. Then repeat steps 1-3.

b. Example for Case VII. Use the conditions for Case I, and consider the 800-acre pond.

Step 1

As a starting point, assume that the condenser intake water temperature is at the equilibrium temperature.

$$T_{IN} = T_{EQ} + \Delta T_c = 82.3 + 15.0 = 97.3°F .$$

Step 2

$$t_r = \frac{V\rho C_p \Delta T_c}{Q_h} = \frac{(3.485 \times 48{,}900 \times 15)(62.4)(1)(15)}{10{,}900} = 4.48 \text{ days} .$$

Step 3a

$$(\Theta_i - \Theta_{EQ}) = T_{IN} - T_{EQ} = 97.3 - 82.3 = 15.0°F .$$

From Fig. 8.6 at $\Delta\Theta = 15.0°F$ and $(a_{12} + a_{13}W) = 6190$, find $f_{2_0 \text{ days}} = 5.6 \times 10^{-3}$.

$$t = t_f - t_i = 4.48 - 0 = 4.48 \text{ days} .$$

$$f_{2_{4.48 \text{ days}}} = f_{2_0} + \frac{t}{\rho C_p (V/A)}$$

$$= 5.6 \times 10^{-3} + \frac{4.48}{(62.4)(1)(15)} = 10.39 \times 10^{-3} .$$

From Fig. 8.6 at $f_{2_{4.48}} = 1.039 \times 10^{-2}$ and $a_{12} + a_{13}W = 6190$, find $\Delta\Theta = 6°F$.

The value of $T_f = 4.48$ was used because the desired temperature was the effluent temperature. If a temperature at a point other than the effluent was desired, one would determine the area the slug of water had traversed to that point, ΔA, and apply Eq. 8.26 to find t_f.

$$T_{EFF_{4.48}} = T_{EQ} + \Delta\Theta = 82.3 + 6.0 = 88.3°F .$$

At $t = 4.48$ days, the water is leaving the pond; therefore, to continue, ΔT_c must be added to $T_{EFF_{4.48}}$ and step 3 repeated.

<u>Step 3b</u>

$$\therefore T_{IN} = 88.3 + 15.0 = 103.3°F ;$$

$$\Delta\Theta = T_{IN} - T_{EQ} = 103.3 - 82.3 = 21.0°F .$$

From Fig. 8.6 at $\Delta\Theta = 21.0°F$ and $a_{12} + a_{13}W = 6190$, find $f_{2_{4.48}} = 3.8 \times 10^{-3}$.

$$t = 8.96 - 4.48 = 4.48 \text{ days} ;$$

$$f_{2_{8.96}} = 3.8 \times 10^{-3} + 4.48/936 = 8.6 \times 10^{-3} .$$

From Fig. 8.6 at $f_{2_{8.96}} = 8.6 \times 10^{-3}$ and $a_{12} + a_{13}W = 6190$, find

$$\Delta\Theta = 8.5°F ;$$

$$T_{EFF_{8.96}} = 82.3 + 8.5 = 90.8°F .$$

Step 3c

Repeat Step 3b using new T_{EFF}.

$$T_{IN} = 90.8 + 15 = 105.8°F \ ;$$

$$\Delta\Theta = 105.8 - 82.3 = 23.5 \ .$$

From Fig. 8.6 at $\Delta\Theta = 23.5°F$ and $a_{12} + a_{13}W = 6190$, find $f_{2_{8.96}} = 3.3 \times 10^{-3}$.

$$t = 13.44 - 8.96 = 4.48 \text{ days} \ ;$$

$$f_{2_{13.44}} = 3.3 \times 10^{-3} + 4.48/936 = 8.1 \times 10^{-3} \ .$$

From Fig. 8.6 at $f_{2_{13.44}} = 8.1 \times 10^{-3}$ and $a_{12} + a_{13}W = 6190$, find

$$\Delta\Theta = 9.5°F \ .$$

$$\therefore T_{EFF_{13.44}} = 82.3 + 9.5 = 91.8°F \ .$$

Step 3d

$$T_{IN} = 91.8 + 15 = 106.8°F \ ;$$

$$\Delta\Theta = 106.8 - 82.3 = 24.5°F \ .$$

From Fig. 8.6 at $\Delta\Theta = 24.5°F$ and $a_{12} + a_{13}W = 6190$, find $f_{2_{17.92}} = 3.1 \times 10^{-3}$.

$$t = 17.92 - 13.44 = 4.48 \text{ days} \ ;$$

$$f_{2_{17.92}} = 3.1 \times 10^{-3} + 4.8 \times 10^{-3} = 7.9 \times 10^{-3} \ .$$

From Fig. 8.6 at $f_{2_{17.92}} = 7.9 \times 10^{-3}$ and $a_{12} + a_{13}W = 6190$, find $\Delta\Theta = 10.0°F$.

$$T_{EFF_{17.92}} = 82.3 + 10.0 = 92.3°F \ .$$

$T_{EFF_{17.92}} = T_{ss}$; therefore, for the rest of June, this would be the effluent temperature. Starting the month of July, the new T_{IN} would be

$$T_{IN} = 92.3 + 15 = 107.3°F \ .$$

Figure 8.8 shows the change of effluent temperature with time for the plug-flow pond.

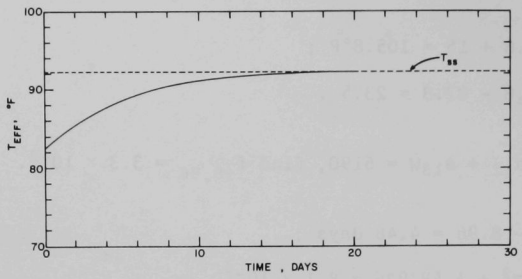

Fig. 8.8.

Transient Effluent Temperature for 800-acre, Plug-flow Pond.

8. Case VIII: Plug Flow, Transient Operation, with a Specified Linear Vertical Temperature Gradient

Use equation listed within Case II to find Θ_s, and substitute Θ_s for Θ in Case VII.

F. Expected Accuracy from Idealized Models

To help provide a feel for the results of the idealized models, the same problem has been used for all the examples. The results are plotted in Fig. 8.9.

The choice of evaporation formula was discussed in the Chapter III. From Fig. 8.9, one can see the extreme effect this choice can make. In the Edinger-Geyer once-through, completely mixed pond, the difference in effluent temperatures was better than 9°F for both the completely mixed 800-acre pond and the plug-flow 800-acre pond. However, this 800-acre pond is heavily loaded. For

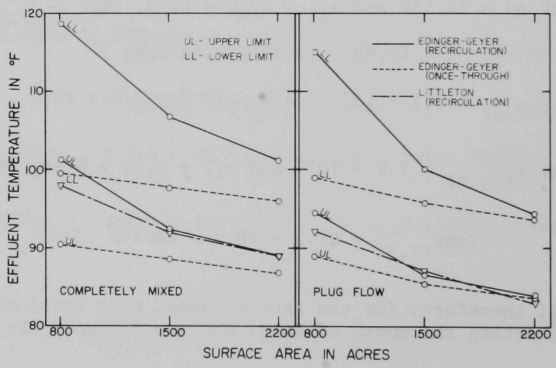

Fig. 8.9. Results from Examples for Steady-state, Completely Mixed and Plug-flow Ponds.

the 2200-acre pond, where the loading was smaller, the difference in the effluent temperatures due to different evaporation formulas was about the same for the once-through pond. For the recirculating pond, this difference is only about 12.3°F as compared to 20.9°F for the 800-acre pond. Therefore, depending on the type of pond used, the choice of an improper evaporation formula can introduce an effective error of 9-17.5°F. In fact, if actual evaporation lay somewhere between the limits given by the formulas, the error introduced would be less than these limits. However, substantial error can result from mishandling the evaporation term. The proper evaporation formula should be chosen on the basis of available data for the location if possible. Data for most general locations are frequently available from organizations such as the Weather Bureau, the Corps of Engineers, or the Geological Survey. Again caution should be used in relating data from other places. Evaporation characteristics can be localized, depending on such things as degree of exposure of water to wind, width of cooling pond, and any energy input or output that affects the water-surface temperature.

In addition to sensitivity to the evaporation terms, the idealized models overlook dead regions in the pond and neglect entrance mixing. These will be discussed in the next two sections.

G. Entrance Entrainment Model

Modeling of a real pond requires a method that allows one to predict performance curves between those of completely mixed and plug-flow ponds, since neither type of pond will completely describe the real pond. One method of arriving at this objective is to schematically represent the real pond. Ryan[119] uses such a representation by assuming that a real pond can be described as two regions of plug flow. One region receives mixed inflow and returned waters at its origin from the second region; the second region serves as the return loop for the mixing water. The flow in Region I is the plant flow plus diluting water. The flow in Region II is the diluting water being brought in to mix into the discharge waters. Figure 8.10 is a diagram of this model. Looking at point 1, the following equation can be written:

$$T_{MIX} = \frac{T_{IN} + (D - 1)T_D}{D}, \tag{8.28}$$

where D is a coefficient representing the dilution due to lateral mixing with the ambient pond waters. Assuming steady-state conditions, the heat loss by Region I can be expressed as

$$\frac{T_{EFF} - T_{EQ}}{T_{MIX} - T_{EQ}} = \exp(-r_1) \tag{8.29}$$

where T_{EFF} is the temperature of the water at the end of Region 1 and

$$r_1 = \frac{KA}{\rho C_p (2D - 1) q_p} , \tag{8.30}$$

where A is the surface area of the related region. Assuming steady state, the cooling in Region II can be expressed as

$$\frac{T_D - T_{EQ}}{T_{EFF} - T_{EQ}} = \exp(-r_1) . \tag{8.31}$$

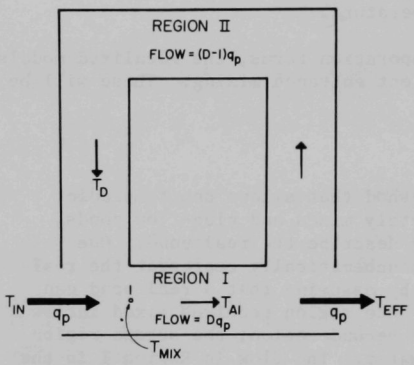

Fig. 8.10.

Schematic Drawing of Entrance Entrainment Model.

Combining Eqs. 8.28, 8.29, and 8.31 results in

$$\frac{T_{EFF} - T_{EQ}}{T_{IN} - T_{EQ}} = \frac{\exp[-r/(2D - 1)]}{D - (D - 1)\exp[-2r/(2D - 1)]} , \tag{8.32}$$

where $r = \frac{KA}{\rho C_p q_p}$ and A is the total surface area of both regions.

Varying the value of D within Eq. 8.32 shows the effect entrance entrainment has on pond performance. Plotted results of varying D are shown in Fig. 8.11. Pure plug-flow operation occurs at D = 1 (this implies zero dilution), and as D increases, the performance curves approach that of a completely mixed pond.

Use of this type of schematic representation requires the following assumptions:

1. The lateral mixing is much greater than the vertical mixing.

2. The total surface area of the pond plays an active part in heat dissipation.

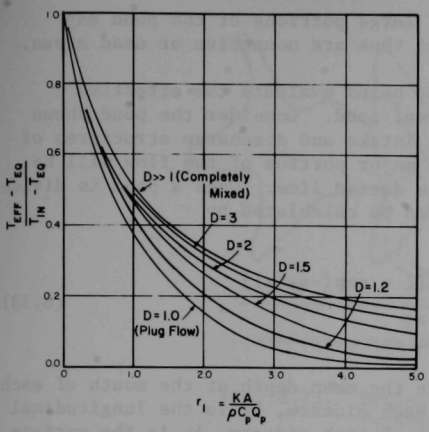

Fig. 8.11.

Temperature Excess of Shallow Pond with Entrance Mixing.[119]

3. The area of each region is proportional to its flow rate; therefore, if D = 2, then Region I would have two-thirds of the area and Region II would have one-third. D = 2 implies that the discharge water mixes with volume of water exactly equal to itself.

Although Assumption 1 is easily justified in a cooling pond because of density differences, Assumption 2 is much more difficult to justify. In a real pond, where portions of the pond would most adequatly be classed as dead area, this assumption would give false results. In effect, as a larger fraction of a pond becomes dead area, this assumption forces the value of D to increase. Thus, a pond that has considerable dead area but strong plug flow in the active areas might be analyzed as a completely mixed pond. This assumption could be reinforced, however, if the active area could be evaluated and only this area of a pond modeled. Assumption 3 is made for mathematical convenience and essentially assumes a pond of uniform depth. Therefore, the validity of this assumption will be based on pond geometry.

Despite the inadequacies of some of the above assumptions, this type of representation does offer a means of comparing different ponds in their performance capabilities. It must be strongly emphasized that methods do exist for predicting D for designs that use typical outlet channels. The method of Stolzenbach and Harleman[131] for example, as shown in Chapter V, enables D to be predicted as a function of the discharge densimetric Froude number, the channel width-to-depth ratio, and local geometry for a rectangular discharge channel. The designer therefore has available to him the means of controlling entrance mixing by the specific design of the outlet channel. In addition, he can analyze the effect of a variety of different designs on overall pond performance. One gross measure could be obtained for a given outlet channel design by predicting D theoretically and then using the simple model outlined in this section.

H. Active-region Model

Up to this point in the discussion of cooling ponds, the modeling has been limited to the hydraulically active portion of the pond. In a real pond,

due to sidearms and tributary embayments, large portions of the pond may have extremely long flow-through times and thus are nonactive or dead areas.

Edinger[34] has developed a method that helps evaluate the effective cooling potential one can expect from a real pond. Consider the pond shown in Fig. 8.12. Due to the location of the intake and discharge structures of the power plant and the pond's shape, the major portion of the flow will be confined within the region outlined by the dotted line. Once a pond is divided into these regions, a shape factor (F_s) can be calculated by

$$F_s = \frac{k}{q_p} \sum \frac{\exp(-kAi/q_p)[1 - \exp(-a_i S_i)]}{a_i}, \tag{8.33}$$

where $k = K/\rho C_p$, $a_i = (k/h_i W_i^2 D_L)^{1/2}$, h_i is the mean depth at the mouth of each sidearm, W_i is the width at the mouth of each sidearm, D_L is the longitudinal mixing coefficient, S_i is the surface area of each sidearm, A_i is the surface area along the main flow path from the discharge to the center of the mouth of each sidearm, and q_p is the plant flow. The shape factor is a term representative of the amount of heat dissipated by all the sidearms. The amount of heat dissipated in a single sidearm is represented by the right side of Eq. 8.33 without the summation sign. This single-sidearm heat-dissipation term, f_i, is derived from the integration of the net heat moving into and out of the sidearm, where it was assumed that heat transfer between mainstream and sidearm is completely described by the longitudinal mixing term, D_L. If there were no sidearms, then F_s would be equal to zero, indicating that heat loss due to sidearms would also be zero. Once the shape factor has been calculated, the pond's effluent temperature can be calculated using the equation

$$\frac{T_{EFF} - T_{EQ}}{\Delta T_c} = \frac{\exp(-kA_m/q_p)}{1 + F_s - \exp(-kA_m/q_p)}, \tag{8.34}$$

where A_m is the total surface area of the main flow path, and $\Delta T_c = Q_h/\rho C_p q_p$. Except for the term F_s, the right side of Eq. 8.34 relates to the cooling taking place in the main flow path. If $F_s = 0$ (corresponding to no sidearm areas), the result is a recirculating plug-flow pond, and under these conditions Eq. 8.34 does in fact reduce to Eq. 8.10.

Using Fig. 8.12 as an example, this method can be demonstrated. The initial step is to calculate F_s, as in Table 8.5.

Based on the calculations in Table 8.5, one can calculate $F_s = (k/q_p)\Sigma f_i = 0.41$. Then, using Eq. 8.34, the intake-condenser temperature rise ratio is $(T_{EFF} - T_{EQ})/\Delta T_c = 0.68$.

The value of D_L is a function of wind mixing, density flows due to temperature differences near the sidearm, the size and geometry of the sidearm, and possibly the plant pumping rates. Its value is about 5-10 × 10^6 ft^2/day.[34] In the above example, D_L was just assumed. Although field tests would be

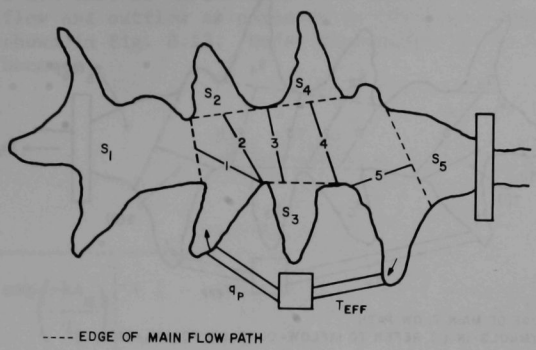

Fig. 8.12. Definition of Main Flow and Tributary Sidearm for Shape-factor Computations.[34]

Table 8.5. Computation of Lake Shape Factor[a] (Ref. 34)

Sidearm No. (1)	S_i, 10^7 ft^2 (2)	*Width,* W_i, *ft* (3)	*Depth,* h_i, *ft* (4)	A_i, 10^7 ft^2 (5)	a_i, 10^{-7} ft^{-2} (6)	f_i,[b] 10^7 ft^2 (7)
1	2.5	1700	6	0.6	1.57	0.535
2	0.9	1400	4	0.9	2.32	0.304
3	0.5	2000	5	1.1	1.46	0.275
4	0.3	1300	7	1.3	1.89	0.220
5	0.3	1500	12	1.9	1.25	0.342
						$f_i = 1.656 \times 10^7$ ft^2

[a]*For* $A_m = 2.3 \times 10^7$ ft^2, $\Sigma S_i = 4.5 \times 10^7$ ft^2, $q_p = 8.5 \times 10^7$ ft^3/day, $k = 1.1$ ft/day ($K = 130$ Btu/ft^2-day-°F), $D_L = 5.0 \times 10^6$ ft^2/day.

[b]
$$f_i = \frac{[\exp(-kA_i/q_p)][1 - \exp(-a_i S_i)]}{a_i}$$

required to determine the exact value of D_L, one can assume a value somewhere within the above range and this should not affect the use of this method for comparing different locations of power plant intakes and effluents. To demonstrate the usefulness of this method for comparing alternatives, consider the same pond, but move the power plant's effluent to a new location as shown in Fig. 8.13. The calculations of the new shape factor are shown in Table 8.6.

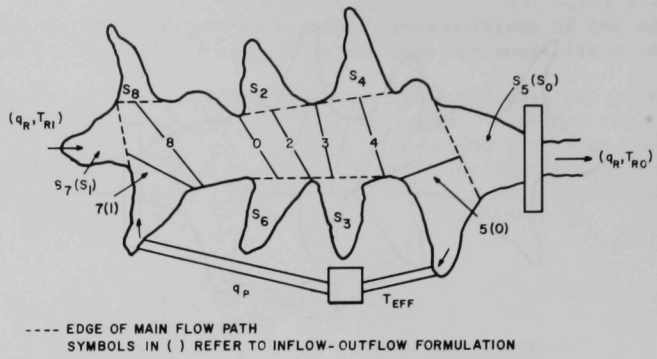

Fig. 8.13. Partitioning of Cooling Lake for Alternative Scheme and for Inflow-Outflow Formulations.[34]

Table 8.6. Lake Shape Factor for Alternative Scheme[a] (Ref. 34)

Sidearm No. (1)	S_i, 10^7 ft^2 (2)	W_i, *ft* (3)	h_i, *ft* (4)	A_i, 10^7 ft^2 (5)	a_i, 10^{-7} ft^{-2} (6)	f_i, 10^7 ft^2 (7)
6	0.5	1100	6	1.4	2.42	0.205
7	0.8	1500	5	0.4	1.95	0.364
8	0.5	1200	4	0.7	2.71	0.232
2	0.9	1400	4	2.1	2.32	0.225
3	0.5	2000	5	2.3	1.46	0.204
4	0.3	1300	7	2.5	1.89	0.163
5	0.3	1500	12	3.1	1.25	0.253
						f_i=1.646 × 10^7 ft^2

[a] $A_m = 4.1 \times 10^7$ ft^2, $\Sigma S_i = 2.7 \times 10^7$ ft^2; *other conditions are the same as in Table 8.5.*

The values in Table 8.6 yield a value for $F_s = (k/q_p)\,\Sigma f_i = 0.41$. Use of this alternative scheme results in an intake-condenser temperature rise ratio of $(T_{EFF} - T_{EQ})\Delta T_c = 0.34$. Because the lowest effluent temperature possible is desired, the second scheme is more advantageous. This should have also been obvious from intuition, as there is a significantly greater distance, and hence more pond involved, than in the first case.

This method can also be extended to flow-through ponds. These ponds have a large inflow and outflow as compared to the plant pumping rate. Consider the pond shown in Fig. 8.13. Under the condition of a flow-through pond, Eq. 8.34 becomes

$$\frac{T_{Eff} - T_{EQ}}{\Delta T_c} = \frac{\exp(-kA_m/q_t)}{\frac{q_t}{q_p}\left[1 - \exp\left(\frac{-kA_m}{q_t}\right)\right] + 1 - \exp\left[\frac{-k(A_m - A_D)}{q_p}\right] + \frac{q_r}{q_p}\left[1 - \exp\left(\frac{-kA_I}{q_p}\right)\right] + F_s}, \tag{8.35}$$

in which A_I is the main flow path at the inflow arm, q_r is the inflow rate, $q_t = q_r + q_p$, and A_D is the main flow path area at the outflow arm. In evaluating the impact of a power plant on a stream, the outlet temperature of the pond, T_{RO}, may be of concern. If the inflow temperature is known, the following relation can be used to determine T_{RO}:

$$\frac{T_{RO} - T_{EQ}}{T_{EFF} - T_{EQ}} = \exp[k(A_m - A_D)/q_t] \exp(-kS_o/q_r) \ . \tag{8.36}$$

where S_o is the area of this arm.

As with earlier models, caution should be used with this model in accepting the results at their absolute value rather than accepting them as values to compare alternative schemes evaluated by the same method. It does, however, provide a simple means for trying to estimate effects of dead areas. More sophisticated models are probably not yet justified on the basis of current understanding of ponds.

I. Evaporation Losses from Ponds

In arid regions, the loss of water due to evaporation can be a major problem. However, calculations of water loss are at best based on empirical equations. The following discussion will be divided into water losses from completely mixed ponds and from plug-flow ponds.

1. Completely Mixed Ponds

Calculation of evaporation losses in a completely mixed pond is simpler because the surface temperature is constant everywhere on the pond's surface. This means that once the heat loss due to evaporation is determined, the amount of water loss is directly obtained.

As discussed in the Chapter III, Edinger and Geyer[32] use the following general formula to determine the heat loss due to evaporation, Q_e:

$$Q_e = (a + bW)(P_W - P_A) \text{ Btu/ft}^2\text{-day} , \tag{8.37}$$

where a and b are empirical coefficients for the studies listed in Table 3.1, W is the wind speed in miles per hour, P_W (mm H_g) is the saturated vapor pressure corresponding to the temperature of the water, and P_A (mm H_g) is the water-vapor pressure of the air.

Once Q_e is determined from Eq. 8.37, the following equation can be used to determine the rate of water loss due to evaporation, M_E:

$$M_E = \frac{Q_e A}{\Delta h} \text{ lb}_m\text{/day} , \tag{8.38}$$

where A (ft^2) is the surface area of the completely mixed pond, and Δh is the heat of vaporization, taken as 1070 Btu/lb_m as an average value for the expected range of pond temperatures.

Therefore, the methods discussed in earlier sections of this chapter to determine the water-surface temperature for completely mixed ponds, plus Eqs. 8.37 and 8.38, allow one to determine M_E. The evaporation rate, E, in feet per day can be computed by

$$E = \frac{M_E}{\rho A} . \tag{8.39}$$

Edinger and Geyer also developed the following equation to relate Q_e to the heat-exchange coefficient, K:

$$Q_e = \frac{K - 15.7}{0.26 + \beta} (P_W - P_A) , \tag{8.40}$$

in which β is the proportionality coefficient for linearizing the temperature/vapor-pressure relation for given temperature ranges (see Fig. 3.3).

Hogan *et al.*[56] use the same general form as Eq. 8.37 to develop another procedure for estimating water loss due to evaporation from a completely mixed pond. They use the polynomial expansion

$$P_W = a_1 + a_2\Theta + a_3\Theta^2 + a_4\Theta^3 \tag{8.41}$$

and substitute this into Eq. 8.37 to obtain

$$M_E \frac{\Delta h}{A} \frac{1}{a + bW} = (a_1 + a_2\Theta + a_3\Theta^2 + a_4\Theta^3) - P_A' , \qquad (8.42)$$

in which $a = a_{12} = 3730$, $b = a_{13} = 373$, Θ is the pond surface temperature relative to 32°F, and P_A' is the vapor pressure of atmospheric air, in psia. The left-hand side of Eq. 8.42 is plotted in Fig. 8.14 as a function of Θ versus P_A. Therefore, one T_P and P_A are calculated.

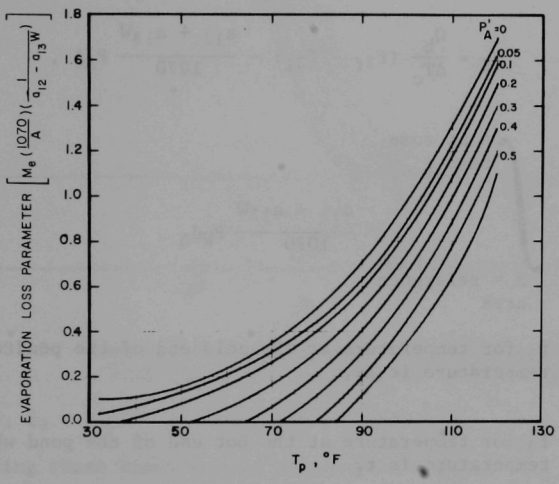

Fig. 8.14. Evaporation-loss Parameter for Mixed Pond in Steady State as a Function of Temperature.[56]

We can determine the value of the left-hand side of Eq. 8.42. Then, knowing A, Δh, and W, we can calculate M directly. The evaporation in length/time can be obtained from Eq. 8.39.

As an example problem, assume the conditions in Case I (Sec. VIII.E.1) for the 800-acre pond, where $T_{SS} = 98.0$°F, $A = 2.485 \times 10^7$ ft^2, $P_A' = 0.348$ psia, and $a_{12} + a_{13}W = 6190$. Therefore, from Fig. 8.14,

$$M_E \frac{1070}{A} \frac{1}{a_{12} + a_{13}W} = 0.5 ,$$

$$M_E = 0.5 \frac{A}{1070} (a_{12} + a_{13}W) = 0.5 \frac{3.485 \times 10^7 \text{ ft}^2}{1070} 6190 = 10.1 \times 10^7 \text{ lb}_m/\text{day} ,$$

and

$$E = \frac{10.1 \times 10^7 \text{ lb}_m/\text{day}}{(62.4 \text{ lb}_m/\text{ft}^3)(3.485 \times 10^7 \text{ ft}^2)} = 0.0464 \text{ ft/day} .$$

2. Plug-flow Pond

Calculation of evaporation losses in a plug-flow pond is complicated because the water-surface temperature is a function of location in the pond.

Hogan *et al.* use Eqs. 8.37 and 8.19 to derive

$$M_E = \frac{Q_b}{\Delta T_c}(f_{3f} - f_{3i}) - \frac{a_{12} + a_{13}W}{1070} P_A' A , \tag{8.43}$$

where $$f_3 = \int_{A = \text{reference area}}^{A \text{ at some temp } T} \frac{a_{12} + a_{13}W}{1070} P_W d_A ,$$

f_{3i} = f_3 for temperature at the cold end of the pond where the temperature is T_i,

and

f_{3f} = f_3 for temperature at the hot end of the pond where the temperature is t_f.

Values for f_3 are calculated from a plot of $\Delta\Theta$ versus f_3 for certain values of T_{EQ}, where $\Delta\Theta_i = T_i - T_{EQ}$ and $\Delta\Theta_f = T_f - T_{EQ}$. Thus, knowing T_{EQ}, T_i, and T_f from Fig. 8.15, one can find f_{3i} and f_3. Inserting these values into Eq. 8.43 along with the other known values allows rapid determination of the rate of evaporation losses, M.

The values of f_3 physically represent the P_W term in Eq. 8.42. However, because Eq. 8.43 is for a plug-flow pond, this term must be integrated over the area it has passed. Before the P_W term can be integrated, the way in which the surface temperature (and hence P_W) varies with the pond area must be known. This is where Eq. 8.19 is used and why Fig. 8.15 is used. Because P_A does not vary along the pond's length, it does not require integration.

As an example, consider the problem in Case V (Sec. VIII.E.5) for an 800-acre pond.

Here $\Delta T_c = 15°F$, $A = 3.485 \times 10^7$ ft^2, $T_i = 107.4°F$, $T_f = 92.3°F$, and $T_{EQ} = 82.3°F$. Therefore $\Delta\Theta_i = T_i - T_{EQ} = 107.4 - 82.3 = 25.1°F$, and $\Delta\Theta_f = T_f - T_{EQ} = 92.3 - 82.3 = 10.0°F$.

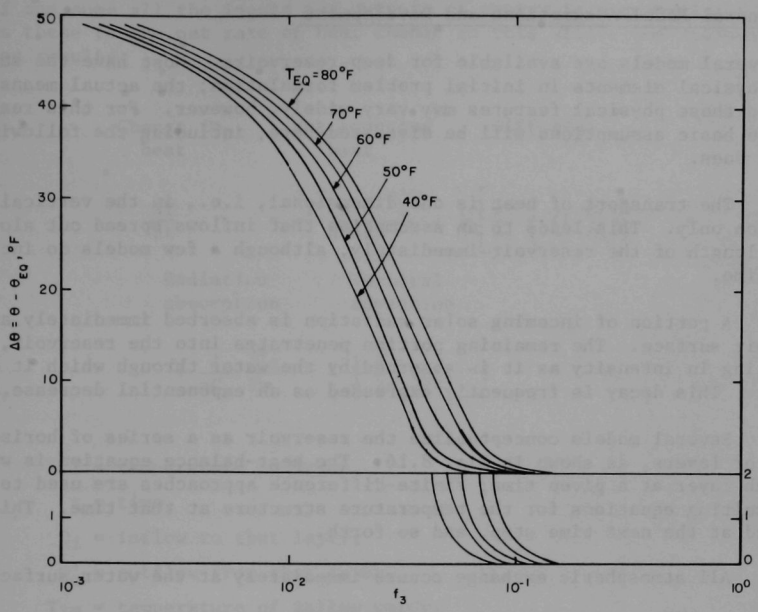

Fig. 8.15. Evaporation-loss Parameter vs. Temperature for a Plug-flow Pond Operating in Steady State.[56]

From Fig. 8.15, $f_3 = 2.65 \times 10^{-2}$ and $f_{3f} = 5.05 \times 10^{-2}$.

Substituting these known values into Eq. 8.43 gives

$$M_E = \frac{10{,}900 \times 10^7}{15} (5.05 \times 10^{-2} - 2.65 \times 10^{-2})$$

$$- \frac{6190}{1070} 0.348(3.485 \times 10^7)$$

$$= 17.45 \times 10^7 - 7.00 \times 10^7 = 10.45 \times 10^7 \text{ lb/day} .$$

J. Deep-pond Modeling

A cooling pond more than about 30 ft deep may develop a cycle of stratification through the year characteristic of many deep lakes and reservoirs. In this case, inflows and outflows from sources other than the power plant may also draw water from one level and return it at another. For these deeper ponds, analysis may require a model to predict vertical temperature structure in the lake. Such models will be called deep-reservoir models herein.

1. General Model Assumptions and Development

Several models are available for deep reservoirs. Most have the same basic physical elements in initial problem formulation; the actual means of treating these physical features may vary widely, however. For this reason, only the basic assumptions will be discussed here, including the following typical ones.

a. The transport of heat is one-dimensional, i.e., in the vertical direction only. This leads to an assumption that inflows spread out along the entire length of the reservoir immediately, although a few models do include a lag time.

b. A portion of incoming solar radiation is absorbed immediately at the reservoir surface. The remaining portion penetrates into the reservoir, decreasing in intensity as it is absorbed by the water through which it is passing. This decay is frequently expressed as an exponential decrease.[28]

c. Several models conceptualize the reservoir as a series of horizontal slices or layers, as shown in Fig. 8.16. The heat-balance equation is written for each layer at a given time; finite-difference approaches are used to solve the resulting equations for the temperature structure at that time. This is repeated at the next time step, and so forth.

d. All atmospheric exchange occurs immediately at the water surface.

Figure 8.16 illustrates the physical factors to be included in such a model. Inflows and outflows must be included, possibly including the vertical distribution of velocities due to these motions. Some models include the capability for handling more than one inflow and several outlets at different elevations. Atmospheric exchange and absorbed solar radiation have been mentioned. Vertical advection is the vertical motion of water due to inflows and outflows. For example, if, during a given time period, inflow below a certain elevation is greater than outflow below that point, a water particle initially sitting at that elevation will move up. Diffusion is the movement of heat in the direction of the temperature gradient. It may consist of simple molecular diffusion, and some authors also include turbulent diffusion.

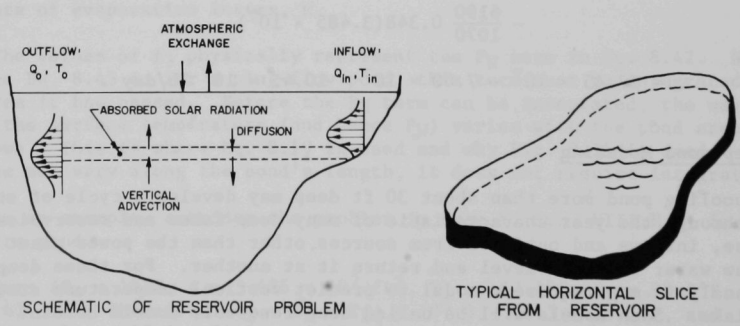

Fig. 8.16. Schematic Diagram of Reservoir Problem.

If one sums all the inputs and outputs of energy to a general slice and equates these to the net rate of heat change in this slice, the following equation results:

$$\underbrace{\frac{\partial T}{\partial t}}_{\text{Change in heat}} = \underbrace{\frac{Q_i T_{IN} - Q_o' T}{A\ \delta z}}_{\text{Net advected heat}} + \underbrace{\frac{1}{A}\left[\frac{\partial}{\partial z}\left(AE'\ \frac{\partial T}{\partial z}\right)\right]}_{\text{Diffusion}} \tag{8.44}$$

$$+ \underbrace{\frac{1}{\rho C_p}\frac{\partial \phi_z}{\partial z}}_{\text{Radiation absorption}} - \underbrace{\frac{1}{A}\frac{\partial}{\partial z}(Q_v' T)}_{\text{Vertical advection}} ,$$

where T = temperature in layer,

t = time,

Q_i = inflow to that layer,

Q_o' = outflow from that layer,

T_{IN} = temperature of inflow water,

A = area of slice in plan view,

E' = diffusion coefficient,

ϕ_z = solar-radiation flux past elevation z,

Q_v' = vertical advective flow rate past elevation z, and

δ_z = thickness of slice.

Solution of Eq. 8.44 requires two boundary conditions (reservoir bottom and surface) and an initial condition, which would be any known temperature profile in the lake. For simplicity, the initial condition is often taken as the early spring isothermal condition. The bottom boundary condition is usually assumed to allow no heat exchange across the bottom of the reservoir. Huber and Harleman[61] note that the surface boundary condition requires that the heat diffused past the reservoir surface must equal the net exchange of heat with the atmosphere.

These solutions are usually performed by finite-difference techniques on a digital computer. Inputs usually require various meteorological data (often daily averages), reservoir geometry, inflows and inflow temperatures, outflows, diffusion coefficients, and possibly some other empirical parameters. Output from these programs is the temperature structure with depth at every time step (often one day), as well as outflow temperatures.

2. Available Models

Numerous models are available. Among the most prominent are those by Water Resources Engineers (Refs. 26, 97, and 141), MIT (Refs. 61, 62, and 120) and Cornell (Ref. 134). Readers are referred to these sources for details and programs. A study at Vanderbilt University is reviewing these and several other models to test model sensitivity and accuracy.

3. Application of Deep-reservoir Models to Cooling Ponds

Slotta and Van Dyke[127] have adapted the MIT model to study the possible use of Lake Norman as a cooling pond for a proposed new steam plant. The Cornell model was initially developed to study effects of heated discharges on the stratification in Lake Cayuga.

The use of the MIT model by Slotta and Van Dyke is indicative of possible uses of such models. Three withdrawal levels were included: one at a hydroelectric dam, one for the Marshall steam plant, and one for the proposed McGuire plant. The model was first verified by testing predicted against measured temperatures for 1969 data. Then, the model was used to simulate what might happen when the new steam plant went on line. A discharge amounting to required cooling-water flow was withdrawn from the 100-ft depth in the model simulation. This flow rate was given an increase in temperature, ΔT_c (the condenser rise), and returned to the reservoir as a part of the inflow. This method simulates both the addition of heat and possible effects on reservoir hydrodynamics due to added withdrawal and inflow. One of the most important items in obtaining good model fit to data lies in accounting for entrance mixing at inflow points. Unfortunately, the model as it was actually applied to the Lake Norman case was inappropriate. An initial dilution of 5 was used in the model by Slotta and Van Dyke, while the actual discharges exhibit dilutions more on the order of 1.5-2.

The model is then used to estimate changes in reservoir temperatures and degrees of stratification, outflow temperatures at the hydroelectric dam and intake water temperatures at the Marshall Plant. Fall results are in the report.[127]

4. Summary on Deep-reservoir Models

Several models, with programs and documentation, are available for use on the deep-pond problem. The effects of new plants, even with different users on the pond, can be estimated. These models, of course, do require an extensive amount of data for use. However, where several competing uses exist for water in a lake, the effort required to obtain these data and run the model may well be justified.

5. Models for Other Deep-pond Cases

The deep-reservoir models outlined in the immediately preceding sections are valid if the pond does, in fact, exhibit horizontal isotherms so that the important transfer processes are essentially vertical in character. In some ponds, however, both horizontal and vertical temperature gradients exist. Ryan[119] mentions this case. The epilimnion then acts very much like a shallow pond. Use of the deep-reservoir models already discussed will enable the

thickness of this upper layer to be determined. The various shallow-pond models can then be applied to approximate the behavior of the pond.

A third type of deep pond discussed by Ryan is similar to the deep, flow-through pond described in the preceding paragraph, but the power-plant discharge is large enough, relative to the pond size, to dominate the action of the pond. Hogan *et al.*[56] obtained good results using their plug-flow, transient-condition model to analyze the Mt. Storm cooling pond in West Virginia. Good agreement of predicted and observed plant-intake temperatures was obtained. Ryan notes that this good agreement is interesting, inasmuch as considerable horizontal mixing (entrance mixing) does occur at this plant.

Ryan proposes a simple model for accounting for entrance mixing in deep ponds. He treats a deep, relatively narrow pond with a hot inflow rate of Q_p and temperature of T_{IN} and a dilution factor D. Here, D = (discharge flow plus entrained ambient fluid)/discharge flow. He assumes that the mixed flow moves to the end of the pond as a plug flow utilizing the full surface area of the pond; it then returns to the plant intake underneath the surface layer. Therefore, the temperature at the far end of the pond will equal the temperature of the water returning along the pond bottom. Assuming no further heat loss on the return along the bottom due to no exposure to the atmosphere, the temperature of this flow equals T_{EFF}, the plant-intake temperature. Let T_{MIX} = the temperature of the flow after dilution by entrance mixing. Therefore,

$$T_{MIX} = \frac{T_{IN} + (D - 1)T_{EFF}}{D} . \tag{8.45}$$

With appropriate redefinition of terms, the solution to the plug-flow problem in the surface layer is the same as that found in Eq. 8.6 and can be written as

$$\frac{T_{EFF} - T_{EQ}}{T_{MIX} - T_{EQ}} = \exp(-r_1) , \tag{8.46}$$

in which

$$r_1 = \frac{KA}{\rho C_p D Q_p} . \tag{8.47}$$

Combination of Eqs. 8.45 and 8.46 yields, after rearrangement,

$$\frac{T_{EFF} - T_{EQ}}{T_{IN} - T_{EQ}} = \frac{\exp(-r_1)}{D - (D - 1)\exp(-r_1)} \tag{8.48}$$

or

$$\frac{T_{EFF} - T_{EQ}}{T_{IN} - T_{EQ}} = \frac{\exp(-r/D)}{D - (D - 1)\exp(-r/D)} \tag{8.49}$$

in which $r = KA/(\rho C_p Q_p)$, as defined earlier.

Recall that a similar expression has been developed for shallow ponds and is shown in Eq. 8.32 and Fig. 8.11. Comparison with those results shows that entrance mixing has a smaller influence on the performance of a deep pond than in a shallow one, where both outgoing and return flows are at the surface and exposed to atmospheric cooling. As an example, consider $r = 2$ and $D = 4$. For plug flow ($D = 1$), Eqs. 8.32 and 8.49 give identical results, or an excess temperature ratio = $(T_{EFF} - T_{EQ})/(T_{IN} - T_{EQ})$, of 0.135. Insertion of $r = 2$ and $D = 4$ into Eqs. 8.32 and 8.49 yields excess temperature ratios of 0.328 and 0.278 for the shallow and deep ponds, respectively. Therefore, entrance mixing here decreased the cooling capacity of the shallow pond more than that of the deep pond. Consider this case with $T_{EQ} = 80.0°F$ and $T_{IN} = 95.0°F$. Then, T_{EFF} would equal 82.0, 84.9, and 84.2°F for the plug flow, shallow pond with $D = 4$, and deep pond with $D = 4$, respectively.

Although this entrance mixing model was developed as an idealized representation of a real cooling pond, preliminary laboratory data at Massachusetts Institute of Technology indicate reasonable agreement of the model with measurements. At present, it seems a reasonable beginning point to use this model to account for entrance mixing in deep ponds. The dilution factor, D, is a function of the discharge-channel design and can be therefore controlled by the designer. One of the surface-discharge analysis techniques presented in Chapter 5 can be used to evaluate D. Especially applicable is the Stolzenbach-Harleman model. As with any pond analysis, however, all factors affecting pond behavior must be studied carefully and a large portion of good judgement applied.

6. Summary on Deep-pond Modeling

An effort has been made to summarize some of the available thought on deep cooling ponds. When ponds are more than about 20-30 ft deep, these methods should be investigated. Whatever analysis technique is used, some estimate of the impact of entrance mixing is essential. It is also necessary to estimate whether one has a horizontally mixed pond or one with horizontal, in addition to vertical, temperature gradients existing. In the former case, one of the available deep-reservoir models can be used. In the latter case, the method selected varies according to how heavily loaded the pond is, as noted earlier and by Ryan.[119] These models should be treated as guides to decisions on pond design and performance, for the current state of the art does not admit to sufficient experience to yield full confidence in predictions.

K. Conclusion

The methods for cooling-pond analysis presented in this chapter are felt to be among the best available. However, the state of the art in cooling-pond analysis requires that these methods be applied judiciously. A major portion

of this chapter deals with the idealized models. A review of the literature will show that most of the effort in cooling-pond analysis has also been directed toward analysis of idealized ponds. Direct application of idealized models to real ponds may lead to questionable results. An attempt is made in this chapter to show the range of answers one can obtain for a single problem using the various idealized models. The section on expected accuracy from idealized models will help the reader realize just how wide this range can be. This does not mean, however, that the idealized models are useless. With proper care in analyzing such major terms as the coefficients for evaporation, idealized models can be used for those ponds that satisfy the hydraulic assumptions made in these models.

When the hydraulic assumptions of idealized models are not met, one must rely on intuition as well as a thorough assessment of all pertinent factors. The entrance entrainment model presented in this chapter gives the reader a feel for the significant effect entrance mixing can have on cooling-pond analysis. Experience with application of deep-reservoir analysis to a cooling lake verifies this.

At present the model is not verified as a predictive tool. However, future application of the model to data from existing ponds may enable its extension to proposed ponds with similar entrance geometry. Work is underway at MIT to develop a better approach to the entrance-mixing problem.

The active-region model is the only one presented in this chapter that analyzes the total pond for nonidealized flow. Although the approach taken in this model requires one to select dead and active regions by intuition, if proper care is taken in selecting regions the results of this model can be fairly reliable. Recall that density currents can play an important part in moving heated water into usually dead areas.

When making an analysis, the reader is encouraged to use all the models presented. A suggested approach would include the following steps:

1. Make complete analysis of the meteorological data for the region. Emphasis is placed on the evaluation of the evaporation term.

2. Perform an analysis of the entrance region of the pond. In this analysis, the geometry of the inlet structure and the general shape of the pond in this region are of major importance. If entrance entrainment is determined to be a major factor, a possible approach is to treat this entrance region as a separate pond that discharges along its entire width into a second pond that represents the remaining portion of the physical pond.

3. Determine the active and dead regions of the pond. Application of the active-region model can then be made. Once the various regions are determined, another possible approach is to apply the idealized models to the active regions. This approach should allow one to bracket the actual performance by assuming plug flow for the best performance and completely mixed flow for the worst. This performance bracket can be moved up or down the performance scale by allowing more or less heat to be lost through the areas of the dead regions. The worst level of the performance bracket corresponds to the assumption that no heat is lost from the area of the dead regions.

If the pond is strongly stratified and the intake and discharge are on the surface, the epilimnion might easily be treated as a shallow pond. On the other hand, if intake or discharges are located in the hypolimnion, it may be necessary to use a deep-reservoir computer model to simulate the response of the pond to various proposed plant arrangements and operating schedules. However, if horizontal temperature gradients are expected in the pond, a model other than the deep-reservoir model must be used.

As a final word, those charged with designing cooling ponds or evaluating them for impact should consider alternative pond designs to optimize pond behavior. This analysis should include an assessment of land costs, reduction in plant capacity due to back pressure, cost of makeup water, effect of discharge temperature, and temperature rise across the condensers. Effects of winds, density currents, and any other factors should be evaluated to effect an optimum design.

APPENDIX A

Shirazi *et al.* Model, Including the Effect of Ambient Turbulence on Buoyant Jets

Shirazi *et al.** have analyzed the data collected by McQuivey *et al.*[90] These data covered the important ranges $0.3 \leq k \leq 10$ and $4 \leq F_j \leq 200$. Most measurements were taken for s/D_o greater than about 15 and were therefore outside the ZOFE. By use of dimensional analysis and regression techniques, Shirazi *et al.* find the following relationships:

Coflowing ($\theta_0' = 0°$)

$$\frac{\Delta T}{\Delta T_o} = 16.0 F_j^{-0.43}\, k^{1.3}\, (s/D_o)^{-1.5} \; ; \tag{A.1}$$

$$\frac{w}{D_o} = 0.15 F_j^{0.42}\, k^{-0.56}\, (s/D_o)^{0.90} \; ; \tag{A.2}$$

$$\frac{Z}{D_o} = 0.20 F_j^{-0.82}\, k^{0.89}\, (s/D_o)^{0.98} \; . \tag{A.3}$$

Crossflow ($\theta_0' = 90°$)

$$\frac{\Delta T}{\Delta T_o} = 0.38 F_j^{0.50}\, k^{-0.66}\, (s/D_o)^{-0.73} \; ; \tag{A.4}$$

$$\frac{w}{D_o} = 0.66 F_j^{-0.011}\, k^{0.60}\, (s/D_o)^{0.40} \; ; \tag{A.5}$$

$$\frac{z}{D_o} = 1.7 F_j^{-0.23}\, k^{0.95}\, (s/D_o)^{0.37} \; . \tag{A.6}$$

The example problem used in Sec. VI.K to illustrate the Fan[38] and Hirst[54] models in Chapter VI can be used here. Recall the basic data: $\theta_0' = 0°$, $u_o = 8.5$ fps, $U_o = u_o + U_a \cos\theta_0 = 8.5 + 2 = 10.5$ fps, $D_o = 16$ ft, $T_o = 77°F$ with $\rho_1 = 0.99707$, and $T_a = 59°F$ with $\rho_0 = \rho_a = 0.99913$. As shown in Sec. VI.K.2.a, this yields values of $F_j = 10.2$ and $k = 5.25$.

---

*M. A. Shirazi, L. R. Davis, and K. V. Byram, Effects of Ambient Turbulence on Buoyant Jets Discharged into a Flowing Environment, Pacific Northwest Environmental Research Laboratory, Working Paper No. 2, Environmental Protection Agency, Corvallis, Oregon (Jan 1973).

Compare the results given by the Shirazi regression equations at the water surface, the terminal point in this case. Equation A.3 enables evaluation of s/D_o at the surface:

$$Z/D_o = 160/16 = 10 = 0.20(10.2)^{-0.82}\ (5.25)^{0.89}\ (s/D_o)^{0.98}\ .$$

Solving this yields

$$s/D_o = 83.8\ .$$

Thus, s = axial distance to surface = 83.8(16) = 1340 ft.

Use of this axial distance in Eq. A.1 enables evaluation of the temperature rise at the surface.

$$\frac{\Delta T}{\Delta T_o} = 16(10.2)^{-0.43}\ (5.25)^{1.3}\ (s/D_o)^{-1.5}$$

$$= 51.1(s/D_o)^{-1.5} = 51.1(83.8)^{-1.5} = 1/15 = 0.067\ .$$

Therefore, the surface dilution is about 15, or the surface temperature rise, ΔT_s, is

$$\Delta T_s = 0.067(18) = 1.2°F\ .$$

These values compare with predictions for s/D_o at the surface = 569 ft and surface dilution = 22.2 by the Hirst model. These differences are significant. On the basis of fits to available coflow data, Shirazi recommends use of Eqs. A.1, A.2, and A.3 as the best available model for coflowing discharges.

APPENDIX B

Koh-Fan Jet Model, Modified to Account for Changes in the Zone of Flow Establishment (ZOFE)

After this report was completed, but before it went to press, some additional information was discovered on analytical treatment of submerged discharges into stagnant receiving waters.

Shirazi and Davis have made extremely thoughtful reviews of available submerged jet data and theory to prepare their workbook.[123] They now recommend use of a modified version of the Koh-Fan model[73] for horizontal discharges into stagnant media, rather than the Fan-Brooks model[39] recommended in this report. Shirazi and Davis reason that for F_j less than about 10, buoyancy forces are sufficient to force the jet up within the ZOFE, thereby making the angle, θ_0, at the end of this zone, not equal to the initial discharge angle, θ_0'. Recall that the Fan-Brooks model suggests use of $\theta_0' = \theta_0$ for all values of F_j. Shirazi and Davis attempt to account for buoyancy by use of the Abraham model[2] until the end of the ZOFE. Conditions at this point then become the input to the Koh-Fan computer program (described in Chapter VII) for the remainder of the jet trajectory.

Since the Koh-Fan model for a single port is essentially identical to the Fan-Brooks model, the only change lies in an improved description of the ZOFE by splicing the Abraham and Koh-Fan models together.

ACKNOWLEDGMENTS

This report was performed under Contract No. 31-109-38-2701 between the University of Chicago (Operator of Argonne National Laboratory) and Barry A. Benedict. The comments and critique recieved from Mr. Barton M. Hoglund, Dr. Philip F. Gustafson, and their associates at Argonne National Laboratory are gratefully acknowledged.

Thanks are also expressed to several workers in the field of thermal discharges who shared their thoughts with the authors by telephone during the writing of the report. These include Mr. Robert Baca, Water Resources Section, Battelle-Northwest; Dr. Eric Hirst, Oak Ridge National Laboratory; Dr. Keith Stolzenbah, Tennessee Valley Authority; and Drs. Loren Davis and Mostafa Shirazi, Pacific Northwest Water Laboratory, Environmental Protection Agency. In addition, earlier discussions with Mr. John V. Tokar and Dr. Anthony J. Policastro were helpful in the final report preparation. Numerous other communications with these and other workers over the last few years should not be discounted in their impact in the discussion herein.

Dr. Frank L. Parker, our colleague at Vanderbilt University, provided helpful review and thoughtful commentary on sections of the report. His efforts of the last several years have been important in providing the background at Vanderbilt to prepare such a summary.

REFERENCES

1. Abraham, G., *Jet Diffusion in Stagnant Ambient Fluid*, Delft Hydraulics Laboratory, No. 29 (1963).

2. Abraham, G., *The Flow of Round Jets Issuing Vertically into Ambient Fluid Flowing in a Horizontal Direction*, Proceedings of the 5th International Water Pollution Research Conference, San Francisco, III 15/1 - III 15/7 (1970).

3. Abramovich, G. N., *The Theory of Turbulent Jets*, The Massachusetts Institute of Technology Press, Cambridge, Mass. (1963).

4. Ackers, P., *Modeling of Heated Water Discharges*, Engineering Aspects of Thermal Pollution, Vanderbilt University Press, Nashville, Tenn. (1969).

5. Albertson, M. L., Y. B. Dai, R. A. Jensen, and H. Rouse, *Diffusion of Submerged Jets*, Trans. Am. Soc. Civil Eng. 115, 639-697 (1950).

6. Anderson, E. R., *Energy-Budget Studies, Water-Loss Investigations: Vol. 1--Lake Hefner Studies, Tech. Report*, U. S. Geological Survey Circ. 229, Washington, D. C. (1952).

7. Anderson, E. R., *Energy-Budget Studies, Water-Loss Investigations: Lake Hefner Studies*, Prof. Paper 269, U. S. Geological Survey, Washington, D. C. (1954).

8. Anderson, J. L., *Negatively Buoyant Jets in a Cross Flow*, Environmental and Water Resources Engineering Department, dissertation, Vanderbilt University, Nashville, Tenn. (1972).

9. Ayers, J. C., R. F. Anderson, N. W. O'Hara, and C. C. Kidd, *Cook Plant Preoperational Studies, 1969*, Benton Harbor Power Plant Limnological Studies, Part IV, Special Report No. 44 of the Great Lakes Research Division, the University of Michigan, Ann Arbor (Mar. 1970).

10. Baca, R. G., *A Computer Program for Thermal Plume Modeling*, Technical Memo, Battelle Pacific Northwest Laboratories, Richland, Wash. (1971).

11. Baca, R. G., unpublished notes defining derivation of equation for submerged jet in three space dimensions (1972).

12. Barnes, H. H., *Roughness Characteristics of Natural Channels*, U. S. Government Printing Office, Washington, D. C. (1967).

13. Bata, G. L., *Recirculation of Cooling Water in Rivers and Canals*, J. Hydraul. Div., Am. Soc. Civil Eng., 83(HY3), 1265-1 to 1265-26 (1957).

13a. Baumgartner, D. J., D. S. Trent, and K. V. Byram, *User's Guide and Documentation for Outfall Plume Model*, Working Paper No. 80, Environmental Protection Agency, Pacific Northwest Water Laboratory, Corvallis, Oregon (May 1971).

14. Beer, L. P., and W. O. Pipes, *Environmental Effects of Condenser Water Discharge in Southwest Lake Michigan*, Consulting Engineering Report, Environmental Sciences Industrial Bio-Test Laboratory, Inc. (1969).

15. Benedict, B. A., *Heated Surface Jet Model Applied to Lakes*, Meeting Preprint 1603, National Water Resources Engineering Meeting, ASCE, Atlanta, Georgia, January 24-28, 1972.

16. Bosanquet, C. H., W. H. Carey, and E. M. Halton, *Dust Deposition from Chimney Stacks*, Proc. Inst. Mech. Eng. (London) 162, 355 (1950).

17. Bowen, I. S., *The Ratio of Heat Losses by Conduction and by Evaporation from Any Water Surface*, Phys. Rev. 27 (June 1926).

18. Brady, D. K., W. L. Graves, and J. C. Geyer, *Surface Heat Exchange at Power Plant Cooling Lakes*, Publication No. 69-901, Edison Electric Institute, New York (1969).

19. Brooks, N. H., *Diffusion of Sewage Effluents in an Ocean Current*, Proceedings of First International Conference on Waste Disposal in the Marine Environment, E. A. Pearson, Editor, Pergamon Press, New York, 246 (1960).

20. Callaway, R. J., K. V. Byram, and G. R. Ditsworth, *Mathematical Model of the Columbia River from the Pacific Ocean to Bonneville Dam: Part I, Theory, Program Notes and Programs*, Federal Water Pollution Control Administration, Northwest Region, Pacific Northwest Water Laboratory, Corvallis, Oregon (Nov. 1969).

21. Carter, H. H., *A Preliminary Report on the Characteristics of Heated Jet Discharged Horizontally into a Transverse Current: Part I -- Constant Depth*, Chesapeake Bay Institute, The Johns Hopkins University, Reference 69-14, Technical Report 61 (Nov. 1969).

22. Cederwall, K., *Hydraulics of Marine Waste Water Disposal*, Report No. 42, Hydraulic Division, Chalmers Institute of Technology, Göteborg, Sweden (1968).

23. Cederwall, K., and N. Brooks, *A Buoyant Slot Jet into a Stagnant or Flowing Environment*, W. M. Keck Laboratory Report No. KH-R-25, California Institute of Technology, Pasadena (1971).

24. Chikwendu, L. N., and J. R. D. Francis, *Arrested Warm Water Layers in Curved Rivers*, J. Inst. Water Eng. 21(3), 351-366 (1967).

25. Chow, V. T., *Open-Channel Hydraulics*, McGraw-Hill, New York (1959).

26. Corps of Engineers, *Application of WRE Reservoir Temperature Simulation Model NPD Computer Program 723-K5-G067*, North Pacific Division, U. S. Army Corps of Engineers (Sept. 1970).

27. Csanady, G. T., *Dispersal of Effluents in the Great Lakes*, Water Research, 4, 79-114 (Jan. 1970).

28. Dake, J. M. K., and D. R. F. Harleman, *Thermal Stratification in Lakes: Analytical and Laboratory Studies*, Water Resour. Res. 5(2), 484-495 (Apr. 1969).

29. Davis, L., personal communication (1972).

30. Ditmars, J. D., *Computer Program for Round Buoyant Jets into Stratified Ambient Environments*, W. M. Keck Laboratory Tech. Memo. 69-1, California Institute of Technology, Pasadena (1969).

31. Ditmars, J. D., *Submerged Discharges: Single-Port and Multiple-Port Diffusers*, Chapter 5 in Engineering Aspects of Heat Disposal from Power Generation, MIT Summer Session Short Course Proceedings, Ralph M. Parsons Laboratory for Water Resources and Hydrodynamics, Cambridge, Mass., June 28-July 2, 1971.

32. Edinger, John E., and John C. Geyer, *Heat Exchange in the Environment*, Publication No. 65-902, Edison Electric Institute, New York (1965).

33. Edinger, J. E., and E. M. Polk, Jr., *Initial Mixing of Thermal Discharges into a Uniform Current*, Report No. 1, National Center for Research and Training in the Hydrologic and Hydraulic Aspects of Water Pollution Control, Vanderbilt University, Nashville, Tenn. (Oct. 1969).

34. Edinger, J. E., *Shape Factors for Cooling Lakes*, J. Power Div., Proc. Am. Soc. Civil Eng. 97(PO4), 861-867 (Dec. 1971).

35. Edinger, J. E., *Estuarine Temperature Distributions*, in Estuarine Modeling: An Assessment, Capabilities and Limitations for Resource Management and Pollution Control, edited by G. H. Ward, Jr., and W. H. Espey, Jr., Tracor, Inc., Austin, Tex. (Feb. 1971).

36. Edinger, J. E., and N. Yanagida, *Cooling Water Density Wedges in Streams*, J. Hydraul. Div., Am. Soc. Civil Eng. 98(HY2), 412-413 (Feb. 1972).

37. Ellison, T. H., and J. S. Turner, *Turbulent Entrainment in Stratified Flow*, J. Fluid Mech. 6(3), 423-448 (1959).

38. Fan, L. N., *Turbulent Buoyant Jets into Stratified or Flowing Ambient Fluids*, W. M. Keck Laboratory Report No. KH-R-15, California Institute of Technology, Pasadena, Cal. (1967).

39. Fan, L. N., and N. H. Brooks, *Numerical Solution of Turbulent Buoyant Jet Problems*, W. M. Keck Laboratory Report No. KH-R-18, California Institute of Technology, Pasadena, Cal. (1969).

40. Federal Water Pollution Control Administration, Industrial Guide on Thermal Pollution, Pacific Northwest Laboratory, Corvallis, Oregon (1968).

41. Fischer, H. B., *A Method for Predicting Pollutant Transport in Tidal Waters*, Hydraulic Laboratory, University of California, Berkeley (Mar. 1970).

42. Fitch, N. R., *Temperature Surveys of St. Croix River, 1969-1970, for the Allen S. King Generating Plant, Oak Park Heights, Minnesota*, Northern State Power Company Environmental Monitoring Program Report (Dec. 1970).

43. Fox, D. G., *Forced Plume in a Stratified Fluid*, J. Geophys. Res. 75(33), 6818-35 (1970).

44. Gördier, R. L., *Studies on Fluid Jets Discharging Normally into Moving Liquid*, Technical Report No. 28, Series B., St. Anthony Falls Hydraulic Laboratory, University of Minnesota, Minneapolis (Aug. 1959).

45. Harleman, D. R. F., *Stratified Flow*, Handbook of Fluid Dynamics, McGraw-Hill, New York (1961).

46. Harleman, D. R. F., *Pollution in Estuaries*, Chapter 14 in Estuary and Coastline Hydrodynamics, edited by A. T. Ippen, McGraw-Hill Book Co., Inc., New York (1966).

47. Harleman, D. R. F., *Mechanics of Condenser Water Discharge from Thermal Power Plants*, Engineering Aspects of Thermal Pollution, Vanderbilt University Press, Nashville, Tenn. (1969).

48. Harleman, D. R. F., *Longitudinal Temperature Distributions in Rivers and Estuaries: One-Dimensional Mathematical Models*, Chapter 8 in Engineering Aspects of Heat Disposal from Power Generation, MIT Summer Session Short Course Proceedings, Ralph M. Parsons Laboratory for Water Resources and Hydrodynamics, Cambridge, Mass., June 28-July 2, 1971.

49. Harleman, D. R. F., *Physical Hydraulic Models*, in Estuarine Modeling: An Assessment, edited by G. H. Ward, Jr., and W. H. Espey, Jr., EPA Water Pollution Control Research Series, No. 16070 DZV 02/71, pp. 215-254 (Feb. 1971).

50. Harleman, D. R. F., G. Jirka, and K. D. Stolzenbach, *A Study of Submerged Multi-Port Diffusers for Condenser Water Discharge with Application to the Shoreham Nuclear Power Station*, Ralph M. Parsons Laboratory Report No. 139, MIT, Boston, Mass. (July 1971).

51. Harleman, D. R. F., C. H. Lee, and L. Hall, *Numerical Studies of Unsteady Dispersion in Estuaries*, J. Sanitary Div., Am. Soc. Civil Eng. 94, SA5 (Oct. 1968).

52. Harleman, D. R. F., and K. D. Stolzenbach, *A Model Study of Thermal Stratification Produced by Condenser Water Discharge*, MIT Hydrodynamics Laboratory Report No. 107, Cambridge, Mass. (Oct. 1967).

53. Hindley, P. D., R. M. Miner, and R. F. Cayot, *Thermal Discharge: A Model-Prototype Comparison*, J. Power Div., Am. Soc. Civil Eng. 97(PO4), (Dec. 1971).

54. Hirst, E. A., *Analysis of Round, Turbulent, Buoyant Jets Discharged to Flowing Stratified Ambients*, ORNL-4685 (1971).

55. Hirst, E. A., personal communication (1972).

56. Hogan, W. T., A. A. Liepins, and F. E. Reed, *An Engineering-Economic Study of Cooling Pond Performance*, Environmental Protection Agency, Water Pollution Control Research Series, No. 16130 DFX05/70, Washington, D. C. (May 1970).

57. Holley, E. R., *Unified View of Diffusion and Dispersion*, J. Hydraul. Div., Am. Soc. Civil Eng. 95, HY2, Proceeding Paper 6462, 621-631 (Mar. 1969).

58. Holley, E. R., D. R. F. Harleman, and H. B. Fischer, *Disperson in Homogeneous Estuary Flow*, Proc. J. Hydraul. Div., Am. Soc. Civil Eng. 96, HY8 (Aug 1970).

59. Hoopes, J. A., R. W. Zeller, and G. A. Rohlich, *Heat Dissipation and Induced Circulations from Condenser Cooling Water Discharges into Lake Monona*, Report No. 35, Department of Civil Engineering, The University of Wisconsin, Madison (Feb. 1968).

60. Hoult, D. P., J. A. Fay, and L. J. Forney, *A Theory of Plume Rise Compared with Field Observations*, J. Air Poll. Cont. Assn. 20(6), 391-97 (1969).

61. Huber, W. C., and D. R. F. Harleman, *Laboratory and Analytical Studies of the Thermal Stratification of Reservoirs*, MIT Hydrodynamics Laboratory Report No. 122, Cambridge, Mass. (Oct. 1968).

62. Huber, W. C., D. R. F. Harleman, and P. J. Ryan, *Temperature Prediction in Stratified Reservoirs*, J. Hydraul. Div., Am. Soc. Civil Eng. 98(HY4), 645-666 (Apr. 1972).

63. Hutchinson, G. E., *A Treatise on Limnology, Volume I, Geography, Physics, and Chemistry*, John Wiley and Sons, Inc., New York (1957).

64. Ippen, A. T., and D. R. F. Harleman, *Steady State Characteristics of Subsurface Flow*, Gravity Waves Symposium, National Bureau of Standards, Circulation 521 (June 1951).

65. Jaske, R. T., *A Test Simulation of the Temperature of the Illinois River and a Prediction of the Effects of Dresden 2 and Dresden 3 Reactors*, Pacific Northwest Laboratory, AEC Research and Development (Apr. 1969).

66. Jordinson, R., *Flow in a Jet Directed Normal to the Wind*, Aero. Research Council, Report and Memo No. 3074 (1956).

67. Keffer, J. E., and W. D. Baines, *The Round Turbulent Jet in a Cross-Wind*, J. Fluid Mech. 15 481-496 (1963).

68. Keulegan, G., *Wind Tides in Small Closed Channels*, J. Res. Nat. Bur. Stan. 46, 358 (1951).

69. Keulegan, G. H., *Eleventh Progress Report on Model Laws for Density Currents: Form Characteristics of Arrested Saline Wedges*, U. S. Department of Commerce, National Bureau of Standards, Report 5482 (1957).

70. Kleinschmidt, R. S., *Hydraulic Design of Detention Tanks*, J. Boston Soc. Civil Eng. 48, No. 4, Sec. 1, 247-294 (Oct. 1961).

71. Koberg, G. E., *Methods to Compute Long Wave Radiation from the Atmosphere and Reflected Solar Radiation from a Water Surface*, U. S. Geological Survey Prof. Paper, 272-F, Washington, D. C. (1964).

72. Koberg, G. E., G. E. Harbeck, and Hughes, *The Effect of the Addition of Heat from a Power Plant on the Thermal Structure and Evaporation of Lake Colorado City, Texas*, U. S. Geological Survey, Prof. Paper No. 272-B (1959).

73. Koh, C. Y., and L. N. Fan, *Mathematical Models for the Prediction of Temperature Distributions Resulting from the Discharge of Heated Water into Large Bodies of Water*, Report No. 16130DWO 10/70, Washington, D. C. (Oct. 1970).

74. Kolesar, D. C., and J. C. Sonnichsen, Jr., *TOPLYR-II -- A Two-Dimensional Thermal-Energy Transport Code*, Hanford Engineering Development Laboratory, Richland, Wash. (Oct. 1971).

75. Krenkel, P. A., and F. L. Parker, editors, *Biological Aspects of Thermal Pollution*, Vanderbilt University Press, Nashville, Tenn. (1969).

76. Larsen, J., and G. E. Hecker, *Design of Submerged Diffusers and Jet Interaction*, Preprint No. 1614, presented at the American Society of Civil Engineers National Water Resources Engineering Meeting, Atlanta, Ga. (Jan. 1972).

77. Lauff, G. H., *Estuaries*, Publication No. 83, American Association for the Advancement of Science, Washington, D. C. (1967).

78. Lee, S. L., and H. W. Emmons, *A Study of Natural Convection above a Line of Fire*, J. Fluid Mech. 11, 353-68 (1961).

79. Lee, C. H., and D. R. F. Harleman, *One-Dimensional, Real-Time Model for Estuarine Water Quality Prediction*, Water Quality Office Report No. 16070DGW, Environmental Protection Agency, Washington, D. C. (1971).

80. Leendertse, J. J., *Aspects of a Computational Model for Long-Period Water-Wave Propagation*, Memorandum RM-5294-PR, the Rand Corporation, Santa Monica, Cal. (May 1967).

81. Leendertse, J. J., *A Water-Quality Simulation Model for Well-Mixed Estuaries and Coastal Seas: Volume I, Principles of Computation*, Memorandum RM-6230-RC, the Rand Corporation, Santa Monica, Cal. (Feb. 1970).

82. Leendertse, J. J., and E. C. Gritton, *A Water-Quality Simulation Model for Well Mixed Estuaries and Coastal Seas: Vol. II, Computation Procedures*, Study R-708-NYC, The New York City Rand Institute (July 1971).

83. Leendertse, J. J., and E. C. Gritton, *A Water-Quality Simulation Model for Well Mixed Estuaries and Coastal Seas: Vol. III, Jamaica Bay Simulation*, Study R-709-NYC, The New York City Rand Institute (July 1971).

84. Levenspiel, O., *Chemical Reaction Engineering: An Introduction to the Design of Chemical Reactors*, John Wiley and Sons, Inc., New York (1962).

85. Linsley, R. K., M. A. Kohler, and J. L. Paulhus, *Hydrology for Engineers*, McGraw-Hill Book Co., New York, p. 98 (1959).

86. Liseth, P., *Mixing of Merging Buoyant Jets from a Manifold in Stagnant Receiving Water of Uniform Density*, Hydraulic Engineering Laboratory Report No. 23-1, University of California, Berkeley (1970).

87. Liseth, P., *Mixing of Merging Buoyant Jets from a Manifold in Stagnant Receiving Water of Uniform Density*, paper presented at 6th International Water Pollution Research Conference, Jerusalem, Israel (June 1972).

88. Mangelson, K. A., *Hydraulics of Waste Stabilization Ponds and Its Influence on Treatment Efficiency*, PhD dissertation, Utah State University, Logan (1971).

89. Marciano, J. J., and G. F. Harbeck, *Mass Transfer Studies in Water-Loss Investigation: Lake Hefner Studies*, U. S. Geological Survey Prof. Paper 269, Washington, D. C. (1954).

90. McQuivey, R. S., T. N. Keefer, and M. A. Shirazi, *Basic Data Report on the Turbulent Spread of Heat and Matter*, U. S. Geological Survey Open-File Report, Fort Collins, Col. (Aug. 1971).

91. Morton, B. R., *On a Momentum-Flux Diagram for Turbulent Jets, Plumes and Wakes*, J. Fluid Mech. 10, 101-112 (1961).

92. Morton, B. R., G. I. Taylor, and J. S. Turner, *Turbulent Gravitational Convection from Maintained and Instantaneous Sources*, Proc. Royal Soc. London, 234A, 1196, 1-23 (1956).

93. Motz, L. H., and B. A. Benedict, *Heated Surface Jet Discharged into a Flowing Ambient Stream*, National Center for Research and Training in the Hydrologic and Hydraulic Aspects of Water Pollution Control, Report No. 4, Vanderbilt University, Nashville, Tenn. (1970).

94. Motz, L. H., and B. A. Benedict, *Heated Surface Jet Discharged into a Flowing Ambient Stream*, Environmental Protection Agency, Water Pollution Control Research Series, No. 16130FDQ 03/71, Washington, D. C. (Mar. 1971).

95. Motz, L. H., and B. A. Benedict, *Surface Jet Model for Heated Discharges*, J. Hydraul. Div., Am. Soc. Civil Eng. 98(HY1), 181-199 (Jan. 1972).

96. Orlob, G. T., *Estuarial System Analysis Quantity and Quality Considerations*, Proceedings, National Symposium on the Analysis of Water Resources Systems, American Water Resources Association, Denver, Col. (July 1968).

97. Orlob, G. T., and L. G. Selna, *Temperature Variations in Deep Reservoirs*, J. Hydraul. Div., Am. Soc. Civil Eng. 96(HY2), 392-410 (Feb. 1970).

98. Orlob, G. T., R. P. Shubinski, and K. D. Feigner, *Mathematical Modeling of Water Quality in Estuarial Systems*, National Symposium on Estuarine Pollution, Stanford University (1967).

99. Parker, F. L., and P. A. Krenkel, editors, *Engineering Aspects of Thermal Pollution*, Vanderbilt Unitersity Press, Nashville, Tenn. (1969).

100. Parker, F. L., and P. A. Krenkel, editors, *Thermal Pollution: Status of the Art*, National Center for Research and Training in the Hydrologic and Hydraulic Aspects of Water Pollution Control, Report No. 3, Vanderbilt University, Nashville, Tenn. (1969).

101. Pearce, A. F., *Critical Reynolds Number for Fully-Developed Turbulence in Circular Submerged Water Jets*, National Mechanical Engineering Research Institute, Council for Scientific and Industrial Research, CS IR Report MEG475, Pretoria, South Africa (Aug. 1966).

102. Plate, E. J., *Water Surface Velocities Induced by Wind Shear*, J. Eng. Mech. Div., Am. Soc. Civil Eng. 96(EM3), 295-312 (June 1970).

103. Platten, J. L., and J. F. Keffer, *Entrainment in Deflected Axisymmetric Jets at Various Angles to the Stream*, Department of Mechanical Engineering Publication No. 6808, University of Toronto (1968).

104. Policastro, A. J., and J. V. Tokar, *Heated Effluent Dispersion in Large Lakes: State-of-the-Art of Analytical Modeling. Part I. Critique of Model Formulations*, ANL/ES-11 (Jan. 1972).

105. Polk, E. M., Jr., B. A. Benedict, and F. L. Parker, *Cooling Water Density Wedges in Streams*, J. Hydraul. Div., Am. Soc. Civil Eng. 97(HY10), 1639-1652 (Oct. 1971).

106. Pratte, B. D., and Baines, W. D., *Profiles of the Round Turbulent Jet in a Cross Flow*, J. Hydraul. Div., Am. Soc. Civil Eng. 92(HY6), Proc. Paper 5556, pp. 53-64 (Nov. 1967).

107. Pritchard, D. W., *What is an Estuary: Physical Viewpoint*, Estuaries, G. H. Lauff, Ed., American Association for Advancement of Science, Pub. No. 83, Washington, D. C. 3-5 (1967).

108. Pritchard, D. W., *Dispersion and Flushing of Pollutants in Estuaries*, J. Hydraul. Div., Am. Soc. Civil Eng. 95(HY1), 115-124 (Jan. 1969).

109. Pritchard, D. W., before the State of Maryland Hearing Board on Water Use Permit Work; also appears in the Governor's (Maryland) Task Force Report (1970).

110. Pritchard, D. W., comments at public hearings, Illinois Pollution Control Board, R-70, Chicago, Ill. (1971).

111. Pritchard, D. W., *Design and Siting Criteria for Once-Through Cooling Systems*, AIChE, 68th Annual Meeting, Houston, Texas (1971).

112. Raphael, J. M., *Prediction of Temperature in Rivers and Reservoirs*, J. Power Div., ASCE, 88(PO2) (July 1962).

113. Rawn, A. M., and H. K. Palmer, *Pre-determining the Extent of a Sewage Field in Sea Water*, Trans. Am. Soc. Civil Eng. 94, 1750, 1036-1081 (1930).

114. Reynolds, J. Z., *Some Water Quality Considerations of Pumped Storage Reservoirs*, PhD dissertation, University of Michigan, Ann Arbor (1966).

115. Richards, J. M., *Experiments on the Motion of Isolated Cylindrical Thermals through Unstratified Surroundings*, Int. J. Air Water Poll. 7, 17-34 (1963).

116. Romberg, G. P., W. Prepejchal, and D. M. Nelson, *Thermal Plume Measurements*, Proceedings of the 14th Conference on Great Lakes Research, 1971, by International Association for Great Lakes Research.

117. Rouse, H., C. S. Yih, and H. W. Humphreys, *Graviational Convection from a Boundary Source*, Tellus 4, 201-210 (1952).

118. Rouse, H., *Diffusion in the Lee of a Two-Dimensional Jet*, 9th Congress International de Mechanique Appliquee, Vol. I, 307-312 (1957).

119. Ryan, P. J., *Cooling Ponds*, Chapter 12 in Engineering Aspects of Heat Disposal -- from Power Generation, MIT Summer Session Short Course, Ralph M. Parsons Laboratory, Cambridge, Mass., June 28-July 2, 1971.

120. Ryan, P. J., and D. R. F. Harleman, *Prediction of the Annual Cycle of Temperature Changes in a Stratified Lake or Reservoir: Mathematical Model and User's Manual*, Ralph M. Parsons Laboratory Report No. 137, Department of Civil Engineering, Massachusetts Institute of Technology, Cambridge (Apr. 1971).

121. Schijf, J. B., and J. C. Schönfeld, *Theoretical Considerations on the Motion of Salt and Fresh Water*, Proceedings, Minnesota International Hydraulics Convention (1953).

122. Schlichting, H., *Boundary Layer Theory*, translated by J. Kestin, 4th Edition, McGray-Hill Book Co., Inc., New York (1960).

123. Shirazi, M. A., and L. R. Davis, *Workbook of Thermal Plume Prediction: Vol. I, Submerged Discharge*, National Environmental Research Center, Corvallis, Oregon (Aug. 1972).

124. Shubinski, R. P., J. C. McCarty, and M. R. Lindorf, *Computer Simulation of Estuarial Networks*, J. Hydraul. Div., Am. Soc. Civil Eng. 91(HY5), 33-49 (Sept. 1965).

125. Silberman, E., and H. Stefan, *Physical (Hydraulic) Modeling of Heat Dispersion in Large Lakes: A Review of the State of the Art*, St. Anthony Falls Hydraulic Laboratory, University of Minnesota, Minneapolis (1970).

126. Simmons, H. B., *Field Experience in Estuaries*, in Estuary and Coastline Hydrodynamics, A. T. Ippen, Ed., McGraw-Hill, Inc., New York, 673-690 (1966).

127. Slotta, L. S., and P. Van Dyke, *Numerical Simulation of the Thermal Regime in Lake Norman*, Hydronautics, Inc., Tech. Report 7908-1 (Oct. 1970).

128. Sotil, C. A., *Computer Program for Slot Buoyant Jets into Stratified Ambient Environments*, W. M. Keck Laboratory of Hydraulics and Water Resources, Tech. Memo 71-2 (June 1971).

129. Stolzenbach, K. D., *Heated Surface Discharges*, Chapter 6 in Engineering Aspects of Heat Disposal -- from Power Generation, MIT Summer Session Short Course, Ralph M. Parsons Laboratory, Cambridge, Mass., June 28-July 2, 1971.

130. Stolzenbach, K. D., personal communication (1972).

131. Stolzenbach, K. D., and D. R. F. Harleman, *An Analytical and Experimental Investigation of Surface Discharges of Heated Water*, MIT, Department of Civil Engineering, Ralph M. Parsons Laboratory, Report No. 135 (Mar. 1971).

132. Stover, J. E., W. D. Bergman, and R. J. Huston, *Mathematical Modeling of Thermal Discharges into Shallow Estuaries*, Document No. T70-AU-7425-U, Tracor, Inc., Austin, Texas (1971).

133. Sundaram, T. R., C. C. Easterbrook, K. R. Piech, and G. Rudinger, *An Investigation of the Physical Effects of Thermal Discharges into Cayuga Lake (Analytical Study)*, CAL No. VT-2616-0-2, Cornell Aeronautical Laboratory, Inc. (Nov. 1969).

134. Sundaram, T. R., R. G. Rehm, G. Rudinger, and G. E. Merritt, *Research on the Physical Aspects of Thermal Pollution*, Cornell Aeronautical Laboratory, Inc., Buffalo, N. Y. (1970). Also available in EPA Water Pollution Control Research Series, No. 16130DPU 02/71 (Feb. 1971).

135. Taimi, T. M., *Effects of Velocity Ratio on Heated Surface Jets*, MS thesis, Vanderbilt University, Nashville, Tenn. (Mar. 1972).

136. Thackston, E. L., and F. L. Parker, *Effect of Geographical Location on Cooling Pond Requirements and Performance*, Environmental Protection Agency, Water Pollution Control Research Series, No. 16130FDQ 03/71, Washington, D. C. (Mar. 1971).

137. Tracor, Inc., *Water Quality Analysis of the Nueces Bay Generating Station*, Document No. T70-AU-7203-U-R, Tracor, Inc., Austin, Texas (1970).

138. Tracor, Inc., *Water Quality Analysis of the Cedar Bayou Generating Station*, Document No. T-70-AU-7252-U (Revision 1), Tracor, Inc., Austin, Texas (1970).

138a. Trent, D. S., and J. R. Welty, *Numerical Thermal Plume Model for Vertical Outfalls in Shallow Water*, Report EPA-R2-73-162, Environmental Protection Agency, Washington, D. C. (Mar. 1973).

ARGONNE NATIONAL LAB WEST
3 4444 00012262 2

X

B